

Group 3 Complexes of Rigid Neutral and Monoanionic Ligands

Group 3 Metal Complexes of Rigid Neutral and Monoanionic Pincer Ligands

By

Aathith Vasanthakumar, H.B.Sc.

A Thesis

Submitted to the School of Graduate Studies

in Partial Fulfilment of the Requirements

for the Degree

Doctor of Philosophy of Science

McMaster University

© Copyright by Aathith Vasanthakumar. September 2020

Doctor of Philosophy of Science (2020) McMaster University

(Department of Chemistry and Chemical Biology) Hamilton, Ontario

TITLE: Group 3 Metal Complexes of Rigid Neutral and Monoanionic Pincer Ligands

AUTHOR: Aathith Vasanthakumar, H.B.Sc.

SUPERVISOR: Dr. David J.H. Emslie

NUMBER OF PAGES: ixliii, 280

Lay Abstract

Cationic group 3 alkyl complexes are underreported in comparison to analogous group 4 complexes. The scarcity of these complexes can be attributed to their propensity to engage in undesirable reactions such as ligand redistribution and cyclometallation. To increase the thermal stability of such complexes, design features, such as carefully positioned steric bulk and ligand rigidity are beneficial. Additionally, such ligands must also have considerable donor ability, in order to stabilize inherently electron deficient cationic metal centers. This work details the synthesis of a variety of neutral and monoanionic ligands that incorporate the aforementioned design features, which were utilized in the successful synthesis of a variety of neutral, monocationic and extremely rare dicationic group 3 alkyl complexes. The cationic monoalkyl complex in this work proved to be a highly potent intramolecular hydroamination catalyst. Furthermore, a rare dicationic scandium complex was highly active for ethylene polymerization.

Abstract

The synthesis of a rigid 4,5-bis(triphenylphosphinimino)-2,7-di-*tert*-butyl-9,9-dimethylxanthene $(\text{Ph}_3\text{PN})_2\text{XT}$ (**1**) ligand is outlined, along with a modified synthesis for previously reported 1,8-bis(triphenylphosphinimino)naphthalene $(\text{Ph}_3\text{PN})_2\text{NAP}$ (**3**). Reaction of neutral $(\text{Ph}_3\text{PN})_2\text{XT}$ with $[\text{Y}(\text{CH}_2\text{SiMe}_3)_3(\text{THF})_2]$ resulted in double cyclometallation, yielding the base-free monoalkyl complex, $[(\{\text{Ph}_2(\text{C}_6\text{H}_4)\text{PN}\}_2\text{XT})\text{Y}(\text{CH}_2\text{SiMe}_3)]$ (**2**). Layering a concentrated THF solution of **2** with hexanes at $-28\text{ }^\circ\text{C}$ afforded THF-coordinated $[(\{\text{Ph}_2(\text{C}_6\text{H}_4)\text{PN}\}_2\text{XT})\text{Y}(\text{CH}_2\text{SiMe}_3)(\text{THF})]\cdot 2\text{THF}$ (**2-THF** $\cdot 2\text{THF}$), with a distorted pentagonal bipyramidal geometry and approximately meridional coordination of the pentadentate $\{\text{Ph}_2(\text{C}_6\text{H}_4)\text{PN}\}_2\text{XT}$ dianion. Similarly, $(\text{Ph}_3\text{PN})_2\text{NAP}$ reacted with $[\text{Y}(\text{CH}_2\text{SiMe}_3)_3(\text{THF})_2]$ to afford a THF-coordinated monoalkyl complex, $[(\{\text{Ph}_2(\text{C}_6\text{H}_4)\text{PN}\}_2\text{NAP})\text{Y}(\text{CH}_2\text{SiMe}_3)(\text{THF})]$ (**4-THF**). Layering a DME solution of **4-THF** with hexanes at $-28\text{ }^\circ\text{C}$ afforded X-ray quality crystals of $[(\{\text{Ph}_2(\text{C}_6\text{H}_4)\text{PN}\}_2\text{NAP})\text{Y}(\text{CH}_2\text{SiMe}_3)(\kappa^2\text{-DME})]\cdot \text{hexane}$ (**4-DME** $\cdot \text{hexane}$), with a highly distorted pentagonal bipyramidal geometry and a facial coordination mode of the tetradentate $\{\text{Ph}_2(\text{C}_6\text{H}_4)\text{PN}\}_2\text{NAP}$ dianion

The synthesis of a rigid 4,5-bis(1,3-diisopropylimidazol-2-imine)-2,7,9,9-tetramethylacridan H(AII₂) ligand (**5**) was achieved via a Buchwald-Hartwig cross-coupling reaction. Reaction of the proligand H(AII₂) with [M(CH₂SiMe₃)₃(THF)₂] (M = Y(**6**), Sc(**8**)) yielded the base free dialkyl complexes [(AII₂)Y(CH₂SiMe₃)₂] (**6**) and [(AII₂)Sc(CH₂SiMe₃)₂] (**8**). The reaction of **6** with one equivalent of [CPh₃][B(C₆F₅)₄] yielded [(AII₂)Y(CH₂SiMe₃)][B(C₆F₅)₄] (**7**) in-situ. Complex **7** proved to be a potent intramolecular hydroamination catalyst for a variety of aminoalkane substrates.

The attempted synthesis of 4,5-bis(1,3-diisopropylimidazol-2-imine)-2,7-di-*tert*-butyl-9,9-dimethylxanthene (XII₂) via the Staudinger reaction resulted in the isolation of the triazene intermediate 4,5-bis(1,3-diisopropylimidazol-2-ylidene{triazene})-2,7-di-*tert*-butyl-9,9-dimethylxanthene XIA₂ (**9**). Reaction of XIA₂ with one equivalent of [Y(CH₂SiMe₃)₃(THF)₂] led to the isolation of [(XIA₂)Y(CH₂SiMe₃)₃] (**10**). Synthesis of XII₂ (**11**) was achieved via a Buchwald-Hartwig cross-coupling reaction. Reaction of XII₂ with one equivalent of YCl₃(THF)_{3.5} resulted in the isolation of [(XII₂)YCl₃] (**12**). In contrast, the reaction of XII₂ with one equivalent of [Y(CH₂SiMe₃)₃(THF)₂] led to several unidentified products. Reaction of XII₂ with 1 equivalent of [H(Et₂O)₂][B(C₆F₅)₄] led to the isolation of the precursor [H(XII₂)][B(C₆F₅)₄] (**13**). The reaction of **13** with 1.1 equivalents of [M(CH₂SiMe₃)₃(THF)₂] (M = {Y(**14**), Sc(**15**)} led to the isolation of the monocationic [(XII₂)M(CH₂SiMe₃)₂][B(C₆F₅)₄] complexes. The reaction of [(XII₂)Sc(CH₂SiMe₃)₂][B(C₆F₅)₄] with 1.1 equivalents of B(C₆F₅)₃ led to the

abstraction of a methyl anion from the silicon center, with concomitant migration of the remaining alkyl group to the positively charged silicon, forming a new $\text{CH}_2\text{SiMe}_2\text{CH}_2\text{SiMe}_3$ alkyl group. This process is accompanied by $\text{MeB}(\text{C}_6\text{F}_5)_3$ anion formation, forming a contact ion pair to afford the dicationic species $[(\text{XII})_2\text{Sc}(\text{CH}_2\text{SiMe}_3)][\text{MeB}(\text{C}_6\text{F}_5)_3][\text{B}(\text{C}_6\text{F}_5)_4]$ **16**. In contrast, the reaction of **15** with 1.3 equivalents of $[\text{CPh}_3][\text{B}(\text{C}_6\text{F}_5)_4]$ in the presence of 5 equivalents of toluene resulted in the synthesis of $[(\text{XII})_2\text{Sc}(\text{CH}_2\text{SiMe}_3)(\eta^x\text{-toluene})][\text{B}(\text{C}_6\text{F}_5)_4]_2$ **17** in-situ. Complex **17** is a highly potent ethylene polymerization catalyst with an activity of 868 kg/mol·atm·h. The reaction of **15** with $[\text{HNMe}_2\text{Ph}][\text{B}(\text{C}_6\text{F}_5)_4]$ led to the cyclometallation of the resulting NMe_2Ph byproduct to yield $[(\text{XII})_2\text{Sc}(\text{C}_6\text{H}_4\text{NMe}_2)][\text{B}(\text{C}_6\text{F}_5)_4]_2$ (**18**) in-situ.

The synthesis of a rigid, asymmetric 4-(1,3-diisopropylimidazol-2-imine)-5-(2,6-diisopropylanilido)-2,7-di-*tert*-butyl-9,9-dimethylxanthene XAI (**19**) ligand was achieved by a two step Buchwald-Hartwig cross-coupling reaction with initial cross coupling of 1,3-diisopropylimidazol-2-imine followed by the cross-coupling of 2,6-diisopropylaniline. The reaction of XAI with 1.1 equivalents of $[\text{Y}(\text{CH}_2\text{SiMe}_3)_3(\text{THF})_2]$ yielded $[(\text{XAI})\text{Y}(\text{CH}_2\text{SiMe}_3)_2]$ (**20**). Subsequent reaction of $[(\text{XAI})\text{Y}(\text{CH}_2\text{SiMe}_3)_2]$ with 1 equivalent of $[\text{CPh}_3][\text{B}(\text{C}_6\text{F}_5)_4]$ in the presence of 10 equivalents of toluene resulted in the synthesis of the toluene coordinated $[(\text{XAI})\text{Y}(\text{CH}_2\text{SiMe}_3)(\eta^x\text{-toluene})][\text{B}(\text{C}_6\text{F}_5)_4]$ (**21**) complex. Similar to **7**, complex **21** was highly active for intramolecular hydroamination of various substrates.

Acknowledgements

First and foremost, I would like to thank my supervisor Dr. David J. H. Emslie, for giving me the opportunity to hone my skills as a chemist under his excellent guidance. His enthusiasm for chemistry is highly contagious and fueled my motivation in the lab. Despite my initial difficulties, you helped infuse me with confidence that helped me accomplish the goals I had set for myself, and for that I am eternally indebted to you. Thanks for editing all my work and always being available to chat despite me dropping by at random times of the day. I am glad I have you as a friend that I can go to for future advice or for just cracking open a cold one.

I would like to thank all present and past Emslie group members with whom I have had the opportunity to work with, including Dr. Brad Cowie, Dr. Todd Whitehorne, Dr. Preeti Chadha, Dr. Edwin Wong, Dr. Ya-Dong (Kevin) Yu, Dr. Kelly Motolko, Kristopher Kolpin, Majeda Al Hareri, Novan Gray, Declan DeJordy, Nick Hoffman, Maia Murphy and Kasuni Wedisinghe. I would like to especially thank Dr. Nick Andreychuk for initially training me. Additionally, I would like to thank Dr. Jeffrey Price for being an excellent colleague/friend who was always there to chat about chemistry and or the Simpsons. Finally, to Katarina Paskaruk for being a great friend and for allowing me to steal your pens and chocolate. I have also had the pleasure of training excellent undergraduate students

which include, Novan Gray, Eliza-Jayne Boisvert, Ryan Tretter, Archie Ahilan and John Box. You guys put up with my jokes and were a pleasure to work with.

Thank you to my Ph.D committee members Dr. Gillian Goward and Dr. Yuriy Mozharivskyj for your guidance and support. I appreciate the positive encouragement that you provided at every committee meeting, especially at the most difficult times I have encountered in my graduate career. I would further like to thank Dr. Gary Schrobilgen and Dr. Ignacio Vargas-Baca for the friendly chats we have had and for instructing excellent courses I've had the pleasure of taking.

I would like to thank Dr. Hilary Jenkins and Dr. Bob Berno in the Nuclear Magnetic Resonance Facility for all of their help. I am especially thankful for the help you provided in the last few months of my graduate career and for being so prompt in replying to questions. I would like to thank Dr. Jim Britten from the McMaster X-ray Diffraction Facility for all his help and guidance pertaining to X-ray structures. Thanks Jim for responding no matter what time of day it was, and for taking an active interest in ensuring that I understood certain concepts.

I would like to thank the professors with whom I had the pleasure to work for as a TA. Thanks to Dr. Kalai Saravanamuttu, Dr. Linda Davis and Greg Bahun. A special thanks to Karen Neuman for being extremely helpful during my lab sessions. I would also like to thank Dr. Kylie Luska for all the friendly chats about basketball (Go Raptors!).

I would like to thank the Department of Chemistry and Chemical Biology at McMaster University for their generous financial support.

Lastly, I would like to thank my family. Shankar anna and especially Kowsi acca for being a very supportive sister and for always sending treats my way. To my late aunt Sarasala mummy for being another mother. Thank you for calling to check up on me and for providing me with a lot of home cooked food and coffee while I was writing my transfer report. To my cousins Binthu, Rekha and Suthu for all your support and all the good times. To my parents Vasanthakumar and Rathaluxmy, I cannot express in words how much you mean to me. You have provided me with encouragement and support throughout my life and I consider myself fortunate for having such loving parents. To my sister Kalpana for always being positive and helping me ease my mind even through the most trying times. My brother-in-law Prem for being a brother I can count on and for being an excellent role model that I wish to emulate. Finally, to my little niece Thara for facetimeing me though out my time writing.

Declaration of Academic Achievement

Kristopher Kolpin a former Ph.D. student in the Emslie group was responsible for the synthesis of $B(C_6F_5)_3$. Dr. Carlos Cruz a former Ph.D student in the Emslie group was responsible for the synthesis of 1-amino-2,2-diphenyl-4-pentene. Dr. Kelly Motolko a former Ph.D student in the Emslie group was responsible for the synthesis 1-amino-2,2-diphenyl-4-methyl-4-pentene and 1-amino-2,2-diphenyl-5-hexene. Mr. Joseph Fornefeld from Midwest Microlab Inc. was responsible for performing elemental analysis for all samples. Dr. Jim Britten was responsible for crystal mounting, data acquisition, as well as assistance for refinement and structure solution for several X-ray diffraction experiments. Eliza-Jayne Boisvert, a former undergraduate student was responsible for the initial synthesis of XAI and $[(XAI)Y(CH_2SiMe_3)_2]$ under my guidance. All other results were obtained by myself Aathith Vasanthakumar.

“We are made of star-stuff. We are a way for the cosmos to know itself” ---

Carl Sagan

Table of Contents

Lay Abstract	ii
Abstract.....	iii
Acknowledgements	vi
Declaration of Academic Achievement	ix
Table of Contents	xi
List of Figures.....	xviii
List of Schemes	xxxii
List of Tables	xxxv
List of Abbreviations	xxxvii
List of Compounds.....	xlii
Chapter 1	
Introduction.....	1
1.1 Introduction to Rare Earth Metal Chemistry	1
1.2 Introduction to Olefin Polymerization	6
1.2.1 Introduction to Ethylene Polymerization by Rare-Earth Metal Catalysts.....	8
1.3 Introduction to Intramolecular Hydroamination	11

1.3.1	Intramolecular Hydroamination Mechanism for Rare Earth Metal Complexes	12
1.3.2	Intramolecular Hydroamination – Substrate Reactivity	15
1.4	Ligand Attachment Strategies for the Synthesis of Rare Earth Complexes	17
1.4.2	Neutral Ligand Attachment Strategies.....	22
1.5	Introduction to Rare Earth Alkyl Complexes.....	22
1.5.1	Neutral Cyclopentadienyl Based Rare-Earth Alkyl Complexes.....	23
1.5.2	Neutral Non-Cyclopentadienyl Based Rare-Earth Alkyl Complexes	26
1.5.3	Synthetic Routes to Cationic Alkyl Complexes.....	28
1.5.4	Monocationic Rare-Earth Alkyl Complexes.....	32
1.5.5	Neutral vs. Cationic Rare Earth Intramolecular Hydroamination Catalysts.....	41
1.5.6	Dicationic Rare Earth Alkyl Complexes.....	55
1.6	Ligand Design for Rare Earth Metal Chemistry	61
1.6.1	Introduction to Rigid Pincer Ligands.....	62
1.7	Introduction to Phosphinimine Based Ligands	66
1.7.1	Complexes Containing Phosphinimine Donors in Rare Earth Chemistry.....	68

1.8	Introduction to Imidazol-2-Imine Based Ligands	79
1.8.1	Imidazol-2-imine Donors in Rare Earth Chemistry	81
1.9	Thesis Goals	82

Chapter 2

Alkyl Yttrium Complexes of Doubly Cyclometallated Xanthene- and Naphthalene-Backbone Bis(phosphinimine) Ligands

2.1	Introduction	84
2.2	Synthesis of $(\text{Ph}_3\text{PN})_2\text{XT}$	86
2.3	Synthesis of $(\text{Ph}_3\text{PN})_2\text{NAP}$	97
2.4	Synthesis of $[(\{\text{Ph}_2(\text{C}_6\text{H}_4)\text{PN}\}_2\text{NAP})\text{Y}(\text{CH}_2\text{SiMe}_3)(\text{THF})](2\text{-THF})$	99
2.5	Investigation of Intramolecular Hydroamination and Ethylene Polymerization Catalysis - $[(\{\text{Ph}_2(\text{C}_6\text{H}_4)\text{PN}\}_2\text{NAP})\text{Y}(\text{CH}_2\text{SiMe}_3)(\text{THF})](2\text{-THF})$] and $[(\{\text{Ph}_2(\text{C}_6\text{H}_4)\text{PN}\}_2\text{XT})\text{Y}(\text{CH}_2\text{SiMe}_3)]$	105
2.6	Summary and Conclusions.....	106

Chapter 3

Neutral and Cationic Group 3 Alkyl Complexes of a Rigid Monoanionic NNN-Donor Pincer Ligand: Synthesis and Intramolecular Hydroamination

Activity	107	
3.1	Introduction	107
3.2	Synthesis of $\text{H}[\text{AlI}_2]$	110

3.3	Synthesis of $[(AlI_2)Y(CH_2SiMe_3)_2]$	112
3.3.1	In-situ synthesis of $[(AlI_2)Y(CH_2SiMe_3)_2][B(C_6F_5)_4]$	119
3.4	Synthesis of $[(AlI_2)Sc(CH_2SiMe_3)_2]$	123
3.4.1	Attempted in-situ synthesis of $[(AlI_2)Sc(CH_2SiMe_3)][B(C_6F_5)_4]$	127
3.5	Intramolecular hydroamination	128
3.6	Summary and Conclusions.....	132

Chapter 4

Synthesis of Alkyl Group 3 Cationic and Dicationic Complexes Employing A Neutral Rigid NON-Donor Ligand.....		134
4.1	Introduction	134
4.2	Synthesis of XIA_2	137
4.3	Synthesis of $[(XIA_2)Y(CH_2SiMe_3)_3]$	140
4.4	Synthesis of XII_2	142
4.5	Synthesis of $[(XII_2)YCl_3]$	144
4.6	Synthesis of $[HXII_2][B(C_6F_5)_4]$	146
4.7	Synthesis of $[(XII_2)Y(CH_2SiMe_3)_2][B(C_6F_5)_4]$	148
4.7.1	Attempted Synthesis of $[(XII_2)Y(CH_2SiMe_3)][B(C_6F_5)_4]_2$	153
4.8	Synthesis of $[(XII_2)Sc(CH_2SiMe_3)_2][B(C_6F_5)_4]$	155

4.8.1	In-situ generation of dicationic [(XII ₂)Sc(CH ₂ SiMe ₂ CH ₂ SiMe ₃)][(MeB(C ₆ F ₅) ₃)] [B(C ₆ F ₅) ₄]	160
4.8.2	In-situ generation of [(XII ₂)Sc(CH ₂ SiMe ₃)(η ^x -toluene) _x][B(C ₆ F ₅) ₄] ₂	169
4.8.3	In-situ generation of the dicationic [(XII ₂)Sc(C ₆ H ₄ NMe ₂)] [B(C ₆ F ₅) ₄] ₂	176
4.9	Ethylene Polymerization Catalysis Using [(XII ₂)Sc(CH ₂ SiMe ₃)] [B(C ₆ F ₅) ₄] ₂	180
4.10	Summary and Conclusions	182

Chapter 5

Synthesis of an Alkyl Yttrium Cation Utilizing A Monoanionic Rigid

Asymmetric NON-Donor Ligand 184

5.1	Introduction	184
5.2	Synthesis of H[XAl].....	186
5.3	Synthesis of [(XAl)Y(CH ₂ SiMe ₃) ₂]	189
5.3.1	Synthesis of [(XAl)Y(CH ₂ SiMe ₃)(η ^x -toluene)] [B(C ₆ F ₅) ₄]	194
5.4	Ethylene Polymerization	202
5.5	Intramolecular Hydroamination	203
5.6	Summary and Conclusions	205

Chapter 6

Future Directions and Conclusions 206

6.1	Future directions of rigid neutral NON donor ligands employing imidazol-2-imine donors	206
6.1.1	A bulky symmetric NON donor ligand - ^t BuXII ₂	207
6.1.2	A bulky asymmetric NON donor ligand.....	208
6.2	Reductive chemistry of dicationic rare earth complexes.....	209
6.3	Cationic aluminum alkyl complexes	213
6.3.1	Synthesis of [({Ph ₃ PN} ₂ XT)AlMe ₂][B(C ₆ F ₅) ₄].....	214
6.3.2	Synthesis of [({Ph ₃ PN} ₂ NAP)AlMe ₂][B(C ₆ F ₅) ₄].....	219
6.4	Summary and Conclusions.....	225

Chapter 7

Experimental Methods 227

7.1	General Details.....	227
7.1.1	Laboratory Equipment and Apparatus	227
7.1.2	Solvents.....	228
7.1.3	Starting Materials.....	228
7.1.4	Instrumentation and Analysis	229

7.2 Synthetic Procedures and Characterization Pertaining to the Work of Chapter 2	231
7.3 Synthetic Procedures and Characterization Pertaining to the Work of Chapter 3	237
7.4 Synthetic Procedures and Characterization Pertaining to the Work of Chapter 4	245
7.5 Synthetic Procedures and Characterization Pertaining to the Work of Chapter 5	256
7.6 Synthetic Procedures and Characterization Pertaining to Future Work - Chapter 6	263
Bibliography	267

List of Figures

Figure 1.1: Literature examples of rare earth metal intramolecular hydroamination catalysts.....	12
Figure 1.2: Selected intramolecular hydroamination substrates cyclized by rare earth catalysts. Substrates are arranged in order of decreasing reactivity towards cyclization.	17
Figure 1.3: Literature example - Synthesis of rare earth tetramethylaluminate complexes by reaction with $[\text{Ln}\{(\mu\text{-Me})_2\text{AlMe}_2\}_3]^{32}$	19
Figure 1.4: Literature example - Synthesis of $[\text{M}(\text{CH}_3)_3]_n$ and subsequent Synthesis of $[(\text{Cn})\text{Y}(\text{CH}_3)_3]$ Cn = 1,4,7- trimethyl-1,4,7-triazacyclononane	20
Figure 1.5: First reported base free bis(alkyl) rare-earth complex	24
Figure 1.6: Selected examples of bis(alkyl) rare earth complexes of cyclopentadienyl based ligands.....	25
Figure 1.7: Selected examples of bis(alkyl) rare earth complexes of cyclopentadienyl based ligands with a pendant neutral donor.....	26
Figure 1.8: Selected examples of bis(alkyl) rare earth complexes of non-cyclopentadienyl based ligands.....	27
Figure 1.9: Selected examples of tris(alkyl) rare earth complexes utilizing neutral multidentate ligands	28
Figure 1.10: Literature examples of dimethylaniline coordination to a cationic rare earth complex– Anion: $[\text{B}(\text{C}_6\text{F}_5)_4]$	32

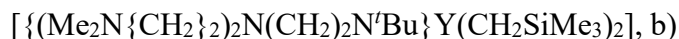
Figure 1.11: First example of a rare earth cationic alkyl complex	
[Cp*La{CH(SiMe ₃) ₂ }][BPh ₄]	33
Figure 1.12: Synthesis of the monomeric contact ion pair [(NacNac ^{tBu, Dipp})Sc(CH ₃)]	
[MeB(C ₆ F ₅) ₃]	34
Figure 1.13: Reaction of [(NacNac ^{Me, Dipp})Sc(CH ₃) ₂] ₂ with 1 or 2 equivalents of B(C ₆ F ₅) ₃	35
Figure 1.14: Reaction of [(NacNac ^{Me, Dipp})Sc(CH ₃) ₂] ₂ with 1 equivalent of [CPh ₃][B(C ₆ F ₅) ₄]	35
Figure 1.15: Reaction of [(NacNac ^{tBu, Dipp})Sc(CH ₂ SiMe ₃) ₂] with B(C ₆ F ₅) ₃	36
Figure 1.16: Reaction of [(2-{(Dipp)NCMe}-6-{(Dipp)NCMe ₂ }C ₃ H ₃ N)Lu(CH ₂ SiMe ₃) ₂] with B(C ₆ F ₅) ₃	37
Figure 1.17: Cationic β-diketiminato Alkyl Yttrium Complexes	39
Figure 1.18: [PhC(N{Dipp}) ₂ M(CH ₂ SiMe ₃) ₂ (THF) _n] reaction with [HNMe ₂ Ph][B(C ₆ F ₅) ₄]	40
Figure 1.19: [(NacNac ^{tBu, Dipp})Sc(CH ₃)][(CH ₃)B(C ₆ F ₅) ₃] (a) catalyst	42
Figure 1.20: Triamine-amide based hydroamination pre-catalysts – ‘b’ and ‘c’ – activated in-situ with 1 eq. [HNMe ₂ Ph][B(C ₆ F ₅) ₄]	44
Figure 1.21: Trifonov’s hydroamination pre-catalysts ‘d’ and ‘e’ – activated in-situ with 1 eq. [CPh ₃][B(C ₆ F ₅) ₄]	46
Figure 1.22: Benzamidinato ligand based rare earth hydroamination pre-catalyst – ‘	49

Figure 1.23: Neutral tridentate (1,4,6-trimethyl-6-pyrrolidin-1-yl-1,4-diazepane) based hydroamination pre-catalyst 'g'	51
Figure 1.24: Coordinatively saturated dicationic alkyl complexes.....	56
Figure 1.25: C—H bond activation of pyridine - $[Y \{\eta^2-(C,N)-C_5H_4N\}(py)_6][BPh_4]_2$	57
Figure 1.26: Synthesis of 12-crown-4 based dicationic monoalkyl yttrium complexes	59
Figure 1.27: Synthesis of a) $[Sc(^iPr\text{-trisox})(CH_2SiMe_3)][B(C_6F_5)_4]_2$, b) $[\{2,6-C_6H_3R_2NCH\}_2CSc(CH_2SiMe_3)][B(C_6F_5)_4]_2$	60
Figure 1.28: The general architecture of a pincer ligand metal complex (A, A' and B represent varying donor groups in a meridional bonding motif).....	63
Figure 1.29: Rigid dianionic pincer ligands – XN_2 and XA_2	64
Figure 1.30: Selected examples of XN_2 and XA_2 metal complexes	65
Figure 1.31: Resonance structures of phosphinimine donors	67
Figure 1.32: Phosphinimine-donor ligands employed in rare earth alkyl and aryl chemistry; for ligands 'd' and 'e', dashed bonds are absent in the former, and present in the latter.....	69
Figure 1.33: Rare earth dialkyl complexes of $[N(PPh_2NAr)_2]^-$ ligands.....	70
Figure 1.34: Synthesis of $[\{N(PPh_2NPh)_2\}Sc\{(2,6-iPrC_6H_3)\}(DMAP)_2]$	70
Figure 1.35: Synthesis of $[(1-\{NAr\}-2-\{PR_2NAr\}C_6H_4)ScMe_2]$ containing ligand type 'e'	71

Figure 1.36: Cyclometallation of [(1-{NDipp}-2-{PPh ₂ NMes})C ₆ H ₄)ScMe ₂] and [(1-{NDipp}-2-{PPh ₂ NDipp})C ₆ H ₄)ScMe ₂] containing ligand type ‘e’	72
Figure 1.37: [{1-(MeC ₄ H ₂ SCH ₂ N)-2-(PPh ₂ NAr-C ₆ H ₄)}M(CH ₂ SiMe ₃) ₂ (THF) _n] complexes containing phosphinimine ligand ‘f’	72
Figure 1.38: [(2-{Ph ₂ PN(Ar)})C ₆ H ₄ {NC(‘Bu)N(Xyl)}]M(CH ₂ SiMe ₃) ₂] containing phosphinimine ligand ‘g’	73
Figure 1.39: Literature examples of [(NP ^{fc})YR] complexes containing phosphinimine ligand ‘h’	74
Figure 1.40: Literature examples of rare earth dialkyl heteroscorpionate complexes employing a pendant phosphinimine donor (ligand type ‘i’).....	75
Figure 1.41: Cyclometallation of [{(PippN=PC ₄ H ₈) ₂ DMC}Sc(CH ₂ SiMe ₃) ₂] containing ligand type ‘j’	76
Figure 1.42: Cyclometallation of [{(PippN=PC ₄ H ₈) ₂ DMC}Lu(CH ₂ SiMe ₃) ₂] containing ligand type ‘j’	77
Figure 1.43: Cyclometallation of [{(ArN=PPh ₂) ₂ DMC}M(CH ₂ SiMe ₃) ₂] containing ligand type ‘j’	77
Figure 1.0.44: [{(PiipNPPH ₂) ₂ pyr}M(CH ₂ SiMe ₃) ₂] containing ligand type ‘k’ ...	78
Figure 1.45: Decomposition of [{(PiipNPPH ₂) ₂ pyr}Sm(CH ₂ SiMe ₃) ₂ (THF) _n] containing ligand type ‘k’	79
Figure 1.46: Resonance forms for imidazol-2-imine ligands	79
Figure 1.47: Literature examples of imidazol-2-imine donor ligands employed in rare earth chemistry.....	82

Figure 2.1: Dianionic XN_2 and XA_2 Ligands, and their relationship to the neutral NON-donor in this work	85
Figure 2.2: ^1H NMR Spectrum of $(\text{N}_3)_2\text{XT}$ (600 MHz, CD_2Cl_2).....	88
Figure 2.3: ^1H NMR Spectrum of $(\text{Ph}_3\text{PN})_2\text{XT}$ (1) (600 MHz, C_6D_6)	89
Figure 2.4: ^{31}P NMR Spectrum of $(\text{Ph}_3\text{PN})_2\text{XT}$ (1) (243 MHz, C_6D_6).....	89
Figure 2.5: ^1H NMR Spectrum of $[(\{\text{Ph}_2(\text{C}_6\text{H}_4)\text{PN}\}_2\text{XT})\text{Y}(\text{CH}_2\text{SiMe}_3)]$ (2) (600 MHz, C_6D_6).....	91
Figure 2.6: ^1H NMR Spectrum of $[(\{\text{Ph}_2(\text{C}_6\text{H}_4)\text{PN}\}_2\text{XT})\text{Y}(\text{CH}_2\text{SiMe}_3)]$ (2) (600 MHz, C_6D_6).....	92
Figure 2.7: ^{31}P NMR Spectrum of $[(\{\text{Ph}_2(\text{C}_6\text{H}_4)\text{PN}\}_2\text{XT})\text{Y}(\text{CH}_2\text{SiMe}_3)]$ (2) (243 MHz, C_6D_6)	92
Figure 2.8: X-Ray crystal structure of $[(\{\text{Ph}_2(\text{C}_6\text{H}_4)\text{PN}\}_2\text{XT})\text{Y}(\text{CH}_2\text{SiMe}_3)(\text{THF})] \cdot 2\text{THF}$ (2-THF·2THF). Ellipsoids are set to 50% probability. For clarity, hydrogen atoms, lattice solvent, <i>tert</i> -butyl groups, and non-cyclometallated phenyl rings on phosphorus are omitted, and the xanthene backbone and cyclometallated phenyl rings of the $\{\text{Ph}_2(\text{C}_6\text{H}_4)\text{PN}\}_2\text{XT}$ dianion are shaded in yellow. Selected bond lengths (Å) and angles (°): Y–C(60) 2.465(3), Y–C(24) 2.505(3), Y–C(42) 2.541(3), Y–N(1) 2.440(2), Y–N(2) 2.463(2), Y–O(1) 2.459(2), Y–O(2) 2.439(2), N(1)–P(1) 1.613(2), N(2)–P(2) 1.612(2), N(1)–Y–N(2) 131.31(7), Y–C(60)–Si 127.14(1), C(60)–Y–O(1) 79.21(8), C(60)–Y–O(2) 158.54(9).	94

Figure 2.9: Literature Examples With Similar Y-C Bond Distances to (2-THF): a)



$[\text{Cp}^*\text{Y}(\text{CH}_2\text{SiMe}_3)\{\text{CH}(\text{pz}')_2\}(\text{THF})]$ 96

Figure 2.10: ^1H NMR Spectrum of $(\text{Ph}_3\text{PN})_2\text{NAP}$ (3) (600 MHz, C_6D_6)..... 98

Figure 2.11: ^{31}P NMR Spectrum of $(\text{Ph}_3\text{PN})_2\text{NAP}$ (3) (243 MHz, C_6D_6)..... 99

Figure 2.12: ^1H NMR Spectrum of $[(\{\text{Ph}_2(\text{C}_6\text{H}_4)\text{PN}\}_2\text{NAP})\text{Y}(\text{CH}_2\text{SiMe}_3)(\text{THF})]$
 $(4\text{-THF})(600\text{ MHz, C}_6\text{D}_6)$ 101

Figure 2.13: Expanded Region - ^1H NMR Spectrum of
 $[(\{\text{Ph}_2(\text{C}_6\text{H}_4)\text{PN}\}_2\text{NAP})\text{Y}(\text{CH}_2\text{SiMe}_3)(\text{THF})]$ (4-THF)(600 MHz, C_6D_6)..... 102

Figure 2.14: ^{31}P NMR Spectrum of $[(\{\text{Ph}_2(\text{C}_6\text{H}_4)\text{PN}\}_2\text{NAP})\text{Y}(\text{CH}_2\text{SiMe}_3)(\text{THF})]$
 $(4\text{-THF})(243\text{ MHz, C}_6\text{D}_6)$ 102

Figure 2.15: Two views of the X-ray crystal structure of
 $[(\{\text{Ph}_2(\text{C}_6\text{H}_4)\text{PN}\}_2\text{NAP})\text{Y}(\text{CH}_2\text{SiMe}_3)(\text{DME})]\cdot\text{hexane}$ (4-DME·hexane).

Ellipsoids are set to 50% probability. For clarity, hydrogen atoms, lattice solvent, and non-cyclometallated phenyl rings on phosphorus are omitted, and the naphthalene backbone and cyclometallated phenyl rings of the

$\{\text{Ph}_2(\text{C}_6\text{H}_4)\text{PN}\}_2\text{NAP}$ dianion are shaded in yellow. Selected bond lengths (Å) and angles (°): Y–C(47) 2.520(2), Y–C(17) 2.508(2), Y–C(29) 2.562(2), Y–N(1) 2.518(2), Y–N(2) 2.401(2), Y–O(1) 2.493(2), Y–O(2) 2.534(2), N(1)–P(1) 1.632(1), N(2)–P(2) 1.613(2), N(1)–Y–N(2) 70.69(6), Y–C(47)–Si 139.18(1), C(29)–Y–C(47) 161.70(8), C(17)–Y–C(47) 111.12(8). 104

Figure 3.1: Relationship between the dianionic XA_2 ligand and the monoanionic Alm_2 and AlI_2 ligand	109
Figure 3.2: ^1H NMR Spectrum of $\text{H}[\text{AlI}_2]$ (600 MHz, C_6D_6)	112
Figure 3.3: ^1H NMR Spectrum of $[(\text{AlI}_2)\text{Y}(\text{CH}_2\text{SiMe}_3)_2]$ (6) (600 MHz, C_6D_6)	114
Figure 3.4: Two views of the X-ray crystal structure $[(\text{AlI}_2)\text{Y}(\text{CH}_2\text{SiMe}_3)_2]$ (6) Ellipsoids are set to 50% probability. For clarity, hydrogen atoms have been omitted. Selected bond lengths (Å) and angles (°): Y–N(1) 2.288(2), Y–N(2) 2.421(2), Y–N(3) 2.394(2), Y–C(36) 2.482(2), Y–C(40) 2.434(2), N(2)–C(18) 1.362(2), N(3)–C(27) 1.364(2), N(1)–Y–N(2) 69.26(5), N(1)–Y–N(3) 69.63(5), C(36)–Y–C(40) 110.48(7), Y–C(36)–Si(1) 115.98(9), Y–C(40)–Si(2) 118.55(9)	115
Figure 3.5: Side view of the x-ray crystal structures – (a) $[(\text{AlI}_2)\text{Y}(\text{CH}_2\text{SiMe}_3)_2]$ (6) (b) $[(\text{XA}_2)\text{U}(\text{CH}_2\text{SiMe}_3)_2] \cdot 2$ hexane	118
Figure 3.6: ^1H NMR Spectrum of $[(\text{AlI}_2)\text{Y}(\text{CH}_2\text{SiMe}_3)][\text{B}(\text{C}_6\text{F}_5)_4]$ (7) (600 MHz, $\text{C}_6\text{D}_5\text{Br}$)	120
Figure 3.7: Expanded region - ^1H NMR Spectrum of $[(\text{AlI}_2)\text{Y}(\text{CH}_2\text{SiMe}_3)][\text{B}(\text{C}_6\text{F}_5)_4]$ (7) (600 MHz, $\text{C}_6\text{D}_5\text{Br}$)	121
Figure 3.8: Expanded region - ^1H NMR Spectrum of $[(\text{AlI}_2)\text{Y}(\text{CH}_2\text{SiMe}_3)][\text{B}(\text{C}_6\text{F}_5)_4]$ (7) (600 MHz, $\text{C}_6\text{D}_5\text{Br}$)	121
Figure 3.9: ^{11}B NMR Spectrum of $[(\text{AlI}_2)\text{Y}(\text{CH}_2\text{SiMe}_3)][\text{B}(\text{C}_6\text{F}_5)_4]$ (7) generated in-situ from the reaction of $[(\text{AlI}_2)\text{Y}(\text{CH}_2\text{SiMe}_3)_2]$ (6) with $[\text{CPh}_3][\text{B}(\text{C}_6\text{F}_5)_4]$ (161 MHz, 248 K, $\text{C}_6\text{D}_5\text{Br}$)	122

Figure 3.10: VT- ^{19}F NMR Spectrum of $[(\text{AlI}_2)\text{Y}(\text{CH}_2\text{SiMe}_3)][\text{B}(\text{C}_6\text{F}_5)_4]$ (7) generated in-situ from the reaction of $[(\text{AlI}_2)\text{Y}(\text{CH}_2\text{SiMe}_3)_2]$ (6) with $[\text{CPh}_3][\text{B}(\text{C}_6\text{F}_5)_4]$ (471 MHz, $\text{C}_6\text{D}_5\text{Br}$).....	123
Figure 3.11: ^1H NMR Spectrum of $[(\text{AlI}_2)\text{Sc}(\text{CH}_2\text{SiMe}_3)_2]$ (7) (600 MHz, C_6D_6)	125
Figure 3.12: Two views of the X-ray crystal structure $[(\text{AlI}_2)\text{Sc}(\text{CH}_2\text{SiMe}_3)_2]$ of one of the independent molecules (8) Ellipsoids are set to 50% probability. For clarity, hydrogen atoms have been omitted and only one independent molecule is shown. Sc–N(1) 2.132(2), Sc–N(2) 2.256(2), Sc–N(3) 2.249(2), Sc–C(36) 2.296(2), Sc–C(40) 2.267(2), N(2)–C(18) 1.359(3), N(3)–C(27) 1.369(3), N(1)–Sc–N(2) 72.53(7), N(1)–Sc–N(3) 72.45 (6), C(36)–Sc–C(40) 110.85(9), Sc–C(36)–Si(1) 125.85(1), Sc–C(40)–Si(2) 121.5 (1).....	126
Figure 3.13: Hydroamination of 1-amino-2,2-diphenylpent-4-ene by $[(\text{AlI}_2)\text{Y}(\text{CH}_2\text{SiMe}_3)_2]$ (6) in C_6D_6 . % conversion of substrate vs. time.....	131
Figure 3.14: Hydroamination of 1-amino-2,2-diphenyl-4-methylpent-4-ene by $[(\text{AlI}_2)\text{Y}(\text{CH}_2\text{SiMe}_3)][\text{B}(\text{C}_6\text{F}_5)_4]$ (7) (2 mol%; in-situ generated) at 24 °C in $\text{C}_6\text{D}_5\text{Br}$. % conversion of substrate vs. time	131
Figure 3.15: Hydroamination of 1-amino-2,2-diphenylhex-5-ene by $[(\text{AlI}_2)\text{Y}(\text{CH}_2\text{SiMe}_3)][\text{B}(\text{C}_6\text{F}_5)_4]$ (7) (4 mol%; in-situ generated) at 24 °C in $\text{C}_6\text{D}_5\text{Br}$. % conversion of substrate vs. time	132
Figure 4.1: Relationship between the monoanionic AlI_2 and neutral XII_2 ligands	136

Figure 4.2: ^1H NMR Spectrum of XIA_2 (600 MHz, CD_2Cl_2).....	138
Figure 4.3: X-Ray crystal structure of XIA_2 . Ellipsoids are set to 50 % probability. For clarity, hydrogen atoms, and lattice solvent (DCM, H_2O) are omitted. Selected bond lengths (Å) and angles (°): N(1)—N(2) 1.297(9), N(2)—N(3) 1.31(1), N(3)—C(24) 1.36(1), N(6)—N(7) 1.256(9), N(7)—N(8) 1.341(9), N(8)—C(25) 1.35(1), N(4)-C(24) 1.33(1), N(10)-C25 1.35(1), N(9)-C(25) 1.37(1), N(5)-C(24) 1.35(1), C(25)-(C26) 1.30(2), C(34)-C(35) 1.35(1), N(1)—N(2)—N(3) 110.9(7), N(6)—N(7)—N(8) 111.4(6). R = 9.33 %.....	139
Figure 4.4: Synthesis of $[(\text{XIA})_2\text{Y}(\text{CH}_2\text{SiMe}_3)_3]$:.....	140
Figure 4.5: ^1H NMR Spectrum of $[(\text{XIA})_2\text{Y}(\text{CH}_2\text{SiMe}_3)_3]$ (10) (600 MHz, C_6D_6)	141
Figure 4.6: ^1H NMR Spectrum of XII_2 (11) (600 MHz, C_6D_6)	143
Figure 4.7: ^1H NMR Spectrum of $[(\text{XII})_2\text{YCl}_3]$ (12) (600 MHz, CD_2Cl_2)	146
Figure 4.8: ^1H NMR Spectrum of $[\text{HXII}_2][\text{B}(\text{C}_6\text{F}_5)_4] \cdot 0.5$ hexanes (13) (600 MHz, CD_2Cl_2).....	148
Figure 4.9: ^1H NMR Spectrum of $[(\text{XII})_2\text{Y}(\text{CH}_2\text{SiMe}_3)_2][\text{B}(\text{C}_6\text{F}_5)_4]$ (14) (600 MHz, $\text{C}_6\text{D}_5\text{Br}$).....	150
Figure 4.10: X-Ray crystal structure of $[(\text{XII})_2\text{Y}(\text{CH}_2\text{SiMe}_3)_2][\text{B}(\text{C}_6\text{F}_5)_4]$ (14). Ellipsoids are set to 30 % probability. For clarity, hydrogen atoms, and $\text{B}(\text{C}_6\text{F}_5)_4$ anion are omitted. Selected bond lengths (Å) and angles (°): Y—C(42) 2.389(5), Y—C(46) 2.386(5), Y—O(1) 2.425(3), Y—N(1) 2.336(4), Y—N(2) 2.329(4), N(1)—C(24) 1.369(6), N(2)—C(33) 1.373(6), N(4)—C(24) 1.344(6), N(3)—C(24)	

1.350(6), N(5)—C(33) 1.346(6), N(6)—C(33) 1.362(6), C(25)—C(26) 1.340(7),
 C(34)—C(35) 1.363(7), Y—C(42)—Si(1) 124.9(3), Y—C(46)—Si(2) 119.5(3),
 C(42)—Y—C(46) 107.1(2), N(1)—Y—C(42) 95.3(2), N(1)—Y—C(46) 115.5(2),
 N(2)—Y—C(46) 115.5(2), N(2)—Y—C(42) 102.0(2), C(42)—Y—O 145.31(2). R =
 6.77 % 151

Figure 4.11: ^1H NMR Spectrum of $[(\text{XII}_2)\text{Sc}(\text{CH}_2\text{SiMe}_3)_2][\text{B}(\text{C}_6\text{F}_5)_4]$ (600 MHz,
 $\text{C}_6\text{D}_5\text{Br}$) 156

Figure 4.12: Variable Temperature- ^1H NMR Spectrum of 15 (500 MHz, $\text{C}_6\text{D}_5\text{Br}$)
 157

Figure 4.13: X-Ray crystal structure of $[(\text{XII}_2)\text{Sc}(\text{CH}_2\text{SiMe}_3)_2][\text{B}(\text{C}_6\text{F}_5)_4]$.

Ellipsoids are set to 30 % probability. For clarity, hydrogen atoms, and $\text{B}(\text{C}_6\text{F}_5)_4$
 anion are omitted. Selected bond lengths (Å) and angles ($^\circ$): Sc—C(42) 2.238(3),
 Sc—C(46) 2.210(3), Sc—O(1) 2.283(2), Sc—N(1) 2.191(2), Sc—N(2) 2.190(2),
 N(1)—C(24) 1.368(3), N(2)—C(33) 1.368(4), N(4)—C(24) 1.346(4), N(3)—C(24)
 1.358(4), N(5)—C(33) 1.355(4), N(6)—C(33) 1.344(4), C(25)—C(26) 1.345(4),
 C(34)—C(35) 1.343(5), Sc—C(42)—Si(1) 130.0(2), Sc—C(46)—Si(2) 123.9(2),
 C(42)—Sc—C(46) 104.5(1), N(1)—Sc—C(42) 96.6(1), N(1)—Sc—C(46) 114.2(1),
 N(2)—Sc—C(46) 110.4(1), N(2)—Sc—C(42) 98.9(1), C(42)—Sc—O 150.8(1). R =
 7.55 % 159

Figure 4.14: Variable Temperature - ^1H NMR Spectra of 16 (500 MHz, $\text{C}_6\text{D}_5\text{Br}$)
 163

Figure 4.15: ^1H NMR Spectrum of 16 (500 MHz, 258K, $\text{C}_6\text{D}_5\text{Br}$) 164

Figure 4.16: Expanded region of ^1H NMR spectrum of 16 (500 MHz, 258K, $\text{C}_6\text{D}_5\text{Br}$).....	164
Figure 4.17: Expanded region of ^1H NMR Spectrum of 16 (500 MHz, 258K, $\text{C}_6\text{D}_5\text{Br}$).....	165
Figure 4.18: ^1H - ^{13}C HMBC of 16 (500 MHz ^1H , 126 MHz ^{13}C , 258 K $\text{C}_6\text{D}_5\text{Br}$)	166
Figure 4.19: ^1H - ^{29}Si HMBC of 16 (500 MHz ^1H , 126 MHz ^{29}Si , 258K, $\text{C}_6\text{D}_5\text{Br}$)	167
Figure 4.20: ^{11}B NMR Spectrum of 16 (161 MHz, 258K, $\text{C}_6\text{D}_5\text{Br}$).....	168
Figure 4.21: ^{19}F NMR Spectrum of 16 (471 MHz, 258K, $\text{C}_6\text{D}_5\text{Br}$)	169
Figure 4.22: ^1H NMR Spectrum of 17 generated in the presence of 5 equivalents of toluene (500 MHz, 298K, $\text{C}_6\text{D}_5\text{Br}$)	171
Figure 4.23: Expanded ^1H NMR Spectrum of 17 generated in the presence of 5 equivalents of toluene (161 MHz, 298K, $\text{C}_6\text{D}_5\text{Br}$)	172
Figure 4.24: Expanded ^1H NMR Spectrum of 17 generated in the presence of 5 equivalents of toluene (161 MHz, 298K, $\text{C}_6\text{D}_5\text{Br}$)	172
Figure 4.25: ^{11}B NMR Spectrum of 17 generated in the presence of 5 equivalents of toluene (161 MHz, 298K, $\text{C}_6\text{D}_5\text{Br}$)	173
Figure 4.26: ^{19}F NMR Spectrum of 17 generated in the presence of 5 equivalents of toluene (471 MHz, 258K, $\text{C}_6\text{D}_5\text{Br}$)	174
Figure 4.27: Variable Temperature ^1H NMR Spectra of 17 (500 MHz, $\text{C}_6\text{D}_5\text{Br}$)	175

Figure 4.28: ^1H NMR Spectrum of in-situ generated 18 (600 MHz, 298K, $\text{C}_6\text{D}_5\text{Br}$).....	178
Figure 4.29: ^{11}B NMR Spectrum of in-situ generated 18 (161 MHz, 298K, $\text{C}_6\text{D}_5\text{Br}$).....	178
Figure 4.30: ^{19}F NMR Spectrum of in-situ generated 18 (471 MHz, 298K, $\text{C}_6\text{D}_5\text{Br}$).....	179
Figure 5.1: Relationship between the dianionic XA_2 , and monoanionic AlI_2 and XAl ligands.....	186
Figure 5.2: ^1H NMR Spectrum of $\text{H}[\text{XAl}]$ (600 MHz, CDCl_3).....	188
Figure 5.3: Expanded Region - ^1H NMR Spectrum of $\text{H}[\text{XAl}]$ (600 MHz, CDCl_3)	188
Figure 5.4: Expanded Region - ^1H NMR Spectrum of $\text{H}[\text{XAl}]$ (600 MHz, CDCl_3)	189
Figure 5.5: ^1H NMR Spectrum of $[(\text{XAl})\text{Y}(\text{CH}_2\text{SiMe}_3)_2]$ (600 MHz, C_6D_6).....	191
Figure 5.6: Expanded Region - ^1H NMR Spectrum of $[(\text{XAl})\text{Y}(\text{CH}_2\text{SiMe}_3)_2]$ (600 MHz, C_6D_6).....	191
Figure 5.7: Expanded Region - ^1H NMR Spectrum of $[(\text{XAl})\text{Y}(\text{CH}_2\text{SiMe}_3)_2]$ (600 MHz, C_6D_6).....	192
Figure 5.8: Variable Temperature- ^1H NMR of $[(\text{XAl})\text{Y}(\text{CH}_2\text{SiMe}_3)_2]$ (500 MHz, d^8 -toluene	193
Figure 5.9: ^1H NMR Spectrum of $[(\text{XAl})\text{Y}(\text{CH}_2\text{SiMe}_3)(\eta^x\text{-toluene})][\text{B}(\text{C}_6\text{F}_5)_4]$ (500 MHz, 248 K, $\text{C}_6\text{D}_5\text{Br}$).....	196

Figure 5.10: Expanded Region of the ^1H NMR Spectrum of $[(\text{XAl})\text{Y}(\text{CH}_2\text{SiMe}_3)(\eta^x\text{-toluene})][\text{B}(\text{C}_6\text{F}_5)_4]$ (500 MHz, 248 K, $\text{C}_6\text{D}_5\text{Br}$).....	196
Figure 5.11: Expanded Region of the ^1H NMR Spectrum of $[(\text{XAl})\text{Y}(\text{CH}_2\text{SiMe}_3)(\eta^x\text{-toluene})][\text{B}(\text{C}_6\text{F}_5)_4]$ (500 MHz, 248 K, $\text{C}_6\text{D}_5\text{Br}$).....	197
Figure 5.12: ^1H - ^1H COSY NMR Spectrum of.....	198
Figure 5.13: ^1H - ^1H EXSY NMR Spectrum of $[(\text{XAl})\text{Y}(\text{CH}_2\text{SiMe}_3)(\eta^x\text{-toluene})][\text{B}(\text{C}_6\text{F}_5)_4]$ (500 MHz, 248 K, $\text{C}_6\text{D}_5\text{Br}$)	199
Figure 5.14: ^1H - ^1H NOESY NMR Spectrum of $[(\text{XAl})\text{Y}(\text{CH}_2\text{SiMe}_3)(\eta^x\text{-toluene})][\text{B}(\text{C}_6\text{F}_5)_4]$ (500 MHz, 248 K, $\text{C}_6\text{D}_5\text{Br}$)	199
Figure 5.15: ^{11}B NMR Spectrum of $[(\text{XAl})\text{Y}(\text{CH}_2\text{SiMe}_3)(\eta^x\text{-toluene})][\text{B}(\text{C}_6\text{F}_5)_4]$ (161 MHz, $\text{C}_6\text{D}_5\text{Br}$)	200
Figure 5.16: ^{19}F NMR Spectrum of $[(\text{XAl})\text{Y}(\text{CH}_2\text{SiMe}_3)(\eta^x\text{-toluene})][\text{B}(\text{C}_6\text{F}_5)_4]$ (471 MHz, $\text{C}_6\text{D}_5\text{Br}$)	201
Figure 6.1: Dicationic Aluminum complexes in the literature.....	213
Figure 6.2: ^1H NMR Spectrum of $[(\{\text{Ph}_3\text{PN}\}_2\text{XT})\text{Al}(\text{CH}_3)_2][\text{B}(\text{C}_6\text{F}_5)_4]$ (22a) (500 MHz, C_6D_6).....	216
Figure 6.3: ^{31}P NMR Spectrum of $[(\{\text{Ph}_3\text{PN}\}_2\text{XT})\text{Al}(\text{CH}_3)_2][\text{B}(\text{C}_6\text{F}_5)_4]$ (22a) (203 MHz, C_6D_6).....	217
Figure 6.4: ^{11}B NMR Spectrum of $[(\{\text{Ph}_3\text{PN}\}_2\text{XT})\text{Al}(\text{CH}_3)_2][\text{B}(\text{C}_6\text{F}_5)_4]$ (22aa) (161 MHz, C_6D_6)	217
Figure 6.5: X-Ray crystal structure of $[(\{\text{Ph}_3\text{PN}\}_2\text{XT})\text{Al}(\text{CH}_3)_2][\text{B}(\text{C}_6\text{H}_3\{\text{CF}_3\}_2)_4]$ (22b). Ellipsoids are set to 50 % probability. For clarity, hydrogen atoms,	

[B(C₆H₃{CF₃}₂)₄] anion and toluene are omitted. Selected bond lengths (Å) and angles (°): Al—C(60) 1.971(3), Al—C(61) 1.977(3), Al—N(1) 2.132(2), Al—N(2) 2.141(2), Al—O(1) 1.990(2), N(1)—P(1) 1.621(2), N(2)—P(2) 1.617(2), C(60)—Al—C(61) 137.9(1), N(1)—Al—N(2) 154.36(9), O(1)—Al—N(1) 77.50(8), O(1)—Al—N2 76.96(8), O(1)—Al—C(60) 110.0 (1), O(1)—Al—C(61) 112.0 (1). R= 6.78 % 219

Figure 6.6: Expanded region - ¹H NMR Spectrum of [(Ph₃PN)₂NAP)Al(CH₃)₂][B(C₆F₅)₄] (23a) (600 MHz, C₆D₆) 221

Figure 6.7: Expanded region - ¹H NMR Spectrum of [(Ph₃PN)₂NAP)Al(CH₃)₂][B(C₆F₅)₄] (23a) (600 MHz, C₆D₆) 221

Figure 6.8: ³¹P NMR Spectrum of [(Ph₃PN)₂NAP)Al(CH₃)₂][B(C₆F₅)₄] (23a) (243 MHz, C₆D₆) 222

Figure 6.9: ¹¹B NMR Spectrum of [(Ph₃PN)₂NAP)Al(CH₃)₂][B(C₆F₅)₄] (23a) (161 MHz, C₆D₆) 223

Figure 6.10: X-Ray crystal structure of [(Ph₃PN)₂NAP)Al(CH₃)₂][B(C₆H₃{CF₃}₂)₄] (23b). Ellipsoids are set to 50 % probability. For clarity, hydrogen atoms, [B(C₆H₃{CF₃}₂)₄] anion and toluene are omitted. Selected bond lengths (Å) and angles (°): Al—C(49) 1.962(3), Al—C(50) 1.969(2), Al—N(1) 1.961(2), Al—N(2) 1.916(2), N(1)—P(1) 1.639(2), N(2)—P(2) 1.618(2), C(60)—Al—C(61) 112.5(1), N(1)—Al—N(2) 91.15(7), N(1)—Al—C(49) 107.74(8), N(2)—Al—C(50) 111.58(8). R = 4.83 % 224

List of Schemes

Scheme 1.1: σ -Bond Metathesis Mechanism.....	5
Scheme 1.2: 1,2-Insertion Mechanism.....	6
Scheme 1.3: The Cossee-Arlman Mechanism for Olefin Polymerization.....	9
Scheme 1.4: The Brookhart-Green Mechanism for Olefin Polymerization	9
Scheme 1.5: The β -Hydride Elimination and a β -Hydrogen Transfer Mechanisms for Polymerization Chain Termination	10
Scheme 1.6: Chain Termination via σ -bond metathesis with H ₂ (g)	10
Scheme 1.7: Chain transfer from cationic rare earth catalyst to an aluminium alkyl scavenger.....	11
Scheme 1.8: Intramolecular Hydroamination Mechanism for Neutral or Cationic Rare Earth Complexes (x = 0, 1)	13
Scheme 1.9: Reversible Reaction of Cyclized Product and Substrate ²⁴	15
Scheme 1.10: Strategies for anionic ligand attachment: a) alkane elimination, b) amine elimination, c) salt metathesis	21
Scheme 1.11: Synthetic routes to cationic alkyl complexes	31
Scheme 1.12: Synthetic routes to phosphinimines – a) the Staudinger reaction, b) the Kirsanov reaction	68
Scheme 1.13: Synthetic routes to imidazol-2-imine ligands.....	80
Scheme 1.14: Synthesis of imidazol-2-imine ligand using Buchwald-Hartwig cross-coupling	81

Scheme 2.1: The Synthesis of XBr_2	86
Scheme 2.2: Synthesis of $(Ph_3PN)_2XT$ (1)	87
Scheme 2.3: Synthesis of $[(\{Ph_2(C_6H_4)PN\}_2XT)Y(CH_2SiMe_3)]$ (2).....	90
Scheme 2.4: Synthesis of the $(Ph_3PN)_2NAP$ ligand (3) using the Kirsanov reaction	98
Scheme 2.5: Synthesis of $[(\{Ph_2(C_6H_4)PN\}_2NAP)Y(CH_2SiMe_3)(THF)]$ (4-THF)	100
Scheme 3.1: Synthesis of $H[AlI_2]$ (5) pro-ligand	111
Scheme 3.2: Synthesis of $[(AlI_2)Y(CH_2SiMe_3)_2]$ (6).....	113
Scheme 3.3: In-situ synthesis of $[(AlI_2)Y(CH_2SiMe_3)][B(C_6F_5)_4]$	119
Scheme 3.4: Synthesis of $[(AlI_2)Sc(CH_2SiMe_3)_2]$ (8)	124
Scheme 4.1: Synthesis of XIA_2 (9)	137
Scheme 4.2: Synthesis of XII_2	142
Scheme 4.3: Synthesis of $[(XII_2)YCl_3]$ (12)	145
Scheme 4.4: Synthesis of $[HXII_2][B(C_6F_5)_4]$ (13)	147
Scheme 4.5: Synthesis of $[(XII_2)Y(CH_2SiMe_3)_2][B(C_6F_5)_4]$ (14).....	149
Scheme 4.6: Attempted in-situ generation of $[(XII_2)Y(CH_2SiMe_3)(\eta^x-$ toluene)][$B(C_6F_5)_4$] $_2$ and $[(XII_2)Y(CH_2SiMe_3)(\{MeB(C_6F_5)_3\})][B(C_6F_5)_4]$	154
Scheme 4.7: Synthesis of $[(XII_2)Sc(CH_2SiMe_3)_2][B(C_6F_5)_4]$ (15)	155
Scheme 4.8: Synthesis and proposed mechanism for the formation of $[(XII_2)Sc(CH_2SiMe_2CH_2SiMe_3)][(MeB(C_6F_5)_3)][B(C_6F_5)_4]$ (16).....	161

Scheme 4.9: In-situ generation of $[(XII_2)Sc(CH_2SiMe_3)(\eta^x\text{-toluene})_x][B(C_6F_5)_4]_2$ (17).....	170
Scheme 4.10: In-situ generation of $[(XII_2)Sc(C_6H_4NMe_2)][B(C_6F_5)_4]_2$ (18).....	176
Scheme 5.1: Synthesis of H[XAI]	187
Scheme 5.2: Synthesis of $[(XAI)Y(CH_2SiMe_3)_2]$	190
Scheme 5.3: In-situ generation of $[(XAI)Y(CH_2SiMe_3)(\eta^x\text{-toluene})][B(C_6F_5)_4]$ (21).....	194
Scheme 6.1: Buchwald-Hartwig Synthetic route for $^{tBu}XII_2$	207
Scheme 6.2: Staudinger reaction synthetic route to $^{tBu}XII_2$	208
Scheme 6.3: Buchwald-Hartwig synthetic route for an asymmetric NON-donor ligand.....	209
Scheme 6.4: Proposed reduction of complexes 14 and 15.....	210
Scheme 6.5: Reduction of $[(XII_2)Sc(CH_2SiMe_3)(\eta^x\text{-toluene})_x][B(C_6F_5)_4]$ (17) .	212
Scheme 6.6: Synthesis of $[(\{Ph_3PN\}_2XT)AlMe_2][B(C_6F_5)_4]$ (22a).....	215
Scheme 6.7: Synthesis of $[(\{Ph_3PN\}_2NAP)AlMe_2][B(C_6F_5)_4]$ (23a).....	220

List of Tables

Table 1.1: Calculated Ln ^{3+/Ln2+} Reduction Potentials of Yttrium and the Lanthanides (NHE: Normal Hydrogen Electrode) ⁸	3
Table 1.2: Ionic Radii (M ³⁺) of the Rare Earth Elements	4
Table 1.3: Ethylene Polymerization with [(NacNac ^{tBu,Dipp})Sc(CH ₃) ₂] and various cocatalysts ³⁹	38
Table 1.4: Ethylene Polymerization with [PhC(N{Diip}) ₂ M(CH ₂ SiMe ₃) ₂ (THF) _n] activated by [HNMe ₂ Ph][B(C ₆ F ₅) ₄] ⁵⁴	41
Table 1.5: Intramolecular hydroamination by [(NacNac ^{tBu,Dipp})Sc(CH ₃)][(CH ₃)B(C ₆ F ₅) ₃] – 5 % catalyst loading.	43
Table 1.6: Intramolecular hydroamination of 1-amino-2,2-dimethyl-4-pentene with neutral and cationic ‘b’ and ‘c’ in Figure 1.18, with and without activation by [HNMe ₂ Ph][B(C ₆ F ₅) ₄] ²⁴	45
Table 1.7: Intramolecular hydroamination by ‘d’ (Figure 1.21) activated by [CPh ₃][B(C ₆ F ₅) ₄] ⁵⁶	46
Table 1.8: Intramolecular hydroamination by ‘e’ (Figure 1.21) activated by [CPh ₃][B(C ₆ F ₅) ₄] ⁵⁶	47
Table 1.9: Intramolecular hydroamination of 1-amino-2,2-dimethyl-4-pentene with neutral and cationic ‘f’ in Figure 1.22 with and without activation by [HNMe ₂ Ph][B(C ₆ F ₅) ₄] ²⁴	50

Table 1.10: Intramolecular hydroamination of 1-amino-2,2-diphenyl-4-pentene catalysis by ‘g-Y’, ‘g-La’ (Figure 1.21) ²⁵ , [Y(CH ₂ SiMe ₃) ₃ (THF) ₂] or[La(CH ₂ Ph) ₃ THF) ₃] with and without activation by [HNMe ₂ Ph][B(C ₆ F ₅) ₄]. ...	51
Table 1.11: Intramolecular hydroamination of <i>N</i> -methylpent-4-en-1-amine catalysis by ‘g-Y’, ‘g-La’ (Figure 1.21) ²⁵ , [Y(CH ₂ SiMe ₃) ₃ (THF) ₂] or[La(CH ₂ Ph) ₃ THF) ₃] with and without activation by [HNMe ₂ Ph][B(C ₆ F ₅) ₄]. ²⁵	53
Table 1.12: Ethylene polymerization with [Ln(CH ₂ SiMe ₃) ₃ (THF) ₂] as the catalyst precursor ⁵⁷	58
Table 3.1: Intramolecular hydroamination catalyzed by 7 {2 mol % (Entry 1) or 5 mol % (Entries 2-4)} generated in situ from 6 and [CPh ₃][B(C ₆ F ₅) ₄] at 25 °C. Reactions were conducted in 0.8 mL C ₆ D ₅ Br.....	129
Table 4.1: Ethylene polymerization by 17	181
Table 5.1: Intramolecular hydroamination catalyzed by 21	204

List of Abbreviations

General

°	Degree(s)
°C	Celsius
K	Kelvin
η^n	Denotes the hapticity of the ligand, which is the coordination of a ligand to a metal center via delocalized charge distributions over a series of n atoms.
κ^n	Denotes the denticity of the ligand, which refers to the number of donor groups in a single ligand, n, that bind to the central metal in a coordination complex
μ_n	Refers to a ligand that is bridging between n atoms
Anal. Calcd.	Calculated (Elemental) Analysis
equiv.	Equivalent(s)
h	Hour(s)
Min	Minutes(s)
g	gram(s)
kg	Kilogram(s)
L	Litre(s)
mL	Mililitre(s)

General Cont.

mol	Mole(s)
-----	---------

mmol	Milimole(s)
M	Molarity (mol/L)
atm	Atmosphere(s)
ppm	Parts per million
THF	Tetrahydrofuran
Tol	Toluene
DME	1,2-Dimethoxyethane
MAO	Methylaluminoxane
Fac	Facial
Mer	Meridional
CIP	Contact Ion Pair
SSIP	Solvent-Separated Ion Pair
D	Deuterium
Ln	Lanthanide
An	Actinide
M	General Metal (Unless Otherwise Specified)

Substituents and Ligands

Ar	Aryl
Dipp	2,6-Diisopropylphenyl (2,6- <i>i</i> Pr ₂ -C ₆ H ₃)
Tripp	2,4,6-Triisopropylphenyl (2,4,6- <i>i</i> Pr ₃ -C ₆ H ₂)

Substituents and Ligands Cont.

Pipp	4-isopropylphenyl
Mes	Mesityl
Cp	Cyclopentadienyl
Cp*	Pentamethylcyclopentadienyl
Cyp	Cyclopentyl
Et	Ethyl
Me	Methyl
ⁱ Pr	Isopropyl
^t Bu	<i>tert</i> -Butyl
ⁿ Bu	<i>n</i> -Butyl
Ph	Phenyl
R	Alkyl or Aryl group (Unless otherwise specified)
DPEPhos	Bis{2-(diphenylphosphino)phenyl} ether
NacNac	β -diketiminato
Xanth	Xanthene
NAP	Naphthalene
(Ph ₃ PN ₂)XT	4,5-bis{ <i>N</i> -(triphenylphosphoranylidene)aniline}-2,7-di- <i>tert</i> -butyl-9,9-dimethylxanthene
(Ph ₃ PN ₂)NAP	1,8-bis{ <i>N</i> -(triphenylphosphoranylidene)aniline}-naphthalene

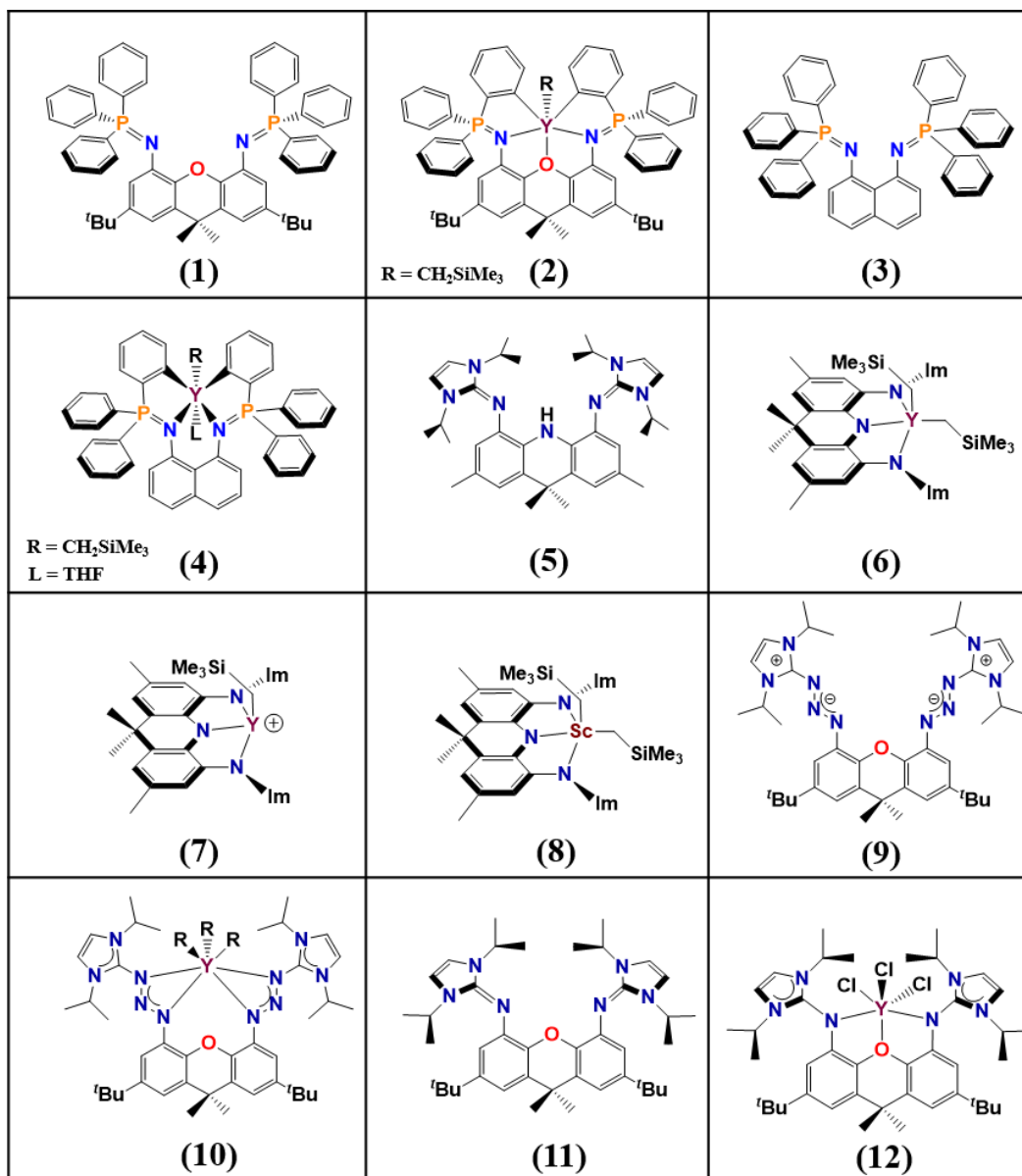
AII ₂	4,5- bis(1,3-diisopropylimidazolin-2-imine)-2,7,9,9-tetramethylacridanide
XII ₂	4,5-bis(1,3-diisopropylimidazolin-2-imine)-2,7-di- <i>tert</i> -butyl-9,9-dimethylxanthene
XIA ₂	4,5- bis{(1,3-diisopropylimidazolin-2-imine)triazene}-2,7-di- <i>tert</i> -butyl-9,9-dimethylxanthene
XAI ₂	4-(1,3-diisopropylimidazolin-2-imine)-5-(2,6-diisorpylanilido)-2,7-di- <i>tert</i> -butyl-9,9-dimethylxanthene

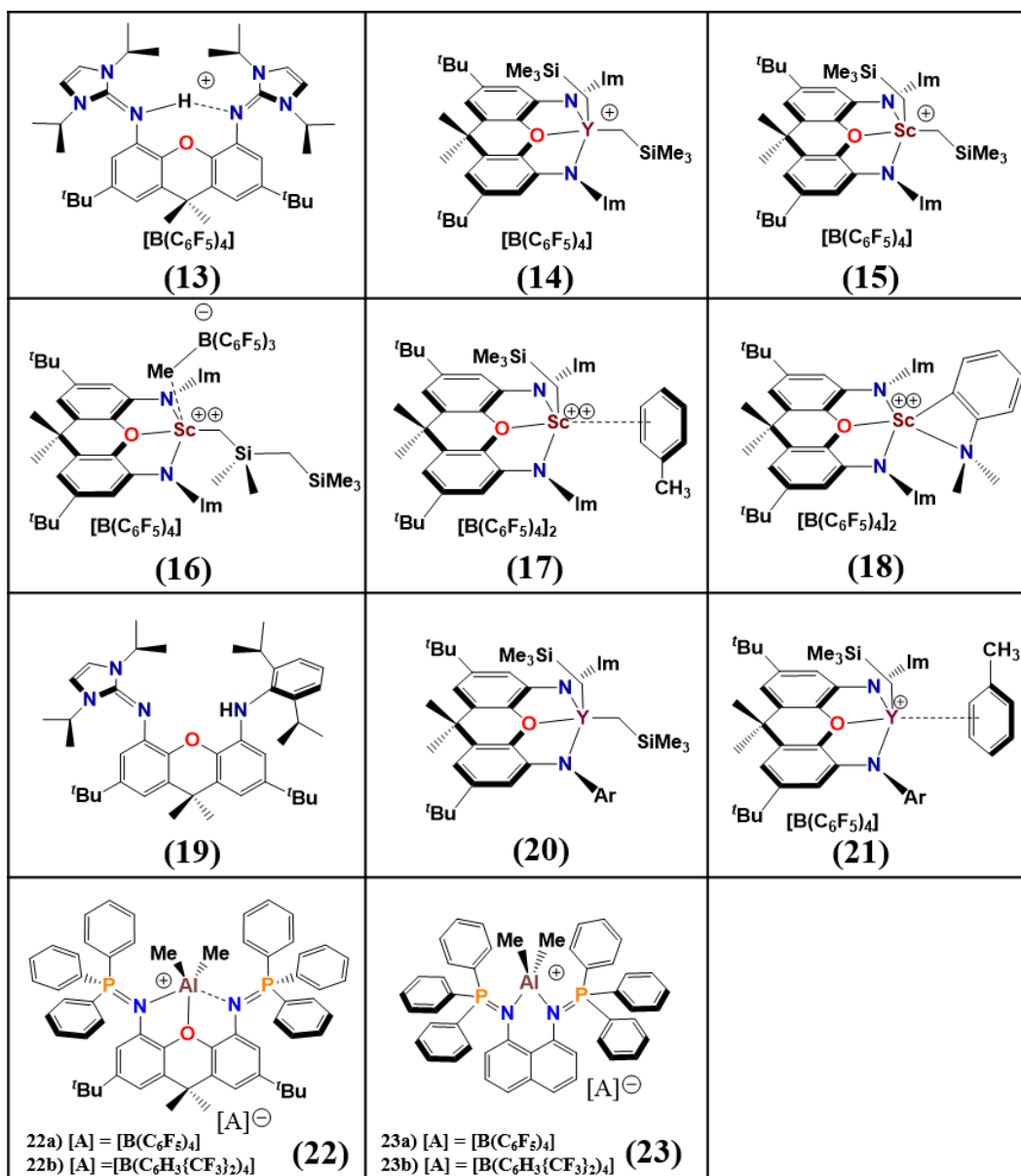
Spectroscopy and Analytical Techniques

Å	Angstrom
δ	NMR Chemical Shift ppm
Hz	Hertz
1D	One Dimesional
2D	Two Dimensional
NMR	Nuclear Magnetic Resonance
{ ¹ H}	Proton Decoupled
COSY	Correlation Spectroscopy
DEPT	Distortionless Enhancement by Polarization Transfer
HMBC	Heteronuclear Multiple Bond Correlation

HSQC	Heteronuclear Single Quantum Coherence
s	Singlet
d	Doublet
t	triplet
sept	Septet
appt.	apparent
PTFE	Polytetrafluoroethylene
m	Multiplet
br.	Broad
J	Symbol for coupling constant
${}^nJ_{X,Y}$	Coupling constant between nuclei X and Y; n = the number of bonds separating X and Y
GC-MS	Gas Chromatography-Mass Spectrometry
DSC	Differential Scanning Calorimetry
GPC	Gel Permeation Chromatography
N_t	Turnover Frequency
M_n	Number Average Molecular Weight
M_w	Weight Average Molecular Weight
PDi	Polydispersity Index

List of Compounds





NOTE: For compound 16 only one possible location of the alkyl group is shown. Alternatively, the MeB(C₆F₅)₃ contact ion pair could be in the plane of the ligand, with the alkyl group located above the plane of the ligand.

Chapter 1

Introduction

1.1 Introduction to Rare Earth Metal Chemistry

The rare-earth elements comprise the lanthanides (La-Yb), as well as the group 3 elements scandium, yttrium and lutetium. Yttrium was the first rare earth element discovered at the end of the 18th century by Finnish chemist and mineralogist Johan Gadolin.¹ By the end of the 19th century all but two of the remaining rare earth metals had been discovered. Lutetium and Promethium were discovered in 1907 and 1947 respectively.¹

Lanthanides together with actinides make up the f-block elements. There are seven degenerate f-orbitals that are mostly commonly used for the f-block elements [fz^3 , fxz^2 , fyz^2 , $fy(3x^2-y^2)$, $fx(x^2-3y^2)$, $fxyz$, $fz(x^2-y^2)$].² Alternatively, the cubic set (fx^3 , fz^3 , fy^3 , $fz(x^2-y^2)$, $fx(z^2-y^2)$, $fx(z^2-x^2)$, $fxyz$) is most suitable for describing octahedral, tetrahedral and cubic ligand fields.^{1,2} Unlike the 5f orbitals of early actinides, the 4f orbitals of lanthanides exhibit poor radial extension, which renders them incapable of effective covalent bonding. As a result, the bonding for rare earth elements is predominantly electrostatic/ionic in nature.

The most common oxidation state for the rare earth metals is 3+.¹ These Ln^{3+} ions are highly Lewis acidic and oxophilic, with highly polar bonds between the metal and anionic ligand, which renders them especially susceptible to protonolysis reactions. Thus, organometallic complexes of Ln^{3+} are highly sensitive to air and moisture and need to be handled under an inert atmosphere. Apart from the M^{3+} oxidation state, Cerium (Ce) and less frequently Praseodymium (Pr), and Terbium (Tb) have been known to exist in the strongly oxidizing Ln^{4+} oxidation state.¹ The Ln^{2+} oxidation state is also accessible. This oxidation state is strongly reducing, and was originally believed to be accessible only for Eu, Yb, Sm.³ The relative ease of accessibility of Eu^{2+} and Yb^{2+} can be attributed to the half filled shell ($4f^7$) for Eu^{2+} , and filled shell ($4f^{14}$) for Yb^{2+} .⁴ Sm^{2+} is also accessible, because it approaches a half filled shell ($4f^6$), although it is significantly more reducing than Eu^{2+} and Yb^{2+} .⁴ Subsequently, molecular complexes of the more highly reducing Tm^{2+} , Dy^{2+} , Nd^{2+} were reported through 1997-2001, although these complexes proved to be rather unstable especially in ethereal solvents such as Et_2O and THF.⁵ This led to the belief that the M^{2+} state would be inaccessible for the remaining trivalent rare earth metals, which have more negative redox potentials for the $\text{M}^{3+}/\text{M}^{2+}$ redox couple (Table 1.1).⁵ However, Lappert and coworkers then reported La(II) and Ce(II) complexes, which demonstrated that early lanthanides could also form Ln(II) complexes.⁶ Recent advances by Evans and coworkers have shown that with the appropriate coordination environment, molecular complexes of the M^{2+} oxidation are accessible for all rare-earth metals.^{5,7}

Table 1.1: Calculated $\text{Ln}^{3+}/\text{Ln}^{2+}$ Reduction Potentials of Yttrium and the Lanthanides (NHE: Normal Hydrogen Electrode) ⁸

Ln	Potential (V vs NHE)	Ln	Potential (V vs NHE)
Eu	- 0.35	Y	- 2.8
Yb	- 1.15	Pr	- 2.9
Sm	- 1.55	Ho	- 2.9
Tm	- 2.3	Er	- 3.1
Dy	- 2.5	La	- 3.1
Nd	- 2.6	Ce	- 3.2
Pm	- 2.7	Tb	- 3.7
Lu	- 2.7	Gd	- 3.9

The lanthanides show a relative decrease of their atomic and ionic radii across the series (Table 1.2).⁸ This trend has been coined “**lanthanide contraction**” and is the result of poor shielding by 4f electrons, resulting in an increase in the effective nuclear charge across the series.^{1, 2, 9} As a result of this trend, Y^{3+} has an ionic radius comparable to the heavier rare earth metals Ho^{3+} and Er^{3+} .

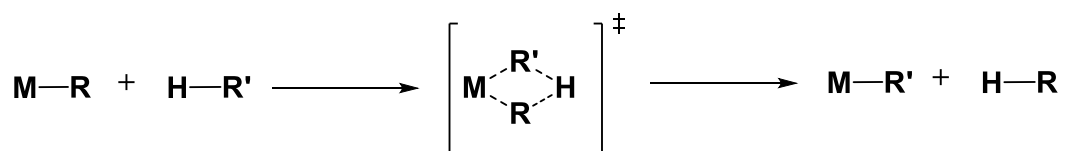
Table 1.2: Ionic Radii (M^{3+}) of the Rare Earth Elements

Element M^{3+}	Ionic radii (\AA)
Sc	0.745
Y	0.900
Lu	0.861
La	1.032
Ce	1.01
Pr	0.99
Nd	0.983
Pm	0.97
Sm	0.958
Eu	0.947
Gd	0.938
Tb	0.923
Dy	0.912
Ho	0.901
Er	0.890
Tm	0.880
Yb	0.868

The inability of Ln^{3+} metals to access an oxidation state two units higher, prevents monometallic complexes from undergoing oxidative addition.

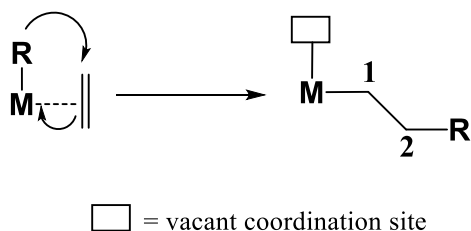
Consequently, the predominant reactions for rare earth organometallic complexes are ones in which the oxidation state is left unchanged, such as σ -bond metathesis and insertion.

The σ -bond metathesis mechanism was elucidated by Bercaw and coworkers in 1987. The mechanism describes a concerted process in which a new M-R bond is formed via a 4-centered transition state, while conserving the oxidation state of the metal (Scheme 1.1).¹⁰



Scheme 1.1: σ -Bond Metathesis Mechanism

Similarly, insertion reactions conserve the oxidation state of the metal throughout the process. For example, 1,2-insertion (Scheme 1.2) involves η^2 -coordination of an unsaturated substrate followed by insertion into the M-R bond.⁹ This process is crucial for catalytic reactions such as olefin polymerization and alkene hydroamination that will be discussed in more detail in Sections 1.2 and 1.3.



Scheme 1.2: 1,2-Insertion Mechanism

1.2 Introduction to Olefin Polymerization

The modern age has seen a high dependence on plastics. Millions of tonnes of plastics are produced each year, with approximately 50% of this production being either polyethylene or polypropylene. In 1894, Hans von Pechmann discovered hydrocarbon based polymers through heating a solution of diazomethane in diethyl ether.¹¹ Forty years later, ethylene polymerization was commercialized using a high pressure radical polymerization mechanism to yield low density polyethylene (LDPE). Karl Ziegler and Giulio Natta then ushered in the epoch of Ziegler-Natta based catalysts, which were able to conduct polymerization at milder temperatures and pressures.¹² These heterogenous catalysts operated using a coordination-insertion mechanism, which resulted in more linear polymers with much more controlled stereoregularity for monomers such as propylene.¹³ Ziegler-Natta based catalysts were then commercialized to produce high density polyethylene (HDPE). The next 60 years has seen several generations of Ziegler Natta catalysts that target improved control over its

predecessor in terms of molecular weight, polymer branching, stereoregularity and catalytic efficiency.¹³ However, these catalysts were still plagued by a broad molecular weight distribution (high polydispersity), which was rectified by the advent of single-site molecular catalysts.¹³

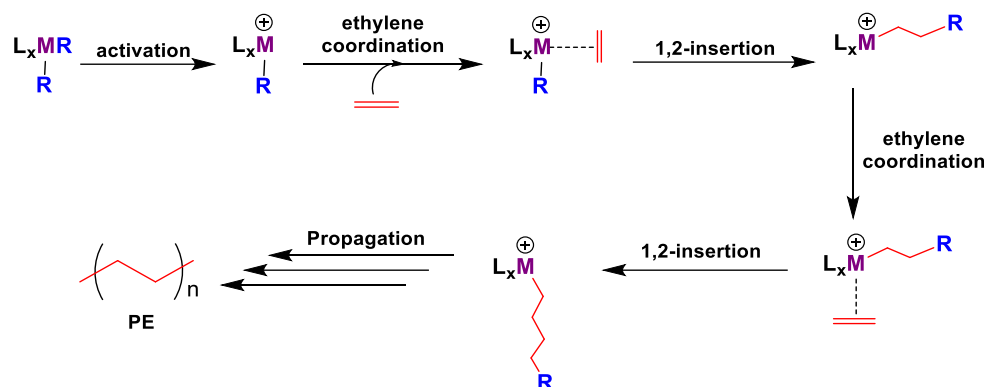
Single site molecular catalysts are coordinated by a supporting ligand that has a significant influence on the polymer characteristics (molecular weight, polydispersity, stereochemistry) in addition to influencing the thermal stability and the catalytic efficiency of the active catalyst.¹⁴ Therefore, significant research has been aimed at modifying the steric and electronic properties of these supporting ligands.¹⁴

Catalysts can be evaluated by comparing their reactivity for polymerization (in kg of polyethylene produced, per mol of catalyst, per hour, per atmosphere of ethylene pressure) as well as characteristics of the generated polymers, which include; density, number average molecular weight (M_n) and weight average molecular weight (M_w).¹⁵ The density of a polymer can elucidate the level of branching of a generated polymer. For example, high density polyethylene is the result of minimal branching, whereas low density polyethene is yielded from high levels of branching. M_n describes the statistical average of all the polymer chains generated. Conversely, M_w describes the weighted average of the polymer chains.¹⁵ The polydispersity index (PDI), which is calculated by dividing M_w by M_n , describes the molecular weight distribution of the polymer chains.¹⁵ PDI is useful

in indicating the stability of the active catalyst, as well as whether one or more active catalysts are present. A truly single site active catalyst that is stable for the lifetime of the catalysis would result in polymers with a narrow PDI, whereas a broad PDI value would indicate either decomposition of the catalyst, or several active sites/catalysts in-situ.

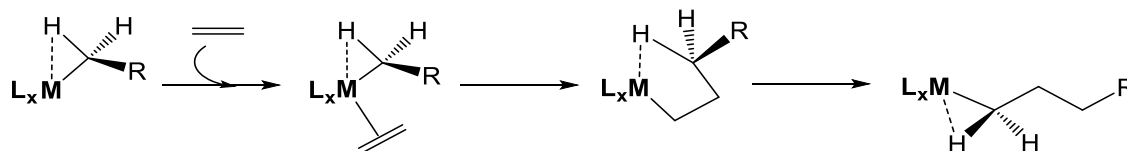
1.2.1 Introduction to Ethylene Polymerization by Rare-Earth Metal Catalysts

The vast majority of ethylene polymerization catalysts are cationic and follow the Cossee-Arman mechanism, as shown in Scheme 1.3.¹⁶ The cationic alkyl catalyst can be generated using the routes discussed later in this thesis (Section 1.5.3). The first step of the mechanism is coordination of the alkene to the metal center. A highly electrophilic metal center along with a vacant coordination site helps promote the coordination of the alkene. The second step in the mechanism is 1,2-insertion, involving an alkyl ligand that is cis to the coordinated alkene, which generates a new vacant coordination site. A second molecule of ethylene can now coordinate the new vacant site, and the cycle repeats numerous times to propagate the polymer until the chain is terminated.



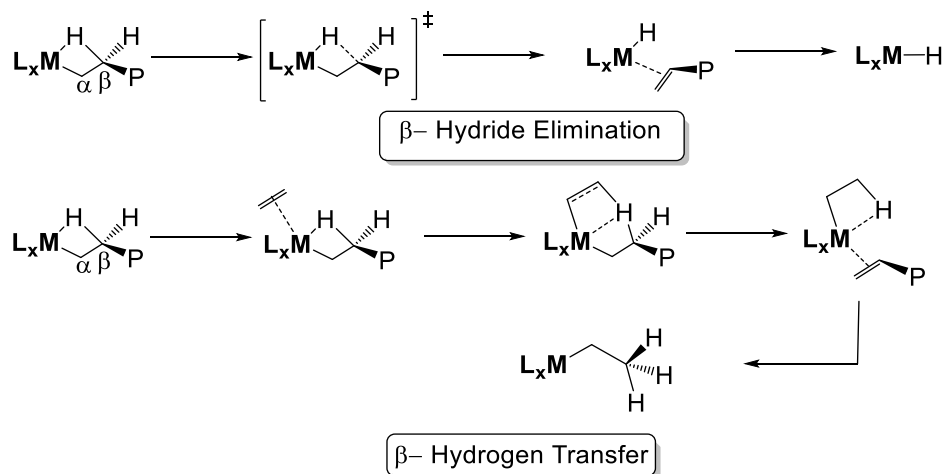
Scheme 1.3: The Cossee-Arlman Mechanism for Olefin Polymerization

In 1983, Brookhart and Green published a modified mechanism for olefin polymerization involving an α -agostic interaction, which assists in stabilizing the metal center, and in facilitating 1,2-insertion as seen in Scheme 1.4.¹⁷



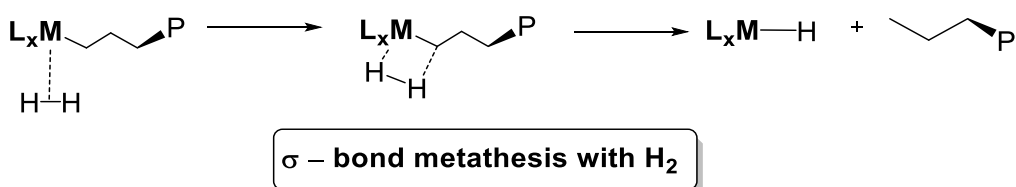
Scheme 1.4: The Brookhart-Green Mechanism for Olefin Polymerization

Termination can occur via addition of an acid to protonate the growing alkyl chain. Alternatively, β -Hydride Elimination and the more common β -Hydrogen Transfer routes can lead to chain termination (Scheme 1.5).¹⁸ When these mechanisms are dominant, the resulting polymers show a characteristic broad polydispersity.



Scheme 1.5: The β -Hydride Elimination and a β -Hydrogen Transfer Mechanisms for Polymerization Chain Termination

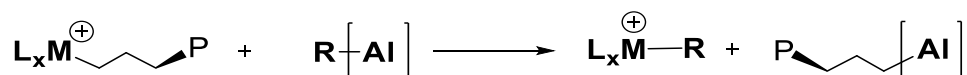
$\text{H}_{2(\text{g})}$ can terminate polymer chain growth via σ -bond metathesis (Scheme 1.6).¹⁹ Therefore, small amounts of $\text{H}_{2(\text{g})}$ are often added to the ethylene feedstock as a way to control the molecular weight of the resulting polyethylene.



Scheme 1.6: Chain Termination via σ -bond metathesis with $\text{H}_{2(\text{g})}$

Aluminium alkyl scavengers (e.g. AlMe_3 , MAO, Al^iBu_3) are often used in a large excess in olefin polymerization reactions, especially in industrial settings, in order to prevent catalyst deactivation by moisture or any other adventitious impurities. However, chain transfer between the catalyst and the aluminum

scavenger (Scheme 1.7) can occur, leading to lower polymer weights and higher polydispersity.²⁰



Scheme 1.7: Chain transfer from cationic rare earth catalyst to an aluminium alkyl scavenger

1.3 Introduction to Intramolecular Hydroamination

Hydroamination involves the reaction of an N–H bond (amine) and an unsaturated C=C bond (alkyne, alkene) to form C–N and C–H bonds. This can either be an intra or an intermolecular process. Catalytic intramolecular hydroamination provides an atom economic route to form N-heterocycles and hence, is a fervently studied area of chemistry. The complex N-heterocycles that can be produced have numerous applications, such as in the pharmaceutical chemistry.²¹

Several highly efficient neutral rare-earth intramolecular hydroamination catalysts have been reported in literature, and selected examples are shown in Figure 1.1.^{21, 22, 23} The M–C σ bonds of rare earth metals are highly reactive, which has rendered rare earth complexes highly potent for hydroamination catalysis.

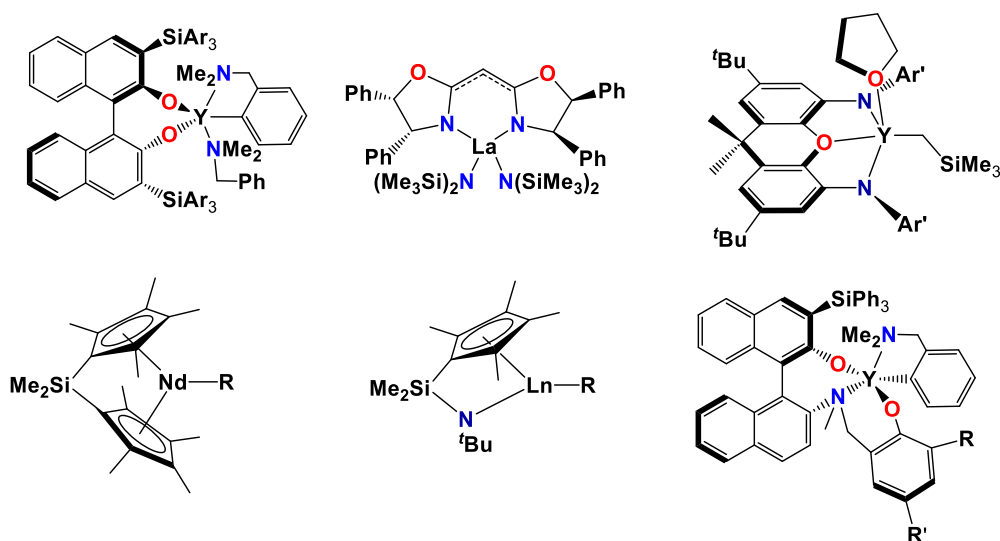


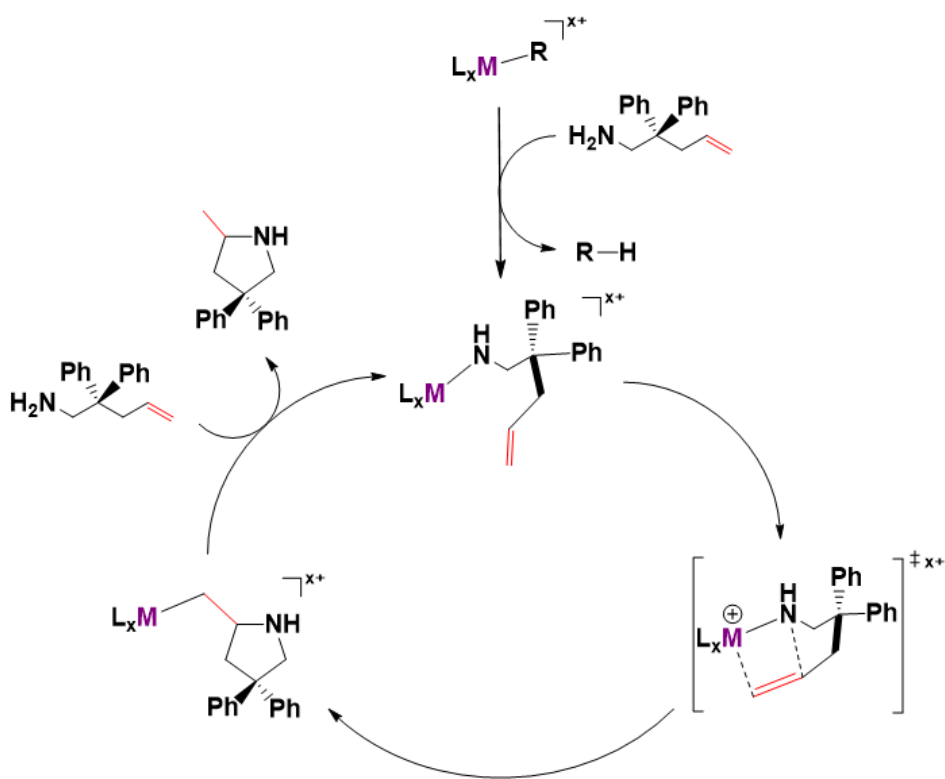
Figure 1.1: Literature examples of rare earth metal intramolecular hydroamination catalysts

Unlike neutral hydroamination catalysts, cationic rare-earth intramolecular hydroamination catalysts are scarcely reported.²⁴⁻²⁷ Section 1.5.5 of this thesis includes a comprehensive discussion of such catalysts. However, it does not include catalysis by neutral group 4, actinide, alkali metal, alkaline earth metal or late transition metal catalysts, as this is not directly relevant to the research in this thesis.

1.3.1 Intramolecular Hydroamination Mechanism for Rare Earth Metal Complexes

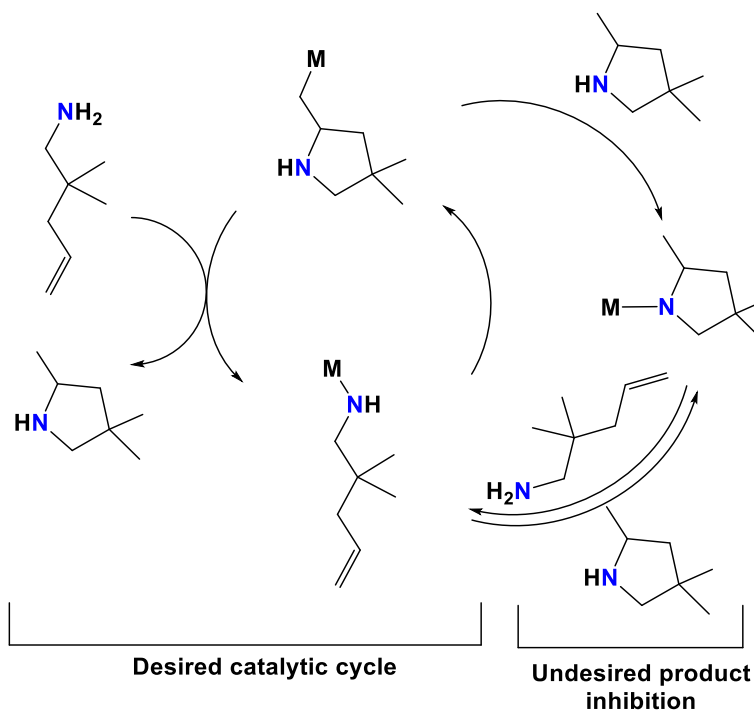
The mechanism for intramolecular hydroamination is the same for both neutral and cationic rare earth mediated catalysis (Scheme 1.8).^{21, 26} The first step

involves protonolysis of the metal-alkyl group (or a metal-amido group if the pre-catalyst is an amido rather than an alkyl complex) by the amine of the substrate. This is followed by alkene coordination to the cationic center, which is subsequently followed by 1,2-insertion of the alkene into the M–N bond resulting in cyclization. A second substrate molecule then protonates off the alkyl group to release the heterocyclic product and thereby regenerate the active catalyst.^{21, 26}



Scheme 1.8: Intramolecular Hydroamination Mechanism for Neutral or Cationic Rare Earth Complexes ($x = 0, 1$)

Generally, intramolecular hydroamination is zero order in respect to substrate concentration, which suggests that the rate limiting step is the insertion of the olefin into the metal-amide bond. However, with increasing conversion, deviation from this behaviour (a shift towards apparent first order dependence is sometimes observed), which suggests either product inhibition (Scheme 1.9) or that protonolysis of the cyclized product becomes the rate limiting step at higher conversions (lower concentration of substrate).^{21, 24} Alternatively, catalysts can demonstrate first order dependence on substrate concentration for the entirety of the conversion, which suggests that protonolysis of the cyclized product by the substrate is the rate limiting step. Finally, sterically unencumbered catalysts can in some cases deviate from zero-order substrate dependence due to substrate inhibition, in which case, the rate of aminoalkene cyclization is observed to accelerate as the reaction proceeds.²¹



Scheme 1.9: Reversible Reaction of Cyclized Product and Substrate²⁴

1.3.2 Intramolecular Hydroamination – Substrate Reactivity

Substrates that are utilized in intramolecular hydroamination contain an unsaturated C—C bond, as well as an amino group. The difficulty in the cyclization of these substrates is dependent on the additional features of the substrate. Figure 1.2 shows selected substrate examples that illustrate the guidelines that effect cyclization.

The Thorpe-Ingold effect/Gem-Disubstituent effect, steric effects and Baldwin's guidelines for ring formation best describe the substrate features that

effect ease of cyclization (Figure 1.2).²⁸ Specifically, the Thorpe-Ingold Effect/Gem-Disubstituent effect describes the influence that substituents elicit on the ease of cyclization. Generally, geminal groups help to promote cyclization by decreasing conformational freedom, which allows the alkene to adopt the suitable orientation required for cyclization. Increased steric bulk of the geminal substituents also helps promote cyclization. This effect can be attributed to the increased repulsion between large substituents, which results in the alkene being drawn closer to the reactive M–N bond thereby promoting cyclization.^{28, 29} The presence of the more bulky phenyl substituents on 1-amino-2,2-diphenyl-4-pentene (**A**) results in an increase in reactivity towards cyclization over the less bulky 1-amino-2,2-dimethyl-4-pentene (**B**), which in turn shows higher reactivity than 1-amino-4-pentene (**C**). Although highly bulky geminal substituents, primarily on the β -position of the aminoalkene substrate help to promote cyclization, substituents on the alkene impede cyclization by hindering the formation of the transition state for C–N bond formation.^{21, 30} This trend is illustrated in Figure 1.2, in which 1-amino-2,2-diphenyl-4-pentene (**A**) is much more reactive towards cyclization, than 1-amino-2,2-diphenyl-4-methyl-4-pentene (**D**), which in turn is more reactive than 1-amino-2,2-diphenyl-4-methyl-4-hexene (**E**). Finally, the Baldwin guideline for cyclization describes the ease of cyclization to form five membered rings over 6 membered rings.³¹ This is evidenced in the ease of cyclization of 1-amino-2,2-diphenyl-4-pentene (**A**) over 1-amino-2,2-diphenyl-5-hexene (**F**), which generally requires higher catalyst loading and higher temperatures for cyclization.

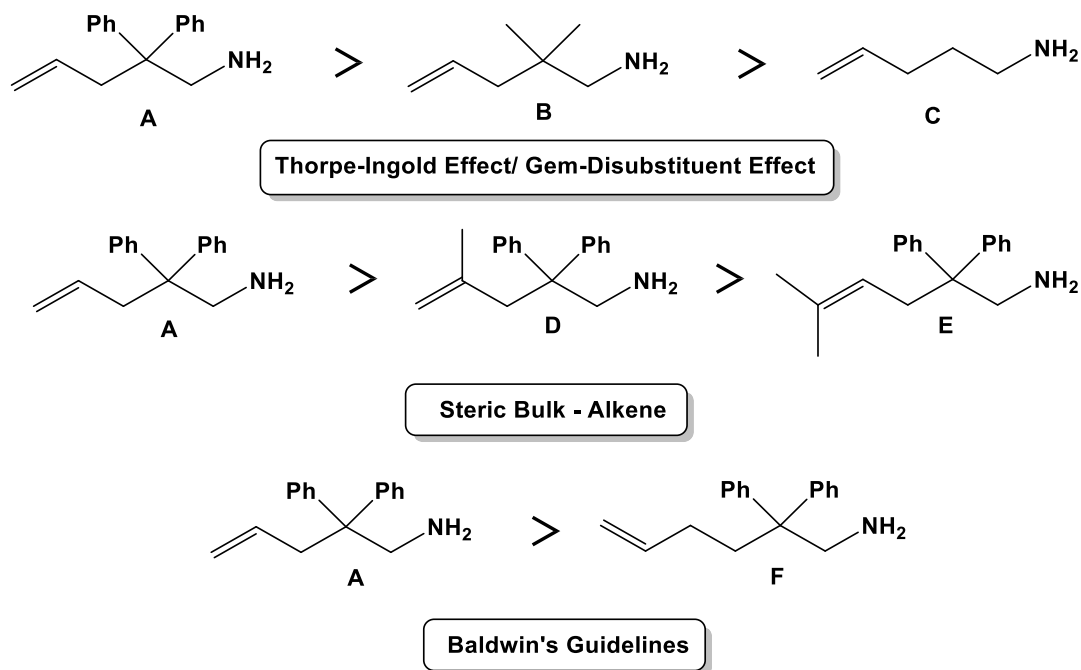


Figure 1.2: Selected intramolecular hydroamination substrates cyclized by rare earth catalysts. Substrates are arranged in order of decreasing reactivity towards cyclization.

1.4 Ligand Attachment Strategies for the Synthesis of Rare Earth Complexes

1.4.1 Anionic Ligand Attachment Strategies

The attachment of an anionic ancillary ligand to a metal center can be achieved utilizing three commonly employed strategies; alkane elimination, amine elimination and salt metathesis (Scheme 1.10 (a)). Alkane elimination allows direct access to metal alkyl complexes via the reaction of protio ligand with a metal alkyl precursor. This results in the elimination of an alkane byproduct, which is generally

volatile, thereby allowing straightforward purification of the target complex. $[\text{M}(\text{CH}_2\text{SiMe}_3)_3(\text{THF})_2]$ is the most commonly utilized group 3 metal alkyl precursor and is heavily utilized in this thesis.³² $[\text{M}(\text{CH}_2\text{Ph})_3(\text{THF})_3]$ is another commonly used benzyl precursor, and has been reported for all the rare earth elements with the exception of Pm^{3+} , Tm^{3+} and Eu^{3+} .³² The lack of a variety of thermally stable rare earth trialkyl precursors, limits the ability to access a range of alkyl complexes. In addition, the instability of the aforementioned precursors at elevated temperatures prevents access to complexes via alkane elimination when heating is required.

$[\text{M}\{(\mu\text{-Me})_2\text{AlMe}_2\}_3]$, has been reported for all rare earth elements with the exception of Sc^{3+} and Pm^{3+} , and has been utilized to synthesize rare earth tetramethylaluminate complexes by reaction with a protio ligand (Figure 1.3).^{32, 33} The reaction is related to alkane elimination, where the AlMe_4 ligands serve as a masked source of methyl ligands. However, such reactions often generate undesired byproducts due to the reaction of the protio ligand with the AlMe_3 byproduct to form an aluminum complex.

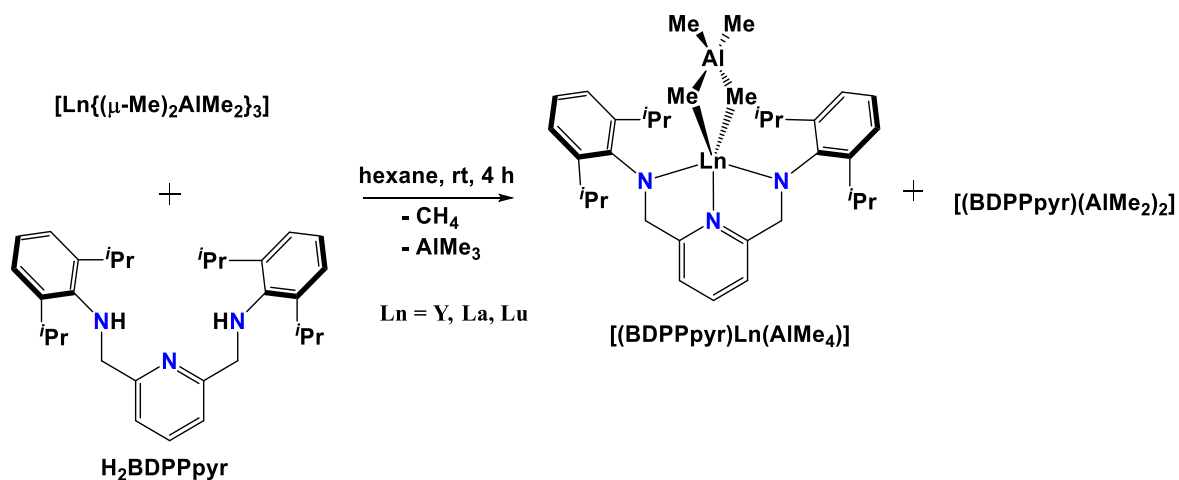


Figure 1.3: Literature example - Synthesis of rare earth tetramethylaluminate complexes by reaction with $[\text{Ln}\{(\mu\text{-Me})_2\text{AlMe}_2\}_3]$ ³²

Anwander and coworkers demonstrated a reversible, donor (THF, Et₂O) induced, tetramethylaluminate cleavage of the $[\text{M}\{(\mu\text{-Me})_2\text{AlMe}_2\}_3]$ (M= Y, Lu) in hexane, to yield polymeric $[\text{M}(\text{CH}_3)_3]_n$ as a white precipitate (Figure 1.4).^{33, 34} Addition of 3 equivalences of AlMe₃ to $[\text{M}(\text{CH}_3)_3]_n$ led to the quantitative reformation of $[\text{M}\{(\mu\text{-Me})_2\text{AlMe}_2\}_3]$. Although both $[\text{Y}(\text{CH}_3)_3]_n$ and $[\text{Lu}(\text{CH}_3)_3]_n$ are air sensitive, the latter has to be handled with additional caution, since it spontaneously detonates in the presence of moisture. $[\text{M}(\text{CH}_3)_3]_n$ have been utilized in literature for isolation of rare earth methyl complexes (Figure 1.4).³²

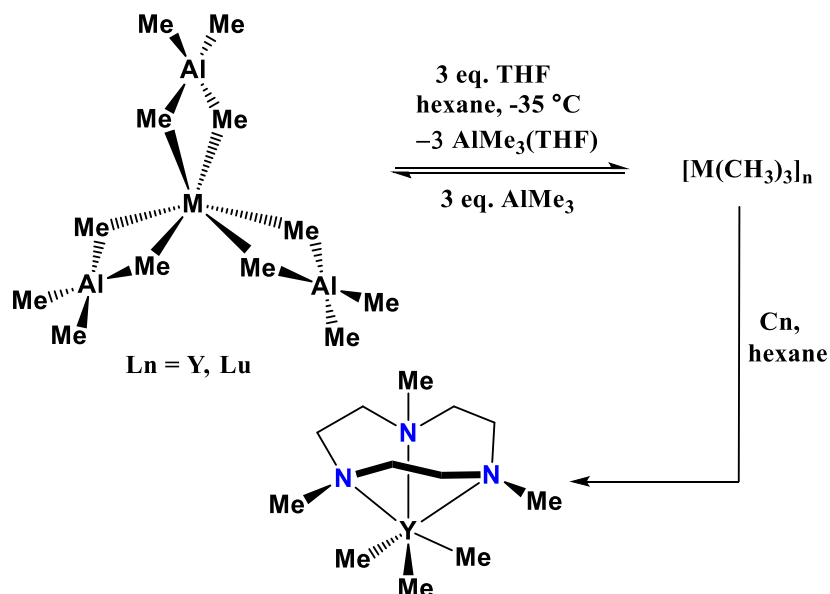
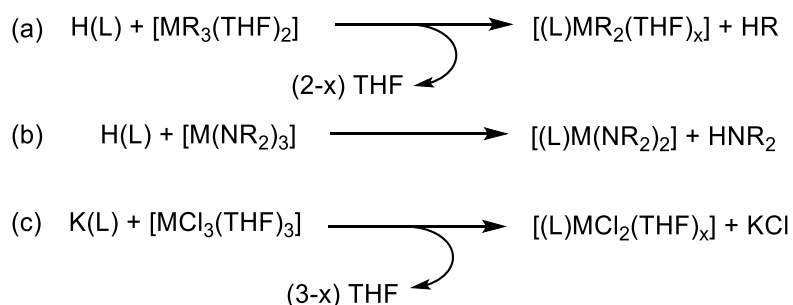


Figure 1.4: Literature example - Synthesis of $[M(\text{CH}_3)_3]_n$ and subsequent Synthesis of $[(\text{C}_n)\text{Y}(\text{CH}_3)_3]$ $\text{C}_n = 1,4,7$ - trimethyl-1,4,7-triazacyclononane

Amine elimination (Scheme 1.10 (b)) is also commonly employed to access metal alkyl chemistry by initially synthesizing a metal amido complex. Unlike alkane elimination, this route requires multiple steps to access potential metal alkyl complexes, and therefore can be more synthetically challenging thereby often resulting in lower yields. This route involves the use of a metal amido precursor, in combination with a pro-ligand, resulting in the elimination of an amine by-product. Metal amido precursors are generally more stable than their analogous metal alkyl precursors, which allows heating to access target complexes. The resulting metal amido complex can then be converted to the corresponding methyl

complex by reaction with AlMe_3 .³⁵ Alternatively, the metal amido complex can be reacted with Me_3SiCl to afford the metal chloride complex.³⁶

The final commonly employed synthetic route for attachment of a ligand to a metal is salt metathesis (Scheme 1.10 (c)). This involves the use of a metal halide precursor in combination with an alkali metal salt of the ligand, resulting in the elimination of an alkali metal halide by-product. The group 3 metal halides tend to be highly insoluble and are thus often utilized in reactions as their THF adducts: $\text{YCl}_3(\text{THF})_{3.5}$ and $\text{ScCl}_3(\text{THF})_3$, which are comparably much more soluble. The resulting metal halide complex can be converted to a range of alkyl complexes utilizing various alkylating agents ($\text{LiCH}_2\text{SiMe}_3$, LiCH_2Ph , MeLi etc.). This allows for greater variability of the alkyl groups that is not straightforward with the aforementioned alkane elimination route. However, this route can be plagued by difficulty in removing the alkyl halide byproduct generated from both the initial salt metathesis reaction, as well as potentially from the alkylation reaction.



Scheme 1.10: Strategies for anionic ligand attachment: a) alkane elimination, b) amine elimination, c) salt metathesis

1.4.2 Neutral Ligand Attachment Strategies

Attachment of a neutral ancillary ligand can often be carried out utilizing either the THF adduct of a metal halide or a metal alkyl precursor, as well as metal amido precursors. In reactions with rare earth metal halide (e.g. $\text{YCl}_3(\text{THF})_{3.5}$, $\text{ScCl}_3(\text{THF})_3$) or alkyl precursors, coordination is likely to result in the elimination of one or more THF molecules. Metal halide complexes can be subsequently converted to alkyl complexes via an alkylating agent (e.g. MeLi , $\text{LiCH}_2\text{SiMe}_3$). In the case of highly rigid pincer ligands, as seen in this thesis, the metal tris(alkyl) unit can prove to be too sterically bulky to fit within the binding pocket of the ligand.

1.5 Introduction to Rare Earth Alkyl Complexes

Rare earth complexes have seen dramatic interest in the last few decades, which can be attributed to the immense potential they demonstrate for catalysis, particularly cationic alkyl derivatives, which have proven to be highly active for olefin polymerization.³⁷⁻³⁹

Rare earth alkyl complexes are highly reactive and the literature is littered with examples of C–H bond activation of the supporting ligand (cyclometallation) resulting in elimination of an alkyl group to form a complex no longer viable as an olefin polymerization catalyst or pre-catalyst.^{37, 40} This section will provide a brief

introduction to neutral rare earth alkyl complexes, with a primary focus on complexes that employ non-cyclopentadienyl based ligands that have demonstrated cyclometallation resistance. Synthetic routes to cationic rare earth alkyl complexes will be described. Literature examples of rare earth cationic alkyl complexes will be discussed with a primary focus on structurally characterized non-coordinatively saturated complexes. A comprehensive review of the scarcely reported dicationic rare earth alkyl complexes will also be provided.

1.5.1 Neutral Cyclopentadienyl Based Rare-Earth Alkyl Complexes

The large size and high electropositivity of the rare earth metals present significant challenges in isolating thermally robust poly(alkyl) complexes. Nevertheless, monoanionic ancillary ligands that contain adequate steric bulk, and electron donation have been utilized to isolate bis(alkyl) complexes of rare-earth metals (LMR_2). Interest in such complexes spawn from the success of metallocene based group 4 olefin polymerization pre-catalysts (Cp^*_2MR_2). The neutral dialkyl complexes of group 4 transition metals, or rare earth elements provide a synthetic route to access cationic monoalkyl complexes for olefin polymerization catalysis. The first synthesized and structurally characterized base free dialkyl rare earth complex, was reported by Schaverien and co-workers in 1989, as seen in Figure 1.5.⁴¹

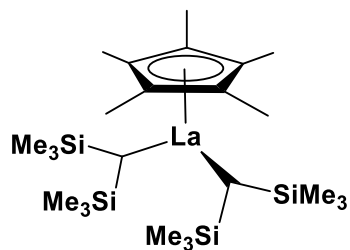


Figure 1.5: First reported base free bis(alkyl) rare-earth complex

Following Schaverien and co-workers' initial work, a number of cyclopentadienyl based rare-earth bis(alkyl) complexes were reported as seen in Figure 1.6.³⁷

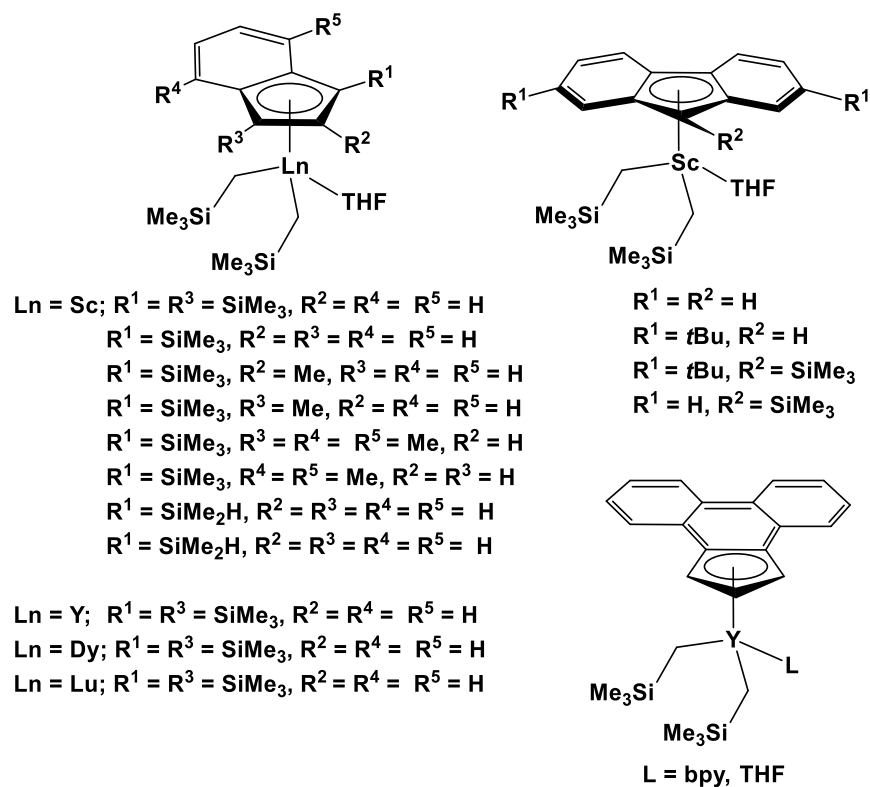


Figure 1.6: Selected examples of bis(alkyl) rare earth complexes of cyclopentadienyl based ligands

The next generation of ligands saw cyclopentadienyl based ligands with various pendant donors such as imines, imidazol-2-imines and phosphininimines (Figure 1.7).³⁷ This allowed for greater variation in the steric and electronic properties of the ligand and the resulting rare-earth dialkyl complexes, and provided sufficient steric bulk to avoid donor solvent (e.g. THF) coordination.

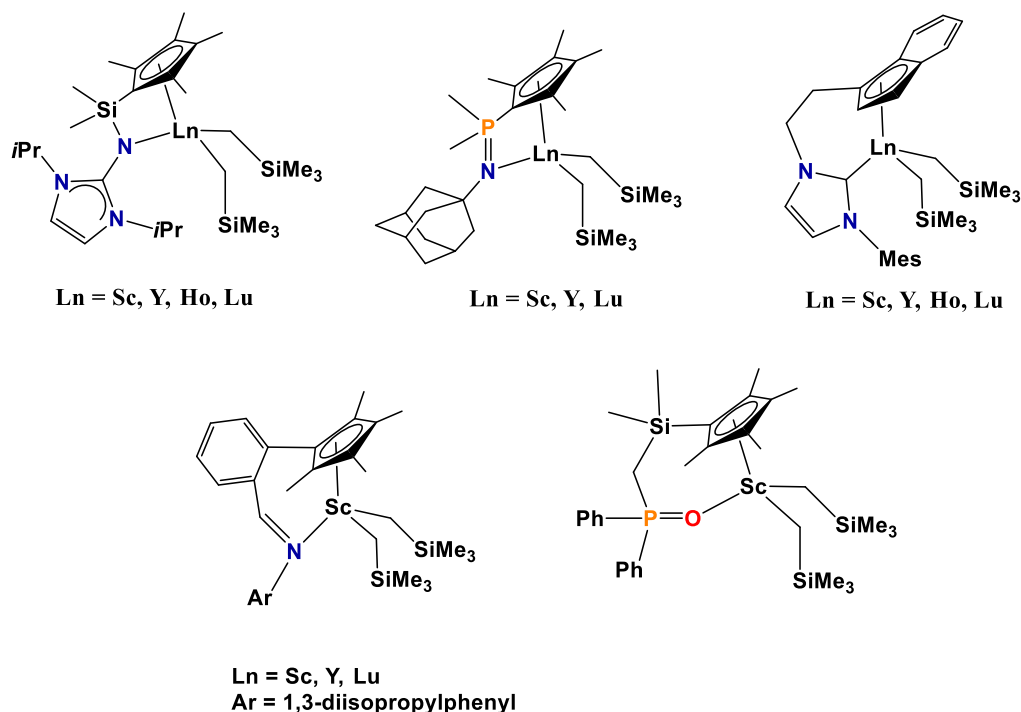


Figure 1.7: Selected examples of bis(alkyl) rare earth complexes of cyclopentadienyl based ligands with a pendant neutral donor

1.5.2 Neutral Non-Cyclopentadienyl Based Rare-Earth Alkyl Complexes

Non-cyclopentadienyl ligands have moved to the forefront of rare earth alkyl chemistry, as a versatile alternative to cyclopentadienyl ligands. Dialkyl rare-earth complexes predominantly employ multidentate ancillary ligands as opposed to monodentate ligands (Figure 1.8) and have proven successful as precursors to cationic monoalkyl complexes.^{37, 38}

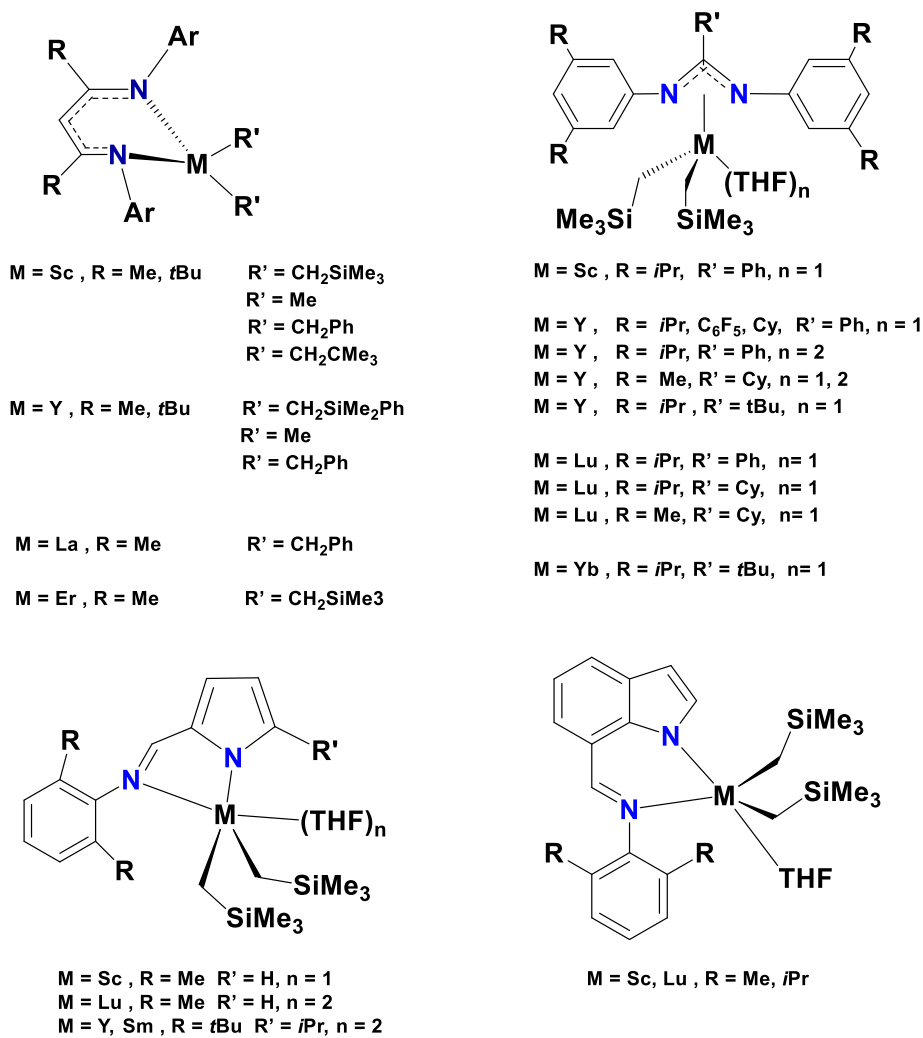


Figure 1.8: Selected examples of bis(alkyl) rare earth complexes of non-cyclopentadienyl based ligands

Although seldom used in comparison to monoanionic ligands, neutral multidentate ligands have also been successfully utilized (Figure 1.9).^{25, 42, 43} These ligands allow for access to neutral trialkyl complexes that can be utilized to access the more scarcely reported dicationic monoalkyl complexes (*vide infra*).

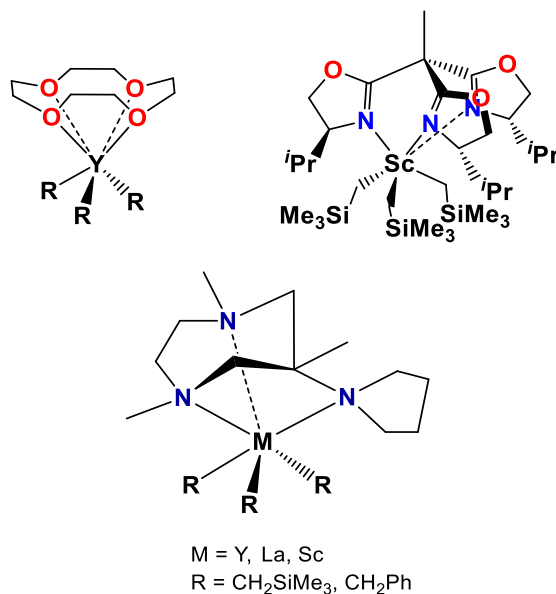


Figure 1.9: Selected examples of tris(alkyl) rare earth complexes utilizing neutral multidentate ligands

1.5.3 Synthetic Routes to Cationic Alkyl Complexes

Interest in cationic rare earth alkyl complexes stems from the high potential these complexes have demonstrated for catalytic processes such as olefin polymerization and intramolecular hydroamination. These complexes are generally accessed by reacting a neutral poly(alkyl) rare-earth complex with a co-reactant that is either a Brønsted acid or a Lewis Acid.³⁸ These co-reactants remove an alkyl anion thereby generating a highly electrophilic, coordinatively unsaturated metal cation, that is primed for substrate binding and catalysis.

One of the most utilized co-reactants is tris(pentafluorophenyl)borane. This highly Lewis acidic co-reactant abstracts an anionic alkyl group (e.g. methyl group)

to generate a coordinatively unsaturated cationic metal center paired with an anionic alkyl borate (Scheme 1.11). Generally, the resulting anionic alkyl borate forms a contact ion pair with the metal via the alkyl with a long M-C bond distance, indicating that the alkyl is strongly associated with the boron as opposed to the metal center.^{44, 45} Abstraction of a trimethylsilylmethyl (CH_2SiMe_3) anion using tris(pentafluorophenyl)borane can similarly lead to the formation of a contact ion pair via the silyl methyl substituents. Alternatively, abstraction of a methyl anion from the silicon center can occur with concomitant migration of the remaining alkyl group to the positively charged silicon in which a new $\text{CH}_2\text{SiMe}_2\text{CH}_2\text{SiMe}_3$ alkyl group is formed, accompanied by $\text{MeB}(\text{C}_6\text{F}_5)_3$ anion formation, forming a contact ion pair. Literature examples of this rearrangement are discussed in Section 1.5.4.^{46, 47} Abstraction of a benzyl (CH_2Ph) group using tris(pentafluorophenyl)borane often results in the generated anionic benzyl borate forming a contact ion pair via η^6 -coordination of the phenyl ring.⁴⁸ The aforementioned contact ion pairs help to stabilize the resulting cationic metal complex, which has in some cases allowed for the isolation of rare earth alkyl cations. However, the contact ion pair can serve to compete with substrate binding to the generated vacant site, which can in turn suppress the catalytic activity of the resulting complex.

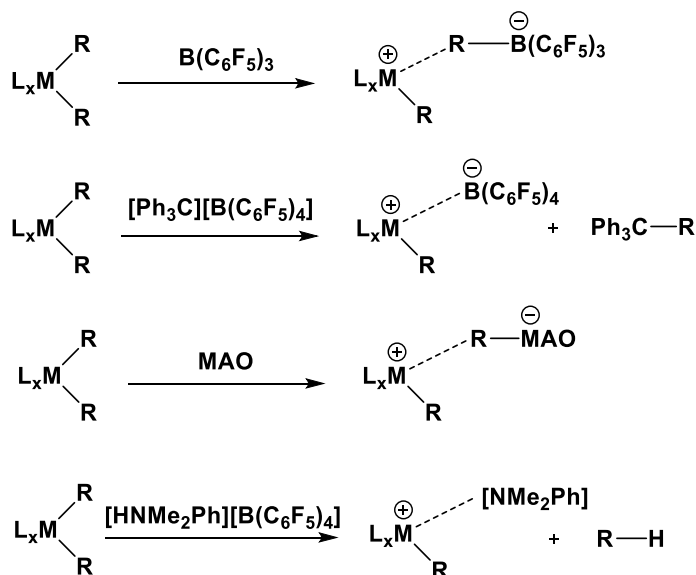
Another commonly utilized co-reactant is trityl tetrakis(pentafluorophenyl)borate, which is a highly Lewis acidic, carbocationic species (Scheme 1.11). In the resulting alkyl cation, evidence of weak interactions between the fluorine substituents on the tetrakis(pentafluorophenyl)borate anion

and the metal center is seen in certain literature examples.⁴⁹ However, the interaction is much weaker than with an alkyl tris(pentafluorophenyl)borate, and as a result, the cationic complexes are significantly more reactive, thermally unstable, and poorly soluble in hydrocarbon solvents.

Methylaluminoxane (MAO) is another commonly utilized alkyl abstraction agent in olefin polymerization catalysis (Scheme 1.11). MAO is generated from the partial hydrolysis of AlMe_3 , and has a non-uniform structure with the general formula $[\text{MeAl}(\mu\text{-O})]_n$.⁵⁰ Unlike the previously mentioned Lewis acidic co-reactants, MAO can be utilized not only with metal alkyls, but can also be utilized with metal chlorides to generate cationic metal alkyl complexes. This is due to the fact that MAO can act as a methylating agent as well as an alkyl abstraction agent. Usually, a 1000-fold excess of MAO is required when utilized as the co-reactant. Although high activity for olefin polymerization is achieved with MAO as the co-reactant, cations generated using MAO are not readily crystallized and isolated.^{9, 44} Hence, MAO is often used as a co-reactant for olefin polymerization studies, but not for the synthesis and isolation of potential cationic rare earth alkyl catalysts.

Apart from Lewis acidic co-reactants, the Brønsted acid co-reactant dimethylanilinium tetrakis(pentafluorophenyl)borate has also been successfully utilized to generate cationic metal complexes. This co-reactant is a source of an acidic proton, which can protonate off an alkyl from a metal alkyl complex, thereby

generating a coordinatively unsaturated cationic metal center, and N,N-dimethylaniline as a by-product (Scheme 1.11).



Scheme 1.11: Synthetic routes to cationic alkyl complexes

Generally, the resulting Me_2NPh by product does not coordinate to the cationic metal center. However, there are group 3 cationic complexes reported in literature that demonstrate Me_2NPh coordination via the amine or η^6 – coordination of the arene. Piers and coworkers reported the reaction of $[(\text{NacNac}^{\text{Me},3,5\text{-tripp-}C_6H_3})\text{Sc}(\text{CH}_2\text{SiMe}_3)_2]$ with $[\text{HNMe}_2\text{Ph}][\text{B}(\text{C}_6\text{F}_5)_4]$, which resulted in a cationic alkyl complex coordinated by Me_2NPh via the amine (Figure 1.10).⁵¹ In contrast, the reaction of $[(\text{NacNac}^{\text{Me},\text{Dipp}})\text{Y}(\text{CH}_2\text{SiMe}_2\text{Ph})_2]$ with $[\text{HNMe}_2\text{Ph}][\text{B}(\text{C}_6\text{F}_5)_4]$, resulted in a cationic monoalkyl complex with η^6 – arene coordination of Me_2NPh

to yttrium (Figure 1.10), which was based on the significant low frequency shift observed for the *para*- and *ortho*- phenyl resonances (*p*-phenyl = 5.79 ppm, *o*-phenyl = 6.11 ppm) as observed by ^1H NMR spectroscopy, relative to free *N,N*-dimethylaniline (*p*-phenyl = 6.74 ppm, *o*-phenyl = 6.60 ppm).⁴⁸

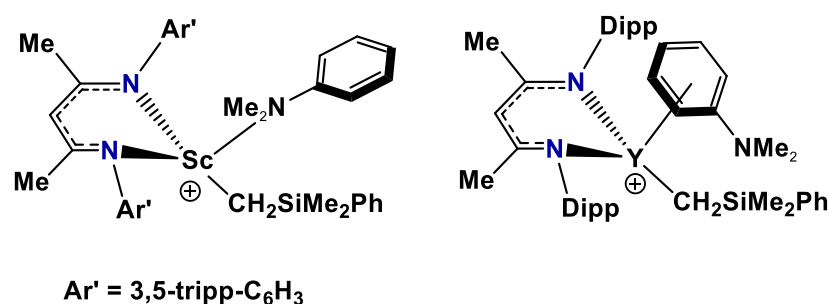


Figure 1.10: Literature examples of dimethylaniline coordination to a cationic rare earth complex– Anion: $[\text{B}(\text{C}_6\text{F}_5)_4]$

1.5.4 Monocationic Rare-Earth Alkyl Complexes

Although a few highly active, neutral rare-earth olefin polymerization catalysts are known, the vast majority are mono-cationic alkyl complexes that capitalize on the highly electrophilic and unsaturated metal center. Hence, accessing cationic alkyl complexes has garnered significant interest. The first example of a rare-earth cationic alkyl complex was reported by Schaverien (Figure 1.11), which was generated by reacting $[\text{Cp}^*\text{La}\{\text{CH}(\text{SiMe}_3)_2\}_2]$ with

[PhNMe₂H][BPh₄]. The resulting complex demonstrated π -coordination of the BPh₄ anion via two of the phenyl rings on boron.⁵²

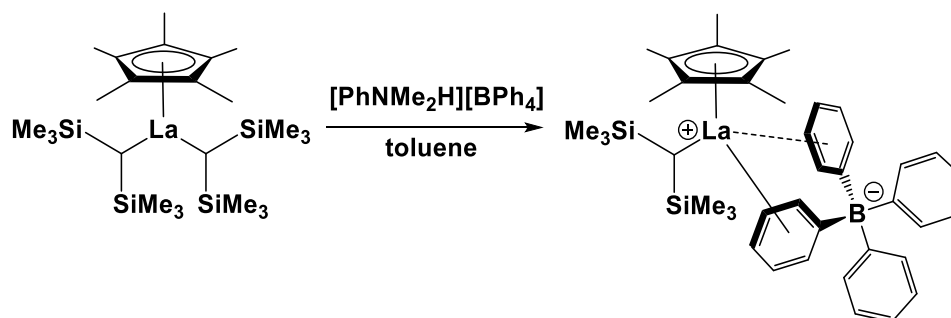


Figure 1.11: First example of a rare earth cationic alkyl complex [Cp*La{CH(SiMe₃)₂}][BPh₄]

The use of monoanionic, non-cyclopentadienyl multidentate ligands has also proven successful in accessing rare earth alkyl cations. The Piers group employed β -diketiminato ligands to synthesize a variety of rare earth dialkyl complexes that have been used to access cationic rare earth alkyl complexes via the strategies that were previously mentioned (*vide supra*). The reaction of [(NacNac^tBu, Dipp)Sc(CH₃)₂] with B(C₆F₅)₃ resulted in the structurally characterized monocationic, contact ion pair seen in Figure 1.12.³⁹

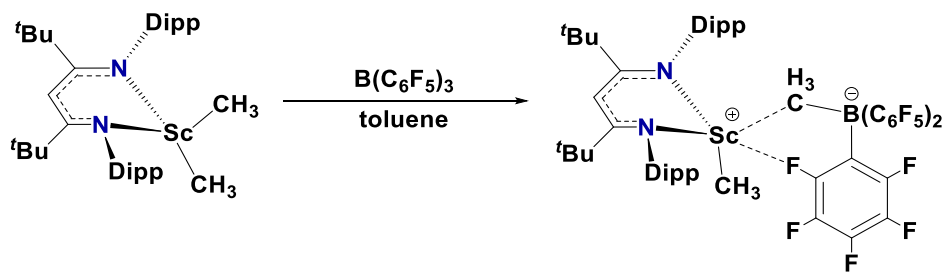


Figure 1.12: Synthesis of the monomeric contact ion pair [(NacNac^{tBu,Dipp}Sc(CH₃))][MeB(C₆F₅)₃]

The reaction of the less sterically bulky [(NacNac^{Me,Dipp})Sc(CH₃)₂] with 1 equivalent of B(C₆F₅)₃ also resulted in [(NacNac^{Me,Dipp})Sc(CH₃)] [MeB(C₆F₅)₃]. However, at temperatures above -35 °C, C₆F₅ ring transfer occurred as shown in Figure 1.13. When 2 equivalents of B(C₆F₅)₃ were used, a dicationic species was generated as observed by ¹H NMR spectroscopy and by the emergence of two sets of signals for the [MeB(C₆F₅)₃] anion in the ¹⁹F NMR spectrum. This complex readily underwent C₆F₅ ring transfer and afforded the monocationic product (Figure 1.13).⁴⁷

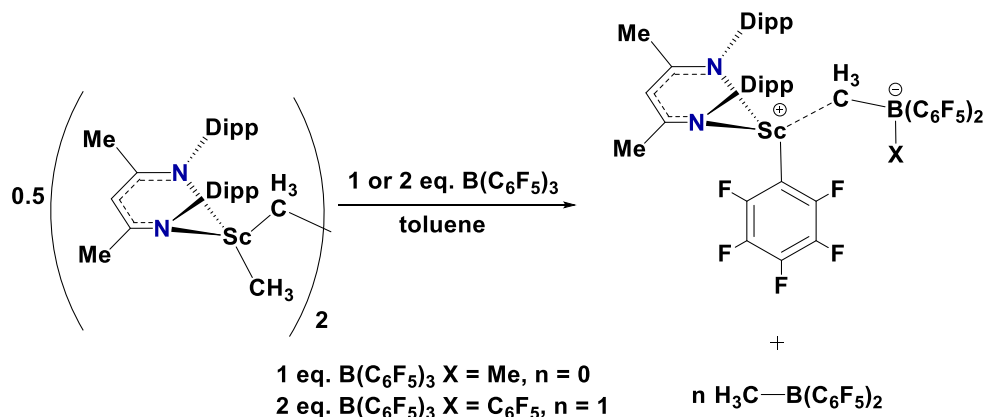


Figure 1.13: Reaction of $[(\text{NacNac}^{\text{Me,Dipp}})\text{Sc}(\text{CH}_3)_2]_2$ with 1 or 2 equivalents of $\text{B}(\text{C}_6\text{F}_5)_3$

In contrast to the aforementioned reactions with $\text{B}(\text{C}_6\text{F}_5)_3$, when $[(\text{NacNac}^{\text{Me,Dipp}})\text{Sc}(\text{CH}_3)_2]$ was reacted with $[\text{CPh}_3][\text{B}(\text{C}_6\text{F}_5)_4]$, C_6F_5 transfer to Scandium was not observed. However, the resulting highly electron deficient cationic complex is coordinated by the arene solvent as shown in Figure 1.14. Competition experiments conducted with the various arenes were in the order of toluene > mesitylene > benzene > > $\text{C}_6\text{H}_5\text{Br}$. The weaker coordination of mesitylene over toluene can be attributed to the steric bulk of the mesitylene. Higher ethylene polymerization activity is seen for the mesitylene coordinated cationic complex due to ethylene displacing mesitylene more readily than the more coordinating toluene.⁵³

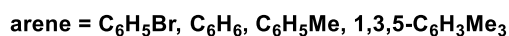
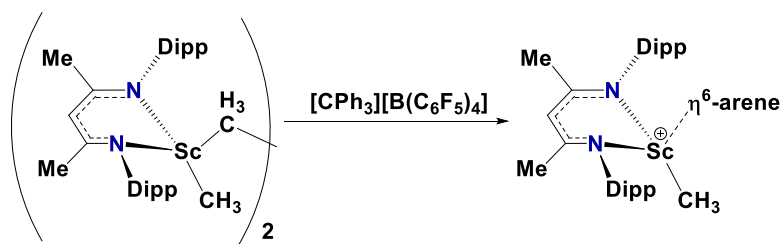


Figure 1.14: Reaction of $[(\text{NacNac}^{\text{Me,Dipp}})\text{Sc}(\text{CH}_3)_2]_2$ with 1 equivalent of $[\text{CPh}_3][\text{B}(\text{C}_6\text{F}_5)_4]$

The Piers group also investigated the reactivity of the bulkier $[(\text{NacNac}^{\text{tBu,Dipp}})\text{Sc}(\text{CH}_2\text{SiMe}_3)_2]$ complex with $\text{B}(\text{C}_6\text{F}_5)_3$.⁴⁷ Unlike the dimethyl scandium complex, the bis(trimethylsilylmethyl) scandium complex follows a unique reaction pathway, in which a new $\text{CH}_2\text{SiMe}_2\text{CH}_2\text{SiMe}_3$ alkyl group is formed, accompanied by $\text{MeB}(\text{C}_6\text{F}_5)_3$ anion formation (Figure 1.15). The proposed mechanism involves the abstraction of a methyl group from silicon with concomitant migration of the remaining alkyl group to the positively charged silicon. This type of rearrangement was also observed by Scott and coworkers in the reaction of $[(2-\{(\text{Dipp})\text{NCMe}\}-6-\{(\text{Dipp})\text{NCMe}_2\}\text{C}_5\text{H}_3\text{N})\text{Lu}(\text{CH}_2\text{SiMe}_3)_2]$ with $\text{B}(\text{C}_6\text{F}_5)_3$ as seen in Figure 1.16.⁴⁶

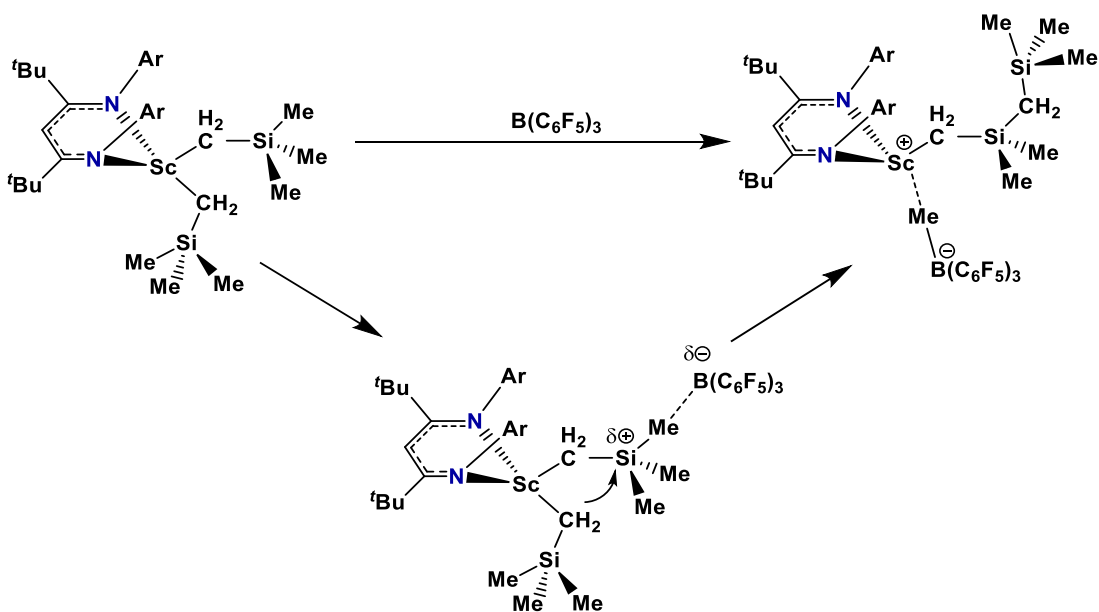


Figure 1.15: Reaction of $[(\text{NacNac}^{\text{tBu,Dipp}})\text{Sc}(\text{CH}_2\text{SiMe}_3)_2]$ with $\text{B}(\text{C}_6\text{F}_5)_3$

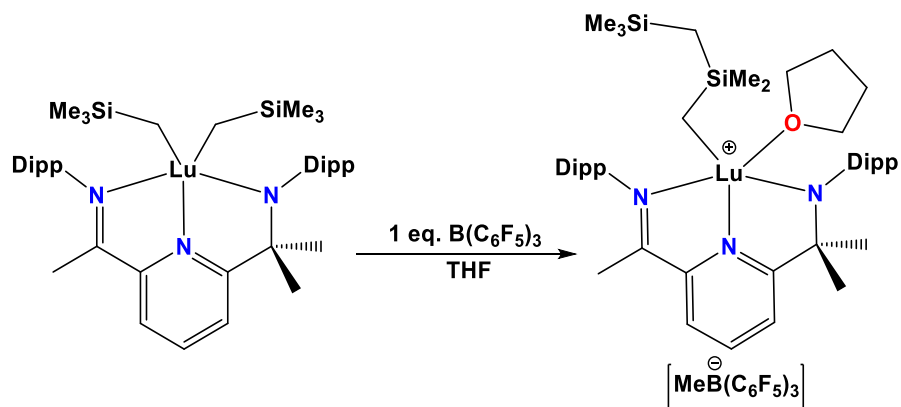


Figure 1.16: Reaction of
 $[(2-\{(\text{Dipp})\text{NCMe}\}-6-\{(\text{Dipp})\text{NCMe}_2\}\text{C}_5\text{H}_3\text{N})\text{Lu}(\text{CH}_2\text{SiMe}_3)_2]$ with $\text{B}(\text{C}_6\text{F}_5)_3$

$[(\text{NacNac}^{\text{Bu,Dipp}})\text{Sc}(\text{CH}_3)_2]$ proved to be a highly effective ethylene polymerization pre-catalyst, and in-situ generated $[(\text{NacNac}^{\text{Bu,Dipp}})\text{Sc}(\text{CH}_3)(\eta^6\text{-toluene})][\text{B}(\text{C}_6\text{F}_5)_4]$ proved to be more active than in-situ generated $[(\text{NacNac}^{\text{Bu,Dipp}})\text{Sc}(\text{CH}_3)][\text{MeB}(\text{C}_6\text{F}_5)_3]$ (Table 1.3).³⁹

Table 1.3: Ethylene Polymerization with [(NacNac^{tBu,Dipp})Sc(CH₃)₂] and various cocatalysts³⁹

Entry	Pre-catalyst	Activator	Activity ^a	M_w ($\times 10^{-3}$)	M_w / M_n
1 ^{b,c}	LScCl ₂	PMAO-IP	99	1357	2.2
2 ^{b,c}	LScR ₂	PMAO-IP	1200	1866	1.98
3 ^{b,d}	LScR ₂	B(C ₆ F ₅) ₃	300	1051	1.7
4 ^{b,d}	LScR ₂	[CPh ₃][B(C ₆ F ₅) ₄]	480	851	2.48

^a Activity in kg PE/mol Sc · h. ^b Polymerization conditions: 50 °C, 300 psi, cyclohexane/toluene, [Sc] = 300 μM, stir rate = 2000 rpm. ^c Al/M = 20. ^d [Cocatalyst] = 315 μM, [PMAO-IP] = 1 mM as scavenger. LScR₂ = [(NacNac^{tBu,Dipp})Sc(CH₃)₂], LScCl₂ = [(NacNac^{tBu,Dipp})ScCl₂]

Piers and co-workers subsequently synthesized yttrium dialkyl complexes employing β-diketiminato ligands. Reaction of neutral [(NacNac^{Me,Dipp})Y(CH₃)₂] with [HNMe₂Ph][B(C₆F₅)₄] afforded a spectroscopically observed monoalkyl cation that shows η⁶-arene coordination of the Me₂NPh byproduct (Figure 1.17).⁴⁸ In contrast, attempts to access cationic complexes via the neutral dibenzyl complex [(NacNac^{tBu,Dipp})Y(CH₂Ph)₂] proved difficult. Reaction of [(NacNac^{tBu,Dipp})Y(CH₂Ph)₂] with B(C₆F₅)₃ generated a cationic complex in which the PhCH₂B(C₆F₅)₃ anion is η⁶-coordinated to yttrium, based on ¹H NMR spectra at -40 °C, but this complex rapidly cyclometallated at room temperature.⁴⁸

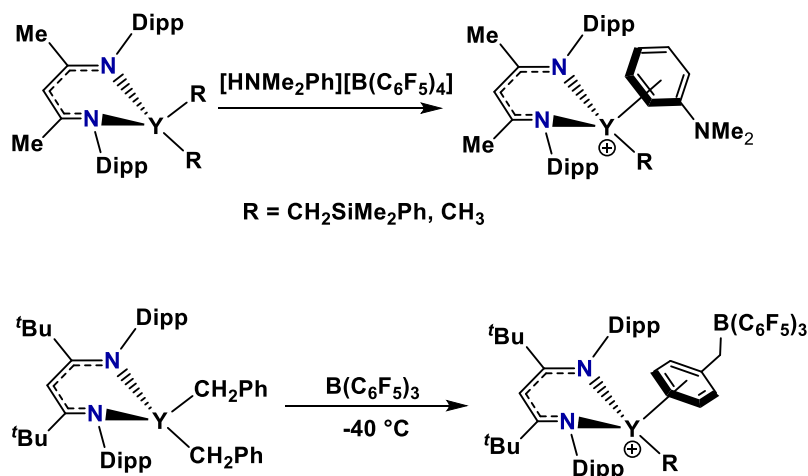


Figure 1.17: Cationic β -diketiminato Alkyl Yttrium Complexes

Hessen and coworkers established a series of neutral rare earth alkyl complexes that allowed for in-situ generation of cationic alkyl complexes (Figure 1.18).⁵⁴ Many of these complexes proved to be highly active for olefin polymerization. The benzamidinato ligand $[\text{PhC}(\text{NAr})_2]^-$, has proven to be successful in accessing highly active olefin polymerization catalysts for a wide variety of rare-earth metals.⁵⁴ Coordinatively saturated THF adducts of the benzamidinato rare earth alkyl cations have been isolated. Generation of the cationic alkyl complexes in toluene as opposed to THF resulted in highly active ethylene polymerization catalysts.^{54, 55}

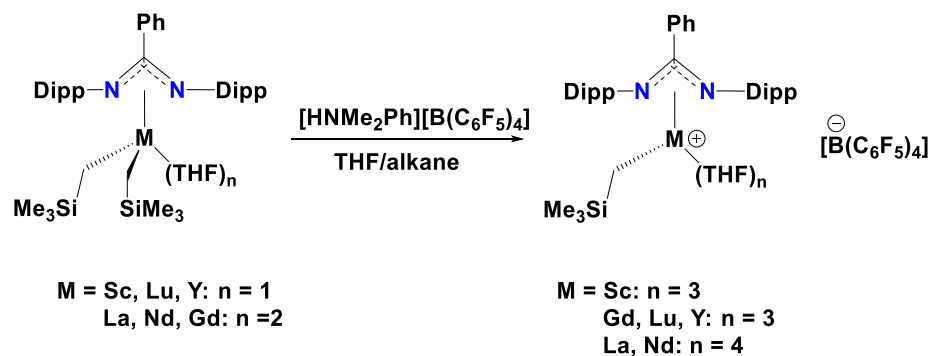


Figure 1.18: $[\text{PhC}(\text{N}\{\text{Dipp}\})_2\text{M}(\text{CH}_2\text{SiMe}_3)_2(\text{THF})_n]$ reaction with $[\text{HNMe}_2\text{Ph}][\text{B}(\text{C}_6\text{F}_5)_4]$

A direct correlation between the ionic radii of the metal and olefin polymerization activity was established for these systems, wherein an increase in activity is generally seen in the order of $\text{Lu} < \text{Sc} < \text{Y}$ (Table 1.4). However, the larger lanthanides showed a decrease in activity with an increase in ionic radius in the order of $\text{Gd} > \text{Nd} > \text{La}$ (Table 1.4). The narrow polydispersity of the resulting polyethylene suggests a single site active catalyst. In the case of the Y catalyst, a narrower polydispersity was achieved in the absence of an alkylaluminum scavenger (tetraisobutyl dialuminoxane). This suggests that a chain transfer mechanism exists in the presence of an alkylaluminum scavenger.⁵⁴

Table 1.4: Ethylene Polymerization with [PhC(N{Diip})₂M(CH₂SiMe₃)₂(THF)_n] activated by [HNMe₂Ph][B(C₆F₅)₄]⁵⁴

M	Radius (Å)	Yield (g)	Activity ^b	M _w (x 10 ⁻³)	M _w /M _n
Sc	0.89	0.20	24	93	1.6
Lu	1.00	2.82	342	496	1.4
Y	1.04	24.80	3006	1666	2.0
Gd	1.07	23.50	2848	1753	2.1
Nd	1.12	16.40	1988	1596	2.2
La	1.17	0.12	14	470	2.5

[PhNMe₂H][B(C₆F₅)₄] as an activator in the presence of TiBAO. Conditions: 5 μmol M; activator/M = 1:1, Al/M = 20, T = 30 °C, pressure = 5 bar ethylene, t = 20 min, toluene solvent (250 mL). ^bkg(PE) mol⁻¹ h⁻¹ bar⁻¹. Sc, Y, Lu: n = 1, Gd, Nd, La: n = 2

1.5.5 Neutral vs. Cationic Rare Earth Intramolecular Hydroamination Catalysts

Cationic rare earth hydroamination catalysts are scarcely found in literature but have shown promise. Piers and Schafer successfully utilized [(NacNac^{tBu}, Dipp)Sc(CH₃)][(CH₃)B(C₆F₅)₃] ‘**a**’ (Figure 1.19) in room temperature intramolecular hydroamination of 1-amino-2,2-diphenyl-4-pentene.²⁶ In contrast,

the neutral dialkyl $[(\text{NacNac}^{t\text{Bu}, \text{Dipp}})\text{Sc}(\text{CH}_3)_2]$ was only able to achieve partial conversion of 1-amino-2,2-diphenyl-4-pentene to the cyclized product. $[(\text{NacNac}^{t\text{Bu}, \text{Dipp}})\text{Sc}(\text{CH}_3)][(\text{CH}_3)\text{B}(\text{C}_6\text{F}_5)_3]$ 'a' was also able to cyclize the more difficult 1-amino-2,2-diphenyl-5-hexene substrate, although the reaction required heating at 65 °C. Attempts to cyclize more difficult substrates proved unsuccessful as seen in Table 1.5 (Entry 4-5).²⁶ Nevertheless, Piers and Schafer were able to demonstrate an increase in catalytic activity for the cationic alkyl complex, in comparison to the neutral alkyl complex. This paved the way for further investigations into the potential of cationic rare earth intramolecular hydroamination catalysts.

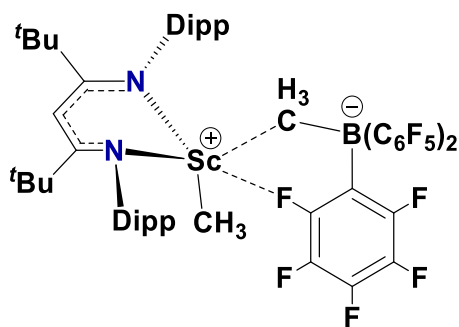
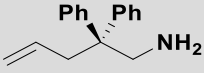
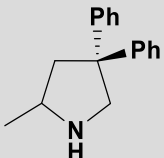
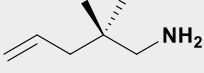
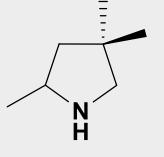
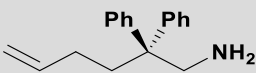
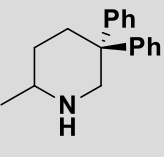
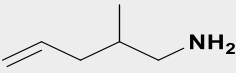
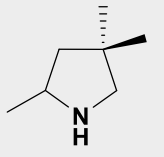
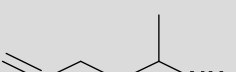
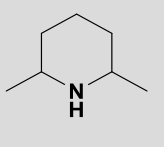


Figure 1.19: $[(\text{NacNac}^{t\text{Bu}, \text{Dipp}})\text{Sc}(\text{CH}_3)][(\text{CH}_3)\text{B}(\text{C}_6\text{F}_5)_3]$ (a) catalyst²⁶

**Table 1.5: Intramolecular hydroamination by [(NacNac^{tBu},
Dipp)Sc(CH₃)][(CH₃)B(C₆F₅)₃] – 5 % catalyst loading.**

	<i>Substrate</i>	<i>Product</i>	<i>Time(h)</i>	<i>%</i>	<i>°C</i>
1			2	95	25
2			24	> 90	65
3			24	> 90	65
4			96	50	65
5			96	0	65

Hessen and coworkers further extended chemistry by demonstrating intramolecular hydroamination activity for a series of cationic complexes generated in-situ (b-c Figure 1.20).²⁴ The rather sterically bulky triamine-amide ligand systems provided promising cationic rare earth alkyl complexes for intramolecular hydroamination. Compound ‘b’ upon activation with 1 equivalent of $[\text{HNMe}_2\text{Ph}][\text{B}(\text{C}_6\text{F}_5)_4]$ (Figure 1.20) completely cyclized 1-amino-2,2-dimethyl-4-pentene within 12 h at 50 °C.²⁴ Similarly, the cationic alkyl derivative of the more sterically encumbered ‘c’ was able to cyclize 77 % of the same substrate under identical experimental conditions.²⁴ In comparison, the neutral ‘b’ and ‘c’ complexes performed poorly for cyclization of 1-amino-2,2-dimethyl-4-pentene, which highlights the benefit of activating to the cationic derivate to access a more potent cationic catalyst (Table 1.6).²⁴

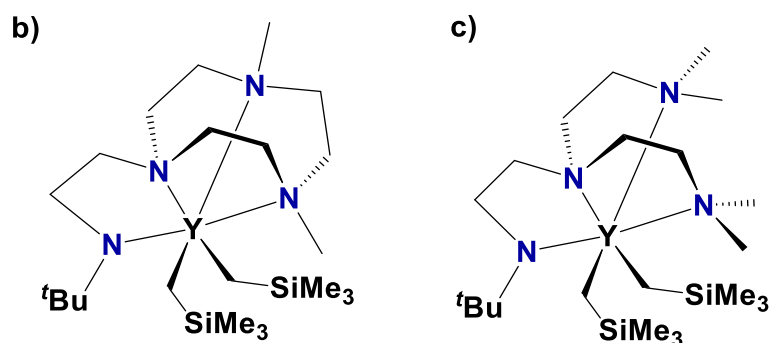


Figure 1.20: Triamine-amide based hydroamination pre-catalysts – ‘b’ and ‘c’ – activated in-situ with 1 eq. $[\text{HNMe}_2\text{Ph}][\text{B}(\text{C}_6\text{F}_5)_4]$

Table 1.6: Intramolecular hydroamination of 1-amino-2,2-dimethyl-4-pentene with neutral and cationic ‘b’ and ‘c’ in Figure 1.18, with and without activation by [HNMe₂Ph][B(C₆F₅)₄]²⁴

Catalyst	Time (h)	% Conversion
b	24	25
b*	12	99
c	24	16
c*	12	77

*Conditions: C₆D₆ solvent (0.5 ml), 50 °C, 10 μmol catalyst *(and [PhNMe₂H][B(C₆F₅)₄] activator where appropriate), 1-amino-2,2-dimethyl-4-pentene 1.0 mmol substrate*

Trifonov and coworkers similarly saw an increase in activity upon activation of ‘d’ and ‘e’ (Figure 1.21) to form a cationic derivative for the cyclization of a variety of primary and secondary aminoalkene substrates (Table 1.7 and 1.8).⁵⁶

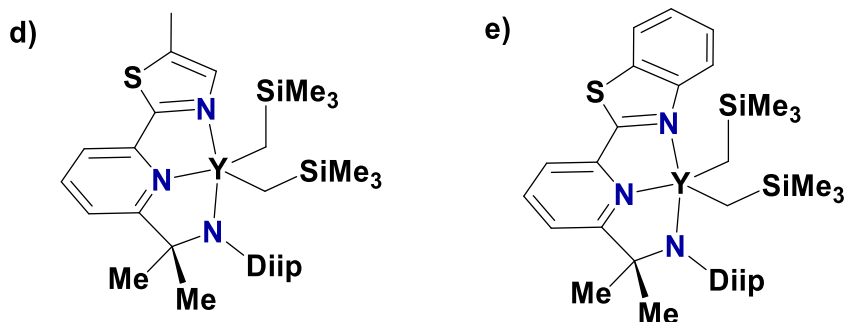
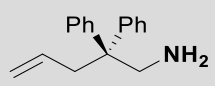
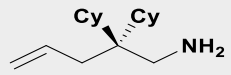
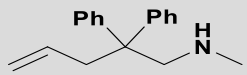
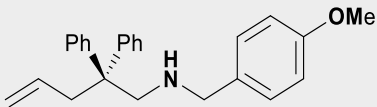
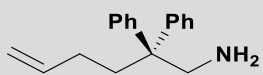


Figure 1.21: Trifonov's hydroamination pre-catalysts 'd' and 'e' – activated in-situ with 1 eq. $[\text{CPh}_3][\text{B}(\text{C}_6\text{F}_5)_4]$

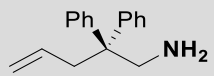
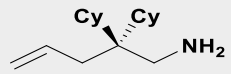
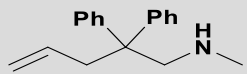
Table 1.7: Intramolecular hydroamination by 'd' (Figure 1.21) activated by $[\text{CPh}_3][\text{B}(\text{C}_6\text{F}_5)_4]$ ⁵⁶

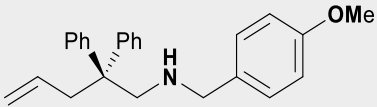
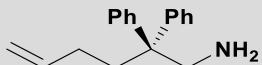

	Substrate	Time (h)	%	°C
1		1.5	97	40
2		2	81	40
3		7	92	80
4		24	31	80

5		5	28	80
---	---	---	----	----

Reaction conditions: *substrate*: 0.21 mmol '*d*': 5 mol% (10.5 μ mol), *solvent*: toluene (2.5 mL). *Activator*: 5 mol% (10.5 μ mol) $[\text{CPh}_3][\text{B}(\text{C}_6\text{F}_5)_4]$. Conversion determined by *in situ* ^1H NMR spectroscopy with ferrocene as internal standard.

Table 1.8: Intramolecular hydroamination by '*e*' (Figure 1.21) activated by $[\text{CPh}_3][\text{B}(\text{C}_6\text{F}_5)_4]$ ⁵⁶

	<i>Substrate</i>	<i>Time (h)</i>	<i>%</i>	<i>°C</i>
1		24	98	23
		1.5	99	40
2		2	94	40
		0.75	99	80
3		4	94	80

4		24	92	80
5		8	28	80
6		3	46	80

Reaction conditions: substrate: 0.21 mmol 'e': 5 mol% (10.5 μ mol), solvent: toluene (2.5 mL). Activator: 5 mol% (10.5 μ mol) $[CPh_3][B(C_6F_5)_4]$. Conversion determined by *in situ* 1H NMR spectroscopy with ferrocene as internal standard. pentene 1.0 mmol substrate

Compared to sterically encumbered (**a-e**) systems, less sterically encumbered '**f**' (Figure 1.22) provided contrasting results in the cyclization of a primary aminoalkene substrate (Table 1.9).²⁴ The neutral amidinate complexes of both Y and Sc '**f**' outperformed their cationic alkyl derivatives. In the case of compound '**f**', the neutral scandium dialkyl complex was able to cyclize more than 90 % of 1-amino-2,2-dimethyl-4-pentene within 6 hours at 50 °C. As expected, the larger neutral yttrium analogue (larger ionic radius) performed vastly more efficiently and was able to complete the conversion of the same substrate in less than an hour at 50 °C. However, upon activation to the cationic alkyl complex via

reaction with $[\text{HNMe}_2\text{Ph}][\text{B}(\text{C}_6\text{F}_5)_4]$, both the Sc and Y analogues became less potent catalysts (Table 1.9).²⁴ This is in contrast to the previously mentioned systems (a-e), which became more active upon activation to their cationic alkyl derivatives. The authors suggested that more sterically congested complexes benefit from activation due to steric relief, thereby allowing substrate binding and efficient cyclization. In the case of less sterically encumbered systems, no such steric relief is required and the strengthening of the M-N bond seen in cationic metal complexes can impede efficient cyclization.²⁴

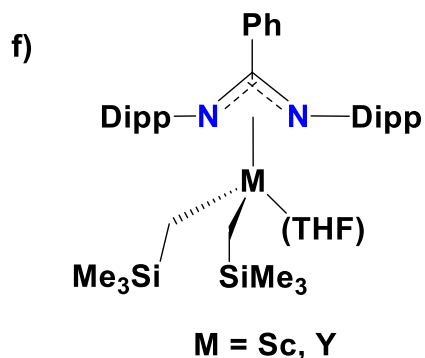


Figure 1.22: Benzamidinato ligand based rare earth hydroamination pre-catalyst – ‘

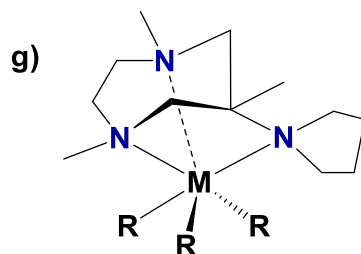
Table 1.9: Intramolecular hydroamination of 1-amino-2,2-dimethyl-4-pentene with neutral and cationic ‘f’ in Figure 1.22 with and without activation by [HNMe₂Ph][B(C₆F₅)₄]²⁴

Catalyst	Time (h)	% Conversion
f - Sc	6	90
f - Y	0.8	99
f* - Sc	24	10
f* - Y	24	13

*Conditions: C₆D₆ solvent (0.5 ml), 50 °C, 10 μmol catalyst *(and [HNMe₂Ph][B(C₆F₅)₄] activator where appropriate), 1-amino-2,2-dimethyl-4-pentene 1.0 mmol substrate*

The aforementioned hydroamination catalysts utilize a monoanionic ancillary ligand. Hessen and coworkers also investigated hydroamination by a rare earth complex ‘g’ employing a neutral ancillary ligand (Figure 1.23).²⁵ Similar to the results observed for sterically congested systems, Hessen and coworkers observed a significant increase in the cyclization efficiency of 1-amino-2,2-diphenyl-4-pentene by the cationic derivatives of ‘g’ (M = Y, La), in comparison to their neutral precursors (Table 1.10).²⁵ However, Hessen observed that the neutral complex ‘g-La’ had the same efficiency as the precursor

[La(CH₂Ph)₃(THF)₃], suggesting dissociation of the neutral ancillary ligand of ‘g-La’ in the presence of excess substrate.²⁵



M = Y, R =
CH₂SiMe₃
M = La R = CH₂Ph

Figure 1.23: Neutral tridentate (1,4,6-trimethyl-6-pyrrolidin-1-yl-1,4-diazepane) based hydroamination pre-catalyst ‘g’.

Table 1.10: Intramolecular hydroamination of 1-amino-2,2-diphenyl-4-pentene catalysis by ‘g-Y’, ‘g-La’ (Figure 1.21)²⁵, [Y(CH₂SiMe₃)₃(THF)₂] or [La(CH₂Ph)₃THF]₃ with and without activation by [HNMe₂Ph][B(C₆F₅)₄].

Catalyst	Time (min)	% Conversion
Y(CH ₂ SiMe ₃) ₃ (THF) ₂	600 ^b	99
g- Y	400 ^b	99

$\text{Y}(\text{CH}_2\text{SiMe}_3)_3(\text{THF})_2^*$	180	88
g* - Y	5	99
$\text{La}(\text{CH}_2\text{Ph})_3(\text{THF})_3$	200	99
g- La	200	99
$\text{La}(\text{CH}_2\text{Ph})_3(\text{THF})_3^*$	240	51
g*- La	70	99

Conditions: C_6D_6 solvent (total volume 0.5 mL), 60 °C, ^b80 °C catalyst (10 μmol), and activator ^{*} $[\text{PhNMe}_2\text{H}][\text{B}(\text{C}_6\text{F}_5)_4]$ (10 μmol), 1-amino-2,2-diphenyl-4-pentene (500 μmol). ^b 80 °C. Determined by *in situ* NMR spectroscopy.

The cyclization of *N*-Methylpent-4-en-1-amine by ‘**g-La**’ similarly suggested the dissociation of the ancillary ligand. In addition, cyclization by the cationic derivative of ‘**g-La**’ had the same efficiency as the cyclization of the substrate by $\text{La}(\text{CH}_2\text{Ph})_3(\text{THF})_3$ activated by $[\text{PhNMe}_2\text{H}][\text{B}(\text{C}_6\text{F}_5)_4]$ (Table 1.11).²⁵ This suggests that under the conditions of hydroamination catalysis, dissociation of the neutral ancillary ligand can occur from both the neutral complex, as well as the corresponding cationic complex. The neutral yttrium analogue ‘**g-Y**’ was observed to be more efficient in the cyclization of *N*-methylpent-4-en-1-amine than its cationic derivative.²⁵ In addition, the results did not suggest the dissociation of the ancillary ligand as was seen for the La derivatives. However, the authors observed the efficiency of ‘**g-Y**’ was less compared to the $[\text{Y}(\text{CH}_2\text{SiMe}_3)_3(\text{THF})_2]$ precursor.

This trend was similarly observed for the cationic derivative of ‘g-Y’, which was less efficient than $[\text{Y}(\text{CH}_2\text{SiMe}_3)_3(\text{THF})_2]$ activated by $[\text{PhNMe}_2\text{H}][\text{B}(\text{C}_6\text{F}_5)_4]$. This suggests that for the sterically bulkier substrate, the ancillary ligand employed impedes catalysis in both the cationic and neutral examples. The authors suggest that this may be due to the increased steric demand of the substrate, in addition to the strong coordination of the supporting ligand resulting in steric crowding of the metal center.²⁵

Table 1.11: Intramolecular hydroamination of *N*-methylpent-4-en-1-amine catalysis by ‘g-Y’, ‘g-La’ (Figure 1.21)²⁵, $[\text{Y}(\text{CH}_2\text{SiMe}_3)_3(\text{THF})_2]$ or $[\text{La}(\text{CH}_2\text{Ph})_3(\text{THF})_3]$ with and without activation by $[\text{HNMe}_2\text{Ph}][\text{B}(\text{C}_6\text{F}_5)_4]$.
25

Catalyst	Time (min)	% Conversion
$\text{Y}(\text{CH}_2\text{SiMe}_3)_3(\text{THF})_2$	25	99
g- Y	40	99
$\text{Y}(\text{CH}_2\text{SiMe}_3)_3(\text{THF})_2^*$	40	99
g* - Y	275	99
$\text{La}(\text{CH}_2\text{Ph})_3(\text{THF})_3$	15	99
g-La	15	99
$\text{La}(\text{CH}_2\text{Ph})_3(\text{THF})_3^*$	10	99
d*- La	10	99

Conditions: C₆D₆ solvent (total volume 0.5 mL), 60 °C, catalyst (10 μmol), and activator [PhNMe₂H][B(C₆F₅)₄](^{}, 10 μmol), where appropriate, substrate (500 μmol). Determined by in situ NMR spectroscopy.*

Hessen and coworkers investigated the kinetic profile for the hydroamination catalyst systems that were reported by their group in the literature. It was observed that sterically encumbered cationic systems demonstrated a first order dependence on substrate concentration, which would suggest that the protonolysis of the cyclized product is the rate determining step.^{24, 25} In contrast, non-sterically encumbered cationic systems were observed to demonstrate zero order dependence for substrate concentrations below 50 %. The zero order dependence on substrate concentration suggests that the insertion step is rate determining, and at higher conversions (>50%), product inhibition takes place, or the product release step becomes rate-limiting.^{24, 25} For example, the neutral and cationic derivatives of the sterically encumbered ‘**b-Y**’ demonstrated first order dependence over the full conversion of the 1-amino-2,2-dimethyl-4-pentene substrate. In contrast, the less sterically encumbered cationic derivatives of ‘**f-M**’ (**M** = **Sc**, **Y**) demonstrated zero order dependence on the substrate concentration at conversions below 50%.²⁴

1.5.6 Dicationic Rare Earth Alkyl Complexes

In comparison to monocationic rare earth alkyl complexes, dicationic alkyl complexes are rarely reported. This can be attributed to the highly electrophilic nature of the metal centres, which makes them highly reactive and susceptible to decomposition. Accessing dicationic alkyl complexes of a trivalent metal requires a neutral ligand, which is inherently less electron donating than a monoanionic ligand. Nevertheless, a few examples in literature exist where coordinatively saturated complexes have been structurally characterized.

Okuda and co-workers were the first to structurally characterize coordinatively saturated dicationic rare earth alkyl complexes and were pivotal in demonstrating their high potential for olefin polymerization.⁵⁷ The reaction of $[\text{Y}(\text{CH}_2\text{SiMe}_3)_3(\text{THF})_2]$ with 3 equivalents (excess) of a Brønsted acid co-reactant $[\text{HNMe}_2\text{Ph}][\text{BPh}_4]$ in THF resulted in the synthesis of dicationic $[\text{Y}(\text{CH}_2\text{SiMe}_3)(\text{THF})_5][\text{BPh}_4]_2$ (Figure 1.24).⁵⁸ Similarly, reaction of $[\text{Y}\{\mu\text{-Me}_2(\text{AlMe}_2)\}_3]$ with excess $[\text{NEt}_3\text{H}][\text{BPh}_4]$ in THF afforded $[\text{Y}(\text{CH}_3)(\text{THF})_6][\text{BPh}_4]_2$ (Figure 1.24).⁵⁸

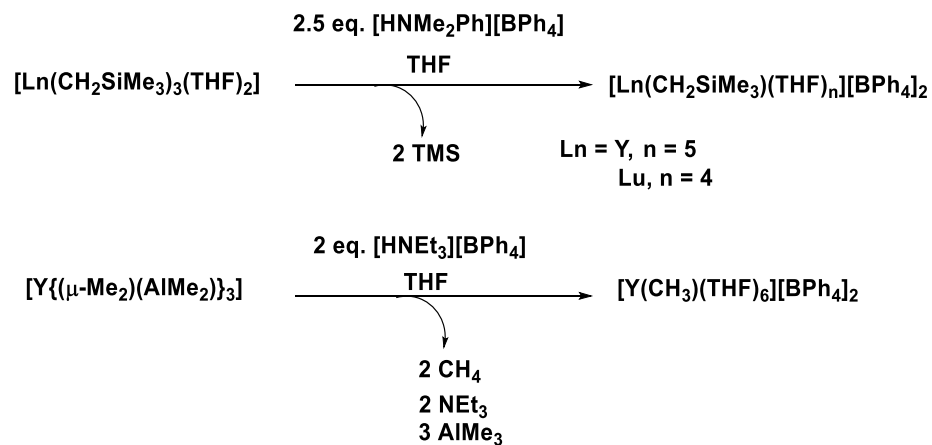


Figure 1.24: Coordinatively saturated dicationic alkyl complexes

Subsequent reaction of $[\text{Y}(\text{CH}_3)(\text{THF})_6][\text{BPh}_4]_2$ with excess pyridine resulted in the complete displacement of THF to form $[\text{Y}(\text{CH}_3)(\text{py})_6][\text{BPh}_4]_2$, which undergoes slow C—H activation of pyridine to yield $[\text{Y}\{\eta^2\text{-(C}_5\text{H}_4\text{N)}\}(\text{py})_6][\text{BPh}_4]_2$ (Figure 1.25).⁵⁹

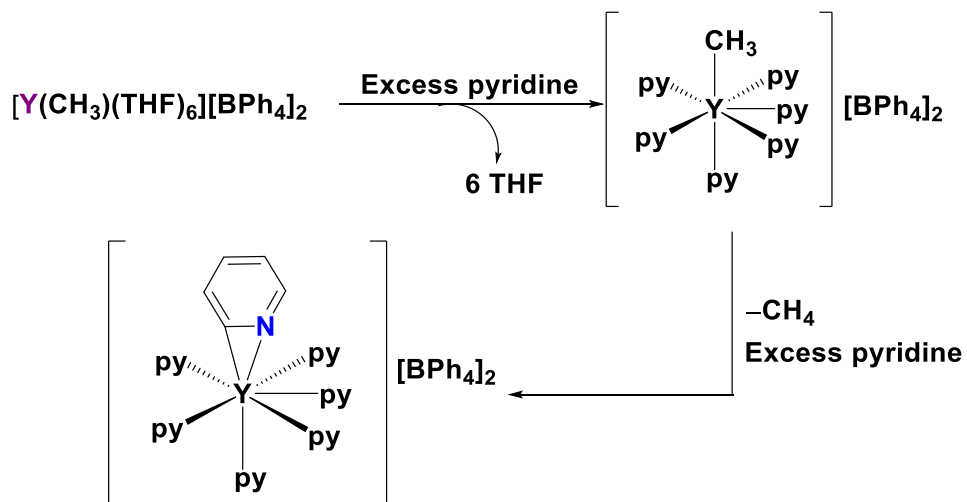


Figure 1.25: C–H bond activation of pyridine - $[\text{Y}\{\eta^2\text{-(C,N)-C}_5\text{H}_4\text{N}\}(\text{py})_6][\text{BPh}_4]_2$

Okuda and coworkers generated a variety of dicationic rare earth alkyl complexes in-situ, in a similar manner to the isolated complexes previously mentioned. However, the in-situ generation was performed in weakly coordinating arene solvents such as toluene and a weakly coordinating anion, $[\text{B}(\text{C}_6\text{F}_5)_4]^-$, was employed, as opposed to $[\text{BPh}_4]^-$. In these experiments, rare earth metals with larger ionic radii demonstrated high activity for ethylene polymerization (Table 1.12).⁵⁷

Table 1.12: Ethylene polymerization with $[\text{Ln}(\text{CH}_2\text{SiMe}_3)_3(\text{THF})_2]$ as the catalyst precursor⁵⁷

M	Radius (Å)	Yield (g)	Activity ^a	M_w/M_n
Sc	0.89	0.03	1	--
Lu	1.00	trace	--	--
Yb	1.01	--	--	--
Tm	1.02	0.76	183	4.1
Er	1.03	0.85	205	5.3
Y	1.04	0.91	272	2.9
Ho	1.04	1.15	275	1.7
Dy	1.05	3.51	842	3.6
Tb	1.06	3.74	899	2.9

$[\text{NMe}_2\text{HPh}][\text{B}(\text{C}_6\text{F}_5)_4]$ as activator in the presence of $\text{Al}i\text{Bu}_3$. Conditions: 5 mmol Ln ; Activator: Ln = 5:1, $\text{Al}:\text{Ln}$ = 200:1, $T = 258$ °C, $p = 5$ bar, $t = 10$ min, $V = 30$ mL (toluene). ^a Activity = $\text{kg}(\text{P.E}) \text{ mol}^{-1} \text{ h}^{-1} \text{ bar}^{-1}$.

A few examples of dicationic rare earth alkyl complexes utilizing multidentate ancillary ligands have been reported in literature. Okuda and coworkers have utilized 12-crown-4 in order to synthesize and structurally characterize monoalkyl yttrium dications.³⁸ The reaction of $[\text{Y}(\text{CH}_2\text{SiMe}_3)_3(12\text{-crown-4})]$ with either the Brønsted acids $[\text{Ph}_2\text{NMe}_2\text{H}][\text{BPh}_4]$, or

$[\text{Ph}_2\text{NMe}_2\text{H}][\text{B}(\text{C}_6\text{F}_5)_4]$, or the Lewis acid BPh_3 in THF, resulted in the THF coordinated 12-crown-4 face-capped, monoalkyl dication as shown in Figure 1.26. Similarly, generation of the dicationic alkyl complex in the presence of an additional equivalent of 12-crown-4 led to a bis(12-crown-4) monoalkyl dication (Figure 1.26).³⁸

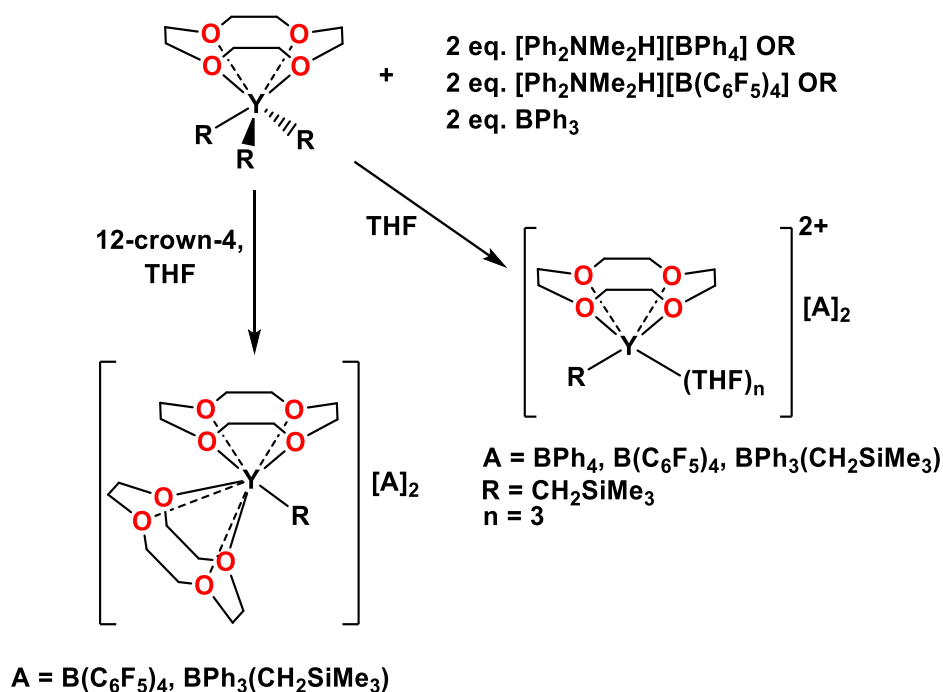


Figure 1.26: Synthesis of 12-crown-4 based dicationic monoalkyl yttrium complexes

The reaction of $[\text{Sc}(\textit{i}\text{Pr-trisox})(\text{CH}_2\text{SiMe}_3)_3]$ with 2 equivalents of $[\text{Ph}_3\text{C}][\text{B}(\text{C}_6\text{F}_5)_4]$ resulted in the in-situ generation of $[\text{Sc}(\textit{i}\text{Pr-trisox})(\text{CH}_2\text{SiMe}_3)][\text{B}(\text{C}_6\text{F}_5)_4]_2$, which was spectroscopically characterized (Figure

1.27 a) but not isolated. $[\text{Sc}(\text{}^i\text{Pr-trisox})(\text{CH}_2\text{SiMe}_3)][\text{B}(\text{C}_6\text{F}_5)_4]_2$ was proposed as the active species in the polymerization of 1-hexene when generated in-situ.⁴² In addition, a N-heterocyclic carbene stabilized scandium trialkyl complex was reacted with 2 equivalents of $[\text{CPh}_3][\text{B}(\text{C}_6\text{F}_5)_4]$ to spectroscopically observe a species that was proposed to be a dicationic scandium monoalkyl complex (Figure 1.27 b). The dicationic species was similarly active for the polymerization of α -olefins (1-hexene, 1-1-octene and 1-decene).⁶⁰

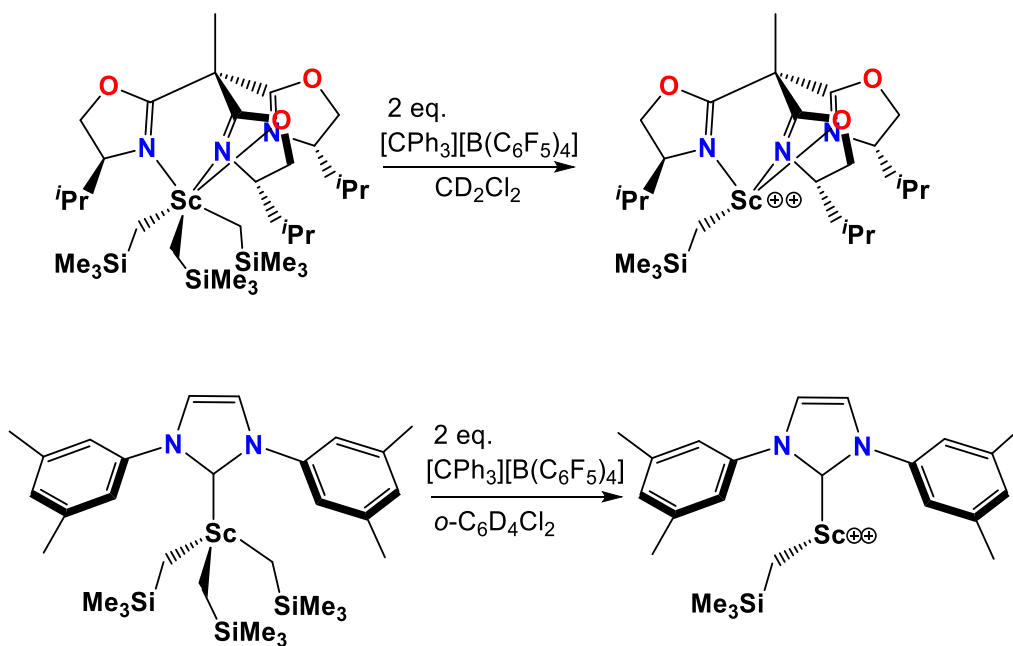


Figure 1.27: Synthesis of a) $[\text{Sc}(\text{}^i\text{Pr-trisox})(\text{CH}_2\text{SiMe}_3)][\text{B}(\text{C}_6\text{F}_5)_4]_2$, b) $[(\{2,6\text{-C}_6\text{H}_3\text{Me}_2\}_2\text{NHC})\text{Sc}(\text{CH}_2\text{SiMe}_3)][\text{B}(\text{C}_6\text{F}_5)_4]_2$

1.6 Ligand Design for Rare Earth Metal Chemistry

Stabilization of potential rare earth alkyl complexes requires careful tuning of the steric and electronic properties of the ligand. Rare earth alkyl complexes tend to follow a variety of undesirable reaction pathways such as dimerization, ligand redistribution, or undesirable coordination of highly donating solvents (e.g. THF).⁶¹ Adequate steric bulk around the metal alkyl center can prevent these pathways and protect the highly reactive metal alkyl. However, excessively bulky ligands can hinder substrate binding to the metal center in catalytic processes such as olefin polymerization and hydroamination. Herein lies the difficulty in fine tuning the steric bulk to allow for substrate binding, while being adequate to stabilize the reactive metal center.

Apart from steric bulk, careful electronic tuning of potential ligands is required in order to stabilize rare earth alkyl complexes. Specifically, electron deficient cationic rare earth alkyl complexes, which show high potential for olefin polymerization, may benefit from highly donating ligands for stabilization.

In addition to steric bulk, compatible electron donating ligands must be utilized in isolating organometallic complexes. Consideration of the Pearson Hard Soft Acid Base principle (HSAB) can aid in identifying suitable donor groups.⁶¹ The terms ‘hard’ and ‘soft’ are indicative of polarizability, with a hard metal/ligand being less polarizable, and a soft metal/ligand being more polarizable.² Rare earth

metals are considered “hard metals”, and therefore preferentially bind to “hard ligands” (e.g. oxygen and nitrogen donors).⁶¹

Another ligand design consideration is the overall charge of the ligand.⁶¹ Utilization of a dianionic ligand may allow access to neutral monoalkyl rare earth (III) complexes, which are of interest due to the high potential these complexes have demonstrated for intra/intermolecular hydroamination catalysis. By contrast, use of a monoanionic or neutral supporting ligand may allow access to monocationic or dicationic alkyl complexes of interest for olefin polymerization.

1.6.1 Introduction to Rigid Pincer Ligands

The modern day definition of “pincer” ligands encapsulates any ligand that is tridentate and adopts a meridional coordination mode, as shown in Figure 1.28.⁶² The first pincer ligand, which employed an ortho-disubstituted phenyl anion with phosphines as neutral flanking donors, was reported by Shawn and Moulton in 1976.⁶² The turn of the century has seen a significant rise in the reporting of pincer ligand based organometallic complexes. Ease of steric and electronic tunability without significant change of the coordination geometry, led to a wide interest in this class of ligands.

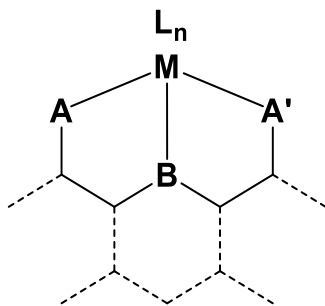


Figure 1.28: The general architecture of a pincer ligand metal complex (A, A' and B represent varying donor groups in a meridional bonding motif)

Within this class of ligand, the Emslie group is particularly interested in highly rigid pincer ligands, in order to carefully position the steric bulk around the metal center, thereby maximizing the steric protection afforded. Rigid ligand frameworks can also impart the desired coordination environment around the metal center despite the preference of the central metal and/or the co-ligands, in addition to mitigation of the entropic loss associated with reduced conformational freedom upon ligand to metal coordination.

Previously the Emslie group reported the synthesis of the dianionic ligands XA_2 and the closely related XN_2 .^{23, 63} Both the aforementioned ligands are highly similar, with XN_2 employing 2,4,6-triisopropylanilino donors as opposed to 2,6-diisopropylanilino donors (XA_2) (Figure 1.29).

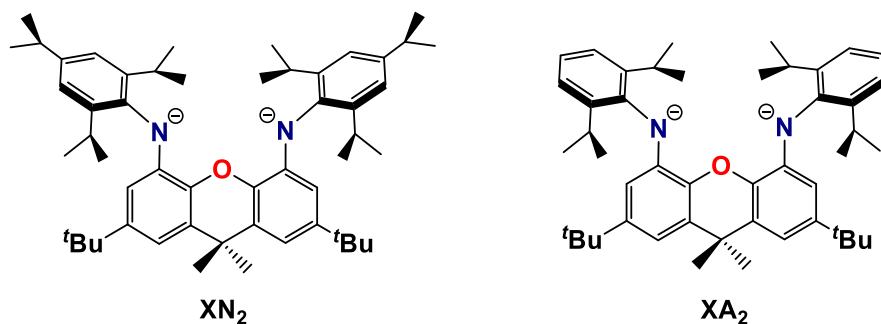


Figure 1.29: Rigid dianionic pincer ligands – XN_2 and XA_2

Utilization of the supporting ligand XN_2 afforded the neutral monoalkyl complex $[(\text{XN}_2)\text{Y}(\text{CH}_2\text{SiMe}_3)(\text{THF})]$, which proved to be a highly efficient intra/intermolecular hydroamination catalyst.²³ In contrast, use of XN_2 with zirconium(IV) allowed for isolation of the neutral dialkyl complex $[(\text{XN}_2)\text{Zr}(\text{CH}_3)_2]$ (Figure 1.30).⁶⁴ This complex was subsequently reacted with $[\text{CPh}_3][\text{B}(\text{C}_6\text{F}_5)_4]$ in toluene to generate in-situ, an η^6 – arene coordinated monoalkyl cation, which proved to be highly efficient for ethylene polymerization. XA_2 was similarly utilized with tetravalent actinide metals such as Th(IV) and U(IV), thereby affording the neutral dialkyl complexes $[(\text{XA}_2)\text{An}(\text{CH}_2\text{SiMe}_3)_2]$ ($\text{An} = \text{U}, \text{Th}$).^{63, 65, 66} Reaction of $[(\text{XA}_2)\text{An}(\text{CH}_2\text{SiMe}_3)_2]$ with $[\text{CPh}_3][\text{B}(\text{C}_6\text{F}_5)_4]$ resulted in η^x – arene coordinated monoalkyl cations (Figure 1.30).^{67, 68} Ethylene polymerization was achieved with the fluoroarene-coordinated cations, while the benzene and toluene coordinated cations were inactive. $[(\text{XA}_2)\text{Th}(\text{CH}_2\text{SiMe}_3)(\eta^x\text{-C}_6\text{H}_5\text{F})][\text{B}(\text{C}_6\text{F}_5)_4]$ is the most active post-metallocene actinide ethylene

polymerization catalyst known in literature (activity = 57.6 kg of polyethylene · (mol of Th)⁻¹ · h⁻¹ · atm⁻¹).⁶⁷

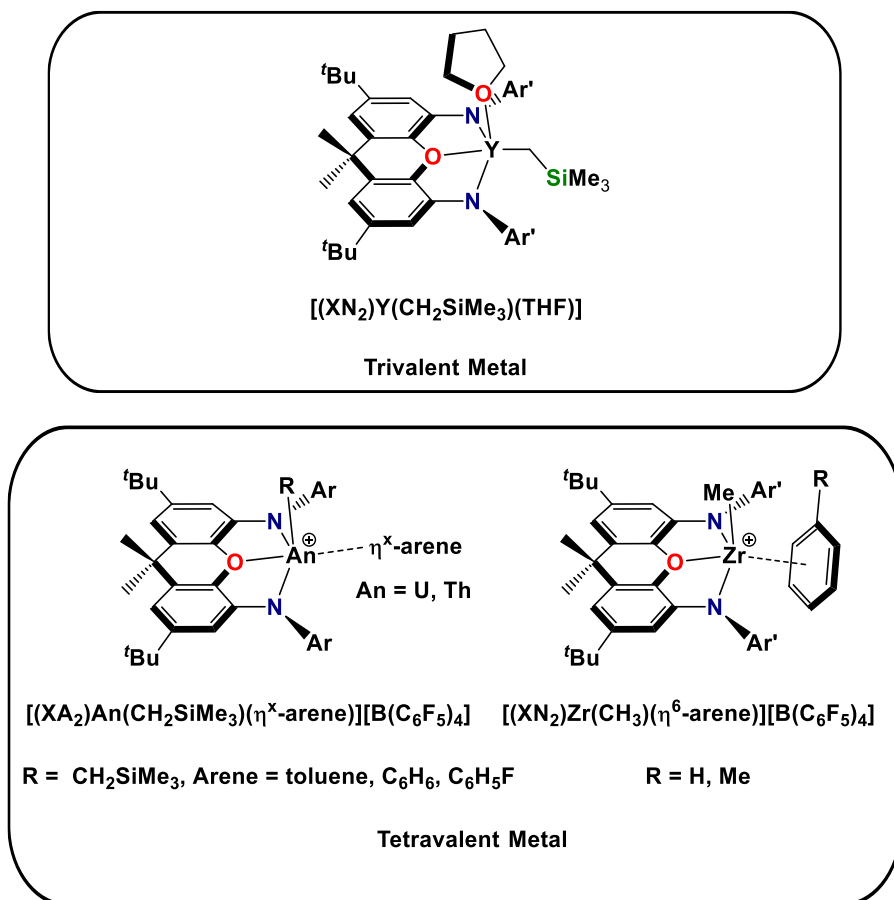


Figure 1.30: Selected examples of XN_2 and XA_2 metal complexes

All of the aforementioned chemistry involves the dianionic XN_2 and XA_2 ligands. However, monocationic or neutral analogues of these ligands could be accessed by replacement of one or both of the flanking amide donors with a neutral donor, where the donor atom is directly linked to the rigid tricyclic ligand backbone.

Potential neutral alternatives are phosphinimine ($-\text{N}=\text{PR}_3$) and imidazol-2-imine ($-\text{N}=\{\text{NHC}\}$) donors, which are discussed in the following sections of the introduction (Sections 1.7 and 1.8 respectively).

Monoanionic ligands can be utilized to generate monocationic monoalkyl complexes of trivalent metals. These cationic monoalkyl rare earth complexes have demonstrated high potential for olefin polymerization catalysis (Section 1.5.4) and are consequently of high interest. Neutral ligands can potentially be utilized to generate highly electron deficient dicationic group 3 alkyl complexes, which are scarcely reported. Although those that have been reported demonstrated high activity for olefin polymerization and are ripe for further exploration.

1.7 Introduction to Phosphinimine Based Ligands

Phosphinimine based ligands have been utilized in the synthesis of various rare earth metal complexes. Steric and electronic properties of phosphinimines are easily tuned by varying the R groups on phosphorus. The highly electron donating capability of these donor groups arises from a significant contribution from the zwitterionic resonance structure, which localizes the negative charge on the nitrogen (Figure 1.31).⁶⁹ These donor groups also afford significant steric protection, which is highly dependent on the specific R groups.

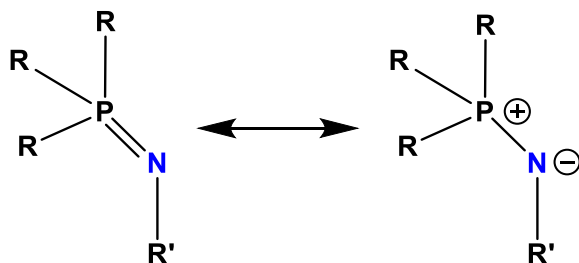


Figure 1.31: Resonance structures of phosphinimine donors

Phosphinimines can be synthesized via two common routes: a) the Staudinger reaction and b) the Kirsanov Reaction (Scheme 1.12).⁷⁰ The Staudinger reaction involves the reaction of an organic azide and a tertiary phosphine, which results in the evolution of nitrogen gas.⁷⁰ In certain cases, the reaction has to be heated in order to liberate nitrogen from the phosphazide intermediate in order to afford the target phosphinimine. The explosive nature of certain organic azides can dissuade researchers from using the Staudinger route.

Apart from the Staudinger reaction, the Kirsanov reaction can also be employed in synthesizing target phosphinimine ligands.⁷¹ This reaction typically involves a phosphine dibromide (e.g. Ph_3PBr_2) and a primary amine, in the presence of a base (e.g. Et_3N , KHMDS) (Scheme 1.12).

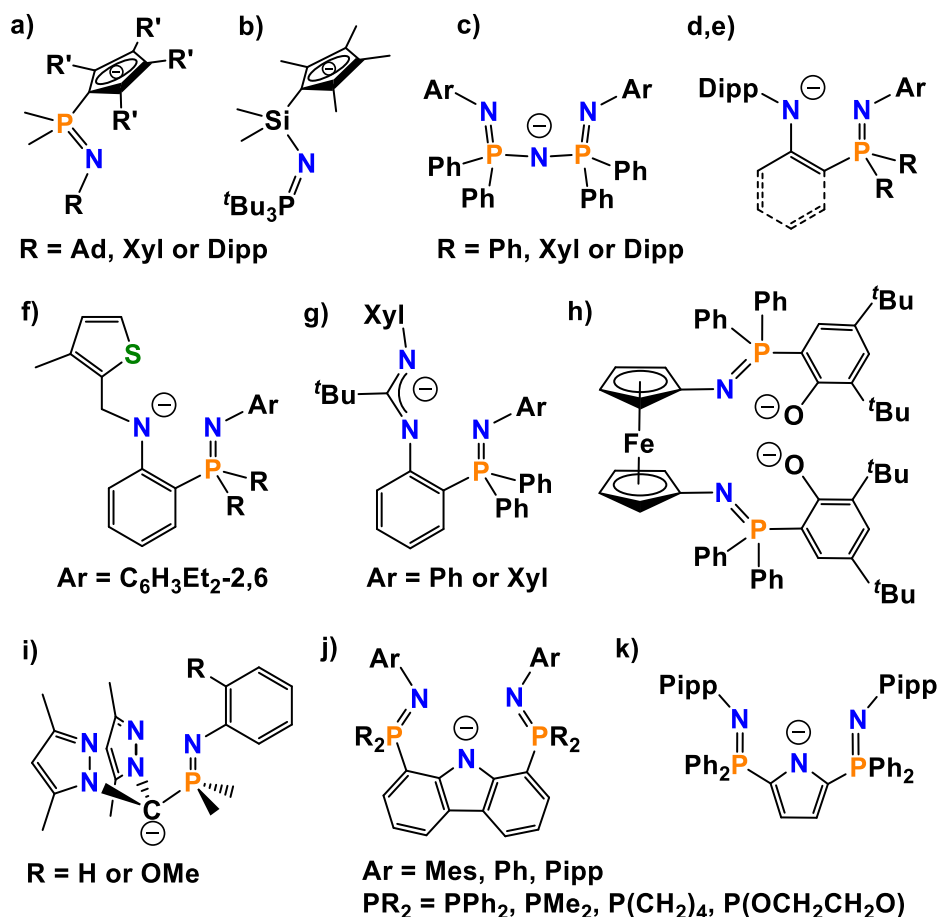


Figure 1.32: Phosphinimine-donor ligands employed in rare earth alkyl and aryl chemistry; for ligands 'd' and 'e', dashed bonds are absent in the former, and present in the latter.

Cui and coworkers utilized the bis-arylated phosphazene pincer ligand 'c' to isolate a series of base free neutral rare earth dialkyl complexes.⁷⁵ The bis-arylated phosphazene ligand adopts a κ^3 -coordination mode via the N atoms (Figure 1.33). $[\{\text{N}(\text{PPh}_2\text{NAr})_2\}\text{Sc}(\text{CH}_2\text{SiMe}_3)_2]$ was further utilized to form a scandium

terminal imido complex by reacting with $i\text{Pr}_2\text{C}_6\text{H}_3\text{NH}_2$ in toluene at -30°C , followed by room temperature treatment with DMAP (Figure 1.34).⁷⁵

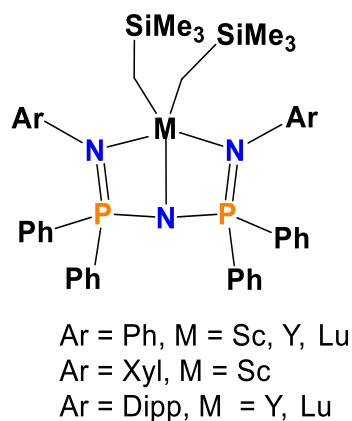


Figure 1.33: Rare earth dialkyl complexes of $[\text{N}(\text{PPh}_2\text{NAr})_2]^-$ ligands

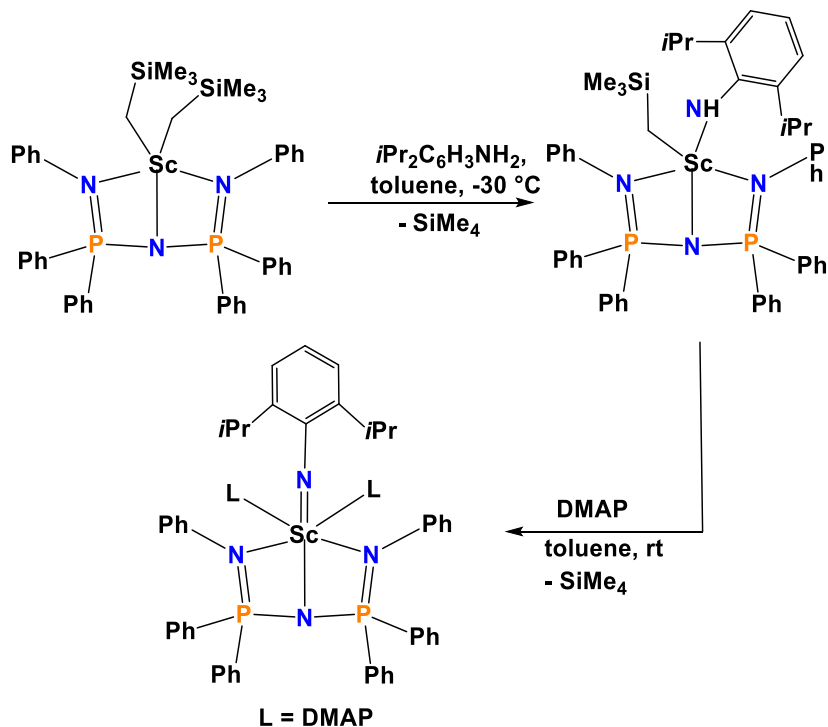


Figure 1.34: Synthesis of $[\{\text{N}(\text{PPh}_2\text{NPh})_2\}\text{Sc}\{(2,6\text{-}i\text{PrC}_6\text{H}_3)\}(\text{DMAP})_2]$

Piers and coworkers were able to synthesize a series of dimethyl scandium complexes employing anilido-phosphinimine ancillary ligands ‘e’.⁷⁶ However, several of the complexes proved to be susceptible to cyclometallation. [(1-{NDipp}-2-{PPh₂NMes}C₆H₄)ScMe₂] underwent a rapid cyclometallation process, in which a methyl group of the mesityl substituent is C–H bond activated at room temperature (Figure 1.35).⁷⁶ In contrast, [(1-{NDipp}-2-{PMe₂NDipp}C₆H₄)ScMe₂] showed C–H bond activation of a PMe₂ methyl group at 65 °C (Figure 1.36).⁷⁶

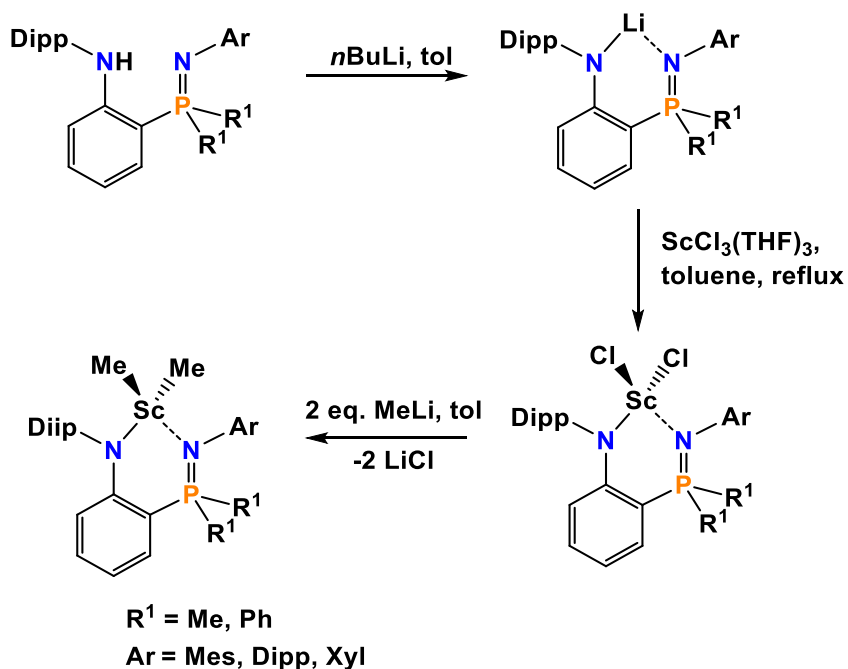


Figure 1.35: Synthesis of [(1-{NAr}-2-{PR₂NAr}C₆H₄)ScMe₂] containing ligand type ‘e’

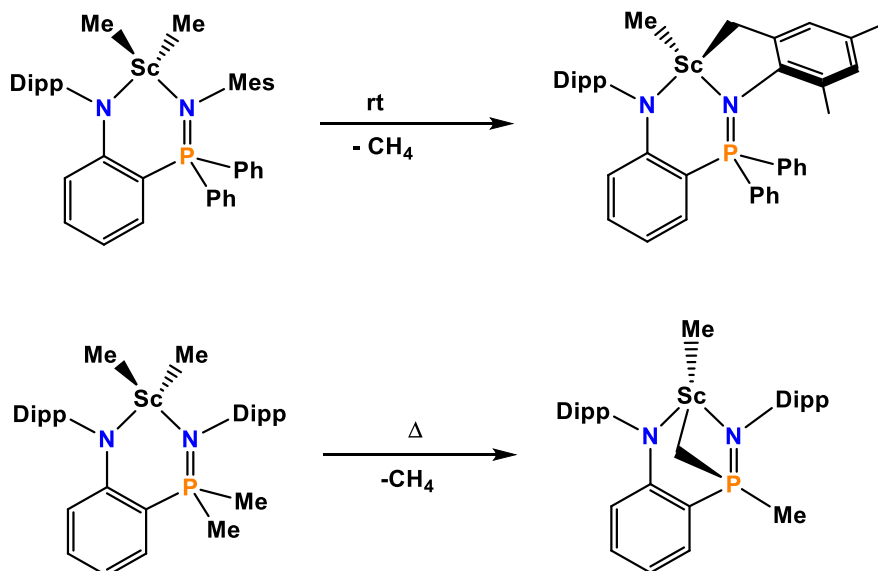


Figure 1.36: Cyclometallation of [(1-{NDipp}-2-{PPh₂NMe})C₆H₄)ScMe₂] and [(1-{NDipp}-2-{PPh₂NDipp})C₆H₄)ScMe₂] containing ligand type ‘e’

Cui and coworkers utilized a thiophenylmethyl- substituted anilido-phosphinimine ligand ‘f’ and isolated a series of rare earth dialkyl complexes (Figure 1.37). X-ray structures of these complexes demonstrated that the thiophene donor does not coordinate to the rare earth center.⁷⁷

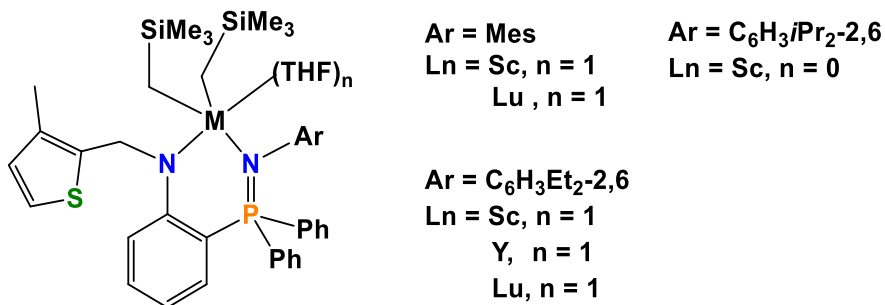


Figure 1.37: [{1-(MeC₄H₂SCH₂N)-2-(PPh₂NAr-C₆H₄)}M(CH₂SiMe₃)₂(THF)_n] complexes containing phosphinimine ligand ‘f’

Ligands designed using an amidinate framework have seen success in isolating rare earth dialkyl complexes. Hessen and coworkers have isolated a series of these complexes as seen in Section 1.5.4. Similarly, Trifonov and coworkers utilized bulky tridentate amidinate ligands bearing pendant phosphinimine donors ‘g’ to isolate a series of rare earth dialkyl complexes (Figure 1.38).⁷⁸

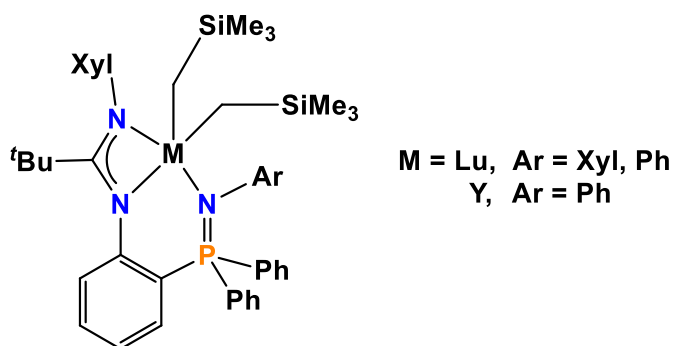


Figure 1.38: [(2-{Ph₂PN(Ar)}C₆H₄{NC(tBu)N(Xyl)})M(CH₂SiMe₃)₂] containing phosphinimine ligand ‘g’

Ancillary ligand designs based on a ferrocene framework have been extensively utilized in transition metal chemistry. Diaconescu and coworkers similarly utilized a ferrocene backbone with two pendant phosphinimine donors ‘h’ to generate [(NP^{fc})Y(CH₂Ph)] and [(NP^{fc})Y(CH₂SiMe₃)] (Figure 1.39).⁷⁹ The

aforementioned complexes were structurally characterized but proved thermally unstable, decomposing at ambient temperature within hours.

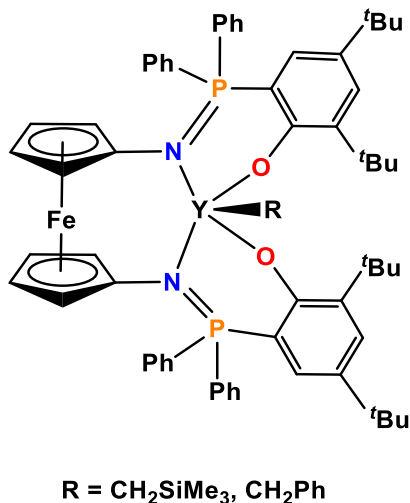


Figure 1.39: Literature examples of [(NP^{fc})YR] complexes containing phosphinimine ligand ‘h’

Apart from pincer ligands, heteroscorpionate ligands have found utility in rare earth chemistry. Both neutral and anionic heteroscorpionate ligands have been reported, and the latter are isolobal to cyclopentadienyl anions (Cp⁻). Cui and coworkers were able to design a phosphinimine modified heteroscorpionate anion (generated in-situ, by C–H bond activation of the central carbon), which afforded the zwitterionic dialkyl rare earth species shown in Figure 1.40.⁸⁰ Structural analysis showed that the carbanion is not directly bonded to the rare earth center,

and the ligand is instead capped on to the metal through κ^3 -coordination of the N donors in the ligand.⁸⁰

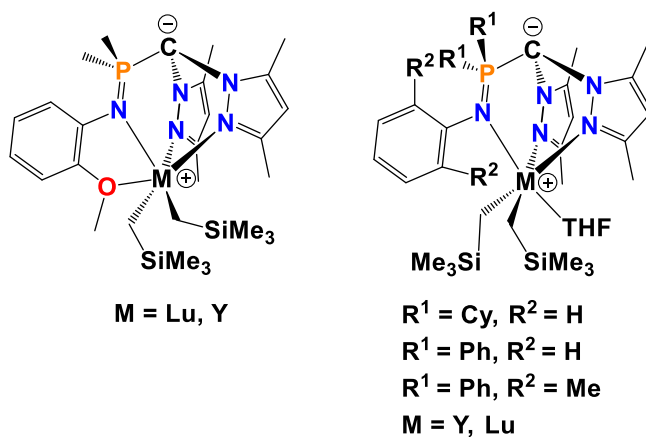


Figure 1.40: Literature examples of rare earth dialkyl heteroscorpionate complexes employing a pendant phosphinimine donor (ligand type ‘i’)

A variety of tridentate anionic ligands in which two phosphinimine donors are linked by an anionic carbazolidate or pyrrolide backbone (‘j’ and ‘k’ in Figure 1.32) have been utilized by the Hayes group to isolate a range of organometallic rare earth complexes. Ligands utilizing the monoanionic ligand framework ‘j’ were employed to isolate Sc, Y and Lu complexes.^{81, 82-85} The aforementioned complexes underwent cyclometallation, with the position of the cyclometallation being dependent on the metal center and the substitution pattern of the ligand.

For example, $[\{(\text{PippN}=\text{PC}_4\text{H}_8)_2\text{DMC}\}\text{Sc}(\text{CH}_2\text{SiMe}_3)_2]$ undergoes stepwise cyclometallation of each phospholane ring under ambient conditions (Figure 1.41).⁸² In contrast, the Lu analogue $[\{(\text{PippN}=\text{PC}_4\text{H}_8)_2\text{DMC}\}\text{Lu}(\text{CH}_2\text{SiMe}_3)_2]$

undergoes cyclometallation of a single ortho C—H bond of an *N*-aryl ring (Figure 1.42).⁸²

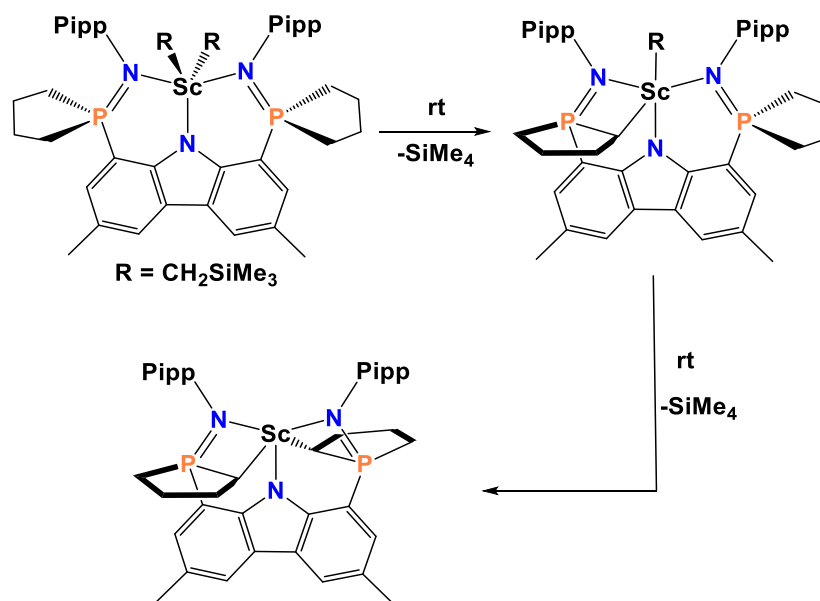


Figure 1.41: Cyclometallation of $[\{(\text{PippN}=\text{PC}_4\text{H}_8)_2\text{DMC}\}\text{Sc}(\text{CH}_2\text{SiMe}_3)_2]$ containing ligand type ‘j’

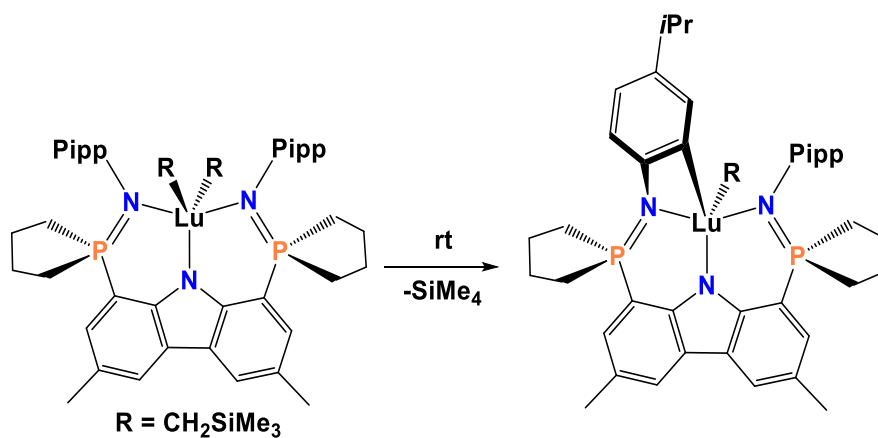


Figure 1.42: Cyclometallation of $[(\text{PippN}=\text{PC}_4\text{H}_8)_2\text{DMC}]\text{Lu}(\text{CH}_2\text{SiMe}_3)_2$ containing ligand type 'j'

Bulkier versions of ligand design 'j' were utilized by Hayes and coworkers to synthesize Y and Lu alkyl complexes. However, cyclometallation was similarly observed for these complexes (Figure 1.43).^{83, 85}

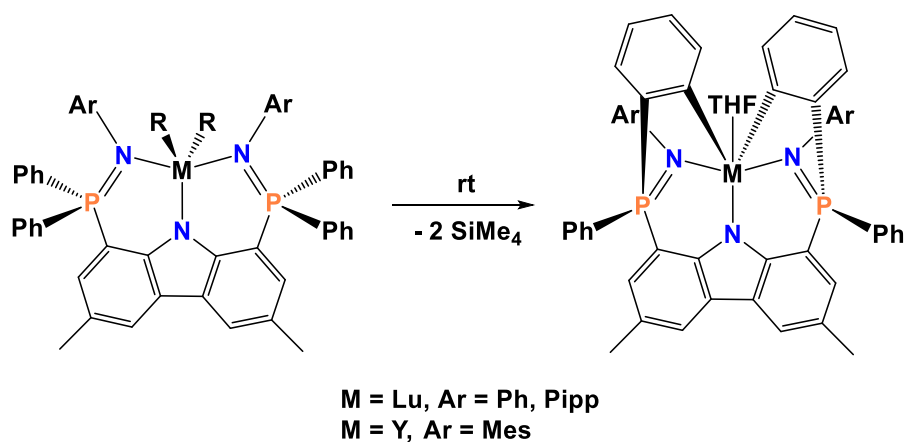
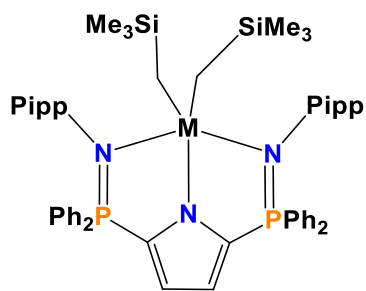


Figure 1.43: Cyclometallation of $[(\text{ArN}=\text{PPh}_2)_2\text{DMC}]\text{M}(\text{CH}_2\text{SiMe}_3)_2$ containing ligand type 'j'

By contrast, dialkyl Sc, Lu, Er and Y complexes of ligand 'k' (Figure 1.44) are stable in solution.^{86, 87} However, switching to the larger Sm(III) ion resulted in rapid orthometallation of a phosphinimine *N*-aryl group, followed by orthometallation of a *P*-phenyl substituent (Figure 1.45).⁸⁷



M = Sc, Er, Lu, Y

Figure 1.0.44: $\{[(\text{PippNPPh}_2)_2\text{pyr}]M(\text{CH}_2\text{SiMe}_3)_2\}$ containing ligand type 'k'

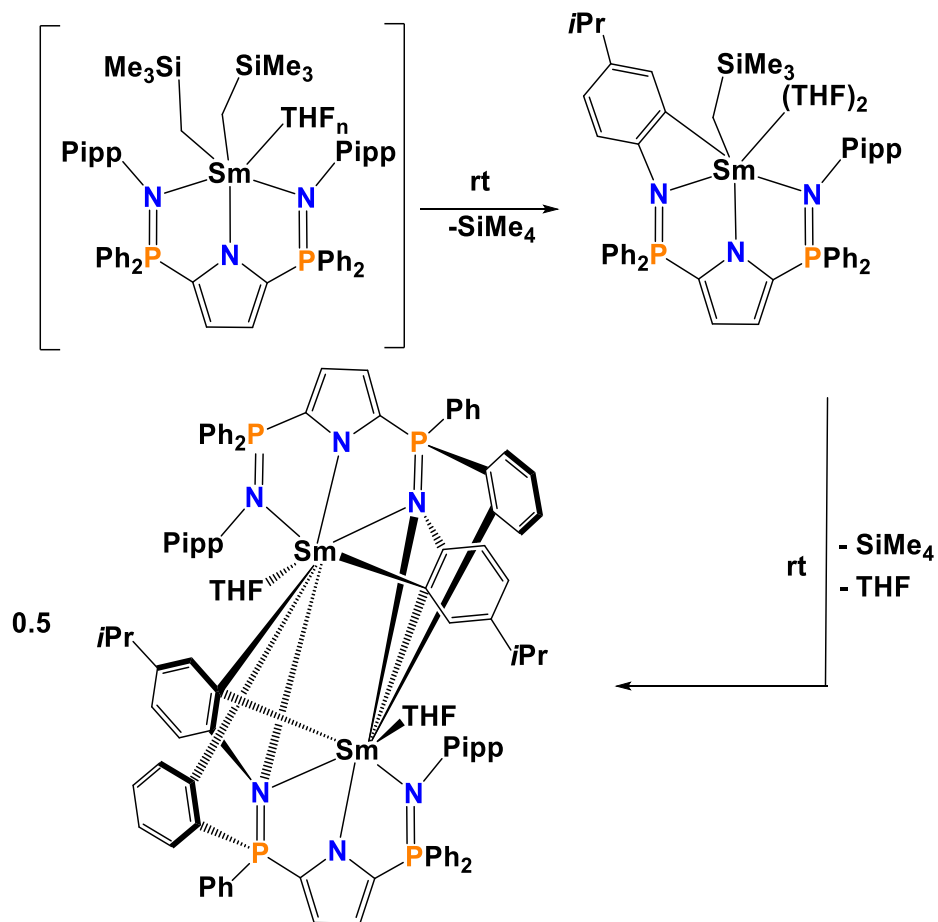


Figure 1.45: Decomposition of $\{[(\text{PiipNPPh}_2)_2\text{pyr}]\text{Sm}(\text{CH}_2\text{SiMe}_3)_2(\text{THF})_n\}$ containing ligand type ‘k’

1.8 Introduction to Imidazol-2-Imine Based Ligands

Following the report of the anionic imidazol-2-iminato ligands by Kuhn and co-workers, Tamm et al. expanded the transition metal chemistry of both the anionic imidazol-2-iminato and the neutral imidazol-2-imine ligands.^{88,89} Although neutral, the imidazol-2-imine donors have a significant contribution from a zwitterionic resonance structure that localizes a negative charge on nitrogen, allowing these donors to be highly electron donating (Figure.1.46).^{89,90} In addition, both the electronic and steric properties of the ligand are easily tunable by varying the R groups on the ring.

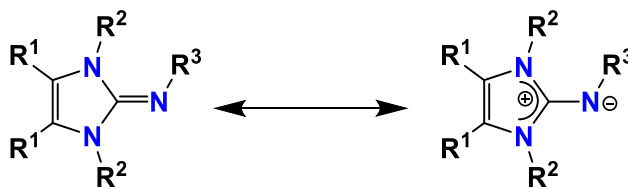
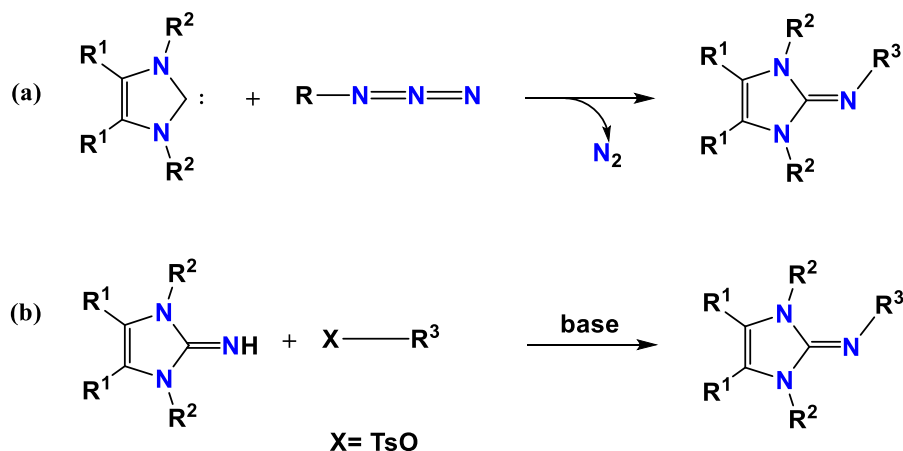


Figure 1.46: Resonance forms for imidazol-2-imine ligands

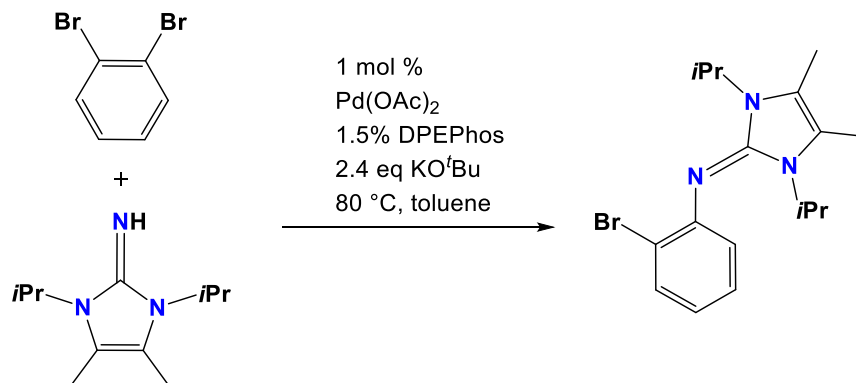
There are two common ways in which imidazol-2-imines are synthesized. The most frequently employed route to synthesize imidazol-2-imine based ligands is an approach similar to the Staudinger reaction, which involves the reaction of a heterocyclic carbene with an organic azide (Scheme 1.13 (a)).⁹¹ The second

approach involves the reaction of a tosylate with the appropriate imidazol-2-imine as seen in Scheme 1.13 (b).⁹²



Scheme 1.13: Synthetic routes to imidazol-2-imine ligands

Alternatively, Buchwald-Hartwig cross-coupling of an imine and an aryl bromide can be achieved, although this approach is underdeveloped in comparison to cross-coupling of primary amines and secondary amines. Existing examples of Buchwald-Hartwig ‘imination’ primarily utilize benzophenone imine ($\text{Ph}_2\text{C}=\text{NH}$). Nevertheless, Tamm and co-workers reported an example of Buchwald-Hartwig cross-coupling of an aryl halide and an imidazol-2-imine as seen in Scheme 1.14.⁹³ This is the only example of this type of coupling reaction.



Scheme 1.14: Synthesis of imidazol-2-imine ligand using Buchwald-Hartwig cross-coupling

1.8.1 Imidazol-2-imine Donors in Rare Earth Chemistry

Imidazol-2-imines are highly under utilized in rare earth chemistry, despite being highly electron donating and having electronic/steric properties that are easily tunable. Ligands ‘a’ and ‘b’ in Figure 1.47 are the only imidazol-2-imine ligands to have been in used in rare earth chemistry. Ligand ‘a’ was utilized to isolate neutral dialkyl complexes of Sc, Y and Lu, which proved to be viable intramolecular hydroamination catalysts.⁹⁴ Ligand ‘b’ was utilized to isolate chloride complexes of Y, Er and Lu.⁹⁰

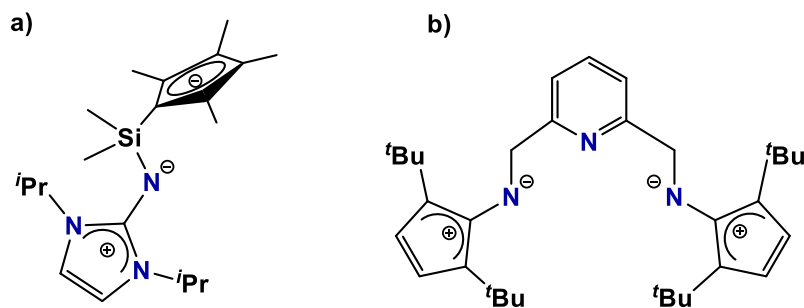


Figure 1.47: Literature examples of imidazol-2-imine donor ligands employed in rare earth chemistry

1.9 Thesis Goals

Cationic group 3 alkyl complexes have demonstrated potential in olefin polymerization and to a lesser extent intramolecular hydroamination. The Emslie group has previously utilized rigid, dianionic XA_2 and XN_2 ligands in successfully isolating a series of cationic actinide (Th, U) and group 4 (Zr) alkyl complexes as outlined in Section 1.6.1. However, accessing cationic group 3 alkyl chemistry would require a monoanionic or neutral ligand. Furthermore, accessing a very rare example of a dicationic rare earth alkyl complex would require a neutral ligand. Due to the inherent electron deficiency of cationic rare earth complexes, highly electron donating groups would ideally be implemented in potential ligand designs. Formally neutral donors such as phosphinimines, and the under utilized imidazol-2-imine groups have a considerable contribution from their zwitterionic resonance

structures, which places a negative charge on the nitrogen, as outlined in Sections 1.7 and 1.8. As a result, the aforementioned donor groups are ideal candidates for potential ligand designs targeted towards accessing cationic and dicationic group 3 alkyl complexes. Therefore the objectives of this Ph.D. research were (1) to synthesize a neutral xanthene based ligand employing flanking phosphinimine donors, and to explore the chemistry of this ligand with group 3 metals (chapter 2), (2) to synthesize the monoanionic acridanide based ligand AII₂ employing flanking imidazol-2-imine donors (steric profile similar to 2,6-diisopropylanilido donors of the XA₂ ligand) and to explore the chemistry of potential monocationic group 3 alkyl complexes (chapter 3). (3) to synthesize a neutral analogue of the AII₂ ligand in which the central anionic donor is replaced with a neutral oxygen donor, thus allowing access to rare examples of dicationic group 3 monoalkyl complexes (chapter 4). (4) to synthesize the asymmetric, monoanionic XAI ligand, which replaces one of the neutral imidazol-2-imine donors of XII₂ with the anionic 2,6-diisopropyl anilido donor group thereby imparting similar steric protection afforded by XA₂ and XN₂ (chapter 5). In addition, this thesis will explore the ethylene polymerization capability of resulting monocationic and dicationic group 3 alkyl complexes. Furthermore, the intramolecular hydroamination capability of monocationic alkyl complexes will be explored. Herein is presented the progress made towards achieving these objectives.

Chapter 2

Alkyl Yttrium Complexes of Doubly Cyclometallated Xanthene- and Naphthalene-Backbone Bis(phosphinimine) Ligands

Adapted with permission from: Vasanthakumar, A.; Emslie, D.J.H; Britten, J.F. *J. Organomet. Chem.* **2019**, *15*, **DOI:** 120980.

2.1 Introduction

Group 3 and f-element alkyl and aryl complexes feature polar metal–carbon bonds, and demonstrate high reactivity of broad applicability in small molecule activation and catalysis.^{27, 38, 61, 95} Organometallic rare earth and actinide chemistry was originally dominated by complexes with carbocyclic supporting ligands, such as cyclopentadienyl anions. However, over the past several decades, rare earth non-cyclopentadienyl chemistry has experienced a surge of interest, due to the enormous steric and electronic variety offered by such ligands.^{27, 38, 61, 95} Our group has previously accessed a range of thermally robust rare earth, thorium and uranium organometallic complexes utilizing rigid dianionic 4,5-di(arylamido)-2,7-di-*tert*-butyl-9,9-dimethylxanthene pincer ligands (e.g. XA₂ and XN₂ in Figure 2.1). These complexes include neutral thorium(IV) and uranium(IV) alkyl complexes,^{63, 65, 66, 96} thorium(IV) monoalkyl cations,^{66, 68} a thorium(IV) dication,⁶⁶ and neutral yttrium(III)

or lutetium(III) monoalkyl complexes; the latter are extremely active for both intramolecular and intermolecular alkene hydroamination.^{23,97}

To further explore the applications of rigid pincer ligands in rare earth chemistry, we became interested in analogues of XA_2 and XN_2 with different overall charges, including neutral ligands where both amido anions have been replaced with neutral N-donors (Figure 2.1). In order to provide a direct analogy, and maximize the rigidity of the metal coordination pocket, the nitrogen donor atoms must be attached directly at the 4- and 5-positions of the xanthene ligand backbone. Therefore, the use of tethered (i.e. not fused to the xanthene backbone) pyridine or related heterocyclic donors is precluded. Acyclic imines are another alternative but are prone to nucleophilic attack at the imine carbon. By contrast, phosphinimine donors are resistant to this mode of decomposition, so are the focus in this work.

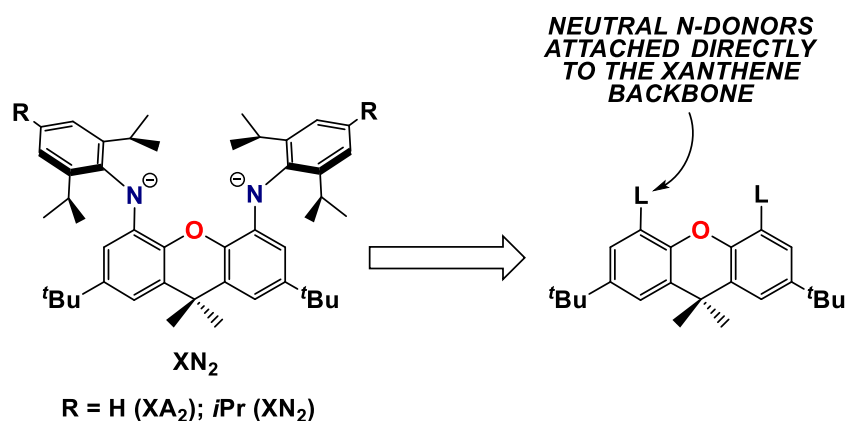
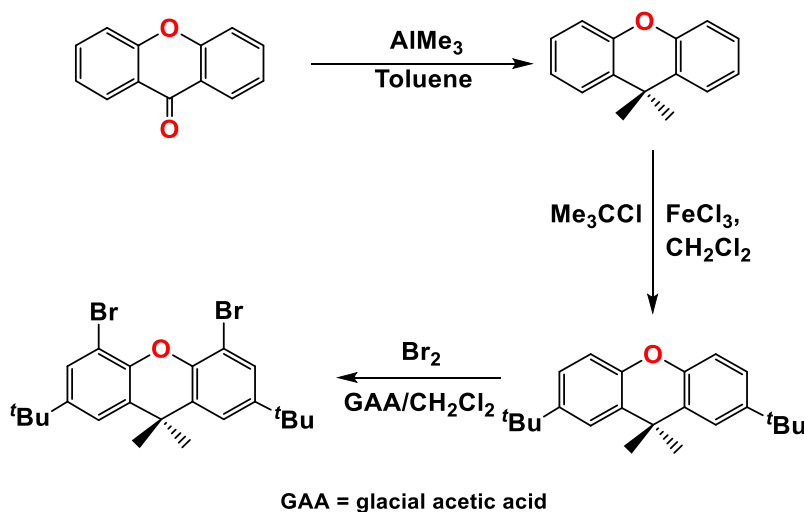


Figure 2.1: Dianionic XN_2 and XA_2 Ligands, and their relationship to the neutral NON-donor in this work

2.2 Synthesis of $(\text{Ph}_3\text{PN})_2\text{XT}$

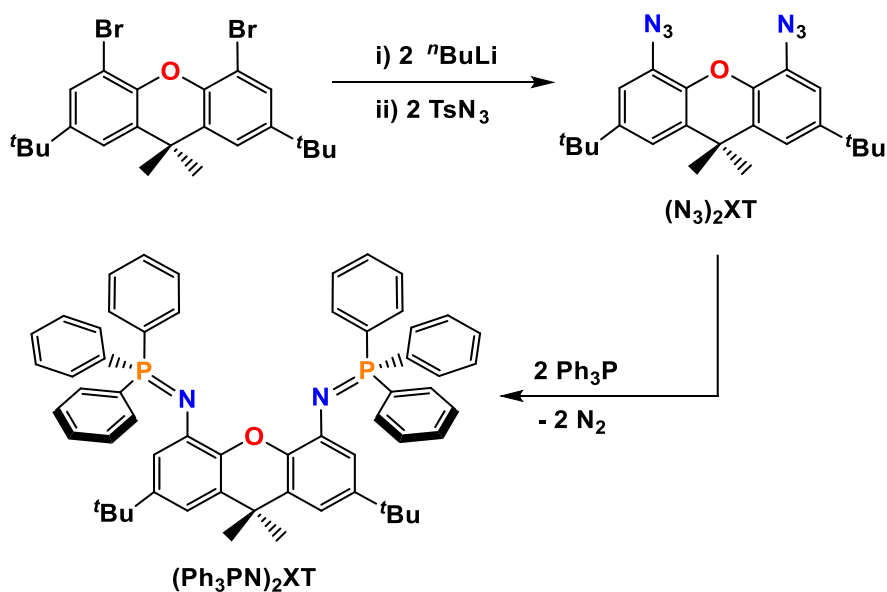
The synthesis of $(\text{Ph}_3\text{PN})_2\text{XT}$ requires the synthesis of the rigid 4,5-dibromo-2,7-di-*tert*-butyl-9,9-dimethylxanthene precursor (XBr_2) (Scheme 2.1).⁹⁸



Scheme 2.1: The Synthesis of XBr_2

The 4,5-dibromo-2,7-di-*tert*-butyl-9,9-dimethylxanthene precursor was dilithiated using 2 equiv. of $^t\text{BuLi}$, and subsequent treatment with 2 equiv. of tosyl azide afforded the diazide species $(\text{N}_3)_2\text{XT}$. Subsequently, $(\text{N}_3)_2\text{XT}$ generated in-situ was reacted with 2 equiv. of PPh_3 to afford $(\text{Ph}_3\text{PN})_2\text{XT}$ (**1**) (Scheme 2.2).

Although the synthesis of **1** was conducted in one pot, $(\text{N}_3)_2\text{XT}$ was independently isolated as a pale orange solid and handled with caution due to the potential for organic azides to be highly shock and temperature sensitive. The ^1H NMR spectrum for $(\text{N}_3)_2\text{XT}$ was consistent with a C_{2v} -symmetric structure (Figure 2.2).



Scheme 2.2: Synthesis of $(\text{Ph}_3\text{PN})_2\text{XT}$ (1)

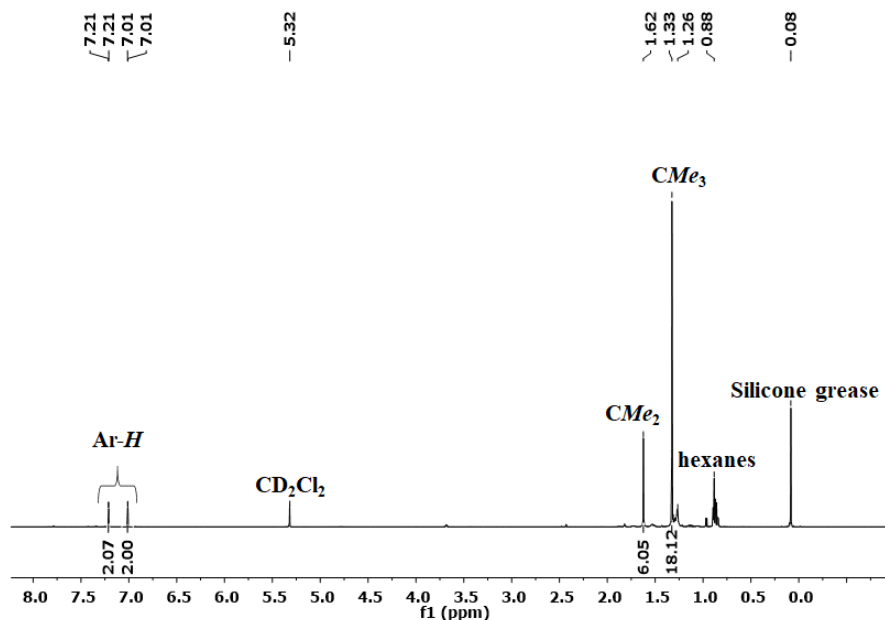


Figure 2.2: ^1H NMR Spectrum of $(\text{N}_3)_2\text{XT}$ (600 MHz, CD_2Cl_2)

The bright yellow $(\text{Ph}_3\text{PN})_2\text{XT}$ ligand is moisture sensitive in solution, but is air- and water-stable as a solid. Solution NMR spectra for $(\text{Ph}_3\text{PN})_2\text{XT}$ (**1**) are consistent with the expected C_{2v} -symmetric structure; a single CMe_2 signal was observed by ^1H (Figure 2.3) and ^{13}C NMR spectroscopy, and the ^{31}P NMR spectrum features a single peak at -1.95 ppm, with a similar chemical shift to other aryl phosphinimines (Figure 2.4).^{83,85} Furthermore, the empirical formula and purity of $(\text{Ph}_3\text{PN})_2\text{XT}$ were confirmed through combustion elemental analysis.

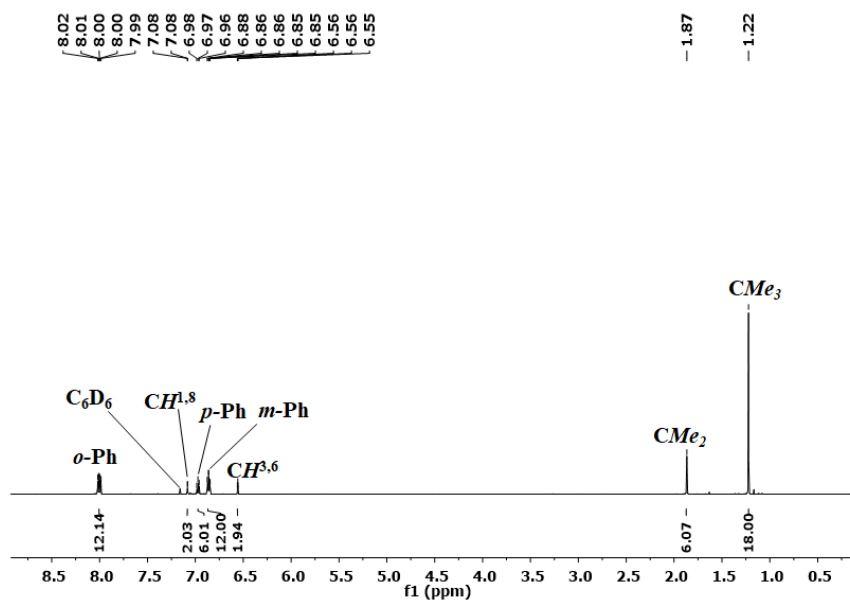


Figure 2.3: ¹H NMR Spectrum of (Ph₃PN)₂XT (1) (600 MHz, C₆D₆)

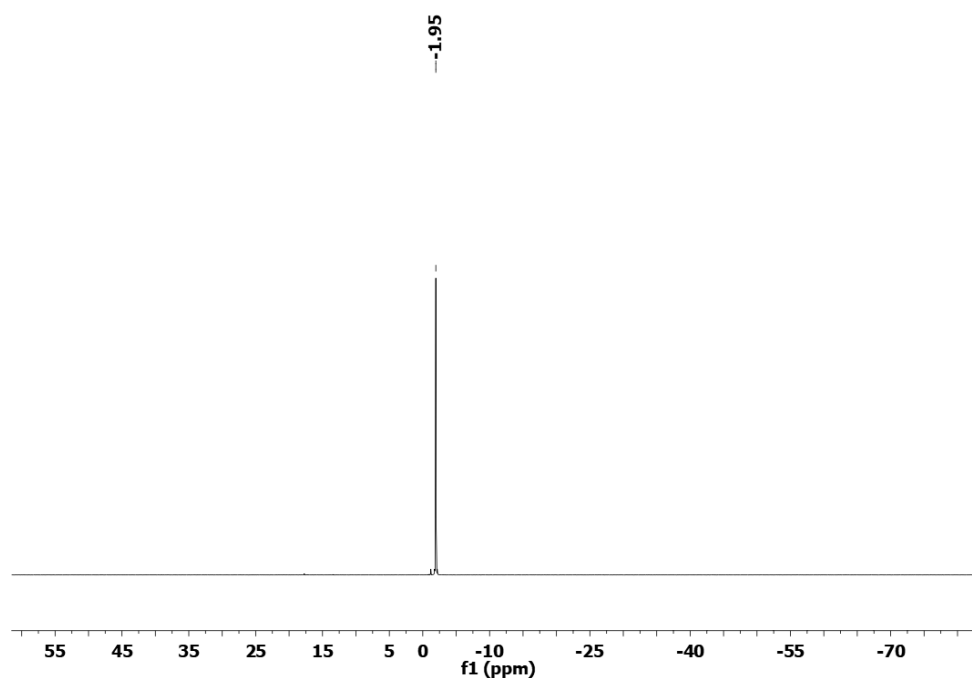
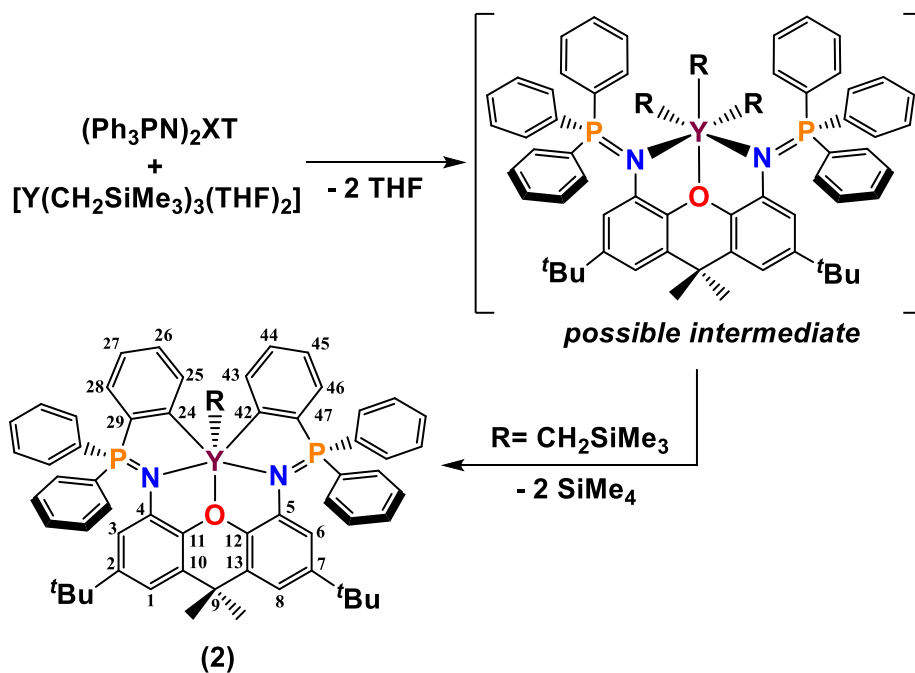


Figure 2.4: ³¹P NMR Spectrum of (Ph₃PN)₂XT (1) (243 MHz, C₆D₆)

2.2 Synthesis of $[(\{\text{Ph}_2(\text{C}_6\text{H}_4)\text{PN}\}_2\text{XT})\text{Y}(\text{CH}_2\text{SiMe}_3)]$

Reaction of $[\text{Y}(\text{CH}_2\text{SiMe}_3)_3(\text{THF})_2]$ with one equiv. of **(1)** in toluene resulted in rapid double cyclometallation, eliminating 2 equiv. of SiMe_4 (Scheme 2.3). This yielded the base-free monoalkyl complex $[(\{\text{Ph}_2(\text{C}_6\text{H}_4)\text{PN}\}_2\text{XT})\text{Y}(\text{CH}_2\text{SiMe}_3)]$ (**(2)**), which was isolated as an analytically pure off-white solid. As noted in the introduction, cyclometallation of multidentate ligands containing neutral $-\text{N}=\text{PAr}_3$ donors has been reported for various rare earth complexes.



Scheme 2.3: Synthesis of $[(\{\text{Ph}_2(\text{C}_6\text{H}_4)\text{PN}\}_2\text{XT})\text{Y}(\text{CH}_2\text{SiMe}_3)]$ (**(2)**)

In solution (C_6D_6 or d^8 -THF), compound **2** is C_s symmetric, resulting in two separate CMe_2 1H and ^{13}C NMR signals; a single ^{31}P NMR signal is seen at 28.85 ppm (d, $^3J_{Y,P}$ 11.4 Hz) in C_6D_6 , at a higher frequency than that of the free ligand (Figures 2.5-2.7). The original $(Ph_3PN)_2XT$ ligand has been cyclometallated at the *ortho* position of a phenyl ring on *each* of the two phosphorus centres, and these equivalent cyclometallated carbon atoms are significantly deshielded, giving rise to a ^{13}C NMR signal at δ 199.63 ppm. This chemical shift is comparable to that in other rare earth aryl complexes.^{99, 100} The YCH_2 1H and ^{13}C NMR signals were observed at 0.19 and 34.68 ppm, respectively, with a $^1J_{C,H}$ coupling constant of 103 Hz, which is smaller than that for a typical sp^3 hybridized carbon atom ($^1J_{C,H}$ = 120-130 Hz), and is characteristic of an α -agostic interaction.^{17, 101, 102}

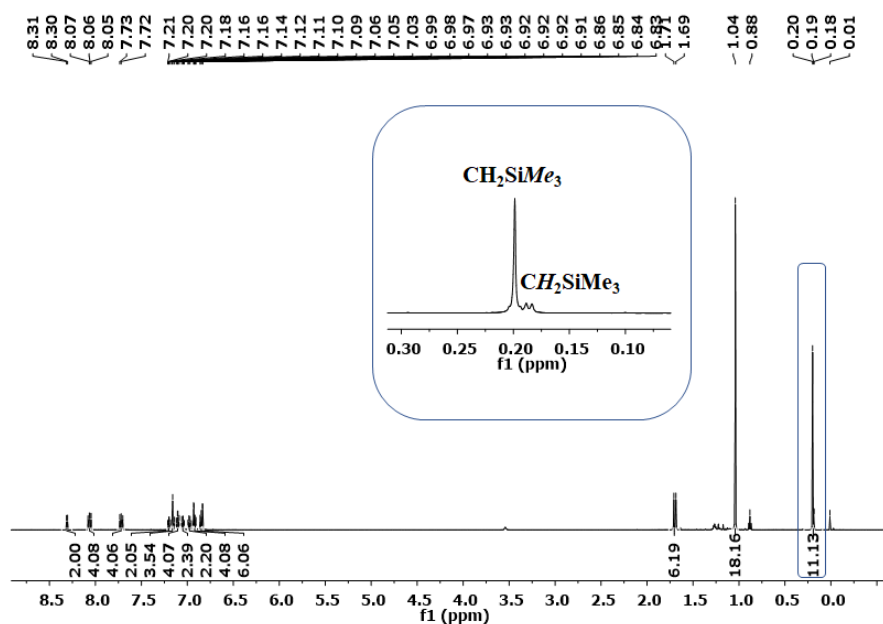


Figure 2.5: 1H NMR Spectrum of $[(\{Ph_2(C_6H_4)PN\}_2XT)Y(CH_2SiMe_3)]$ (**2**) (600 MHz, C_6D_6)

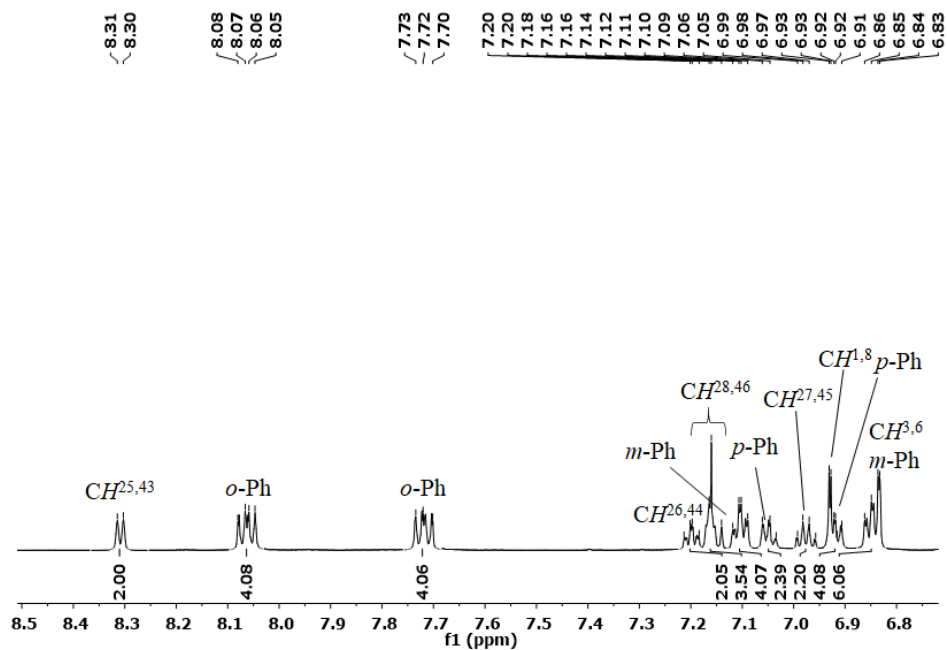


Figure 2.6: ^1H NMR Spectrum of $[(\{\text{Ph}_2(\text{C}_6\text{H}_4)\text{PN}\}_2\text{XT})\text{Y}(\text{CH}_2\text{SiMe}_3)]$ (2) (600 MHz, C_6D_6)

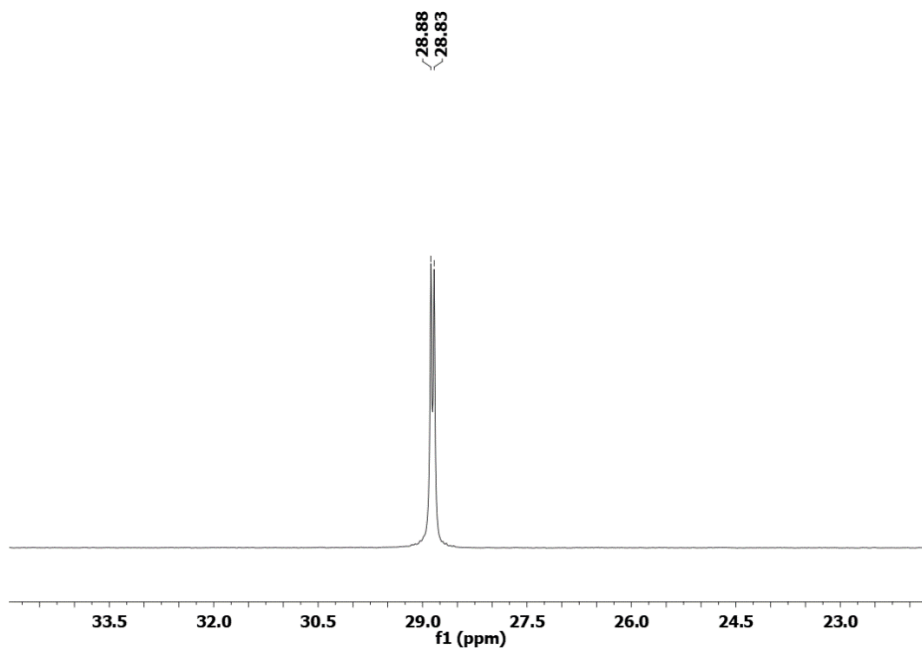


Figure 2.7: ^{31}P NMR Spectrum of $[(\{\text{Ph}_2(\text{C}_6\text{H}_4)\text{PN}\}_2\text{XT})\text{Y}(\text{CH}_2\text{SiMe}_3)]$ (2) (243 MHz, C_6D_6)

Attempts to obtain X-ray quality crystals of base-free **2** were unsuccessful. However, layering a concentrated THF solution of **2** with hexanes at $-28\text{ }^{\circ}\text{C}$ afforded THF-coordinated $[(\{\text{Ph}_2(\text{C}_6\text{H}_4)\text{PN}\}_2\text{XT})\text{Y}(\text{CH}_2\text{SiMe}_3)(\text{THF})]\cdot 2\text{THF}$ (**2-THF** $\cdot 2\text{THF}$) (Figure 2.8). This structure (Figure 2.8) confirmed that cyclometallation had occurred at the *ortho* position of a phenyl ring on each of the two phosphinimine donors, resulting in a series of four edge-sharing 5-membered metallacycles. The coordination geometry of **2-THF** is distorted pentagonal bipyramidal, with the κ^5 -coordinated $\{\text{Ph}_2(\text{C}_6\text{H}_4)\text{PN}\}_2\text{XT}$ ligand in the pentagonal plane, and THF and alkyl ligands in apical positions. Yttrium is located only 0.27 \AA out of the N(1)/O(1)/N(2) plane, displaced in the direction of the alkyl ligand. The aryl donors are coordinated $0.40\text{-}0.69\text{ \AA}$ above and below the plane of the nitrogen and oxygen atoms of the dianion, and the angle between the planes of the two cyclometallated aryl rings is 53° ; this distortion likely occurs in order to minimize unfavorable steric interactions between the *meta-CH* protons on the two rings.

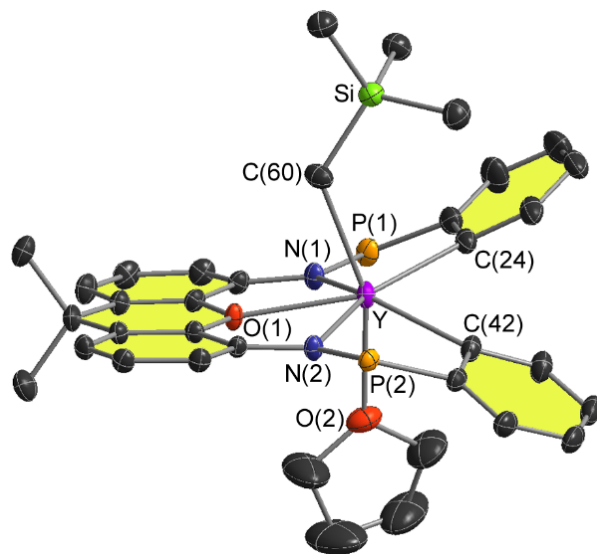


Figure 2.8: X-Ray crystal structure of $[(\{\text{Ph}_2(\text{C}_6\text{H}_4)\text{PN}\}_2\text{XT})\text{Y}(\text{CH}_2\text{SiMe}_3)(\text{THF})] \cdot 2\text{THF}$ (2-THF·2THF). Ellipsoids are set to 50% probability. For clarity, hydrogen atoms, lattice solvent, *tert*-butyl groups, and non-cyclometallated phenyl rings on phosphorus are omitted, and the xanthene backbone and cyclometallated phenyl rings of the $\{\text{Ph}_2(\text{C}_6\text{H}_4)\text{PN}\}_2\text{XT}$ dianion are shaded in yellow. Selected bond lengths (Å) and angles (°): Y–C(60) 2.465(3), Y–C(24) 2.505(3), Y–C(42) 2.541(3), Y–N(1) 2.440(2), Y–N(2) 2.463(2), Y–O(1) 2.459(2), Y–O(2) 2.439(2), N(1)–P(1) 1.613(2), N(2)–P(2) 1.612(2), N(1)–Y–N(2) 131.31(7), Y–C(60)–Si 127.14(1), C(60)–Y–O(1) 79.21(8), C(60)–Y–O(2) 158.54(9).

In complexes of related 4,5-bis(amido)xanthene ligands, the rigidity of the xanthene ligand backbone has been shown to be highly effective in ensuring approximately meridional coordination of the NON-donor array.^{63-66, 68, 96, 103, 104} However, bending at the central non-aromatic ring can still be accommodated, and is most often observed upon coordination to small metal ions such as magnesium(II)

and aluminum(III).^{23, 102} In the case of **2-THF**, the xanthene backbone is essentially planar, with an angle of just 3° between the planes of the two xanthene aryl rings.

The Y–C_{alkyl} distance of 2.465(3) Å falls at the high end of the range reported for neutral yttrium trimethylsilylmethyl complexes (which are more commonly 2.36 to 2.45 Å),¹⁰⁵ presumably due to the high coordination number in **2-THF**. Other trimethylsilylmethyl complexes with similar Y–C distances include [{(Me₂N{CH₂}₂)₂N(CH₂)₂N'Bu}Y(CH₂SiMe₃)₂] (Y–C = 2.463(2) Å),¹⁰⁶ [{}ⁱPr₂TACN(SiMe₂)N'Bu}Y(CH₂SiMe₃)₂] (Y–C = 2.465(4) Å; TACN = 1,4,7-triazacyclononane),¹⁰⁷ and [Cp*Y(CH₂SiMe₃){CH(pz')₂}(THF)] (Y–C = 2.462(2) Å; pz' = 3,5-dimethylpyrazolyl) (Figure 2.9).¹⁰⁸ The Y–C(60)–Si bond angle in **2-THF** is 127.1(1)°, which is larger than typically observed for an sp³ hybridized carbon atom. This is suggestive of an α-agostic interaction, consistent with the small ¹J_{C,H} NMR coupling constant measured for the YCH₂ group of **2** in solution (*vide supra*). The Y–C_{aryl} bonds are 2.505(3) and 2.541(3) Å, again at the upper end of the usual range,¹⁰⁵ likely due to the high coordination number, combined with constraints associated with pentadentate coordination of the rigid ligand framework.

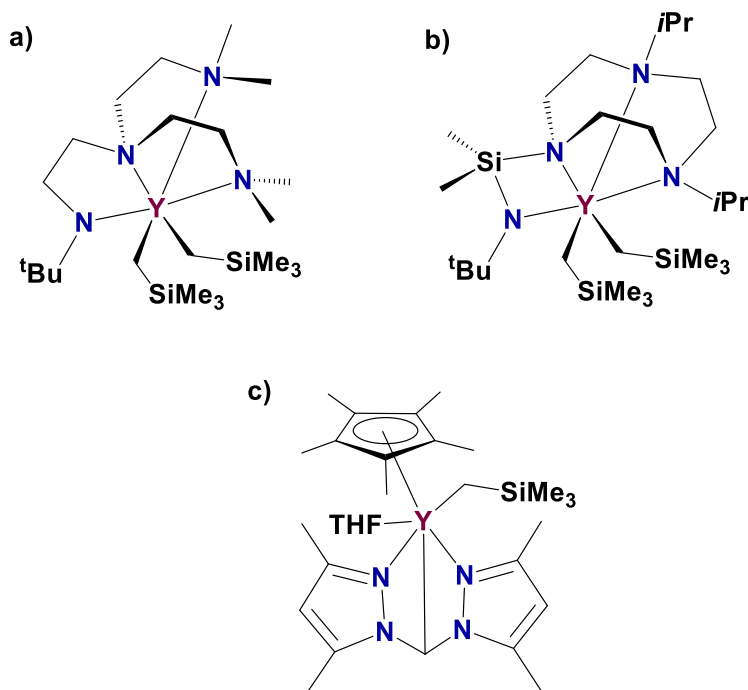


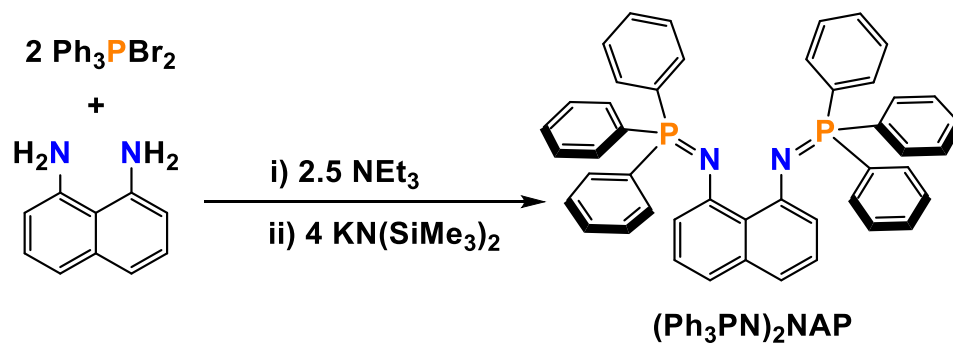
Figure 2.9: Literature Examples With Similar Y-C Bond Distances to (2-THF): a) $[\{(Me_2N\{CH_2\}_2)_2N(CH_2)_2N^tBu\}Y(CH_2SiMe_3)_2]$, b) $[\{iPr_2TACN(SiMe_2)N^tBu\}Y(CH_2SiMe_3)_2]$, c) $[Cp^*Y(CH_2SiMe_3)\{CH(pz')_2\}(THF)]$

The P–N bond distances are 1.61(2) Å; similar to those in related group 3 phosphinimine complexes.^{73, 76, 83} These P–N distances are slightly elongated in comparison to those in uncomplexed phosphinimine ligands, which typically range from 1.56 to 1.58 Å,^{76, 83-85} suggesting some contribution from the zwitterionic resonance structure (with a positive charge on phosphorus and a negative charge on nitrogen). The Y–N bond distances {2.440(2) and 2.463(2) Å} lie at the higher end of the range reported for yttrium phosphinimine complexes,¹⁰⁵ again likely due to

the high coordination number in **2-THF**, combined with constraints imposed by the ligand framework. Similarly, the Y–O(1) distance to the xanthene backbone is 2.459(2) Å, which is longer than that in previously reported [(XN₂)Y(CH₂SiMe₃)(THF)]·O(SiMe₃)₂ {Y–O_{xant} = 2.347(2) Å},²³ which features the same xanthene backbone. The Y–O(2) bond to THF {2.439(2) Å} is only slightly shorter than Y–O(1), and falls within the usual range.¹⁰⁵

2.3 Synthesis of (Ph₃PN)₂NAP

Given that coordination of the (Ph₃PN)₂XT ligand to yttrium resulted in rapid double cyclometallation to afford a κ⁵-coordinated Ph₂(C₆H₄)PN₂XT dianion (*vide supra*), we conjectured that a ligand backbone which reduces the distance between the phosphinimine donors (i.e. a ligand with a smaller metal binding pocket) may disfavor double cyclometallation, affording a mono-cyclometallated dialkyl yttrium complex. Therefore, the synthesis and complexation of a naphthalene-backbone bis-phosphinimine ligand, (Ph₃PN)₂NAP (**3**), was undertaken and was confirmed by solution NMR (Figures 2.10-2.11) and combustion analysis. This ligand was synthesized using a modified version of the literature preparation (Scheme 2.4).¹⁰⁹



Scheme 2.4: Synthesis of the $(\text{Ph}_3\text{PN})_2\text{NAP}$ ligand (3) using the Kirsanov reaction

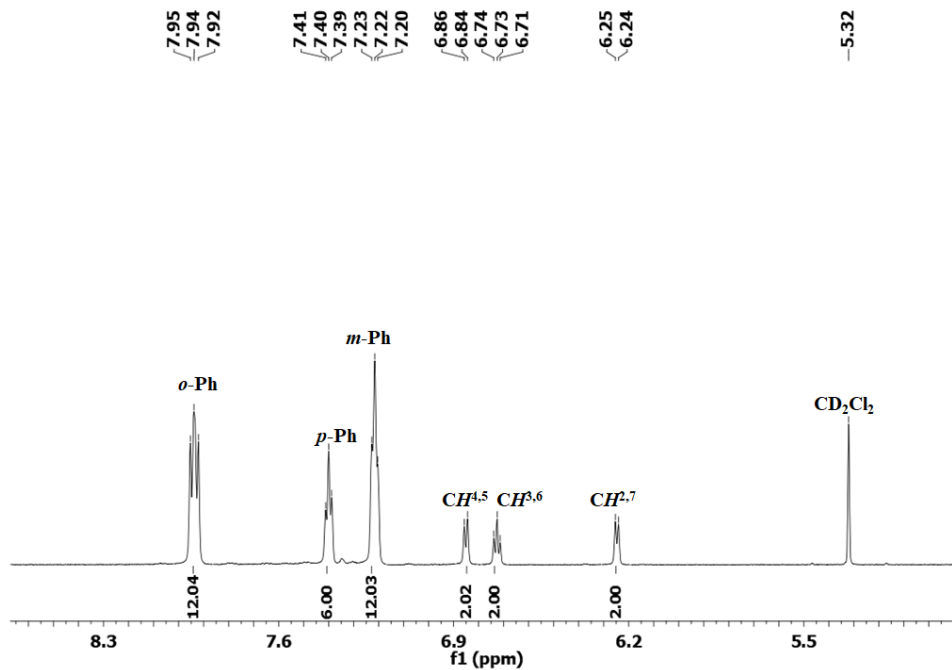


Figure 2.10: ^1H NMR Spectrum of $(\text{Ph}_3\text{PN})_2\text{NAP}$ (3) (600 MHz, C_6D_6)

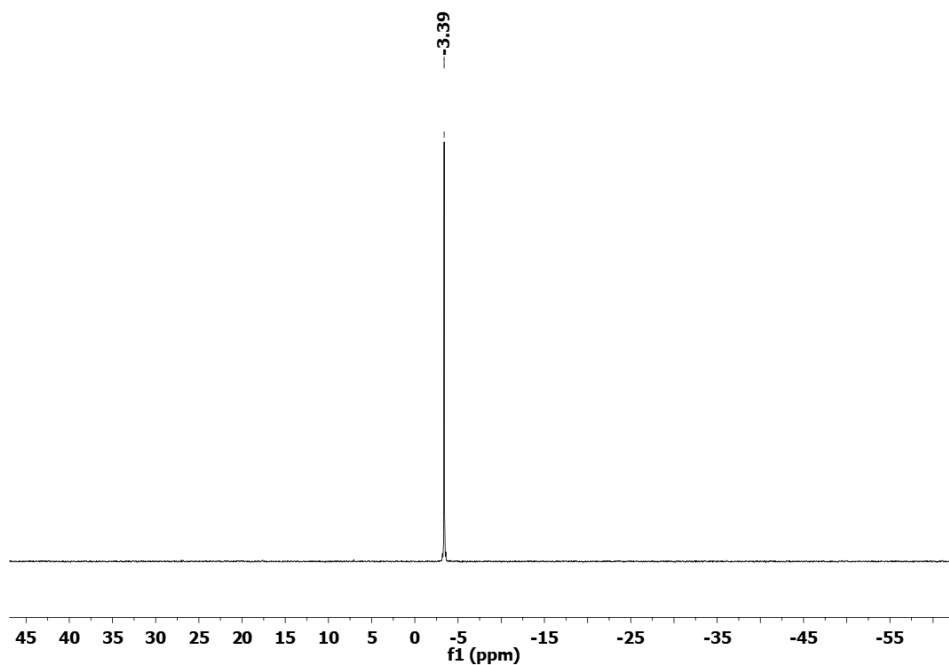
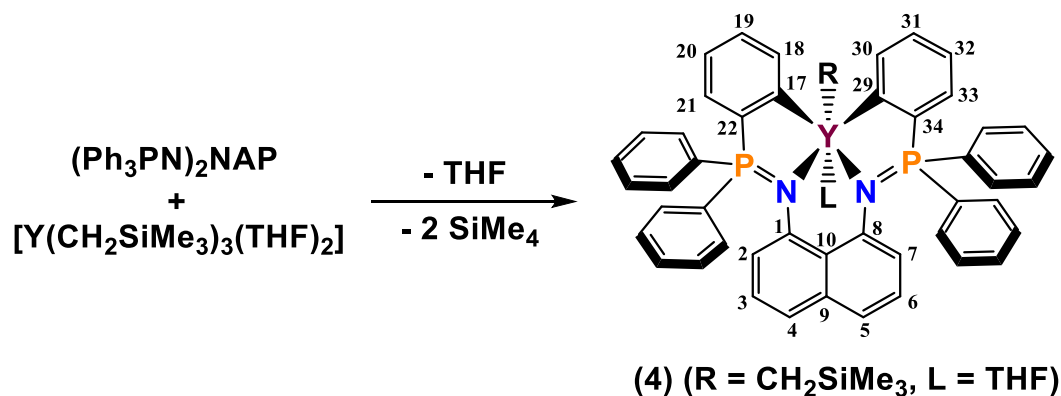


Figure 2.11: ^{31}P NMR Spectrum of $(\text{Ph}_3\text{PN})_2\text{NAP}$ (**3**) (243 MHz, C_6D_6)

2.4 Synthesis of $[(\{\text{Ph}_2(\text{C}_6\text{H}_4)\text{PN}\}_2\text{NAP})\text{Y}(\text{CH}_2\text{SiMe}_3)(\text{THF})](2\text{-THF})$

Similar to the reactivity of $[\text{Y}(\text{CH}_2\text{SiMe}_3)_3(\text{THF})_2]$ with $(\text{Ph}_3\text{PN})_2\text{XT}$, reaction of $[\text{Y}(\text{CH}_2\text{SiMe}_3)_3(\text{THF})_2]$ with 1 equiv. of $(\text{Ph}_3\text{PN})_2\text{NAP}$ afforded a doubly cyclometallated monoalkyl yttrium complex, $[(\{\text{Ph}_2(\text{C}_6\text{H}_4)\text{PN}\}_2\text{NAP})\text{Y}(\text{CH}_2\text{SiMe}_3)(\text{THF})]$ (**4-THF**; Scheme 2.5). However, unlike base-free **1**, THF could not be removed from **4-THF** in vacuo at room

temperature. Furthermore, **4-THF** decomposed to unidentified products at room temperature; over several hours in solution, and several days in the solid state.



Scheme 2.5: Synthesis of $[(\{\text{Ph}_2(\text{C}_6\text{H}_4)\text{PN}\}_2\text{NAP})\text{Y}(\text{CH}_2\text{SiMe}_3)(\text{THF})]$ (**4-THF**)

Room temperature NMR spectra of compound **4-THF** are indicative of C_s symmetry, with a single ^{31}P NMR signal at 28.49 ppm (d, $^2J_{89\text{Y},31\text{P}}$ 12 Hz), and two sets of peaks for the intact phenyl rings on phosphorus (Figures 2.12-2.14). Again, cyclometallation was found to have occurred at the *ortho* position of a phenyl ring on each of the two phosphinimine donors, and the ^{13}C NMR chemical shift for the cyclometallated carbon was 197.52 ppm. The YCH_2 ^1H and ^{13}C NMR signals were located at -0.15 and 30.82 ppm, respectively, with a small $^1J_{\text{C,H}}$ coupling constant

of 102 Hz (nearly identical to that in **2**), indicative of an α -agostic interaction.^{17, 101,}

102

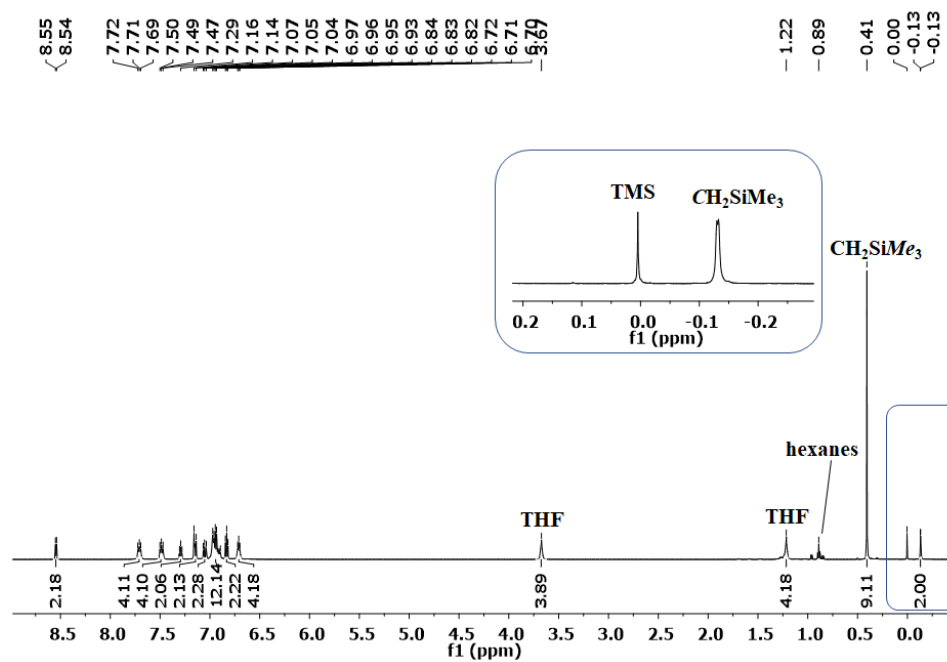


Figure 2.12: ¹H NMR Spectrum of [(Ph₂(C₆H₄)PN)₂NAP]Y(CH₂SiMe₃)(THF) (4-THF) (600 MHz, C₆D₆)

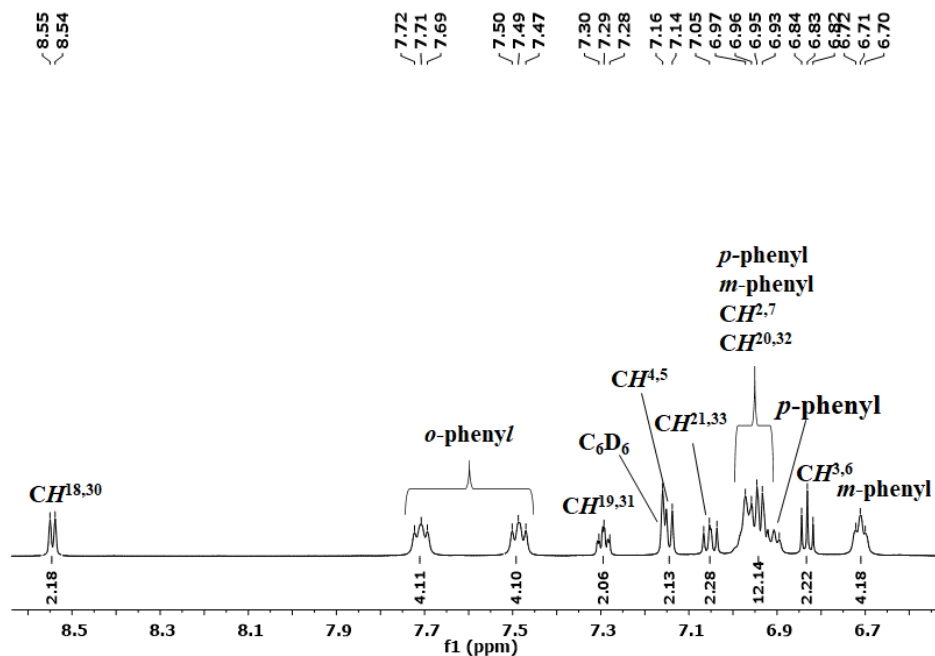


Figure 2.13: Expanded Region - ^1H NMR Spectrum of $[(\{\text{Ph}_2(\text{C}_6\text{H}_4)\text{PN}\}_2\text{NAP})\text{Y}(\text{CH}_2\text{SiMe}_3)(\text{THF})]$ (4-THF)(600 MHz, C_6D_6)

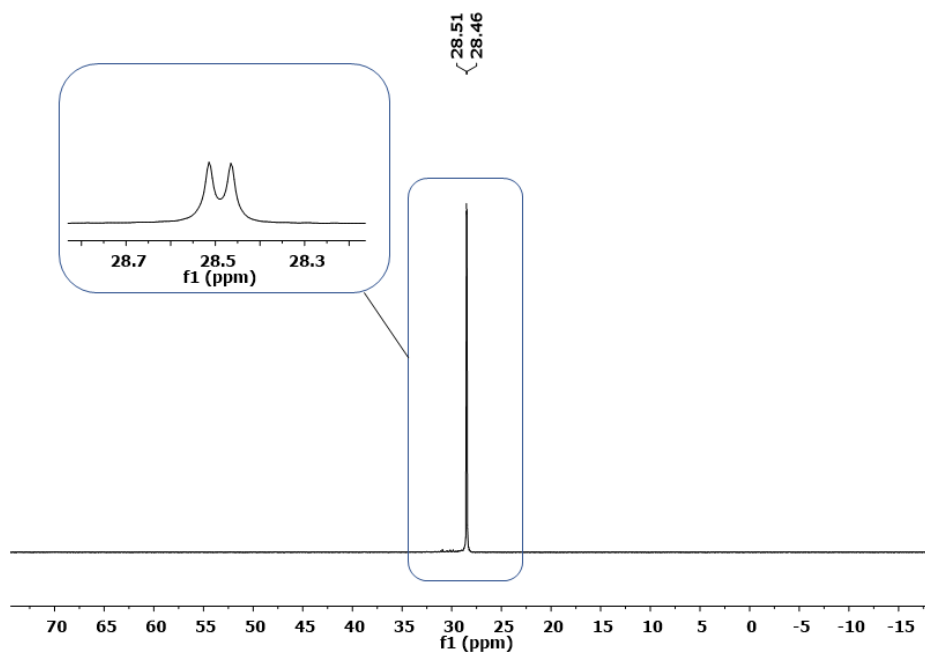


Figure 2.14: ^{31}P NMR Spectrum of $[(\{\text{Ph}_2(\text{C}_6\text{H}_4)\text{PN}\}_2\text{NAP})\text{Y}(\text{CH}_2\text{SiMe}_3)(\text{THF})]$ (4-THF)(243 MHz, C_6D_6)

X-ray quality crystals of **4-THF** proved elusive. However, crystals of $[\{(\text{Ph}_2(\text{C}_6\text{H}_4)\text{PN})_2\text{NAP}\}\text{Y}(\text{CH}_2\text{SiMe}_3)(\kappa^2\text{-DME})]\cdot\text{hexane}$ (**4-DME**·hexane) were obtained from DME/hexanes at $-28\text{ }^\circ\text{C}$ (Figure 2.15). Complex **4-DME** is 7-coordinate (Figure 2.15), and can be described as a highly distorted pentagonal bipyramid, with the alkyl ligand and one of the aryl groups [C(29)] in axial sites. However, unlike the structure of **2-THF**, yttrium lies 1.53 \AA out of the N(1)/C(9)/N(2) plane (cf. 0.27 \AA out of the N(1)/O(1)/N(2) plane in **2-THF**). Effectively, the tetradentate $(\text{Ph}_2(\text{C}_6\text{H}_4)\text{PN})_2\text{NAP}$ dianion adopts a facial coordination mode, whereas the pentadentate $(\text{Ph}_2(\text{C}_6\text{H}_4)\text{PN})_2\text{XT}$ ligand coordinates meridionally.

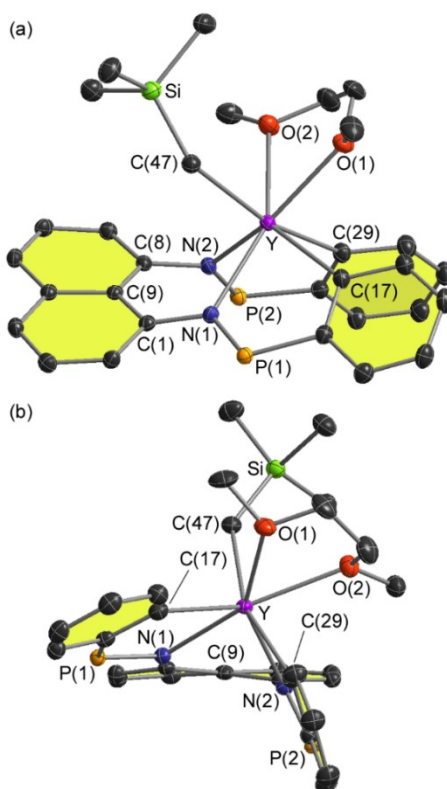


Figure 2.15: Two views of the X-ray crystal structure of $[(\{\text{Ph}_2(\text{C}_6\text{H}_4)\text{PN}\}_2\text{NAP})\text{Y}(\text{CH}_2\text{SiMe}_3)(\text{DME})]\cdot\text{hexane}$ (**4-DME**·hexane). Ellipsoids are set to 50% probability. For clarity, hydrogen atoms, lattice solvent, and non-cyclometallated phenyl rings on phosphorus are omitted, and the naphthalene backbone and cyclometallated phenyl rings of the $\{\text{Ph}_2(\text{C}_6\text{H}_4)\text{PN}\}_2\text{NAP}$ dianion are shaded in yellow. Selected bond lengths (Å) and angles (°): Y–C(47) 2.520(2), Y–C(17) 2.508(2), Y–C(29) 2.562(2), Y–N(1) 2.518(2), Y–N(2) 2.401(2), Y–O(1) 2.493(2), Y–O(2) 2.534(2), N(1)–P(1) 1.632(1), N(2)–P(2) 1.613(2), N(1)–Y–N(2) 70.69(6), Y–C(47)–Si 139.18(1), C(29)–Y–C(47) 161.70(8), C(17)–Y–C(47) 111.12(8).

The Y–C_{aryl} bonds in **4-DME** are 2.508(2) Å [Y–C(17)] and 2.562(2) Å [Y–C(29)], giving an average Y–C_{aryl} distance which is nearly identical to that in compound **2-THF**. By contrast, the Y–C(47) distance is 2.520(2) Å, which is even longer than the corresponding Y–C_{alkyl} distance in **2-THF** {2.465(3) Å}. This can be attributed to the high *trans* influence of the aryl group in the opposing axial site {C(47)–Y–C(29) = 161.70(8)°}, possibly combined with increased steric hindrance resulting from the smaller binding pocket and differently-placed steric bulk of the naphthalene-backbone ligand. The Y–C(47)–Si angle is also notably obtuse, at 139.2(1)°, indicative of an α -agostic interaction, in keeping with the solution NMR data for **4-THF** (*vide supra*). However, given that the $^1J_{\text{C,H}}$ NMR coupling constants for the YCH₂ groups in **2** and **4-THF** are nearly identical, the significantly more obtuse Y–C–Si angle in **4-DME** {cf. 127.1(1)° in **2-THF**} is also suggestive of appreciable steric hindrance. Moreover, steric hindrance is likely responsible for the long Y–O_{DME} distances of 2.493(2) and 2.534(2) Å in **4-DME** {cf. 2.439(2) Å for the Y–O_{THF} bond in **2-THF**}.

The P–N bonds are 1.613(2) and 1.632(2) Å, comparable to those in compound **2-THF**. However, the Y–N(1) and Y–N(2) distances are 2.518(2) and 2.401(2) Å; both longer and shorter than those in **2-THF** {2.440(2) and 2.463(2) Å}. The substantial difference between the Y–N distances in **4-DME** presumably stems from constraints imposed by the ligand framework, which enforces a non-ideal orientation of the lone pair on N(1) relative to yttrium {Y lies 0.59 Å out of the P(1)/N(1)/C(1) plane, compared to 0.03 Å out of the P(2)/N(2)/C(8) plane}.

2.5 Investigation of Intramolecular Hydroamination and Ethylene Polymerization Catalysis - [(Ph₂(C₆H₄)PN)₂NAP)Y(CH₂SiMe₃)(THF)](**2-THF**) and [(Ph₂(C₆H₄)PN)₂XT)Y(CH₂SiMe₃)]

Due to a coordination number of 6 at yttrium, neither **2** nor **4-THF** is active for ethylene polymerization (20 °C, 1 atm). Furthermore, addition of hydroamination substrates resulted in protonation of the aryl anions in the cyclometallated ligands and release of free (Ph₃PN)₂XT or (Ph₃PN)₂NAP. However, to the best of our knowledge, **2** and **4-THF** are the first isolated examples of monometallic rare earth alkyl diaryl complexes.¹¹⁰

2.6 Summary and Conclusions

The rigid xanthene-backbone bis(phosphinimine) ligand, $(\text{Ph}_3\text{PN})_2\text{XT}$, was synthesized in 2 steps (one pot) from 4,5-dibromo-2,7-di-*tert*-butyl-9,9-dimethylxanthene, and a modified synthesis is provided for the $(\text{Ph}_3\text{PN})_2\text{NAP}$ ligand. Both bis(phosphinimine) ligands reacted with $[\text{Y}(\text{CH}_2\text{SiMe}_3)_3(\text{THF})_2]$ to afford doubly cyclometallated monoalkyl yttrium complexes, $[(\{\text{Ph}_2(\text{C}_6\text{H}_4)\text{PN}\}_2\text{XT})\text{Y}(\text{CH}_2\text{SiMe}_3)]$ (**2**) and $[(\{\text{Ph}_2(\text{C}_6\text{H}_4)\text{PN}\}_2\text{NAP})\text{Y}(\text{CH}_2\text{SiMe}_3)(\text{THF})]$ (**4-THF**). Compound **2** is thermally stable at room temperature, whereas **4-THF** slowly decomposed in solution and in the solid state. Crystals of 7-coordinate **2-THF** and **4-DME** were obtained from THF/hexanes and DME/hexanes, respectively. The geometry of **2-THF** is approximately pentagonal bipyramidal, with the pentadentate $(\text{Ph}_2(\text{C}_6\text{H}_4)\text{PN})_2\text{XT}$ dianion coordinating meridionally. By contrast, the $(\text{Ph}_2(\text{C}_6\text{H}_4)\text{PN})_2\text{NAP}$ dianion in **4-DME** adopts a facial coordination mode, resulting in a very different steric environment at the metal, and different co-ligand placement. These differences in coordination mode presumably stem from changes in the distance between the nitrogen atom attachment points on the ligand backbone (4.75 Å in $\text{Ph}_2(\text{C}_6\text{H}_4)\text{PN}\}_2\text{XT}$ vs 2.59 Å in $\text{Ph}_2(\text{C}_6\text{H}_4)\text{PN}\}_2\text{NAP}$), with the shorter distance preventing meridional coordination of the N- and C-donor atoms (due to a binding pocket of insufficient size).

Chapter 3

Neutral and Cationic Group 3 Alkyl Complexes of a Rigid Monoanionic NNN-Donor Pincer Ligand: Synthesis and Intramolecular Hydroamination Activity

3.1 Introduction

Pincer ligands have been used to great effect in the development of late transition metal organometallic chemistry and homogeneous catalysis, and have recently seen increased application in early transition metal and f-element chemistry.^{62, 111} Within this class of ligand, those based on a tricyclic backbone composed of three 6-membered rings (e.g. anthracene, acridine, xanthene or acridan) can provide a particularly rigid coordination environment, and dianionic 4,5-bis(arylamido)xanthene (e.g. XA_2 and XN_2 ; Figure 1.29) have been shown to be highly effective for the isolation of reactive organometallic complexes. For example, our group has used the XA_2 and XN_2 dianions to prepare the first non-cyclopentadienyl thorium alkyl cations,⁶⁸ a unique example of a thorium dication accessed via double alkyl group abstraction,⁶⁶ a range of uranium(IV) dialkyl complexes,⁶⁵ a cationic zirconium alkyl cation with high activity for ethylene polymerization,⁶⁴ and neutral yttrium and lutetium monoalkyl complexes with high activity for

intra- and intermolecular hydroamination.^{23, 97} Furthermore, the XA_2 ligand was recently employed by Goicoechea and Aldridge *et al.* for the synthesis of an anionic aluminium(I) nucleophile, $[(\text{XA}_2)\text{Al}]^-$, which provided access to unique C–H bond activation chemistry,¹¹² reactive monometallic aluminium imide¹¹³ and oxo¹¹⁴ complexes, and a nucleophilic gold complex.¹¹⁵ Additionally, low-valent cobalt and iron complexes of a related 4,5-bis(silylamido)xanthene ligand were recently reported by the Tilley group, extending the chemistry of this ligand class to the late transition metals.¹¹⁶

A limitation of 4,5-bis(amido)xanthene ligands is that their 2– charge does not allow for the synthesis of cationic alkyl complexes of the rare earth elements. Such cationic complexes are of interest as catalysts for alkene polymerization and hydroelementation and would be accessible using a monoanionic analogue of the XA_2 ligand. One strategy to access such a ligand would be to switch from a neutral xanthene backbone with flanking anionic donors to an anionic acridanide backbone with flanking neutral donors (Figure 3.1). However, to maintain high rigidity analogous to that in XA_2 , the flanking donor atoms must be attached directly to the ligand backbone, and most neutral donors do not exhibit cyclometallation resistance comparable to that of ubiquitous 2,6-diisopropylanilido donors. For example, in an initial foray into the synthesis of a monoanionic NNN-donor pincer ligand, we

prepared the Alm_2 anion (Figure 3.1) with neutral $-\text{N}=\text{CPh}_2$ donors on an acridanide backbone. However, reaction with $[\text{Y}(\text{CH}_2\text{SiMe}_3)_3(\text{THF})_2]$ resulted in rapid cyclometallation, concomitant with coordination.¹¹⁷

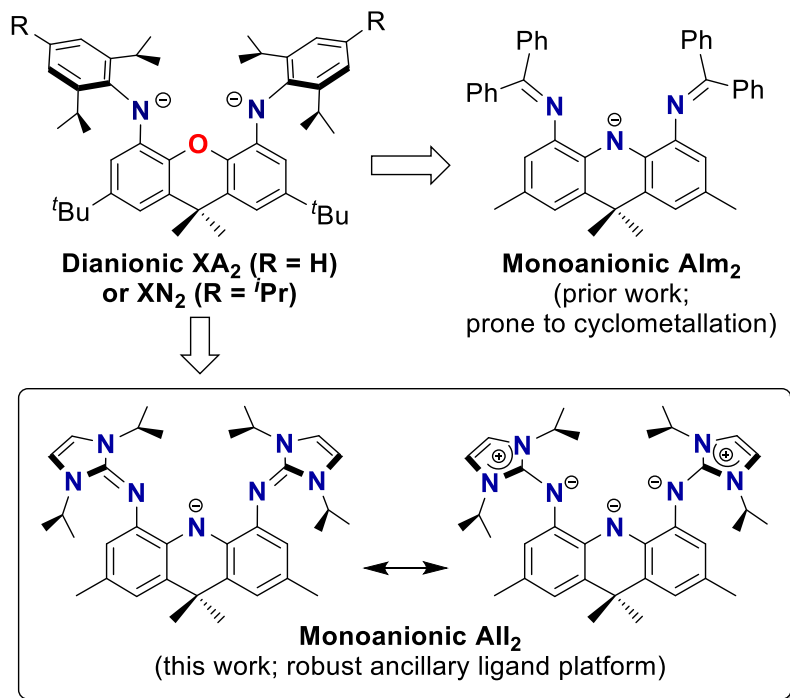


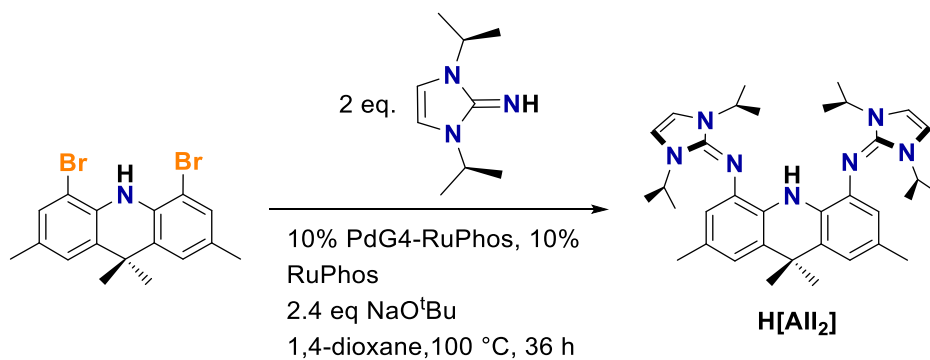
Figure 3.1: Relationship between the dianionic XA_2 ligand and the monoanionic Alm_2 and All_2 ligand

As a more robust alternative, we envisaged a ligand featuring neutral 1,3-diisopropylimidazol-2-imine $\{-\text{N}=(\text{NHC}); \text{NHC} = 1,3\text{-diisopropylimidazol-2-ylidene}\}$ donors in the 4 and 5-positions of an acridanide backbone (All_2 ; Figure 3.1), where a zwitterionic resonance structure can be expected to allow the imidazole rings to lie perpendicular to the plane of the acridanide

backbone, providing a steric profile similar of that of the XA_2 dianion (albeit with isopropyl groups slightly further removed from the metal coordination pocket due to their attachment in the *ortho* positions of a 5-membered rather than a 6-membered ring). Herein we describe the synthesis of the aforementioned AlI_2 ligand (as the protio ligand), alkane elimination reactions to afford room temperature-stable scandium and yttrium dialkyl complexes, generation of a monoalkyl yttrium cation, and a comparison of the catalytic activity of the neutral dialkyl and cationic monoalkyl yttrium complexes for intramolecular alkene hydroamination.

3.2 Synthesis of $\text{H}[\text{AlI}_2]$

The $\text{H}[\text{AlI}_2]$ pro-ligand was synthesized via Pd-catalyzed imination of $\text{H}[\text{ABr}_2]$ with two equivalents of 1,3-diisopropylimidazol-2-imine (Scheme 3.1). Imination reactions utilizing $\text{Ph}_2\text{C}=\text{NH}$ are commonplace, but reactions with other imine substrates have seldom been reported.⁹³ In this work, a 4th generation Ruphos catalyst,¹¹⁸ combined with a high temperature and an extended reaction time was required to access $\text{H}[\text{AlI}_2]$ in good yield.



Scheme 3.1: Synthesis of H[AlI₂] (5) pro-ligand

The room temperature ¹H NMR (Figure 3.2) and ¹³C NMR spectra of H[AlI₂] are consistent with the expected structure, with four equivalent isopropyl groups due the accessibility of the zwitterionic resonance form. The NH signal was observed at δ 8.39 ppm.

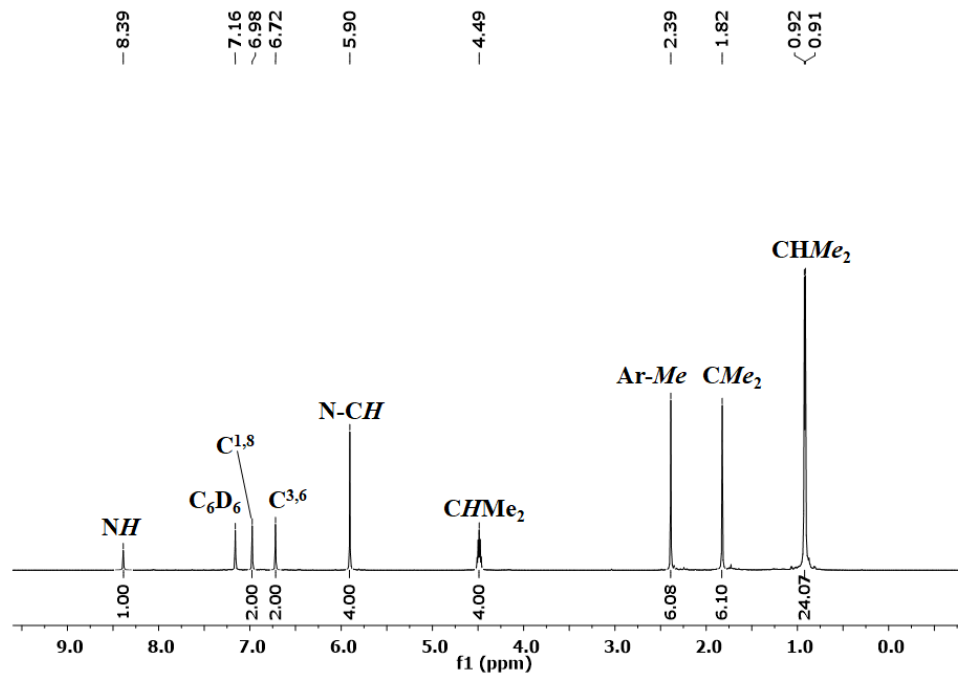
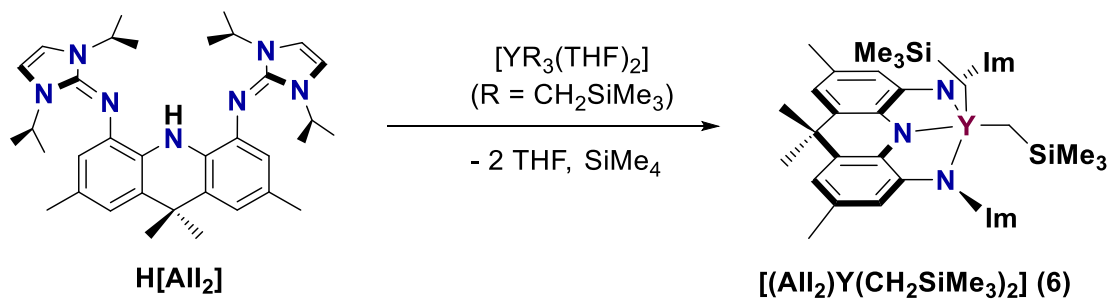


Figure 3.2: ^1H NMR Spectrum of $\text{H}[\text{AlI}_2]$ (600 MHz, C_6D_6)

3.3 Synthesis of $[(\text{AlI}_2)\text{Y}(\text{CH}_2\text{SiMe}_3)_2]$

Reaction of $\text{H}[\text{AlI}_2]$ with one equivalent of $[\text{Y}(\text{CH}_2\text{SiMe}_3)_3(\text{THF})_2]$ yielded the base-free neutral dialkyl complex $[(\text{AlI}_2)\text{Y}(\text{CH}_2\text{SiMe}_3)_2]$ (**6**) as an analytically pure brown solid (Scheme 3.2).



Scheme 3.2: Synthesis of $[(\text{AlI}_2)\text{Y}(\text{CH}_2\text{SiMe}_3)_2]$ (6**)**

$[(\text{AlI}_2)\text{Y}(\text{CH}_2\text{SiMe}_3)_2]$ (**6**) is stable at room temperature, with apparent C_{2v} symmetry as evidenced by a single CMe_2 and CMe_3 peak in the ^1H and ^{13}C NMR spectra (Figure 3.3). The YCH_2 ^1H and ^{13}C NMR signals were located at -0.81 and 28.32 ppm ($^1J_{^{13}\text{C},89\text{Y}}$ 36 Hz; $^2J_{^1\text{H},89\text{Y}}$ 2 Hz) for **6**. The $^1J_{\text{C,H}}$ coupling constant for the YCH_2 signal in **6** is 101 Hz, which is smaller than that for a typical sp^3 hybridized carbon atom ($^1J_{\text{C,H}} = 120 - 130$ Hz), suggestive of an α -agostic interaction.^{101, 102}

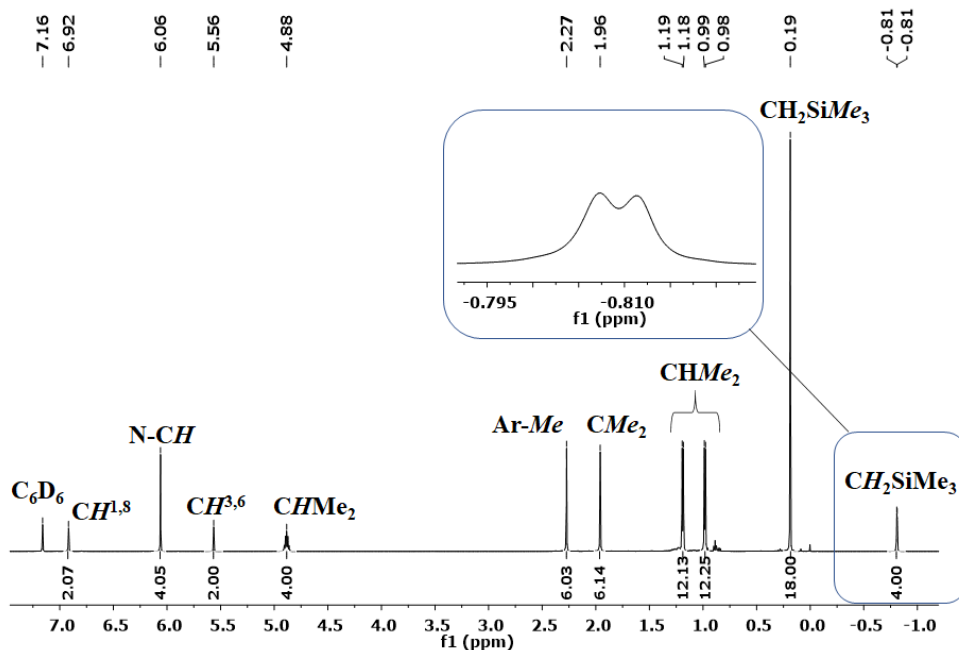


Figure 3.3: ^1H NMR Spectrum of $[(\text{AlI}_2)\text{Y}(\text{CH}_2\text{SiMe}_3)_2]$ (**6**) (600 MHz, C_6D_6)

X-ray quality crystals of **6** were grown from toluene at $-28\text{ }^\circ\text{C}$ (Figure 3.4). In complex **6**, the AlI_2 ligand is κ^3 -coordinated with an angle of 28.6° between the two aryl rings of the acridanide backbone. The metal is 5-coordinate, with one alkyl group $\{\text{C}(36)\}$ located between the flanking imidazole rings, whereas the other $\{\text{C}(40)\}$ is located below the plane, flanked by isopropyl groups. Consequently, the imidazole rings are oriented so as to minimize unfavorable steric interactions between the alkyl group below the plane and the flanking isopropyl groups, resulting in unequal $\text{C}(21)\cdots\text{C}(30)$ and $\text{C}(24)\cdots\text{C}(33)$ distances of 6.55 and 8.21 Å in **6**.

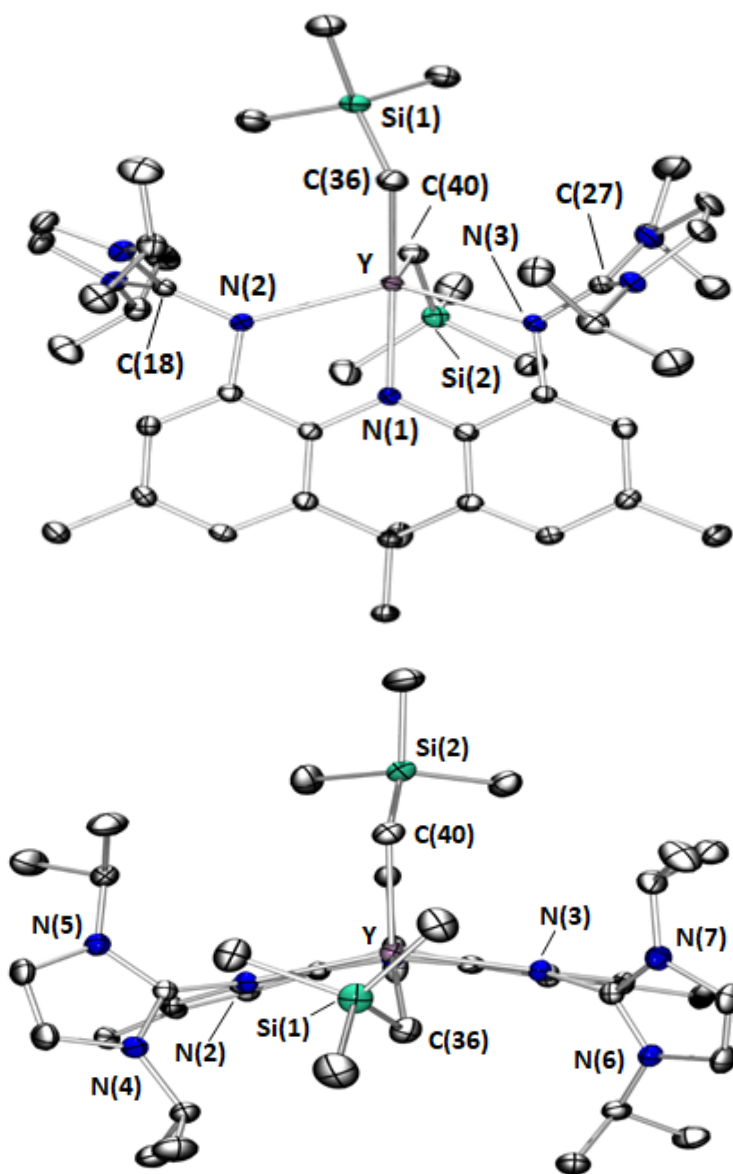


Figure 3.4: Two views of the X-ray crystal structure $[(AlH_2)Y(CH_2SiMe_3)_2]$ (6) Ellipsoids are set to 50% probability. For clarity, hydrogen atoms have been omitted. Selected bond lengths (Å) and angles (°): Y–N(1) 2.288(2), Y–N(2) 2.421(2), Y–N(3) 2.394(2), Y–C(36) 2.482(2), Y–C(40) 2.434(2), N(2)–C(18) 1.362(2), N(3)–C(27) 1.364(2), N(4)–C(18) 1.358(2), N(5)–C(18) 1.364(2), N(6)–C(27) 1.362(2), N(7)–C(27) 1.364(2), N(1)–Y–N(2) 69.26(5), N(1)–Y–N(3) 69.63(5), C(36)–Y–C(40) 110.48(7), Y–C(36)–Si(1) 115.98(9), Y–C(40)–Si(2) 118.55(9)

In compound **6**, the Y–C distances are 2.434(2) and 2.482(2) Å, which lie at the upper end of the range for monometallic yttrium trimethylsilylmethyl complexes (which are commonly 2.36 to 2.47 Å). The Y–N(1) distance to the central amido donor is 2.288(2) Å, whereas the Y–N(2) and Y–N(3) bond lengths are 2.421(2) and 2.394(2) Å, consistent with weaker coordination of the neutral imidazol-2-imine donors. The Y–N_{imine} distances in **6** are shorter than the Y–N_{imine} distances of 2.475(5) and 2.494(4) Å of the intact AIm₂ ligand in [Y(AIm₂)(AIm₂')] (AIm₂' is a cyclometallated AIm₂ ligand),¹¹⁷ but longer than the Y–N_{imine} distances of 2.381(2) and 2.358(2) Å in Tamm's [$\{2,6\text{-C}_5\text{H}_3\text{N}(\text{CH}_2\text{N}=\{\text{NHC}\})_2\}\text{YCl}_3$] (NHC = 1,3-di-*tert*-butylimidazol-2-ylidene).⁹⁰ The Y–C–Si angles {115.98(9)° and 118.55(9)°} in **6** are slightly obtuse (larger than the ideal sp³ carbon angle of 109.5°) and suggesting a potential α -agostic interaction.

The N(2)–C(18) and the N(3)–C(27) bond distances in **6** range from 1.362(2) and 1.357(2) Å, which is significantly longer than in free imidazole-2-imines. For example, the N=C distances in the free imine donors in (NHC)=N{C₆H₄(OMe)-*p*} (NHC = 1,3-diisopropyl-4,5-dimethylimidazol-2-ylidene)¹¹⁹ and [$\{\kappa^2\text{-}2,6\text{-C}_5\text{H}_3\text{N}(\text{CH}_2\text{N}=\{\text{NHC}\})_2\}\text{FeCl}_2$] (NHC = 1,3-di-*tert*-butylimidazol-2-ylidene)¹²⁰ are 1.308(2) and 1.294(3) Å, respectively. Furthermore, the endocyclic N–C(18) and N–C(27) distances in **6** are comparable to N(2)–C(18) and N(3)–C(27), ranging from 1.358(2) to 1.364(2) Å. These features, in combination with the roughly perpendicular

orientation of the imidazole rings relative to the adjacent aryl ring of the acridanide backbone (interplanar angles of 63.5° and 82.5°) in **6**, are indicative of a substantial contribution from the zwitterionic resonance structure with negative charges on N(2) and N(3).

The uranium(IV) complex $[(XA_2)U(CH_2SiMe_3)_2]$ (b in Figure 3.5) provides an opportunity to compare the steric profiles of the monoanionic AlI_2 and dianionic XA_2 ligands, given that the ionic radii of yttrium(III) and uranium(IV) are nearly identical (0.90 vs 0.89 Å). Qualitatively, the structures of **6** and $[(XA_2)U(CH_2SiMe_3)_2]$ (which contains two independent but qualitatively isostructural molecules in the unit cell) are similar, and the C–N–C angles around the flanking nitrogen donors are nearly identical (114 – 121°). However, the N \cdots N distance between the flanking nitrogen donors is substantially shorter (ave. 4.00 Å for the uranium XA_2 vs 4.42 Å for the yttrium AlI_2 complex) due to shorter M–N_{amido} vs M–N_{imine} distances. This contributes to shorter C \cdots C distances between flanking isopropyl methine carbon atoms in the uranium complex {C(30) \cdots C(45) = 4.60 – 4.85 Å; C(33) \cdots C(42) = 7.65 – 7.70 Å}, indicating that the flanking anionic 2,6-diisopropylphenylamido groups in XA_2 exert a greater steric influence than the neutral 1,3-diisopropylimidazol-2-imine donors in AlI_2 . A knock-on effect of the short C(30) \cdots C(45) distance (combined with an average M–C distance that is 0.07 Å shorter in the uranium complex) is that alkyl ligand coordination above the plane of the ligand is more strongly disfavoured,

resulting in O–U–C(52) angles of 94.8(2) and 95.0(2)°, and C(48)–U–C(52) angles of 103.2(2) and 105.0(2) Å, which are more acute than the corresponding N(1)–Y–C(40) and C(36)–Y–C(40) angles in **6** {110.46(6) and 110.48(7), respectively}.

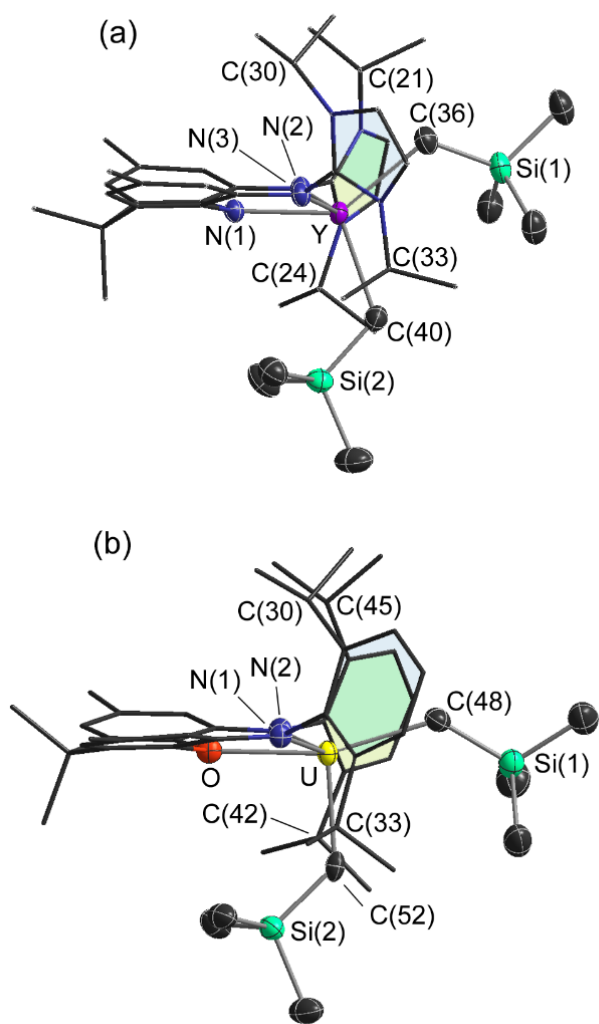
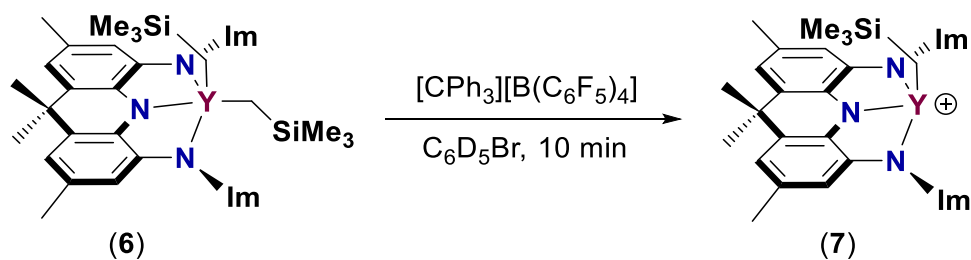


Figure 3.5: Side view of the x-ray crystal structures – (a) $[(AlI_2)Y(CH_2SiMe_3)_2]$ (**6**) (b) $[(XA_2)U(CH_2SiMe_3)_2] \cdot 2$ hexane

3.3.1 In-situ synthesis of $[(AlI_2)Y(CH_2SiMe_3)_2][B(C_6F_5)_4]$

Reaction of **6** with $[CPh_3][B(C_6F_5)_4]$ in C_6D_5Br afforded a dark purple solution of $[(AlI_2)Y(CH_2SiMe_3)][B(C_6F_5)_4]$ (**7**; Scheme 3.3), accompanied by byproducts of trimethylsilylmethyl group abstraction by the trityl cation; Ph_3CH at 5.44 ppm, a singlet at δ 3.37 ppm and $SiMe_3$ signals at -0.24 ppm and -0.31 ppm.¹²¹



Scheme 3.3: In-situ synthesis of $[(AlI_2)Y(CH_2SiMe_3)][B(C_6F_5)_4]$

The room temperature 1H NMR spectrum of **7** features two $CHMe_2$ and CMe_2 signals, indicative of C_s symmetry (Figures 3.6-3.8). Solutions of **7** in C_6D_5Br were entirely decomposed after 45 min at room temperature. The presence of 10 equivalents of a coordinating arene solvent (C_6D_6 , toluene) had a negligible influence on the stability of **7** and the 1H NMR spectra of **7** at -25 °C in C_6D_5Br are identical in the presence and absence of 10 equivalents of toluene. At 25 °C, the YCH_2 signals were observed at -0.88

ppm in the ^1H NMR spectrum (Figure 3.8), and 34.08 ppm in the ^{13}C NMR spectrum, with a $^1J_{\text{H},^{13}\text{C}}$ coupling constant of 100 Hz.

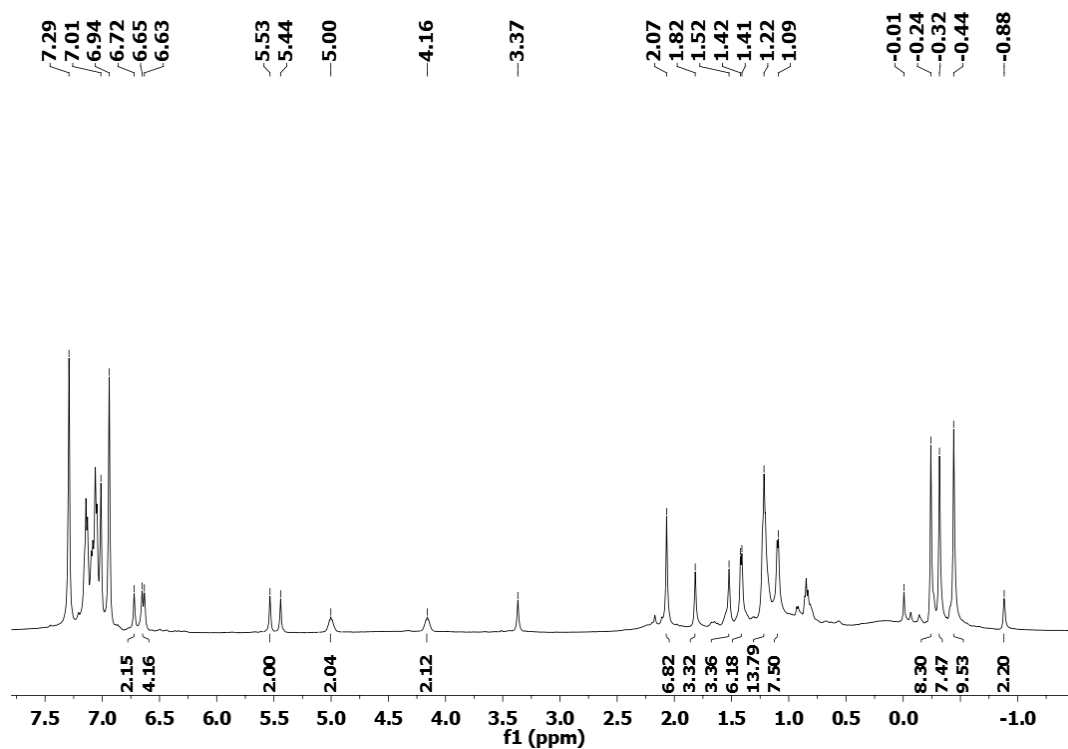


Figure 3.6: ^1H NMR Spectrum of $[(\text{AlI}_2)\text{Y}(\text{CH}_2\text{SiMe}_3)][\text{B}(\text{C}_6\text{F}_5)_4]$ (7) (600 MHz, $\text{C}_6\text{D}_5\text{Br}$)

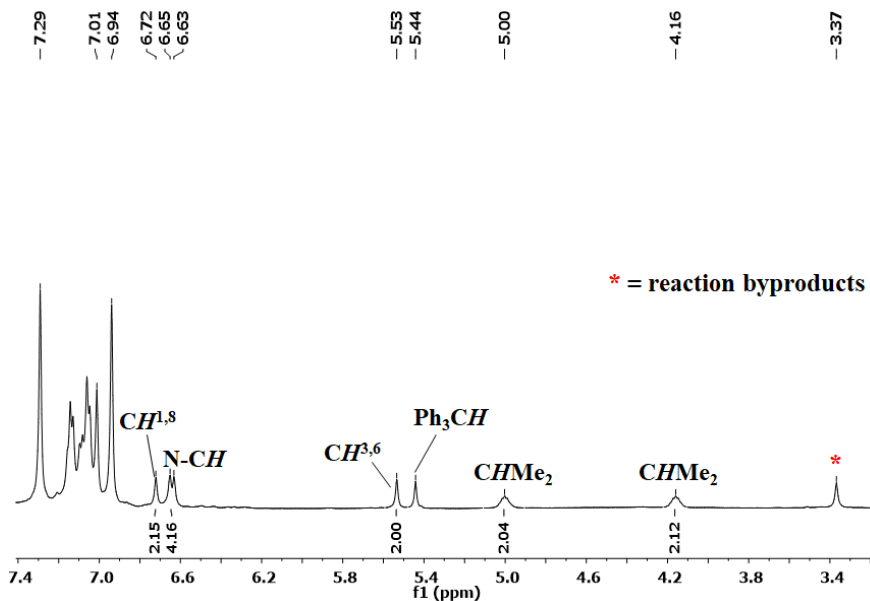


Figure 3.7: Expanded region - 1H NMR Spectrum of $[(AlI_2)Y(CH_2SiMe_3)][B(C_6F_5)_4]$ (7) (600 MHz, C_6D_5Br)

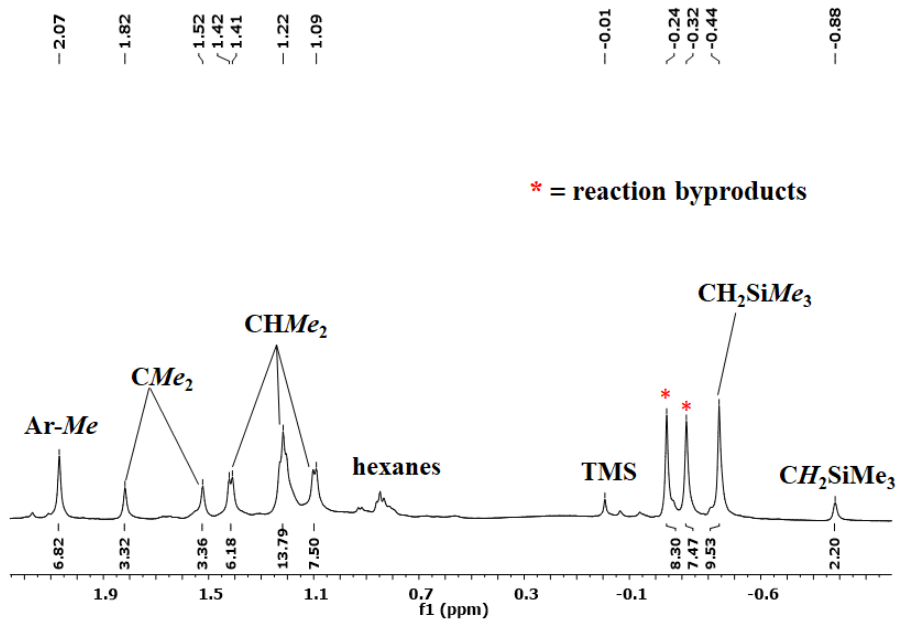


Figure 3.8: Expanded region - 1H NMR Spectrum of $[(AlI_2)Y(CH_2SiMe_3)][B(C_6F_5)_4]$ (7) (600 MHz, C_6D_5Br)

The ^{11}B chemical shift is consistent with an intact $\text{B}(\text{C}_6\text{F}_5)_4^-$ anion at room temperature and at 248 K (Figure 3.9), but in the ^{19}F NMR spectrum, the signals in the expected regions for the *para* and *meta* signals were absent, suggestive of interactions between the borate anion and the cationic metal center resulting in significant broadening of these signals. A single sharp signal at $\delta -131.29$ ppm was observed in the ^{19}F NMR, which is in the expected region for the *ortho*-F signal of the $\text{B}(\text{C}_6\text{F}_5)_4^-$ anion. Low temperature ^{19}F NMR (298 to 248K) spectra were collected, but the spectra remained largely unchanged within the temperature range (Figure 3.10).

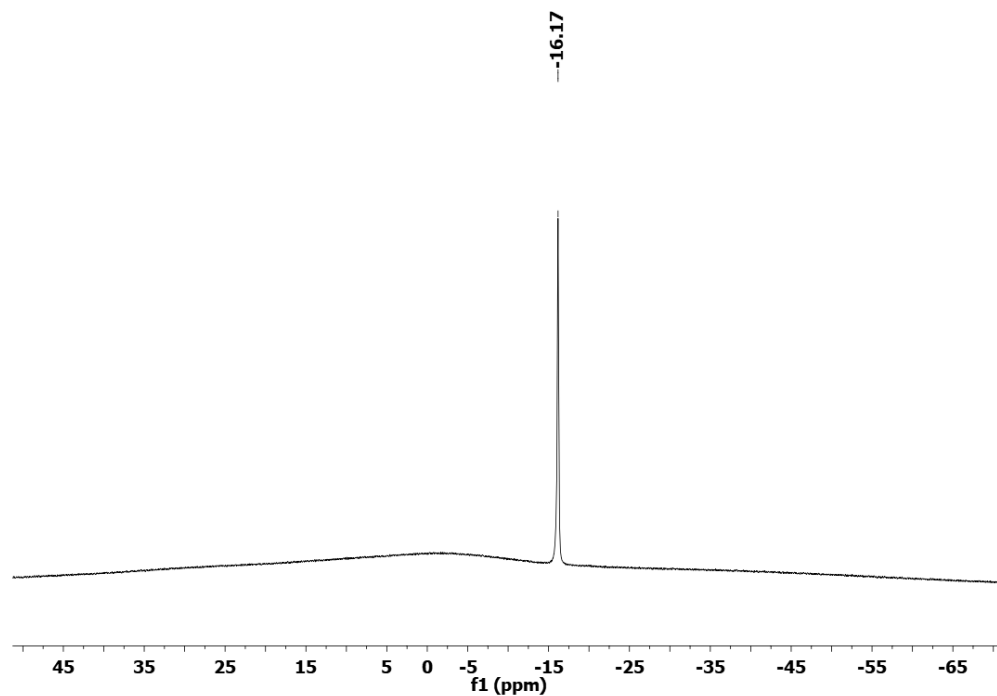


Figure 3.9: ^{11}B NMR Spectrum of $[(\text{AlI}_2)\text{Y}(\text{CH}_2\text{SiMe}_3)][\text{B}(\text{C}_6\text{F}_5)_4]$ (7) generated in-situ from the reaction of $[(\text{AlI}_2)\text{Y}(\text{CH}_2\text{SiMe}_3)_2]$ (6) with $[\text{CPh}_3][\text{B}(\text{C}_6\text{F}_5)_4]$ (161 MHz, 248 K, $\text{C}_6\text{D}_5\text{Br}$).

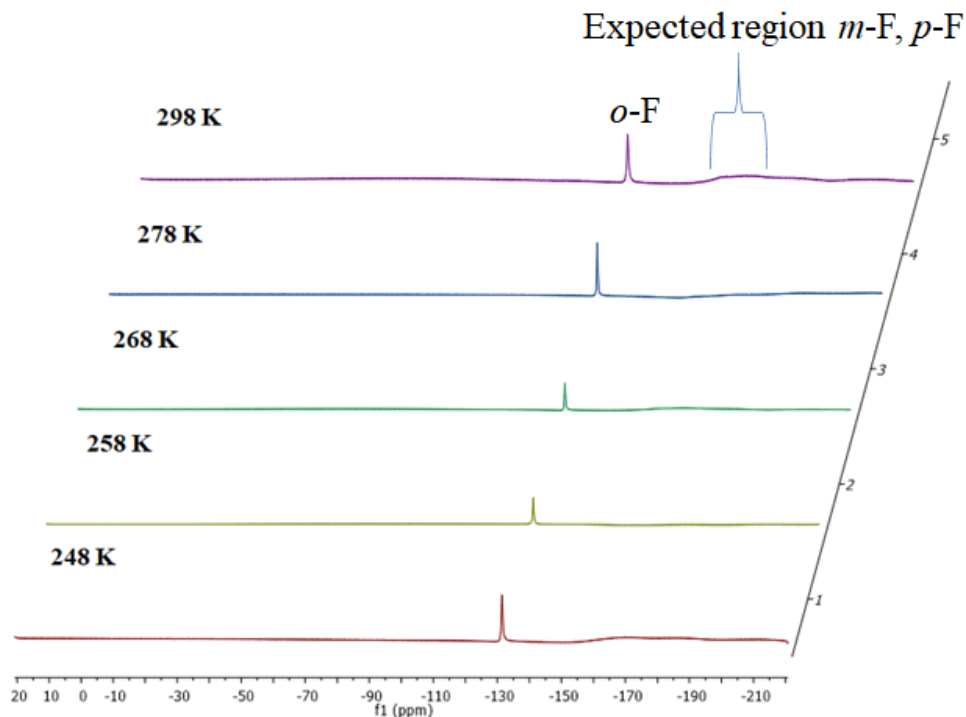
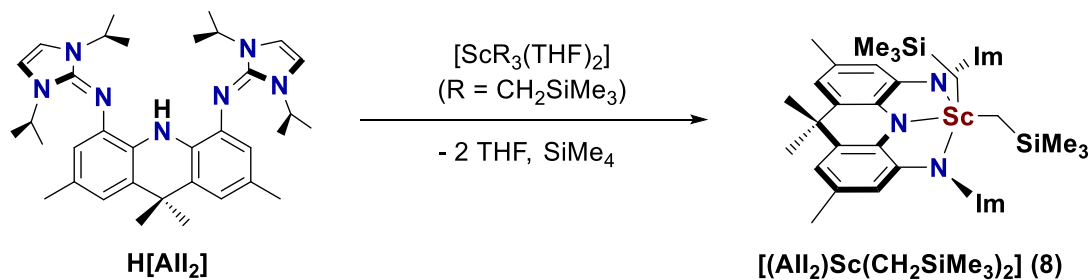


Figure 3.10: VT- ^{19}F NMR Spectrum of $[(\text{AlI}_2)\text{Y}(\text{CH}_2\text{SiMe}_3)][\text{B}(\text{C}_6\text{F}_5)_4]$ (**7**) generated in-situ from the reaction of $[(\text{AlI}_2)\text{Y}(\text{CH}_2\text{SiMe}_3)_2]$ (**6**) with $[\text{CPh}_3][\text{B}(\text{C}_6\text{F}_5)_4]$ (471 MHz, $\text{C}_6\text{D}_5\text{Br}$)

3.4 Synthesis of $[(\text{AlI}_2)\text{Sc}(\text{CH}_2\text{SiMe}_3)_2]$

Reaction of $\text{H}[\text{AlI}_2]$ with one equivalent of $[\text{Sc}(\text{CH}_2\text{SiMe}_3)_3(\text{THF})_2]$ yielded the base-free neutral dialkyl complex $[(\text{AlI}_2)\text{Sc}(\text{CH}_2\text{SiMe}_3)_2]$ (**8**) as an analytically pure brown solid (Scheme 3.4).

Scheme 3.4: Synthesis of $[(\text{AlI}_2)\text{Sc}(\text{CH}_2\text{SiMe}_3)_2]$ (**8**)

$[(\text{AlI}_2)\text{Sc}(\text{CH}_2\text{SiMe}_3)_2]$ (**8**) is stable at room temperature, with apparent C_{2v} symmetry as evidenced by a single CMe_2 and CMe_3 peak in the ^1H (Figure 3.11) and ^{13}C NMR spectra. The ScCH_2 ^1H and ^{13}C NMR signals were located at -0.50 and 30.97 ppm. Similar to **6**, the $^1J_{\text{C,H}}$ coupling constant for the ScCH_2 signal in **8** is 102 Hz, which is smaller than that for a typical sp^3 hybridized carbon atom ($^1J_{\text{C,H}} = 120$ - 130 Hz), suggestive of an α -agostic interaction.

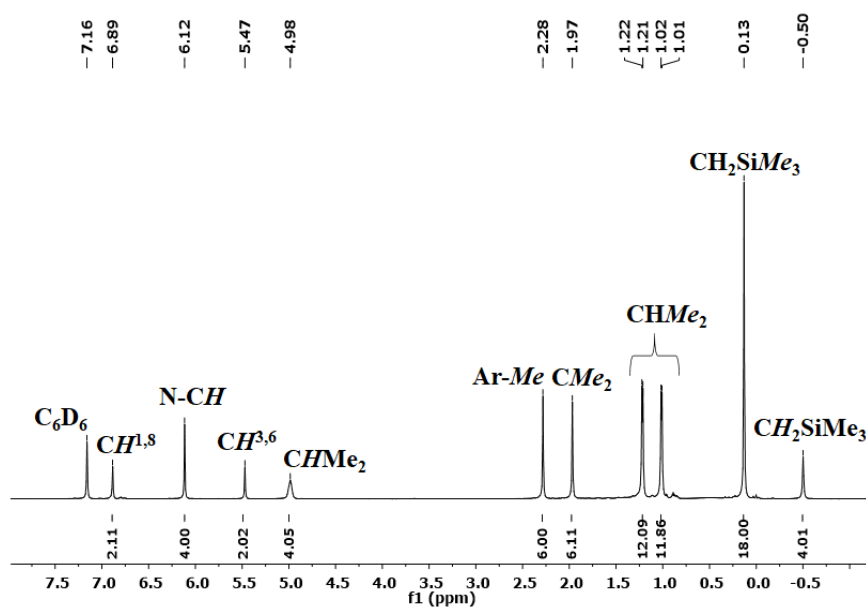
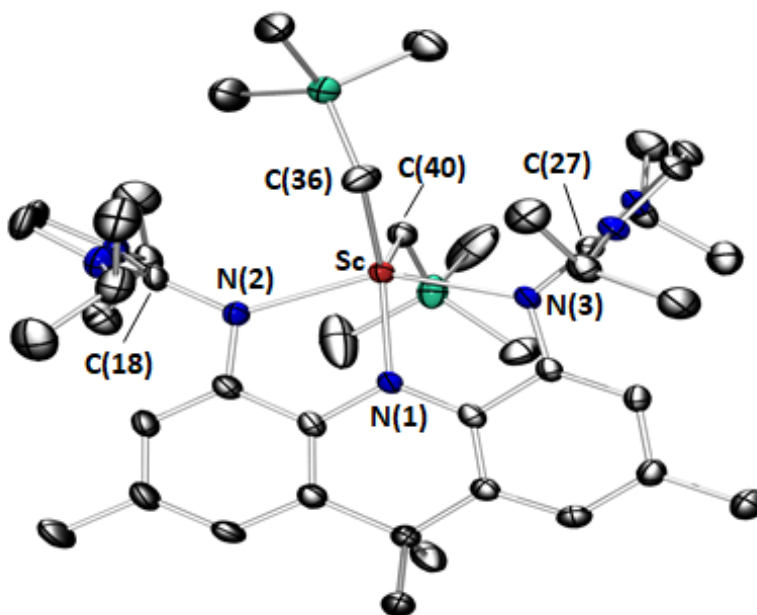


Figure 3.11: ^1H NMR Spectrum of $[(\text{AlI}_2)\text{Sc}(\text{CH}_2\text{SiMe}_3)_2]$ (**7**) (600 MHz, C_6D_6)

X-ray quality crystals of **8** were grown from toluene at $-28\text{ }^\circ\text{C}$ (Figure 3.12). Complex **8** contains two independent but qualitatively isostructural molecules in the unit cell. As observed for **6**, the AlI_2 ligand is κ^3 -coordinated with angles of 12.1° and 19.3° (for **8**) between the two aryl rings of the acridanide backbone. Similar to **6**, complex **8** shows a 5-coordinate geometry with one alkyl group $\{\text{C}(36)\}$ located between the flanking imidazole rings, whereas the other $\{\text{C}(40)\}$ is located below the plane, flanked by isopropyl groups.



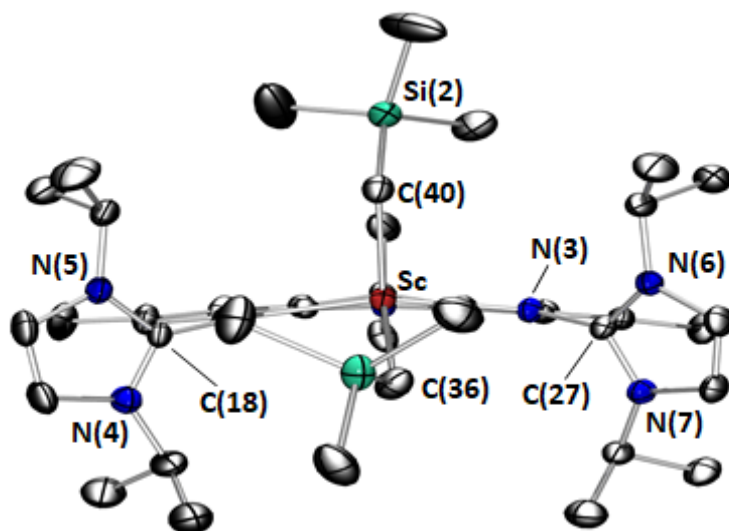


Figure 3.12: Two views of the X-ray crystal structure $[(AlI_2)Sc(CH_2SiMe_3)_2]$ of one of the independent molecules (**8**) Ellipsoids are set to 50% probability. For clarity, hydrogen atoms have been omitted and only one independent molecule is shown. Sc–N(1) 2.132(2), Sc–N(2) 2.256(2), Sc–N(3) 2.249(2), Sc–C(36) 2.296(2), Sc–C(40) 2.267(2), N(2)–C(18) 1.359(3), N(3)–C(27) 1.369(3), N(4)–C(18) 1.359(3), N(5)–C(18) 1.361(3), N(6)–C(27) 1.361(3), N(7)–C(27) 1.360(3), N(1)–Sc–N(2) 72.53(7), N(1)–Sc–N(3) 72.45 (6), C(36)–Sc–C(40) 110.85(9), Sc–C(36)–Si(1) 125.85(1), Sc–C(40)–Si(2) 121.5 (1).

All M–C and M–N bonds in **8** are shorter than those in **6** by 0.15–0.19 Å, primarily reflecting the difference in the ionic radii of Sc(III) and Y(III) (0.745 vs 0.90 Å). The M–C–Si angles range from 121.5(1)–125.9(1)° in **8**, which is again larger than the ideal sp^3 C bond angle of 109.5°.

Similar to **6**, complex **8** demonstrates a significant contribution from the zwitterionic resonance structure. The N(2)–C(18) and the N(3)–C(27) bond distances in **8** range from 1.359(2) to 1.375(3) Å, which is significantly longer than

in free imidazole-2-imines and comparable to those in **6**. Furthermore, the endocyclic N–C(18) and N–C(27) distances in **8** are comparable to N(2)–C(18) and the N(3)–C(27), ranging from 1.351(2) to 1.363(2) Å. These features, in combination with the roughly perpendicular orientation of the imidazole rings relative to the adjacent aryl ring of the acridanide backbone (interplanar angles of 75.6–88.4°), are indicative of a substantial contribution from the zwitterionic resonance structure with negative charges on N(2) and N(3).

3.4.1 Attempted in-situ synthesis of [(AlI₂)Sc(CH₂SiMe₃)] [B(C₆F₅)₄]

Reaction of scandium compound **8** with [CPh₃][B(C₆F₅)₄] in C₆D₅Br also generated a dark purple solution. However, the resulting ¹H NMR spectrum was broad and featureless (between 20 and –25 °C), including signals for protons located in the plane of the ligand backbone (i.e. protons which would be unaffected by a fluxional process involving alkyl group migration between sites above and below the plane of the ligand backbone). Attempts to trap an alkyl cation by the addition of THF or 1,3-diisopropylimidazol-2-ylidene resulted in decomposition to multiple products, so the scandium analogue of **7** was not pursued further.

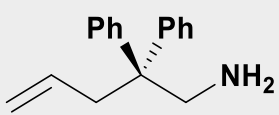
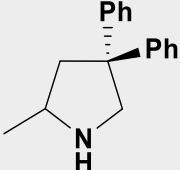
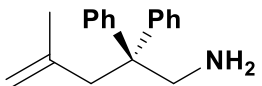
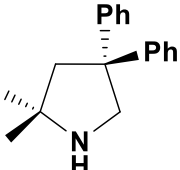
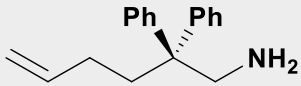
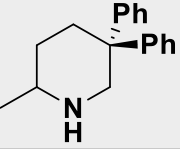
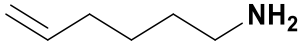
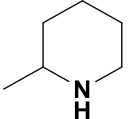
Similarly, a 1:1 reaction of **8** with [HNMe₂Ph][B(C₆F₅)₄] resulted in several unidentified products, and was therefore not pursued further.

3.5 Intramolecular hydroamination

Compound **7** was investigated as a catalyst for intramolecular alkene hydroamination, since only a handful of cationic rare earth hydroamination catalysts have been reported, and the availability of **6** and **7** provides a means to directly compare the catalytic activity of an alkyl cation with the neutral dialkyl precursor.

The cyclization of 1-amino-2,2-diphenyl-4-pentene using 2 mol% of **7** at room temperature (Entry 1 in Table 3.1) was complete after 8 minutes, establishing **7** as a highly active catalyst. Additionally, **7** (5 mol%; Entries 2-3) cyclized 1-amino-2,2-diphenyl-4-methyl-4-pentene and 1-amino-2,2-diphenyl-5-hexene (>99% completion) in just 1.1-1.5 hours at room temperature. These substrates are more challenging than 1-amino-2,2-diphenyl-4-pentene due to increased alkene steric hindrance and less favourable six- versus five-membered ring formation, respectively, and catalysts capable of cyclizing these substrates at room temperature are uncommon. Attempts to cyclize 1-amino-5-hexene proved unsuccessful between 24 and 80 °C (Entry 4). This can be attributed to the absence of cyclization promoting phenyl groups (Thorpe-Ingold effect), and strong coordination of the sterically unencumbered substrate to the cationic yttrium centre.

Table 3.1: Intramolecular hydroamination catalyzed by **7 {2 mol % (Entry 1) or 5 mol % (Entries 2-4)} generated in situ from **6** and $[\text{CPh}_3][\text{B}(\text{C}_6\text{F}_5)_4]$ at 25 °C. Reactions were conducted in 0.8 mL $\text{C}_6\text{D}_5\text{Br}$.**

Substrate	Product	Time (h)	% ^a	$N_t(\text{h}^{-1})$
		≤ 0.13	≥ 99	≥ 385
		1	> 99	20
		1.1	> 99	18.5
		36	0	0

In contrast to the high catalytic activity of **7** for intramolecular hydroamination, a 5 mol% catalyst loading of neutral **6** required 5.1 hours to complete the room temperature cyclization of 1-amino-2,2-diphenyl-4-pentene. Several groups have previously reported an analogous trend, where a cationic rare earth alkyl complex exhibits significantly higher activity than the neutral polyalkyl precursor. However, Hessen *et al.* have also observed examples of the opposite trend, highlighting the extent to which the

availability of a more sterically open and electrophilic metal centre (in cationic complexes) can either be beneficial or detrimental, depending on exact nature of the catalyst and whether the rate determining step is protonation of the insertion product by the substrate to release the cyclized product, or 1,2-insertion.²⁴ In the case of **6** (5 mol%, 24 °C) cyclization of 1-amino-2,2-diphenyl-4-pentene was found to be zero order with respect to substrate concentration over the entire substrate range (Figure 3.13), suggesting that the latter mechanism is operative. Similarly, in the case of **7**, the cyclization of both 1-amino-2,2-diphenyl-4-methyl-4-pentene (2 mol%, 24 °C) (Figure 3.14) and 1-amino-2,2-diphenyl-5-hexene (3.75 mol %, 24 °C) (Figure 3.15) were found to be zero order suggesting that the rate determining step is 1,2-insertion.

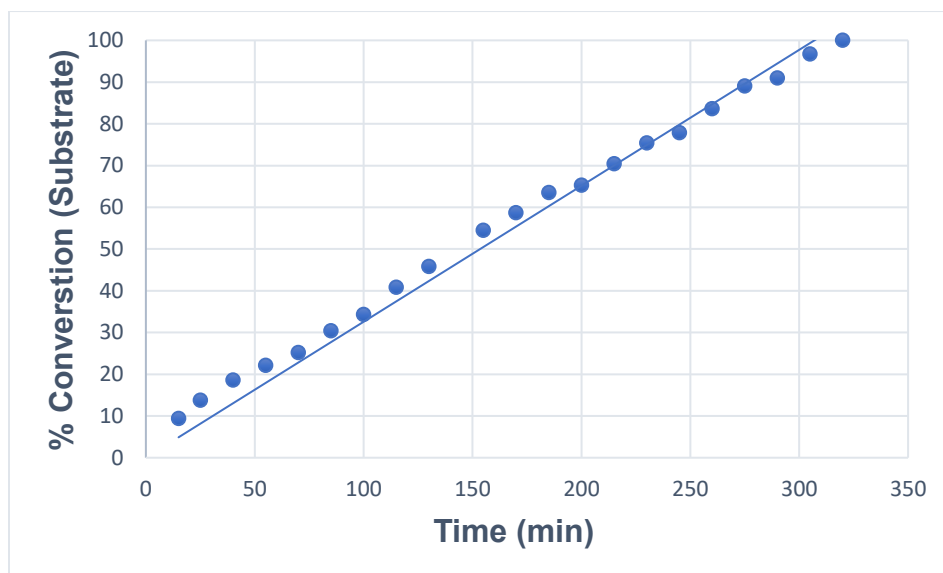


Figure 3.13: Hydroamination of 1-amino-2,2-diphenylpent-4-ene by $[(\text{AlI}_2)\text{Y}(\text{CH}_2\text{SiMe}_3)_2]$ (6) in C_6D_6 . % conversion of substrate vs. time

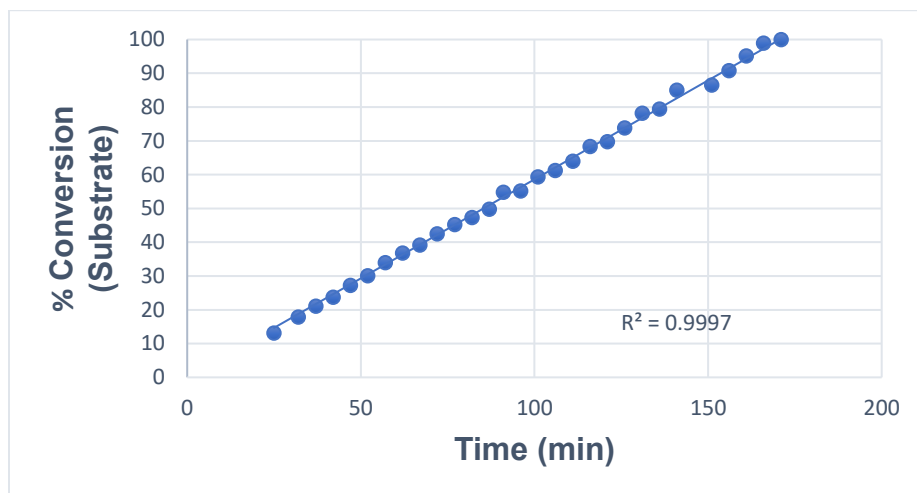


Figure 3.14: Hydroamination of 1-amino-2,2-diphenyl-4-methylpent-4-ene by $[(\text{AlI}_2)\text{Y}(\text{CH}_2\text{SiMe}_3)][\text{B}(\text{C}_6\text{F}_5)_4]$ (7) (2 mol%; in-situ generated) at 24 °C in $\text{C}_6\text{D}_5\text{Br}$. % conversion of substrate vs. time

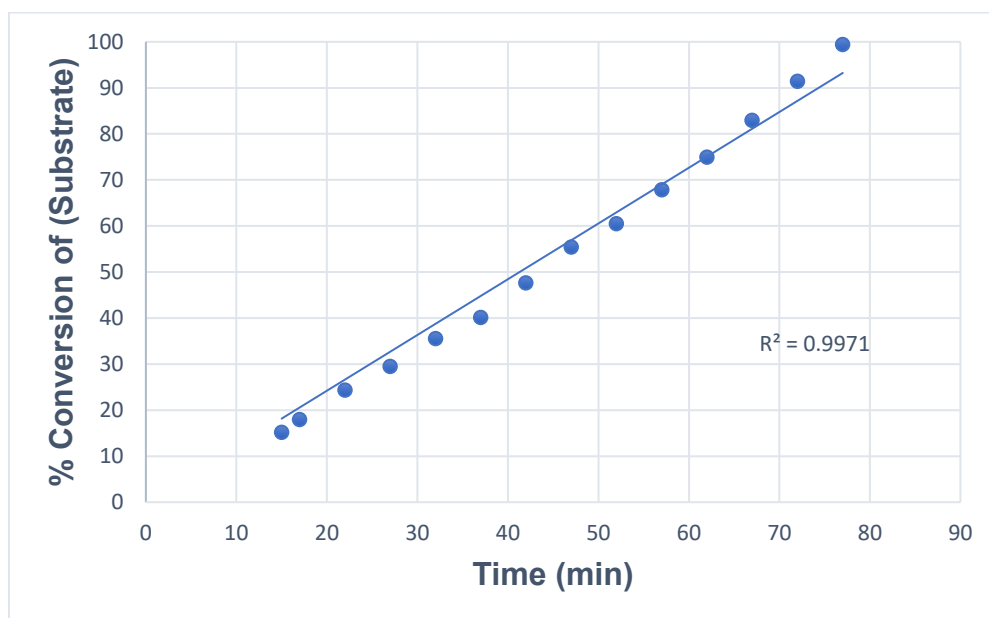


Figure 3.15: Hydroamination of 1-amino-2,2-diphenylhex-5-ene by $[(\text{AlI}_2)\text{Y}(\text{CH}_2\text{SiMe}_3)][\text{B}(\text{C}_6\text{F}_5)_4]$ (7**) (4 mol%; in-situ generated) at 24 °C in $\text{C}_6\text{D}_5\text{Br}$. % conversion of substrate vs. time**

3.6 Summary and Conclusions

In summary, a rigid new NNN-donor pincer ligand employing an anionic acridanide backbone with flanking neutral imidazol-2-imine donors was synthesized (as the protio ligand) and used to access neutral base free dialkyl complexes of yttrium and scandium, $[(\text{AlI}_2)\text{M}(\text{CH}_2\text{SiMe}_3)_2]$ {M = Y (**6**) and Sc (**8**)}. Both dialkyl complexes are stable at room temperature, and the solid state structures highlight the extent to which the monoanionic AlI_2 ligand possesses a similar, but slightly tempered, steric profile to the previously reported XA_2 dianion. Reaction of **6** with $[\text{CPh}_3][\text{B}(\text{C}_6\text{F}_5)_4]$ generated the yttrium monoalkyl cation $[(\text{AlI}_2)\text{Y}(\text{CH}_2\text{SiMe}_3)][\text{B}(\text{C}_6\text{F}_5)_4]$ (**7**), which is a rare example of a cationic rare earth catalyst for alkene hydroamination. Compound **7** readily cyclized 1-amino-2,2-diphenyl-4-pentene, 1-amino-2,2-diphenyl-4-methyl-4-pentene and 1-amino-2,2-diphenyl-5-hexene, and to the best of our knowledge, **7** is the first rare earth alkyl cation that can perform the latter two cyclization reactions at room temperature. Compound **7** is a far more active hydroamination catalyst than the neutral dialkyl precursor **6**, and in both cases, a zero order dependence on substrate concentration suggests

that the rate determining step is 1,2-insertion as opposed to protonation by substrate to release the cyclized product.

Chapter 4

Synthesis of Alkyl Group 3 Cationic and Dicationic Complexes Employing A Neutral Rigid NON-Donor Ligand

4.1 Introduction

Monocationic rare earth alkyl complexes are relatively underreported when compared to cationic group 4 alkyl complexes. Nevertheless, examples of coordinatively unsaturated, monocationic rare earth complexes, which are predominantly generated in-situ, have been reported as detailed in Section 1.5.4. Several of these complexes have proven to be highly efficient olefin polymerization catalysts.^{37, 38}

In comparison, dicationic rare earth alkyl complexes are very scarcely reported in the literature. Okuda and coworkers were the first to report coordinatively saturated examples of dicationic rare earth complexes.^{58, 100} They were further able to demonstrate the potential of dicationic rare earth complexes for ethylene polymerization by reacting $[M(\text{CH}_2\text{SiMe}_3)_3(\text{THF})_2]$ precursors with excess (5 equivalents) $[\text{HNMe}_2\text{Ph}][\text{B}(\text{C}_6\text{F}_5)_4]$ in toluene (Table 1.11, Section 1.5.6), to in-situ generate a dicationic alkyl species.⁵⁷ Following the work by Okuda et.al, only two examples of a spectroscopically observed, coordinatively unsaturated diacationic rare earth alkyl dications have been reported (Section 1.5.6).^{42, 60}

The vast majority of reported rare earth alkyl complexes employ monoanionic ligands. As described in Section 1.5.2, a monoanionic ligand allows access to neutral rare earth dialkyl complexes, which can be utilized to generate monocationic monoalkyl complexes. In contrast, utilizing a neutral ligand can potentially allow access to dicationic complexes of trivalent rare earth metals. However, neutral ligands are underreported relative to monoanionic ligands in rare earth chemistry. This can potentially be attributed to the greater electron donating capability that is intrinsic to anionic ligands, which allows for stabilization of electron deficient cationic metal centers.

Imidazol-2-imine donors are formally neutral donors that are highly electron donating due to the zwitterionic resonance structure, which localizes a negative charge on the nitrogen.^{89, 90} The monoanionic AlI_2 ligand incorporated these neutral donors and was utilized to generate in-situ, the monoalkyl cation $[(\text{AlI}_2)\text{Y}(\text{CH}_2\text{SiMe}_3)][\text{B}(\text{C}_6\text{F}_5)_4]$ as detailed in Chapter 3. $[(\text{AlI}_2)\text{Y}(\text{CH}_2\text{SiMe}_3)][\text{B}(\text{C}_6\text{F}_5)_4]$ was investigated as a potential ethylene polymerization catalyst, but the catalytic activity was found to be under 10 kg of P.E / mol · h · atm. The low ethylene polymerization activity of $[(\text{AlI}_2)\text{Y}(\text{CH}_2\text{SiMe}_3)][\text{B}(\text{C}_6\text{F}_5)_4]$ was attributed to the poor electrophilicity of the cationic metal center due to the highly electron donating monoanionic ancillary ligand (AlI_2). Herein lies the difficulty in designing a ligand that achieves a fine balance in electron donation, which electronically stabilizes, while not drastically reducing the electrophilic nature of the metal center.

To access a more potent ethylene polymerization catalyst, we became interested in designing a neutral ligand analogous to monoanionic AlI_2 . This could allow access to more highly electron deficient, dicationic rare earth alkyl complexes, which would favour ethylene coordination required for polymerization. Conceptually, replacing the central anionic N donor of the acridanide backbone, with the neutral oxygen donor of the xanthene backbone, while utilizing flanking imidazol-2-imine donors affords the target XII_2 ligand design (Figure 4.1).

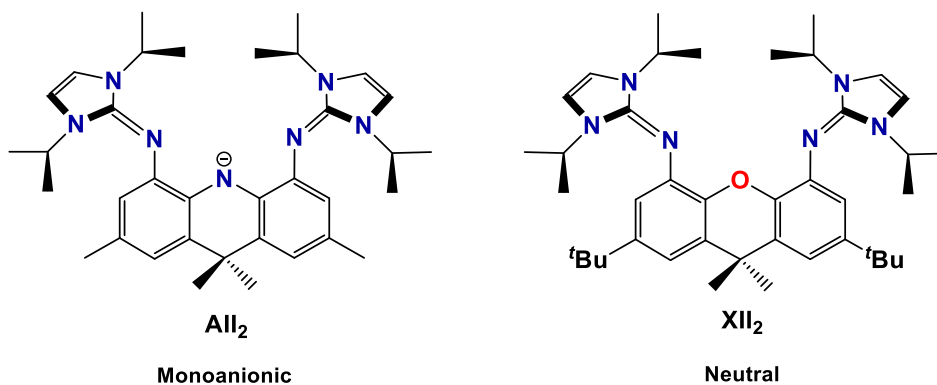
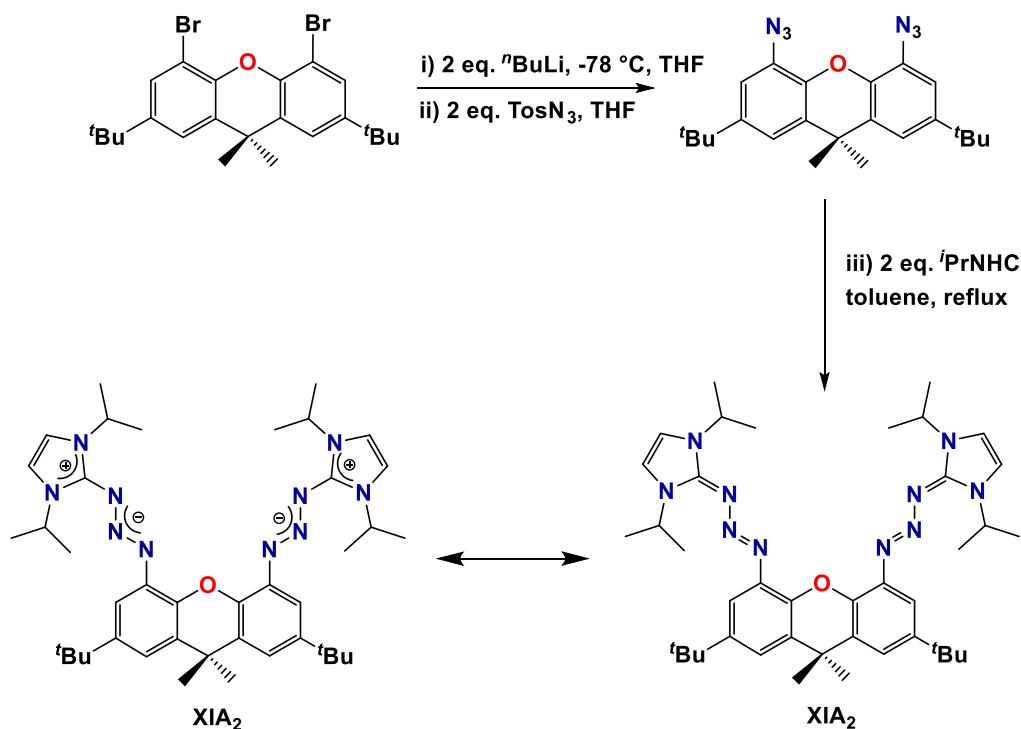


Figure 4.1: Relationship between the monoanionic AlI_2 and neutral XII_2 ligands

4.2 Synthesis of XIA₂

Imidazol-2-imines are commonly synthesized via a reaction similar to the Staudinger reaction utilized to synthesize phosphinimines.⁹¹ In chapter 2, we were able to in-situ generate (N₃)₂XT to synthesize (Ph₃PN)₂XT. Similarly, (N₃)₂XT was generated and treated with 2 eq. of 1,3-diisopropylimidazol-2-ylidene and heated to reflux in toluene. However, the intermediate triazene product (XIA₂) **9**; was highly stable and did not liberate N₂ to yield XII₂ (Scheme 4.1).



Scheme 4.1: Synthesis of XIA₂ (9)

Solution NMR spectra are consistent with a C_{2v} symmetric structure, however distinguishing **9** from the original synthetic target, XII₂ is not possible from solution NMR alone since no distinguishing feature exist via ¹H NMR (Figure 4.2).

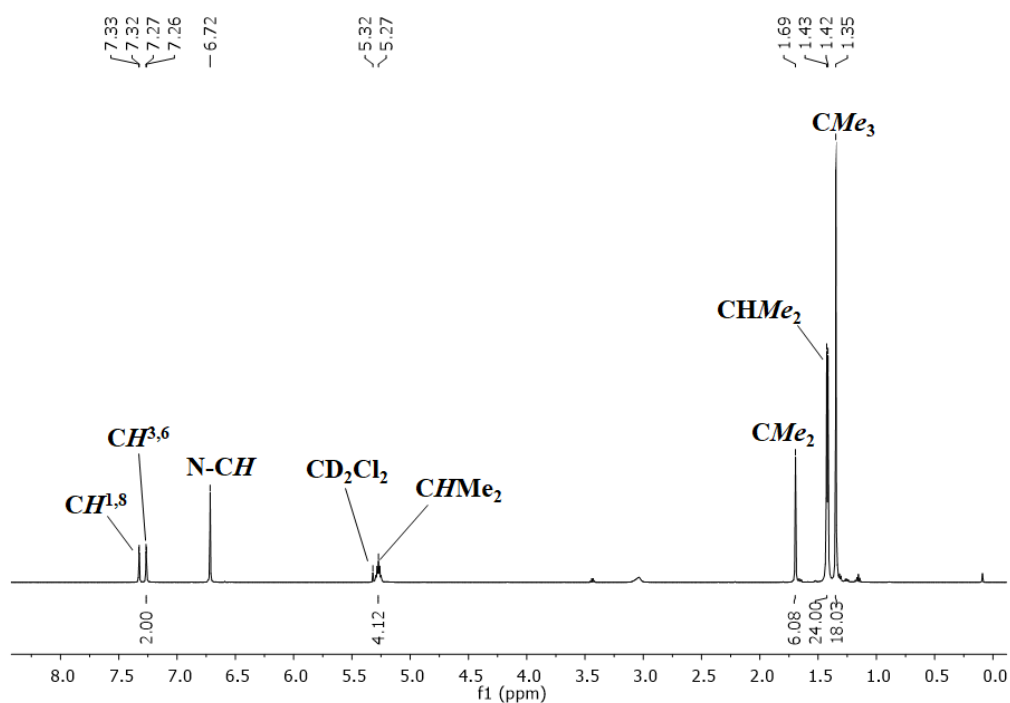


Figure 4.2: ¹H NMR Spectrum of XIA₂ (600 MHz, CD₂Cl₂)

XIA₂ is highly insoluble in non-halogenated aromatic solvents, and sparingly soluble in THF and diethyl ether. However, XIA₂ shows adequate solubility in CH₂Cl₂ and DMF. Attempts at refluxing XIA₂ in DMF (160 °C) led to decomposition to several unidentified products, as opposed to the formation of the target XII₂.

X-ray quality crystals were obtained by layering a solution of XIA₂ in CH₂Cl₂ with hexanes (Figure 4.3). Several structural features suggest a significant contribution of the zwitterionic resonance structure as depicted in Scheme 4.1. For example, the N₃-imidazol unit lies approximately in plane with respect to the xanthene backbone. In addition, N(3)-C(24) and N(8)-C(25) are 1.37(1) Å and 1.35(1) Å respectively which are significantly longer than typical C=N double bonds (1.26-1.29 Å), but not as long as typical C–N single bond, which further suggests a significant contribution by the zwitterionic resonance structure. The N(2)-N(3) and N(7)-N(8) bonds are 1.31(1) Å and 1.341(9) Å, which are shorter than typical N-N single bonds (1.41-1.46 Å).

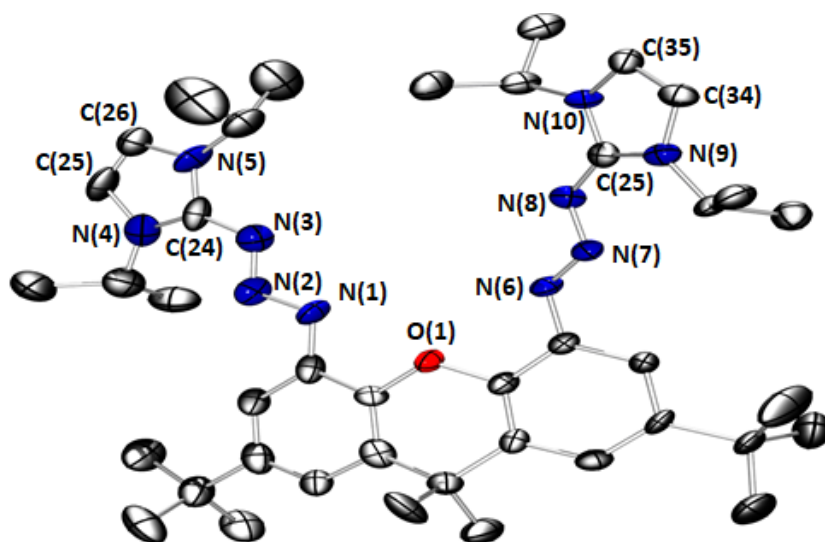


Figure 4.3: X-Ray crystal structure of XIA₂. Ellipsoids are set to 50 % probability. For clarity, hydrogen atoms, and lattice solvent (DCM, H₂O) are omitted. Selected bond lengths (Å) and angles (°): N(1)–N(2) 1.297(9), N(2)–N(3) 1.31(1), N(3)–C(24) 1.37(1), N(6)–N(7) 1.256(9), N(7)–N(8) 1.341(9), N(8)–C(25) 1.35(1), N(4)–C(24) 1.33(1), N(10)–C25 1.35(1), N(9)–C(25) 1.37(1), N(5)–C(24) 1.35(1), C(25)–(C26) 1.30(2), C(34)–C(35) 1.35(1), N(1)–N(2)–N(3) 110.9(7), N(6)–N(7)–N(8) 111.4(6). R = 9.33 %

4.3 Synthesis of $[(XIA_2)Y(CH_2SiMe_3)_3]$

A 1:1 reaction of XIA_2 and $[Y(CH_2SiMe_3)_3(THF)_2]$ in toluene afforded $[(XIA_2)Y(CH_2SiMe_3)_3]$ (**10**) as a carmine colored powder (Figure 4.4). Solution NMR spectra are consistent with a C_{2v} symmetric, tris(alkyl) complex with broad signals integrating 4H and 2H for the CH_2SiMe_3 peaks (Figure 4.5). These spectroscopic features are suggestive of a structure in which two alkyl groups are coordinated above and below the plane of the xanthene backbone, while the third alkyl group lies in the plane of the xanthene backbone. However, the exact coordination mode of the XIA_2 ligand is unknown. In solution, slow decomposition of **10** was observed via 1H NMR spectroscopy, producing TMS and an unidentified insoluble solid.

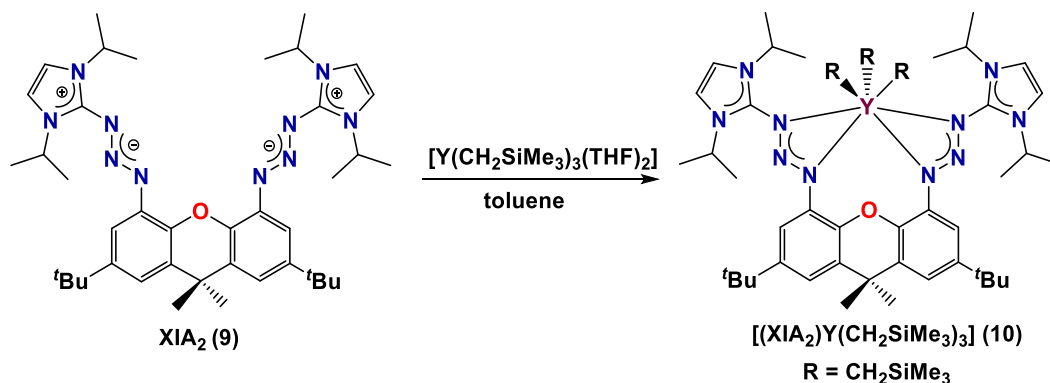


Figure 4.4: Synthesis of $[(XIA)_2Y(CH_2SiMe_3)_3]$:

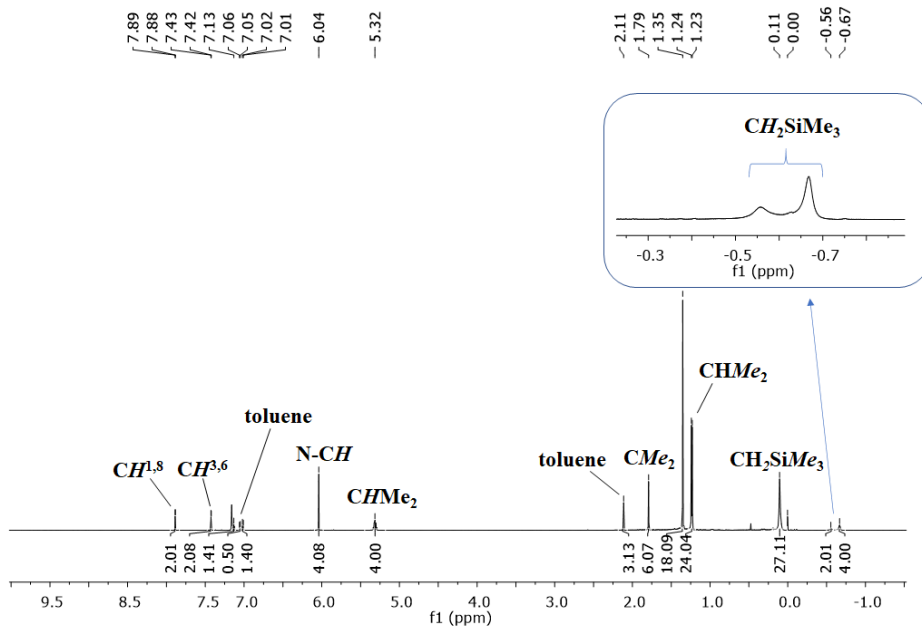


Figure 4.5: ^1H NMR Spectrum of $[(\text{XIA}_2)\text{Y}(\text{CH}_2\text{SiMe}_3)_3]$ (**10**) (600 MHz, C_6D_6)

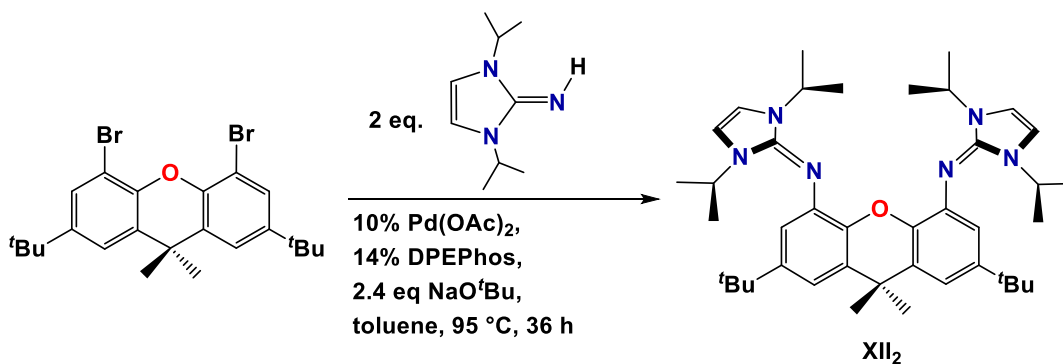
Crystals of **10** were grown from a saturated solution of **10** in toluene at $-28\text{ }^\circ\text{C}$ however, the crystals did not diffract and an X-ray structure was not obtained.

Attempts were made to access a cationic dialkyl complex via treatment of **9** with 1 equivalent of $[\text{CPh}_3][\text{B}(\text{C}_6\text{F}_5)_4]$ in $\text{C}_6\text{D}_5\text{Br}$ in the presence of 10 equivalents of toluene, but numerous unidentified products were produced.

4.4 Synthesis of XII₂

Buchwald-Hartwig amination cross-coupling reactions have been well established for a wide variety of primary amines and secondary amine substrates. In contrast, Buchwald-Hartwig ‘imination’ is scarcely reported, with existing examples primarily confined to benzophenone imine (Ph₂=NH). Tamm and coworkers provided the sole example of Buchwald-Hartwig ‘imination’ of an imidazol-2-imine as discussed in Section 1.8.⁹³

Previously, the Emslie group utilized a catalytic system of 10% Pd(OAc)₂ and 14% DPEPhos in the cross-coupling of 2,6-diisopropylaniline and 2,4,6-triisopropylaniline with Br₂XT to synthesize XA₂ and XN₂ respectively.^{23, 63} Similarly, this catalytic system was employed in the Buchwald Hartwig ‘imination’ of 1,3-diisopropyl-imidazol-2-imine with Br₂XT to synthesize XII₂ (Scheme 4.2).



Scheme 4.2: Synthesis of XII₂

Solution NMR spectra for XII₂ are consistent with the expected C_{2v} symmetric structure; single CMe₃ and CMe₂ signals were observed by ¹H (Figure 4.6) and ¹³C NMR spectroscopy. The CH^{1,8} and CH^{3,6} proton signals have coincidental ¹H NMR chemical shifts. Although the CHMe₂ protons might be expected to be diastereotopic, the signals appear to be equivalent in both the ¹H NMR and ¹³C NMR spectra. This, and the observation of a single CHMe₂ environment, can be attributed to the zwitterionic resonance structure, which allows free rotation of the imidazole rings.

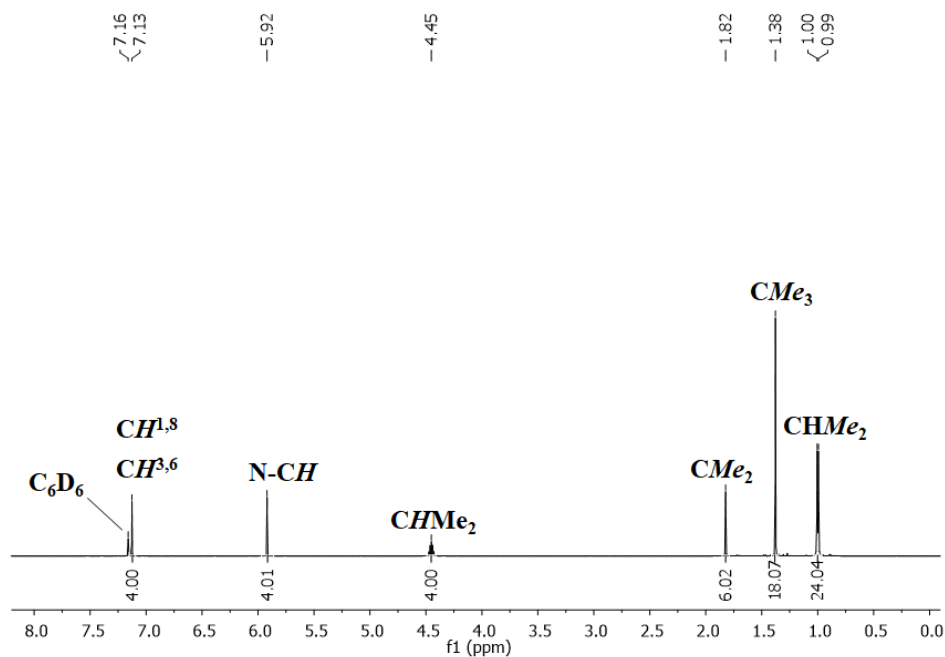


Figure 4.6: ¹H NMR Spectrum of XII₂ (11) (600 MHz, C₆D₆)

In establishing the cross-coupling conditions required for the synthesis of XII₂, it was found that the reaction was particularly sensitive to temperature. The

reaction had to be brought to 95 °C gradually from room temperature as opposed to the reaction mixture being placed directly in a 95 °C oil bath, since the latter resulted in several unknown products as observed via ^1H NMR spectroscopy. In addition, attempts at monitoring the reaction by retrieving aliquots at room temperature followed by reheating resulted in the complete decomposition of the catalyst and several unknown products were generated upon reheating as seen by ^1H NMR spectroscopy.

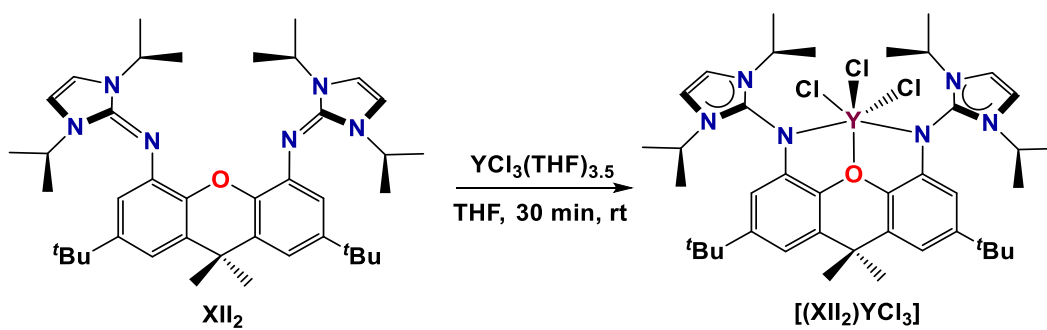
Analogues of the XII₂ ligand were targeted utilizing the catalytic system highlighted in Scheme 4.2. However, attempts at cross-coupling the more sterically bulky 1,3-*tert*-butyl-imidazol-2-imine, as well as 1,3,4,5-tetramethyl-imidazol-2-imine with Br₂XT proved unsuccessful.

4.5 Synthesis of [(XII₂)YCl₃]

Following the synthesis of XII₂, attempts were made to access tris(alkyl) neutral complexes of scandium and yttrium. A 1:1 reaction of XII₂ and [Y(CH₂SiMe₃)₂(THF)₂] did not afford the expected tris(alkyl) complex and instead led to numerous unidentified products. A similar outcome was seen for the reaction with [Sc(CH₂SiMe₃)₂(THF)₂]. This could be because the tris(alkyl) metal unit is too large for the binding pocket of the XII₂ ligand.

An alternative route to access rare earth alkyl complexes is via rare earth halide complexes, as highlighted in Section 1.4.2. Consequently, a 1:1 reaction of

XII₂ and [YCl₃(THF)_{3.5}] in THF, was carried out, and in this case the expected product, [(XII₂)YCl₃] (**12**) was formed cleanly (Scheme 4.3). The ¹H NMR spectrum of **12** is consistent with the expected C_{2v}-symmetric structure (Figure 4.7). The compound is highly insoluble in non-halogenated aromatic solvents.



Scheme 4.3: Synthesis of [(XII₂)YCl₃] (**12**)

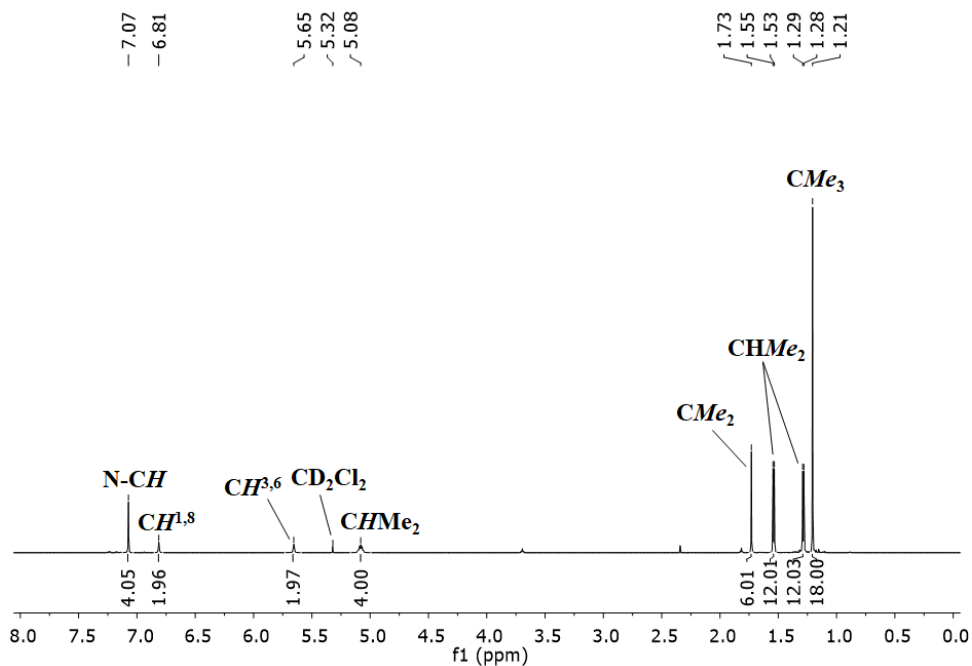


Figure 4.7: ^1H NMR Spectrum of $[(\text{XII}_2)\text{YCl}_3]$ (12) (600 MHz, CD_2Cl_2)

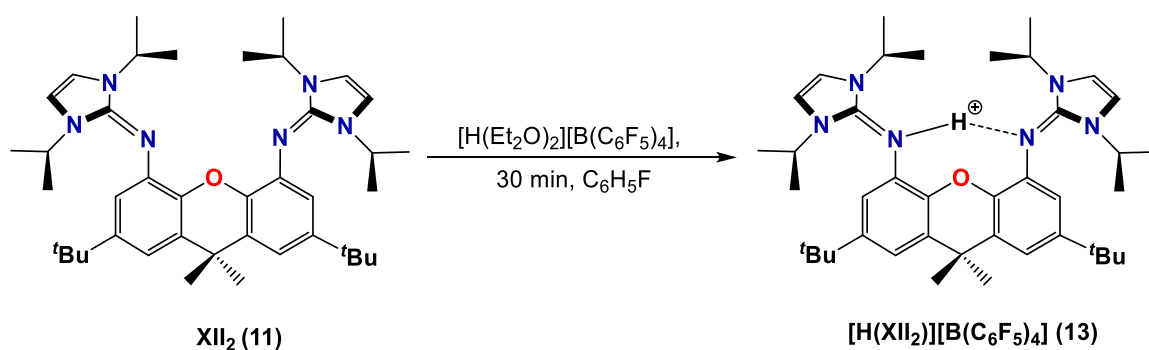
Attempts to access tris(alkyl) complexes via $[(\text{XII}_2)\text{YCl}_3]$ proved unsuccessful. Since it was inferred that the $\text{Y}(\text{CH}_2\text{SiMe}_3)_3$ unit is too large for the binding pocket of XII_2 (*vide supra*), it was hypothesized that smaller methyl groups might allow access to a trimethyl derivative, $[(\text{XII}_2)\text{Y}(\text{CH}_3)_3]$. However, the reaction of $[(\text{XII}_2)\text{YCl}_3]$ with 3 equivalents of MeLi in THF resulted in numerous unidentifiable products in the ^1H NMR spectrum.

4.6 Synthesis of $[\text{HXII}_2][\text{B}(\text{C}_6\text{F}_5)_4]$

Due to the difficulty in accessing tris(alkyl) group 3 complexes employing the XII_2 ligand, an alternative route that allows direct access to a monocationic di(alkyl) group 3 complex was undertaken. Previously, the Emslie group isolated $[(\text{XA}_2)\text{An}(\text{CH}_2\text{SiMe}_3)_2]$ ($\text{An} = \text{U}, \text{Th}$), which suggests that a $\text{Y}(\text{CH}_2\text{SiMe}_3)_2$ unit would be accommodated within the binding pocket of the sterically similar XII_2 ligand.^{63, 65, 66}

In order to directly access di(alkyl) group 3 complexes, a protic co-reactant is necessary for alkane elimination. Since XII_2 is an excellent proton sponge, a 1:1 reaction with $[\text{H}(\text{Et}_2\text{O})_2][\text{B}(\text{C}_6\text{F}_5)_4]$ in $\text{C}_6\text{H}_5\text{F}$ followed by addition of hexanes,

afforded the monoprotonated $[\text{HXII}_2][\text{B}(\text{C}_6\text{F}_5)_4] \cdot 0.5$ hexanes (**13**) ligand precursor as a white powder (Scheme 4.4). In contrast to the reaction in fluorobenzene, the same reaction in benzene or toluene resulted in a mixture of products.



Scheme 4.4: Synthesis of $[\text{HXII}_2][\text{B}(\text{C}_6\text{F}_5)_4]$ (**13**)

Solution NMR spectra of **13** are consistent with a C_{2v} -symmetric structure (Figure 4.8). However, the Ar-*H* signal at δ 6.40 ppm along with the N-*H* signal are significantly broadened, perhaps indicative of a rapid exchange of the proton between the imidazol-2-imine donors.

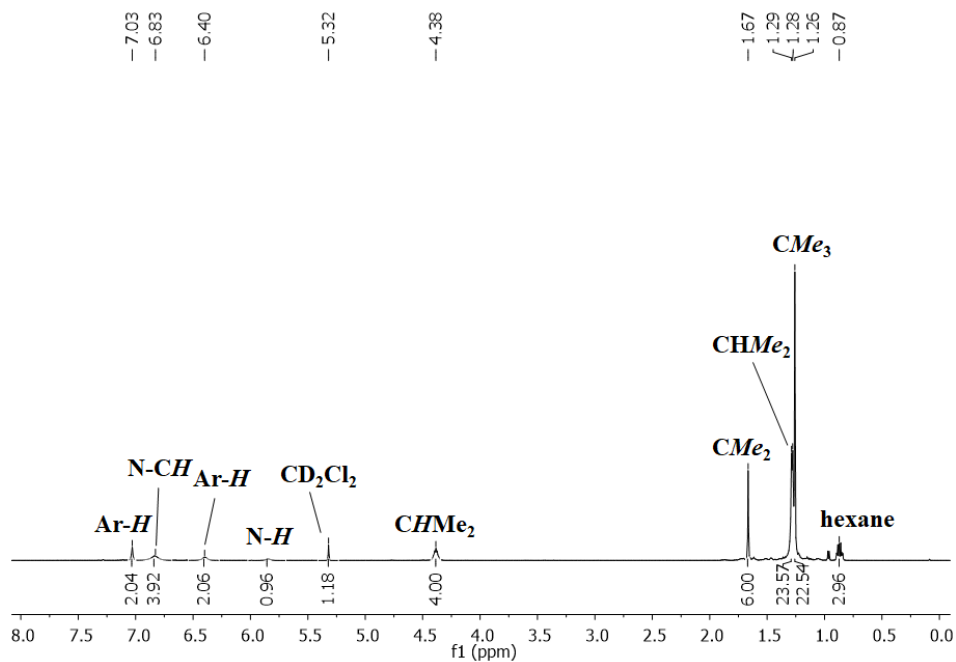
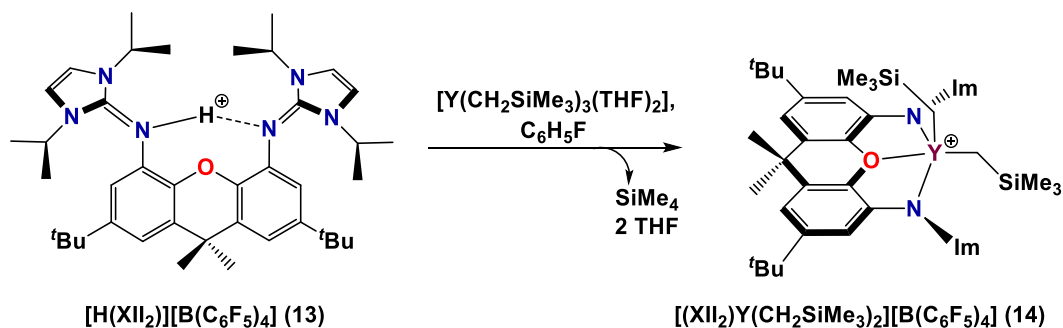


Figure 4.8: ¹H NMR Spectrum of [HXII₂][B(C₆F₅)₄] · 0.5 hexanes (**13**) (600 MHz, CD₂Cl₂)

4.7 Synthesis of [(XII₂)Y(CH₂SiMe₃)₂][B(C₆F₅)₄]

A 1:1 reaction of [HXII₂][B(C₆F₅)₄] with [Y(CH₂SiMe₃)₃(THF)₂] in C₆H₅F afforded the [(XII₂)Y(CH₂SiMe₃)₂][B(C₆F₅)₄] (**14**) as an analytically pure white powder (Scheme 4.5).



Scheme 4.5: Synthesis of $[(XII_2)Y(CH_2SiMe_3)_2][B(C_6F_5)_4]$ (14)

Solution NMR spectra for **14** are consistent with a C_{2v} -symmetric structure; single CMe_2 and CMe_3 signals were observed by 1H (Figure 4.9) and ^{13}C NMR spectroscopy. Several examples of cationic yttrium alkyl complexes have proven to be prone to ligand cyclometallation at room temperature. However, based on integration and the expected alkyl integration, it is evident that no such cyclometallation has occurred. The YCH_2 1H and ^{13}C NMR signals were observed at -0.77 and 37.18 ppm, respectively, with a $^1J_{C,H}$ coupling constant of 100 Hz, which is smaller than that for a typical sp^3 hybridized carbon atom ($^1J_{C,H} = 120-130$ Hz), and is suggestive of the presence of an α -agostic interaction.^{101, 102} The YCH_2 ^{13}C NMR signal is a doublet with a $^1J_{C,Y}$ coupling constant of 41 Hz, which is comparable to the literature examples of cationic yttrium alkyl complexes.⁵⁸ In comparison, neutral $[(AlI_2)Y(CH_2SiMe_3)_2]$ has a smaller $^1J_{C,Y}$ coupling constant of 36 Hz, indicative of a stronger $Y-C$ bond in cationic **14**.

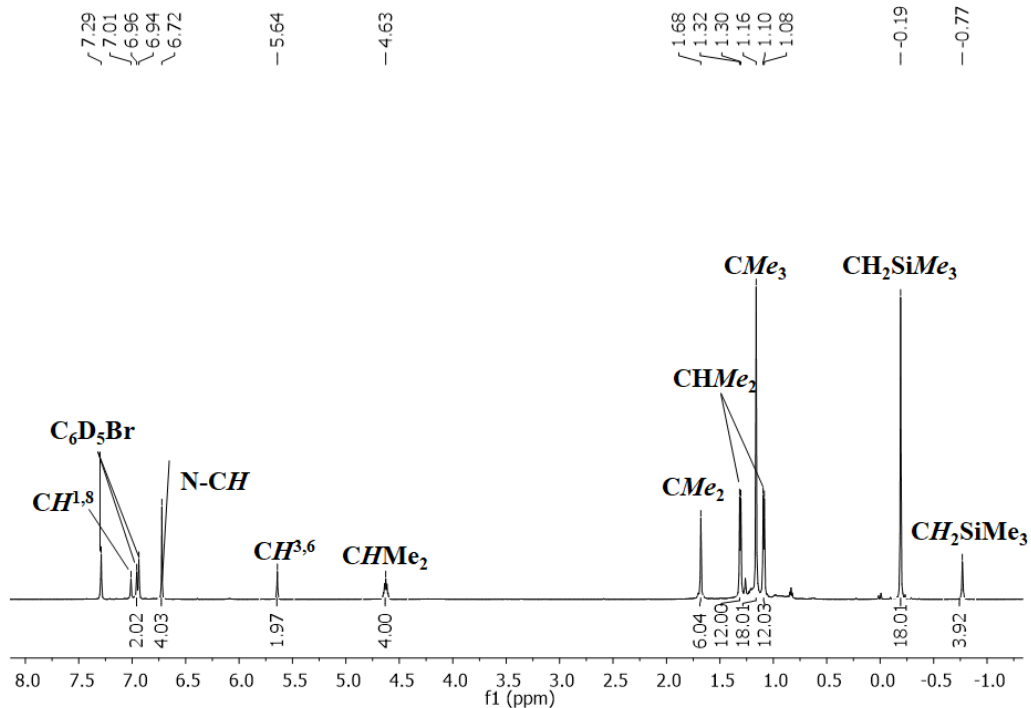


Figure 4.9: 1H NMR Spectrum of $[(XII_2)Y(CH_2SiMe_3)_2][B(C_6F_5)_4]$ (**14**) (600 MHz, C_6D_5Br)

X-ray quality crystals of $[(XII_2)Y(CH_2SiMe_3)_2][B(C_6F_5)_4]$ were grown by layering hexanes onto a solution of $[(XII_2)Y(CH_2SiMe_3)_2][B(C_6F_5)_4]$ in C_6H_5F at -28 °C (Figure 4.10).

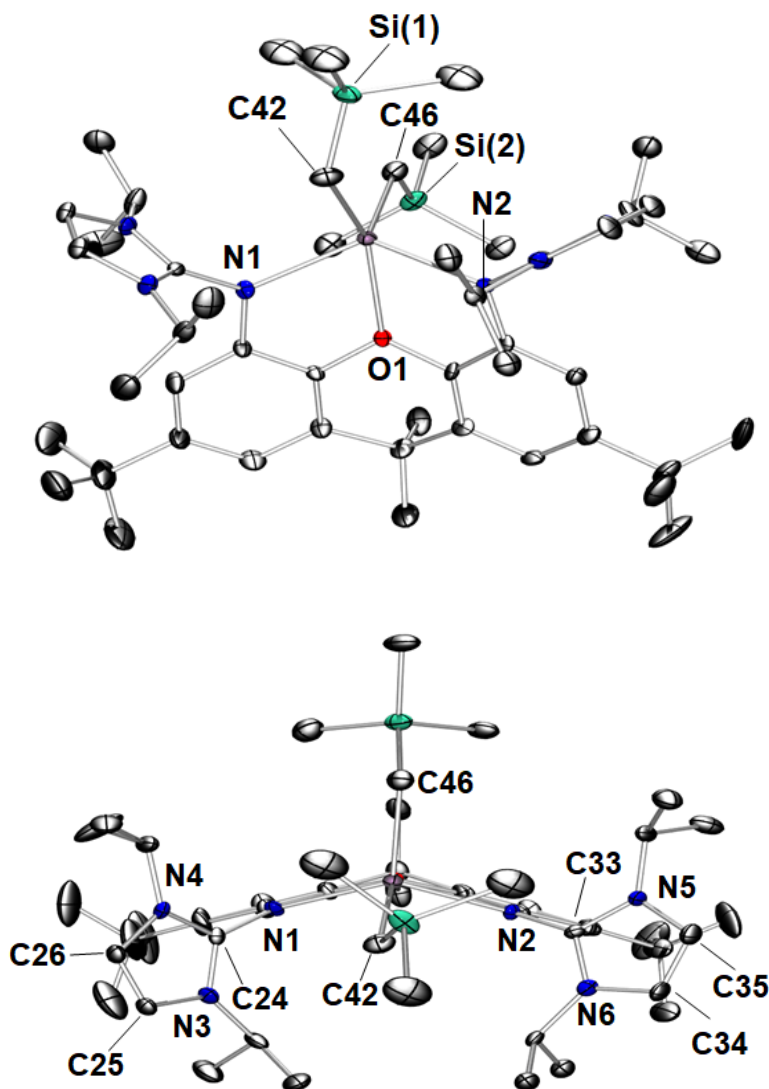


Figure 4.10: X-Ray crystal structure of [(XII₂)Y(CH₂SiMe₃)₂][B(C₆F₅)₄] (14). Ellipsoids are set to 30 % probability. For clarity, hydrogen atoms, and B(C₆F₅)₄ anion are omitted. Selected bond lengths (Å) and angles (°): Y–C(42) 2.389(5), Y–C(46) 2.386(5), Y–O(1) 2.425(3), Y–N(1) 2.336(4), Y–N(2) 2.329(4), N(1)–C(24) 1.369(6), N(2)–C(33) 1.373(6), N(4)–C(24) 1.344(6), N(3)–C(24) 1.350(6), N(5)–C(33) 1.346(6), N(6)–C(33) 1.362(6), C(25)–C(26) 1.340(7), C(34)–C(35) 1.363(7), Y–C(42)–Si(1) 124.9(3), Y–C(46)–Si(2) 119.5(3), C(42)–Y–C(46) 107.1(2), N(1)–Y–C(42) 95.3(2), N(1)–Y–C(46) 115.5(2), N(2)–Y–C(42) 102.0(2), C(42)–Y–O 145.31(2). R = 6.77 %

Complex **14** is 5 coordinate with one alkyl ligand located above the plane of the XII₂ ligand, and one approximately in the plane of the ligand, adopting a distorted square pyramidal geometry. The Y—C distances of 2.389(5) and 2.386(5) respectively, which is on the lower end of the range for monometallic yttrium trimethylsilylmethyl complexes (which are commonly 2.36 to 2.47 Å).¹⁰⁵ This is considerably shorter than the Y—C distances reported for [(AlI₂)Y(CH₂SiMe₃)₂] (2.434(2) and 2.438(2) Å) and can be attributed to the more electron deficient yttrium center of **14**. The Y—N(1) and Y—N(2) distances are 2.336(4) Å and 2.329(4) Å, which are considerably shorter than the Y—N_{imine} distances of the neutral [(AlI₂)Y(CH₂SiMe₃)₂] complex (2.394(2) and 2.421(2) Å) and shorter than the Y—N_{imine} distances of 2.381(2) and 2.358(2) Å in Tamm's [$\{\kappa\text{-}2,6\text{-C}_5\text{H}_3\text{N}(\text{CH}_2\text{N}=\{\text{NHC}\})_2\}\text{YCl}_3$] (NHC = 1,3-di-*tert*-butylimidazol-2-ylidene).⁹⁰ Similar to [(AlI₂)Y(CH₂SiMe₃)₂], the N(1)—C(24) and N(2)—C(33) distances (1.369(6) and 1.373(6)) are more elongated than in literature examples of free imine donors such as (NHC)=N{C₆H₄(OMe)-*p*} (NHC = 1,3-diisopropyl-4,5-dimethylimidazol-2-ylidene)¹¹⁹ and [$\{\kappa\text{-}2,6\text{-C}_5\text{H}_3\text{N}(\text{CH}_2\text{N}=\{\text{NHC}\})_2\}\text{FeCl}_2$] (NHC = 1,3-di-*tert*-butylimidazol-2-ylidene)¹²⁰, which are 1.308(2) and 1.294(3) Å, respectively. In addition, the endocyclic N—C(24) and N—C(33) distances range from 1.344 to 1.362 Å, similar to the 1.358(2) to 1.364(2) Å distances in [(AlI₂)Y(CH₂SiMe₃)₂] suggesting that the zwitterionic resonance contribution of the imidazol-2-imine donors is similar for both compounds. The imidazole rings of [(XII₂)Y(CH₂SiMe₃)₂][B(C₆F₅)₄] are roughly perpendicular in orientation with

respect to the adjacent aryl ring of the xanthene backbone (interplanar angles of 80.2° and 67.4°) further indicative of a considerable zwitterionic resonance contribution localizing a negative charge on N(1) and N(2).

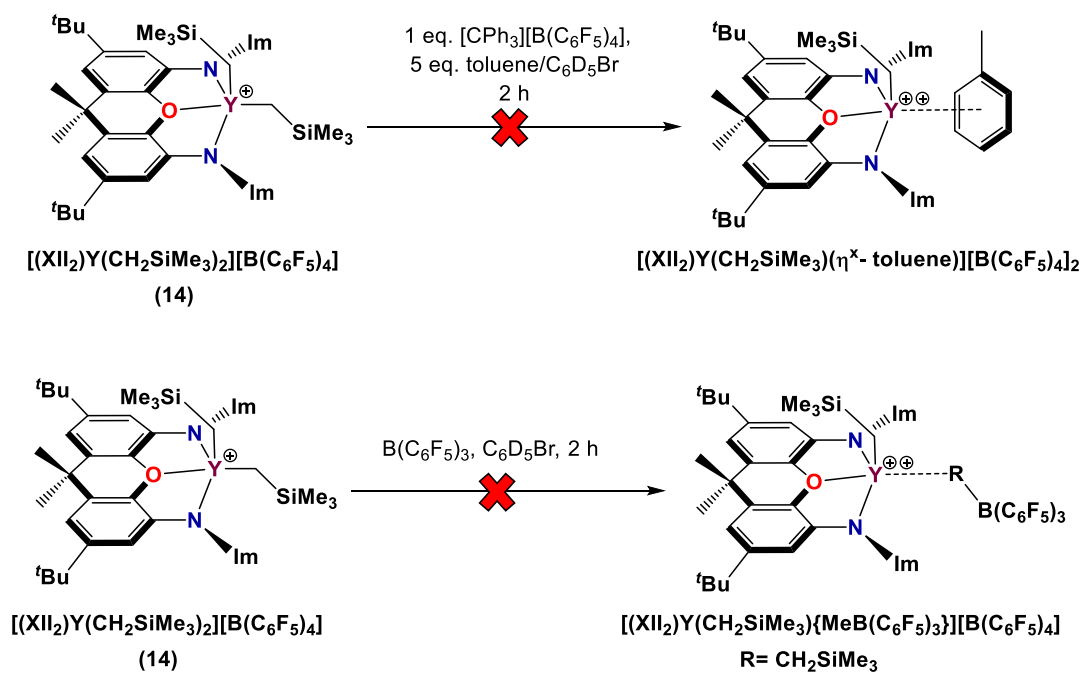
The Y—C(42)—Si(1) and Y—C(46)—Si angles are $124.9(3)^\circ$ and $119.5(3)^\circ$ respectively, which deviates from the ideal 109.5° angle for an sp^3 hybridized carbon and is further indication of an α -agostic interaction.

As previously mentioned, bending at the central non-aromatic ring of xanthene has often been observed, upon coordination to small metal ions such as magnesium(II) and aluminum(III).^{23, 102} [(XII₂)Y(CH₂SiMe₃)₂][B(C₆F₅)₄], a significant bend is observed, with a 38.9° angle between the planes of the two xanthene aryl rings. In comparison, [(AlI₂)Y(CH₂SiMe₃)₂] has a 28.6° bend between the planes of the two acridanide aryl rings. The larger ligand bend angle in cationic **14**, may be due to increased steric hinderance as a consequence of significantly shorter Y—C and Y—N distances.

4.7.1 Attempted Synthesis of [(XII₂)Y(CH₂SiMe₃)] [B(C₆F₅)₄]₂

As previously outlined in Section 1.5.3, Lewis acid activators are often utilized to abstract an alkyl group in order to access a monocationic or dicationic complex. In order to access a potential dicationic complex, a 1:1 reaction of **14** and B(C₆F₅)₃ in C₆D₅Br was attempted (Scheme 4.6). However, the reaction yielded a

complex spectrum with multiple unidentified products, in addition to tetramethylsilane which is indicative of decomposition. Similarly, a 1:1 reaction of **14** and $[\text{CPh}_3][\text{B}(\text{C}_6\text{F}_5)_4]$ in the presence of toluene resulted in several unidentified products and tetramethylsilane (Scheme 4.6).

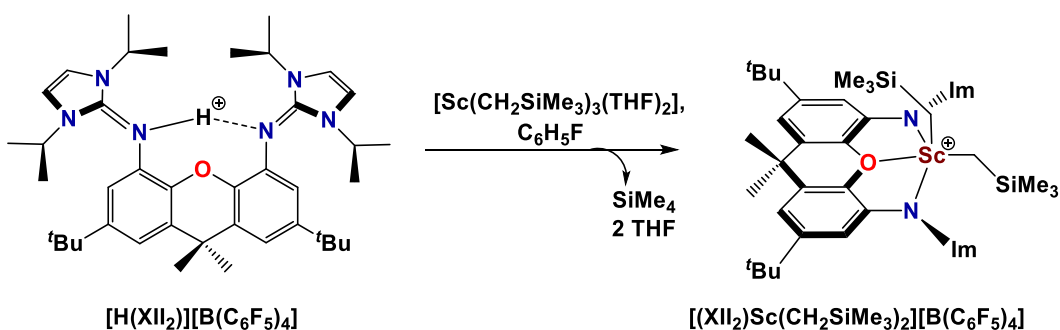


Scheme 4.6: Attempted in-situ generation of $[(\text{XII})_2\text{Y}(\text{CH}_2\text{SiMe}_3)(\eta^x\text{-toluene})][\text{B}(\text{C}_6\text{F}_5)_4]_2$ and $[(\text{XII})_2\text{Y}(\text{CH}_2\text{SiMe}_3)\{\text{MeB}(\text{C}_6\text{F}_5)_3\}][\text{B}(\text{C}_6\text{F}_5)_4]$

The monocationic alkyl complex **14** proved to be inactive towards ethylene polymerization. In-situ activation with both $[\text{CPh}_3][\text{B}(\text{C}_6\text{F}_5)_4]$ and $\text{B}(\text{C}_6\text{F}_5)_3$ similarly did not yield polyethylene, likely due to the instability of the resulting dicationic monoalkyl complex.

4.8 Synthesis of $[(XII_2)Sc(CH_2SiMe_3)_2][B(C_6F_5)_4]$

In an effort to access a more stable monoalkyl dication, the scandium analogue of **14** was synthesized. A 1:1 reaction of $[HXII_2][B(C_6F_5)_4]$ with $[Sc(CH_2SiMe_3)_3(THF)_2]$ in C_6H_5F afforded $[(XII_2)Sc(CH_2SiMe_3)_2][B(C_6F_5)_4]$ (**15**) as an analytically pure white powder (Scheme 4.7).



Scheme 4.7: Synthesis of $[(XII_2)Sc(CH_2SiMe_3)_2][B(C_6F_5)_4]$ (**15**)

Solution NMR spectra for $[(XII_2)Sc(CH_2SiMe_3)_2][B(C_6F_5)_4]$ are consistent with a C_{2v} -symmetric structure; a single CMe_3 and CMe_2 signals were observed by 1H (Figure 4.11) and ^{13}C NMR spectroscopy. However, in contrast to $[(XII_2)Y(CH_2SiMe_3)_2][B(C_6F_5)_4]$, 1H NMR signals for groups that lie above or below the plane of the xanthene backbone are slightly broadened, suggestive of a rapid exchange between scandium alkyl groups located in and out of the plane of the ligand backbone. Similarly, the $Sc-CH_2$ group is observed as a broad singlet at room temperature.

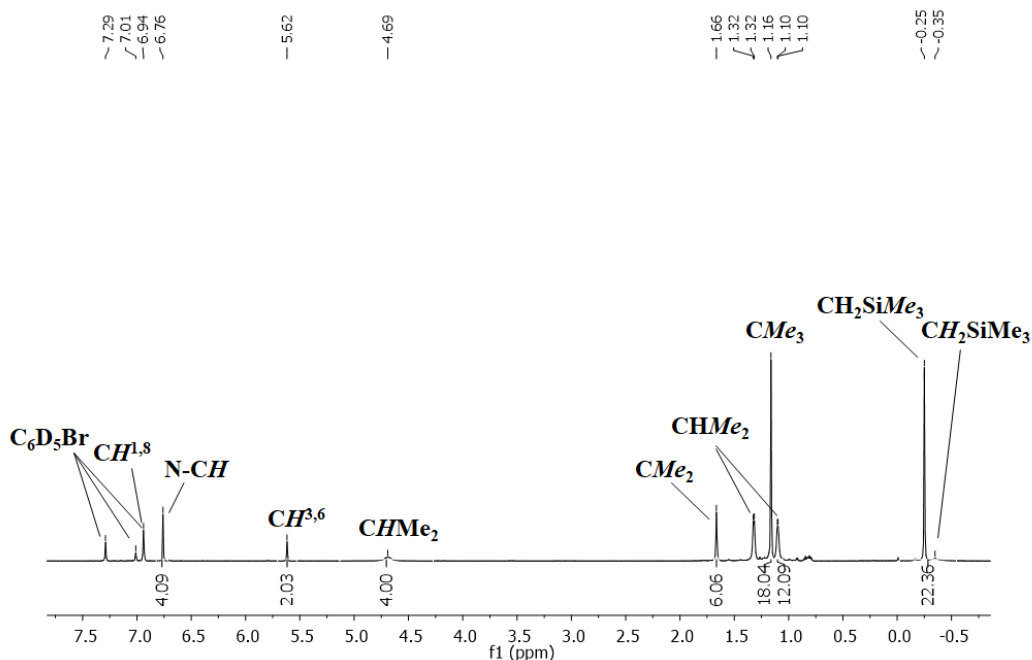


Figure 4.11: ^1H NMR Spectrum of $[(\text{XII})_2\text{Sc}(\text{CH}_2\text{SiMe}_3)_2][\text{B}(\text{C}_6\text{F}_5)_4]$ (600 MHz, $\text{C}_6\text{D}_5\text{Br}$)

High temperature ^1H NMR (35 °C - 50 °C) resulted in the sharpening of signals that correspond to proton signals that lie above/below the plane of the xanthene backbone (Figure 4.12). Low temperature ^1H NMR spectra (-25 °C) was consistent with a C_s symmetric complex as evidenced by two broad CHMe_2 signals (δ 5.03, 4.38 ppm), as well as two broad Sc-CH_2 signals (δ 0.25, -0.86 ppm). Signals for proton environments that lie within the plane of the xanthene backbone remained sharp at low temperatures.

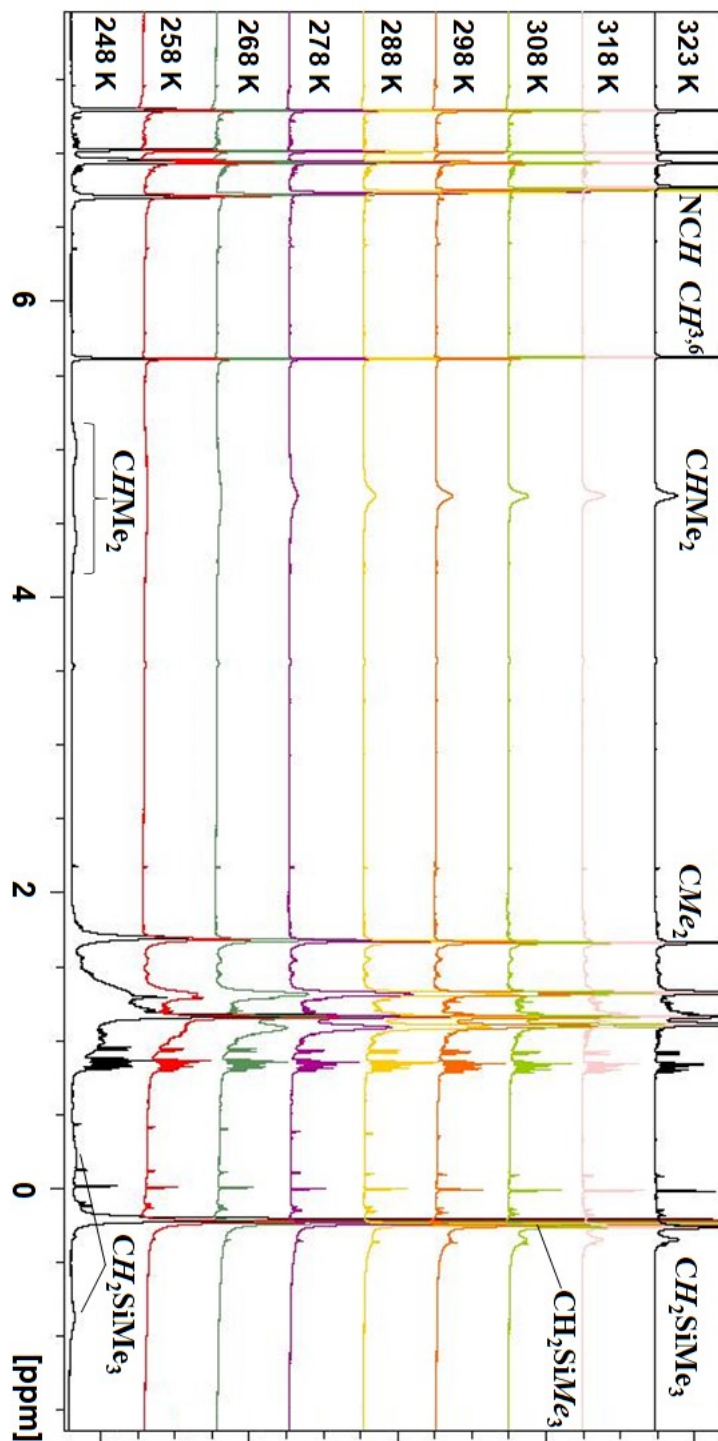


Figure 4.12: Variable Temperature-¹H NMR Spectrum of 15 (500 MHz, C₆D₅Br)

X-ray quality crystals of $[(\text{XII}_2)\text{Sc}(\text{CH}_2\text{SiMe}_3)_2][\text{B}(\text{C}_6\text{F}_5)_4]$ (**15**) were grown by layering hexanes onto a solution of **15** in $\text{C}_6\text{H}_5\text{F}$ followed by cooling at $-28\text{ }^\circ\text{C}$ (Figure 4.13). As with the yttrium analogue, **15** is 5 coordinate with one alkyl ligand located above the plane of the XII_2 ligand, and one approximately in the plane of the ligand, adopting a distorted square pyramidal geometry. The endocyclic N–C(24) and N–C(33) distances range from 1.344(4) to 1.358(4) Å, which is similar to the range for **15** and suggests a considerable zwitterionic resonance contribution localizing a negative charge on N(1) and N(2). All M–C and M–N bonds in **2** are shorter than those in **1** by 0.15–0.18 Å, primarily reflecting the difference in the ionic radii of Sc(III) and Y(III) (0.745 vs 0.90 Å). The Sc–C(42)–Si(1) and Sc–C(46)–Si(2) angles are $129.97(3)^\circ$ and $123.85(3)^\circ$ respectively, again suggestive of an α -agostic interaction.

A significant bend of the xanthene backbone is observed, with a 41.26° angle between the planes of the two xanthene aryl rings, which is slightly larger than seen for **14**, likely in response to the smaller ionic radius of Sc^{3+} in comparison to Y^{3+} .

Compound **15** is stable in solution up to $90\text{ }^\circ\text{C}$, attesting to the steric protection afforded by the XII_2 ligand in addition to the electronic stabilization afforded by the zwitterionic resonance structure contribution of the imidazol-2-imine donors. Decomposition at $110\text{ }^\circ\text{C}$ yielded tetramethylsilane and an unidentified insoluble solid.

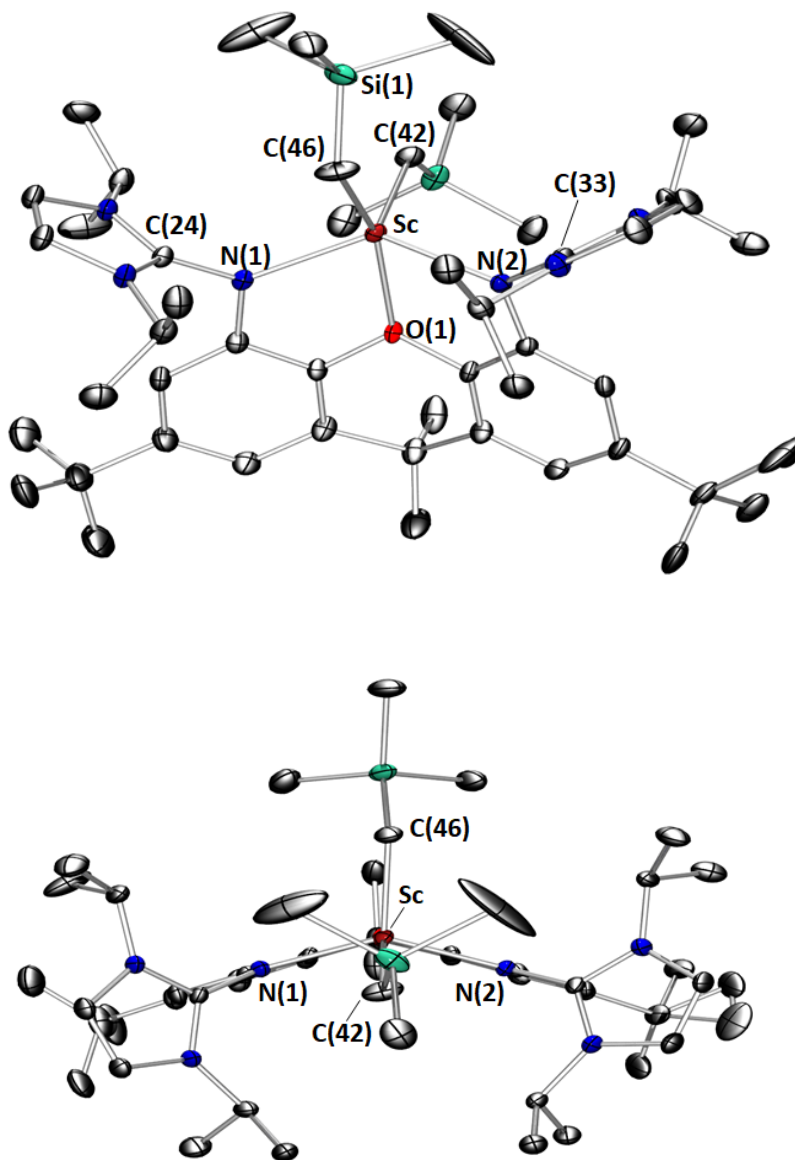


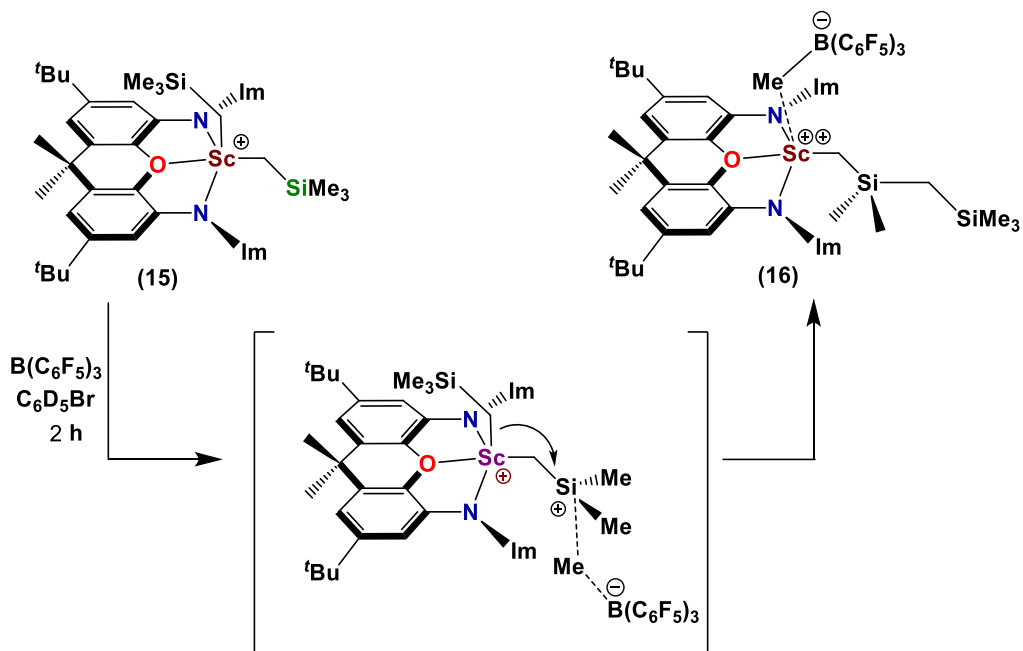
Figure 4.13: X-Ray crystal structure of $[(\text{XII})_2]\text{Sc}(\text{CH}_2\text{SiMe}_3)_2[\text{B}(\text{C}_6\text{F}_5)_4]$. Ellipsoids are set to 30 % probability. For clarity, hydrogen atoms, and $\text{B}(\text{C}_6\text{F}_5)_4$ anion are omitted. Selected bond lengths (Å) and angles (°): Sc—C(42) 2.238(3), Sc—C(46) 2.210(3), Sc—O(1) 2.283(2), Sc—N(1) 2.191(2), Sc—N(2) 2.190(2), N(1)—C(24) 1.368(3), N(2)—C(33) 1.368(4), N(4)—C(24) 1.346(4), N(3)—C(24) 1.358(4), N(5)—C(33) 1.355(4), N(6)—C(33) 1.344(4), C(25)—C(26) 1.345(4), C(34)—C(35) 1.343(5), Sc—C(42)—Si(1) 130.0(2), Sc—C(46)—Si(2) 123.9(2), C(42)—Sc—C(46) 104.5(1), N(1)—Sc—C(42) 96.6(1), N(1)—Sc—C(46)

114.2(1), N(2)—Sc—C(46) 110.4(1), N(2)—Sc—C(42) 98.9(1), C(42)—Sc—O 150.8(1). R = 7.55 %

4.8.1 In-situ generation of dicationic

**[(XII₂)Sc(CH₂SiMe₂CH₂SiMe₃)][(MeB(C₆F₅)₃)] [B(C₆F₅)₄]
(16) complex**

Following the synthesis of [(XII₂)Sc(CH₂SiMe₃)₂][B(C₆F₅)₄], attempts were made to access a dicationic alkyl complex. The reaction of [(XII₂)Sc(CH₂SiMe₃)₂][B(C₆F₅)₄] (**15**) with a slight excess of B(C₆F₅)₃ (1.1 equivalents) did not yield the expected trimethylsilylmethyl abstraction product. Solution NMR studies strongly suggest the abstraction of a methyl anion from the silicon center, with concomitant migration of the remaining alkyl group to the positively charged silicon, forming a new CH₂SiMe₂CH₂SiMe₃ alkyl group. This process is accompanied by MeB(C₆F₅)₃ anion formation, forming a contact ion pair to afford dicationic species **16**, as seen in Scheme 4.8. This type of rearrangement was independently observed by Piers and Scott in reacting to form monocationic complexes as discussed in Section 1.5.4.^{46, 47} However, this is the first example of this type of rearrangement en route to a dicationic complex.



Scheme 4.8: Synthesis and proposed mechanism for the formation of $[(\text{XII})_2\text{Sc}(\text{CH}_2\text{SiMe}_2\text{CH}_2\text{SiMe}_3)][(\text{MeB}(\text{C}_6\text{F}_5)_3)[\text{B}(\text{C}_6\text{F}_5)_4]$ (**16**) - Only one possible location of the alkyl group is shown. Alternatively, the $\text{MeB}(\text{C}_6\text{F}_5)_3$ contact ion pair could be in the plane of the ligand, with the alkyl group located above the plane of the ligand.

Room temperature NMR spectroscopy (298 K) of **16** are consistent with a C_s symmetric complex as evidenced by two distinct CHMe_2 peaks, accompanied by a single CMe_3 signal indicating that side to side symmetry is conserved. The room temperature ^1H NMR spectrum of **16** features sharp signals for proton environments that lie in the plane of the xanthene backbone, whereas significant broadening was seen for protons located above/below the xanthene backbone plane,

particularly the signals associated with the isopropyl groups. This is suggestive of a rapid fluxional process. Complex **16** in solution, was observed to decompose slowly at room temperature with complete decomposition after 12 hours.

A ^1H NMR spectrum of **16** at 258 K resulted in sharper signals for the proton environments above and below the xanthene backbone plane (Figure 4.14). In addition, the N-CH signal decoalesced to two distinct doublets at 258 K. The ^1H NMR spectra are consistent with the proposed $\text{CH}_2\text{SiMe}_2\text{CH}_2\text{SiMe}_3$ alkyl ligand formation, as evidenced by four distinct ^1H signals with a 2:6:2:9 integration. In addition, the proton signals for $\text{CH}_2\text{SiMe}_2\text{CH}_2\text{SiMe}_3$ were observed in regions similar to those reported by Piers et al. for the monocationic contact ion pair $[(\text{NacNac}^{\text{Bu,Dipp}})\text{Sc}(\text{CH}_2\text{SiMe}_2\text{CH}_2\text{SiMe}_3)][\text{MeB}(\text{C}_6\text{F}_5)_3]$. Furthermore, a broad peak at 1.51 ppm integrating to 3 is observed in the region where $\text{MeB}(\text{C}_6\text{F}_5)_3$ has been reported for many rare earth monocationic ion pairs such as $[(\text{NacNac}^{\text{Bu,Dipp}})\text{Sc}(\text{CH}_2\text{SiMe}_2\text{CH}_2\text{SiMe}_3)][\text{MeB}(\text{C}_6\text{F}_5)_3]$ (1.51 ppm) (Figures 4.14-4.17).

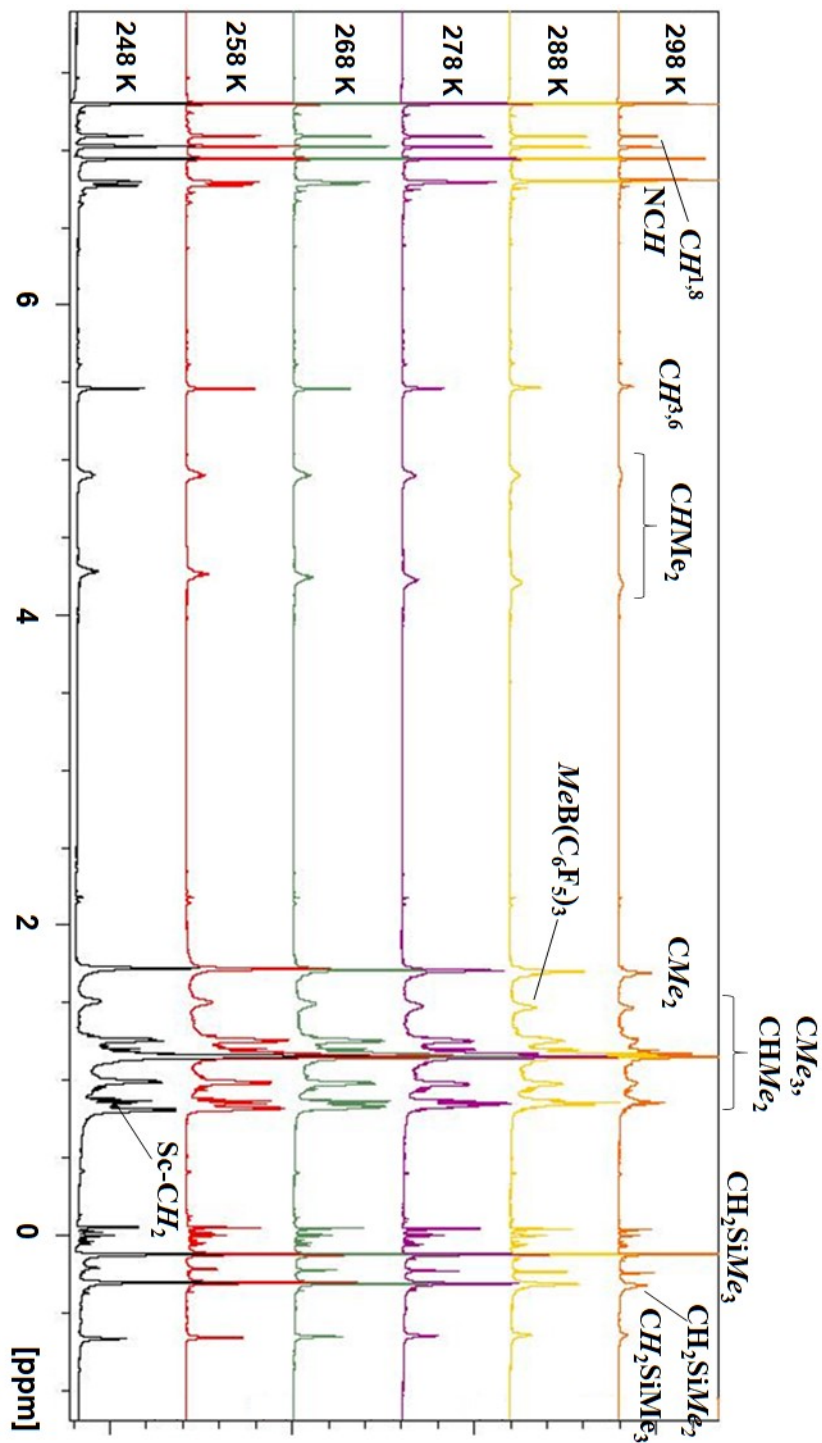


Figure 4.14: Variable Temperature - ^1H NMR Spectra of 16 (500 MHz, $\text{C}_6\text{D}_5\text{Br}$)

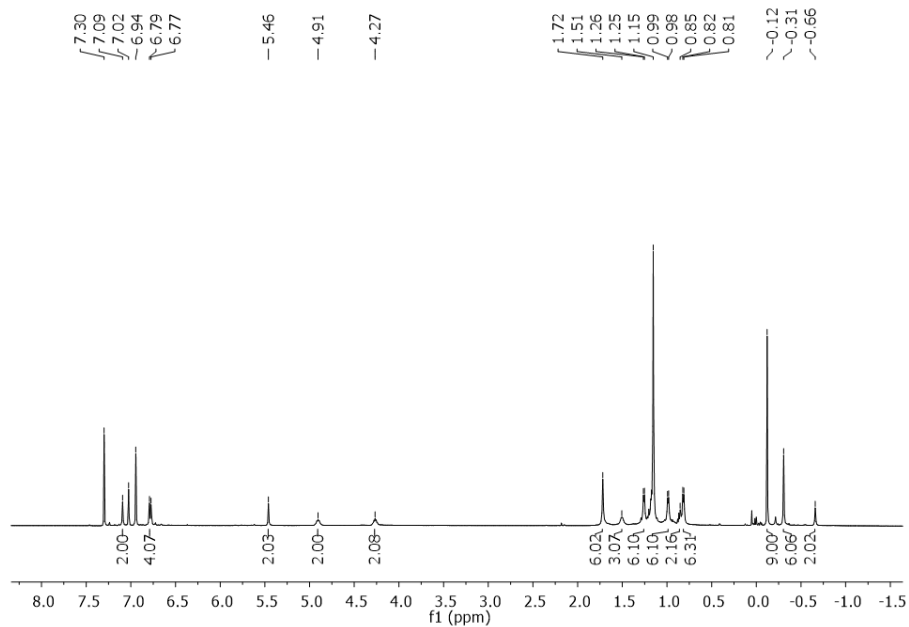


Figure 4.15: ^1H NMR Spectrum of 16 (500 MHz, 258K, $\text{C}_6\text{D}_5\text{Br}$)

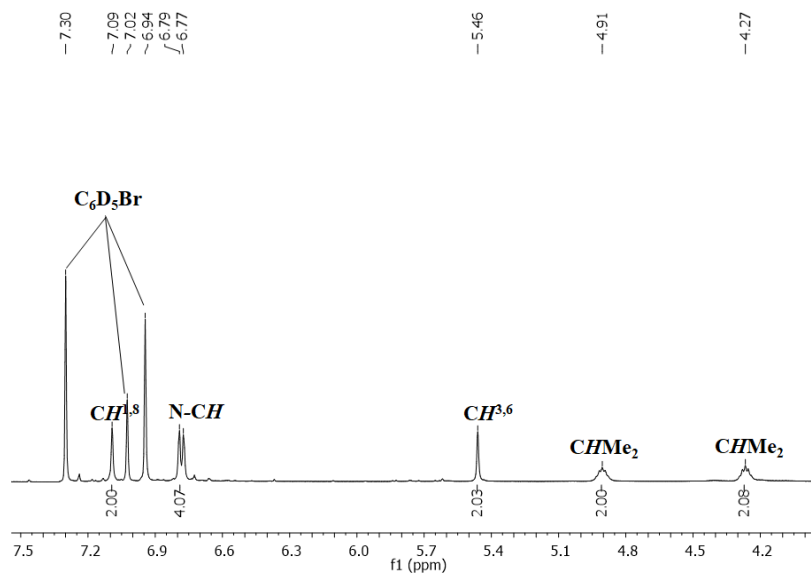


Figure 4.16: Expanded region of ^1H NMR spectrum of 16 (500 MHz, 258K, $\text{C}_6\text{D}_5\text{Br}$)

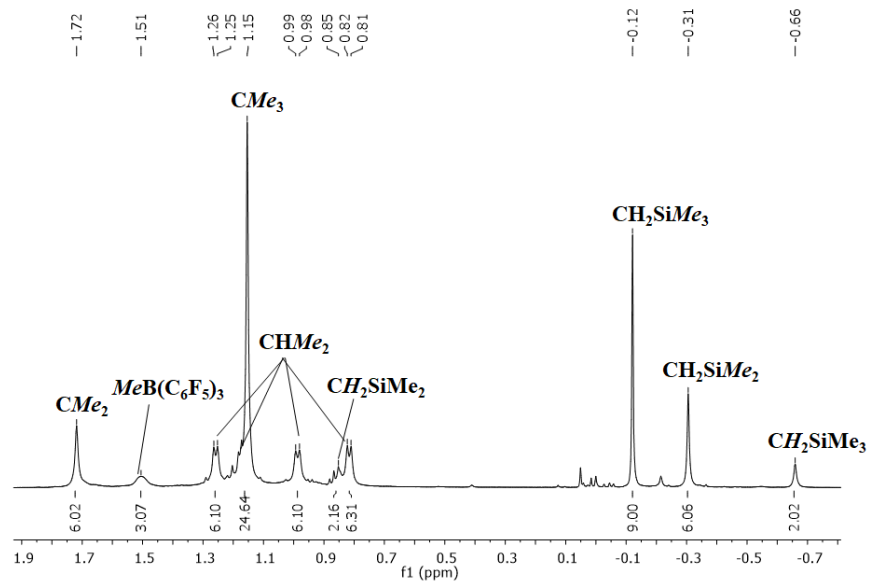


Figure 4.17: Expanded region of ^1H NMR Spectrum of **16 (500 MHz, 258K, $\text{C}_6\text{D}_5\text{Br}$)**

The ^1H - ^{13}C HMBC spectrum for **16** further supports the formation of the $\text{CH}_2\text{SiMe}_2\text{CH}_2\text{SiMe}_3$ ligand. As seen in Figure 4.18, the γ - CH_2 carbon signal couples to the proton signals of the SiMe_2 and SiMe_3 signals, which is consistent with expectations for a $\text{CH}_2\text{SiMe}_2\text{CH}_2\text{SiMe}_3$ alkyl. In addition, the proton signal for the SiMe_2 group was observed to couple with the α - CH_2 and γ - CH_2 carbon signals as seen in Figure 4.18.

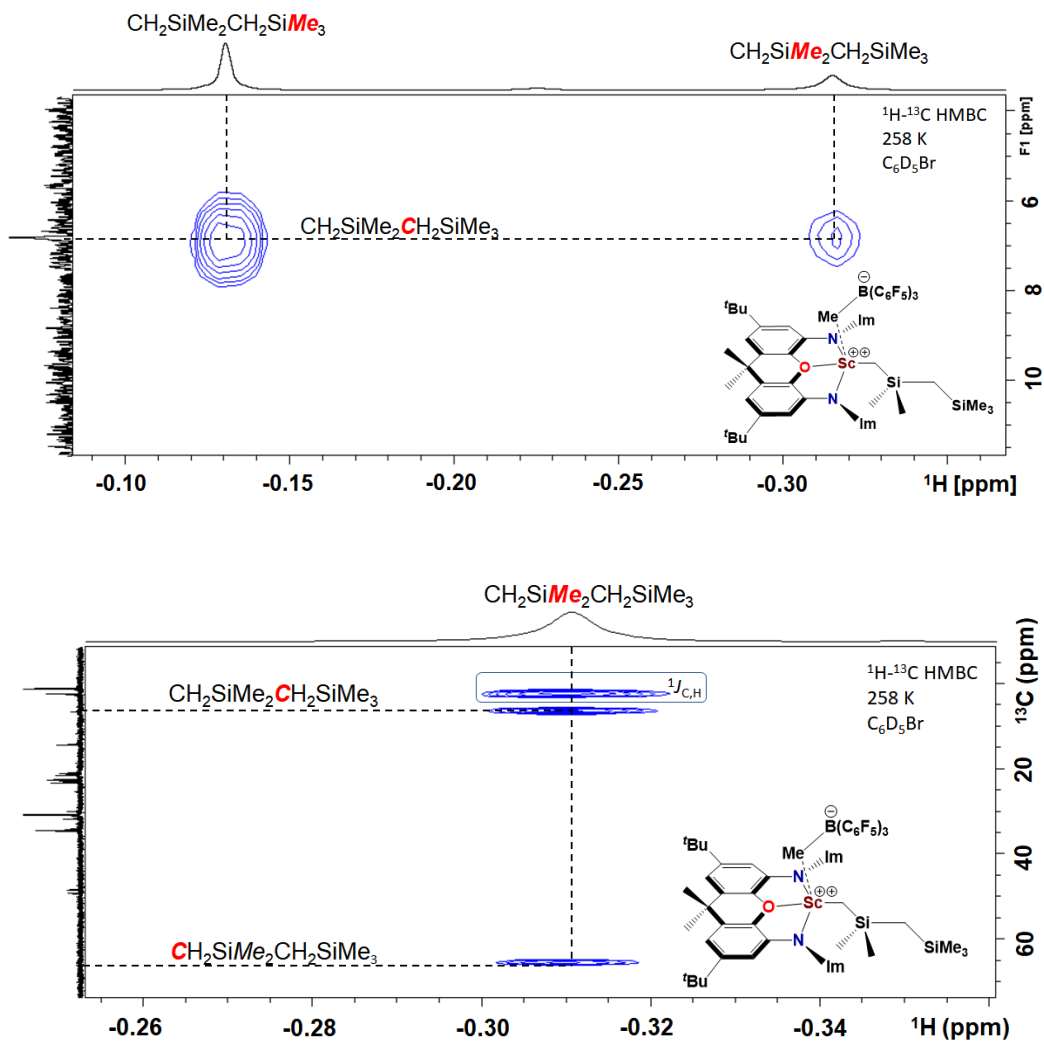


Figure 4.18: ^1H - ^{13}C HMBC of 16 (500 MHz ^1H , 126 MHz ^{13}C , 258 K $\text{C}_6\text{D}_5\text{Br}$)

Two distinct silicon environments were observed from a ^1H - ^{29}Si HMBC as seen in Figure 4.19. The $\alpha\text{-CH}_2$ and the SiMe_2 protons both couple to the same silicon center (SiMe_2), as opposed to the terminal SiMe_3 . The central CH_2 group couples to both silicon centers although this is harder to distinguish due to similar ^{29}Si chemical shifts of the two silicon centers.

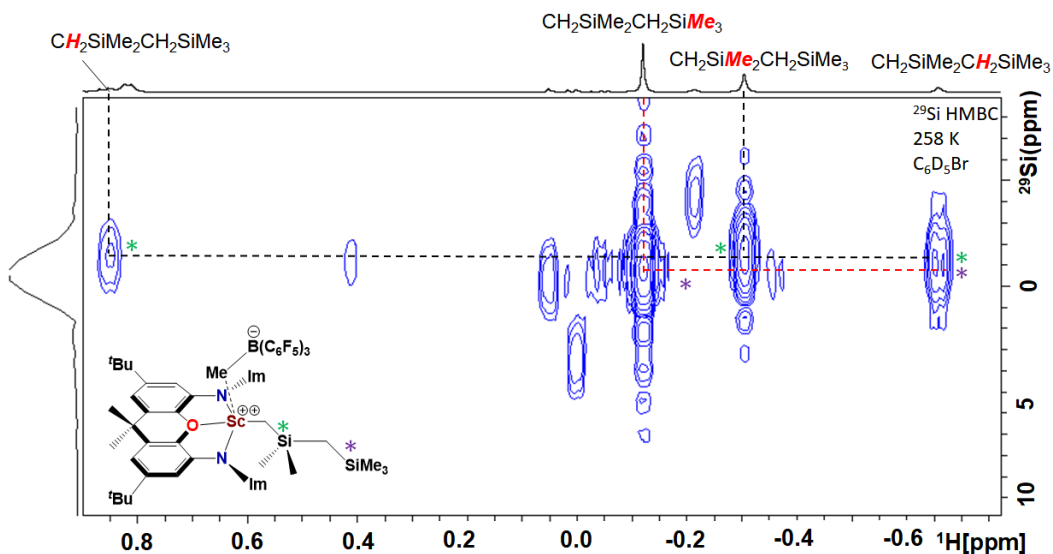


Figure 4.19: ^1H - ^{29}Si HMBC of **16** (500 MHz ^1H , 126 MHz ^{29}Si , 258K, $\text{C}_6\text{D}_5\text{Br}$)

Similar to the previously discussed rare earth alkyl complexes in this thesis, **16** was also observed to have a $^1J_{\text{C,H}}$ coupling constant of 100 Hz suggestive of an α -agostic interaction.^{101, 102}

Two distinct sharp signals are seen in the ^{11}B NMR spectrum of **16** corresponding to the $\text{B}(\text{C}_6\text{F}_5)_4$ anion (δ -16.20 ppm) and the $\text{MeB}(\text{C}_6\text{F}_5)_3$ anion (δ -15.02 ppm) anion (Figure 4.20). The ^{11}B NMR chemical shift of **16** is comparable to literature examples of $\text{MeB}(\text{C}_6\text{F}_5)_3$ rare earth contact ion pair complexes such as $[(\text{NacNac}^{\text{tBu, Dipp}})\text{Sc}(\text{CH}_2\text{SiMe}_2\text{CH}_2\text{SiMe}_3)][\text{MeB}(\text{C}_6\text{F}_5)_3]$ (δ -15.2 ppm) and $[(\text{NacNac}^{\text{tBu, Dipp}})\text{ScCH}_3][\text{MeB}(\text{C}_6\text{F}_5)_3]$ (δ -16.6 ppm).^{39, 47}

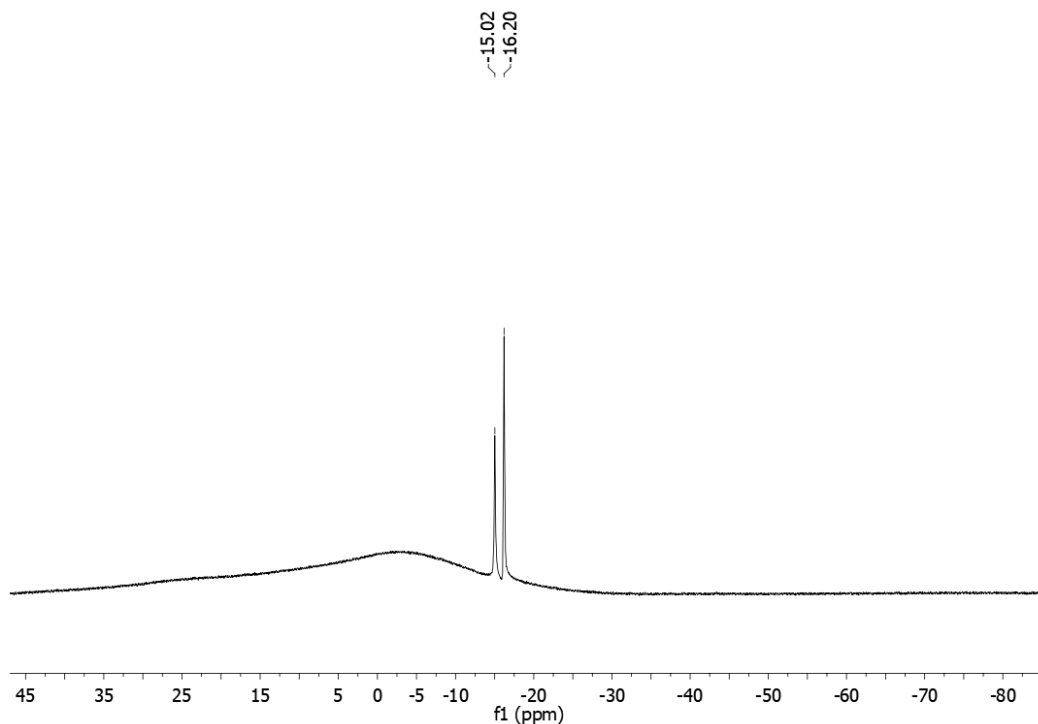


Figure 4.20: ^{11}B NMR Spectrum of **16** (161 MHz, 258K, $\text{C}_6\text{D}_5\text{Br}$)

The ^{19}F NMR spectrum is consistent with the expected signals for the $\text{B}(\text{C}_6\text{F}_5)_4$ and $\text{MeB}(\text{C}_6\text{F}_5)_3$ anions of **16** (Figure 4.21). Horton and coworkers established a probe in which the value of $\Delta\delta(\text{m,p-F})$, the chemical shift difference between the meta and para fluorine signals for the $[\text{RB}(\text{C}_6\text{F}_5)_3]$ ($\text{R} = \text{Me}, \text{CH}_2\text{Ph}$) anion, indicates its coordination/non-coordination to a d^0 metal center (values: 3-6 ppm indicate coordination, < 3 ppm indicates non coordination).¹²² As seen in Figure 4.21, the $\Delta\delta(\text{m,p-F})$ value for $\text{MeB}(\text{C}_6\text{F}_5)_3$ (**16**) is 4.19 ppm, which strongly suggests coordination to the metal center via a methyl bridge.

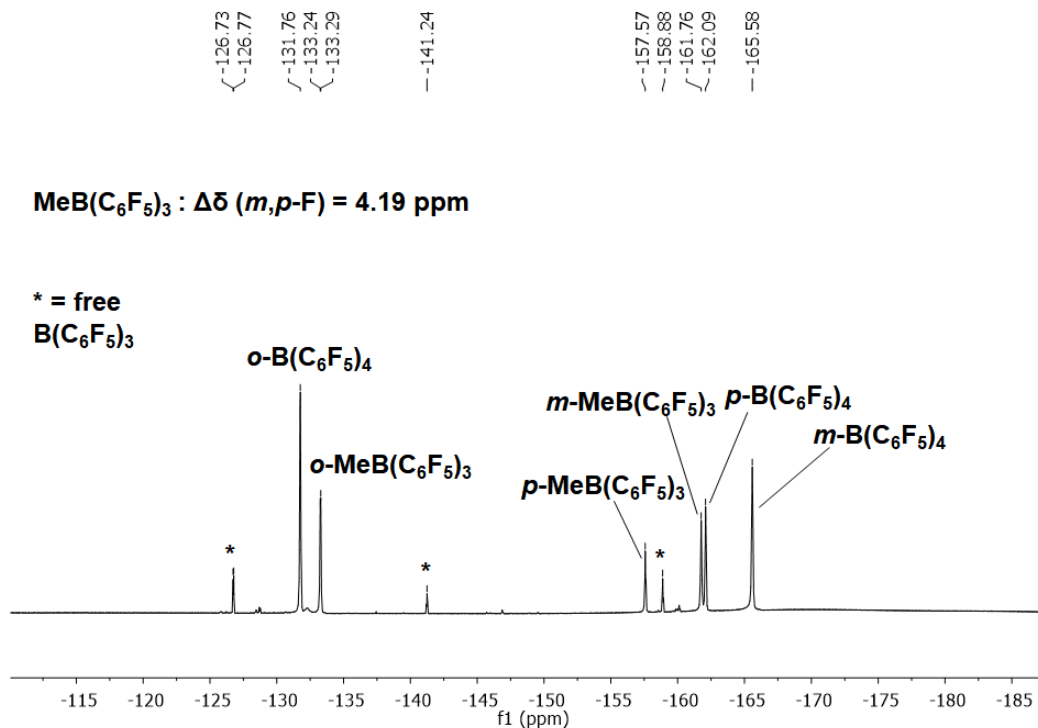
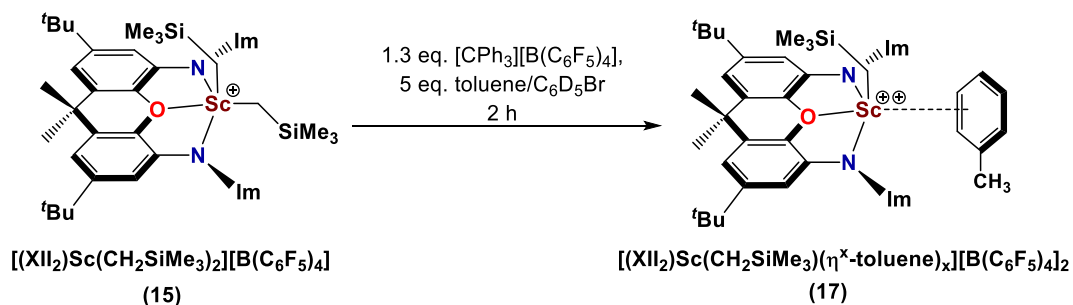


Figure 4.21: ¹⁹F NMR Spectrum of **16** (471 MHz, 258K, C₆D₅Br)

4.8.2 In-situ generation of [(XII)₂Sc(CH₂SiMe₃)(η^x -toluene)_x][B(C₆F₅)₄]₂ (*x* = 0,1)

The reaction of **15** with 1.3 equivalents of [CPh₃][B(C₆F₅)₄] in C₆D₅Br in the presence of 5 equivalents of toluene, afforded a dicationic monoalkyl complex [(XII)₂Sc(CH₂SiMe₃)(η^x -toluene)_x][B(C₆F₅)₄]₂ (**17**; Scheme 4.9), accompanied by the usual byproducts of trimethylsilylmethyl group abstraction by the trityl cation; Ph₃CH, as well as SiMe₃ and CH₂ signals (δ 2.36, -0.02 ppm respectively)

attributed to one isomer of “Ph₃CCH₂SiMe₃”.^{68, 123} The reaction had to be stirred for 2 hours or intermittently sonicated in a J-young tube to observe the generation of **17**. A dark orange oil was observed to precipitate over the 2 hour reaction period and is attributed to **17**'s low solubility in C₆D₅Br. In the presence of 5 equivalents of toluene, **17** was stable for several days and showed slow decomposition to an unidentified insoluble product. Significant decomposition to unidentified products is seen after 4 days at room temperature. In the absence of toluene, a 1:1 reaction of [CPh₃][B(C₆F₅)₄] and **15** in C₆D₅Br resulted in several unidentified products, as well as tetramethylsilane, which is indicative of decomposition. This strongly suggests that toluene stabilizes **17** via π -coordination.



Scheme 4.9: In-situ generation of [(XII₂)Sc(CH₂SiMe₃)(η^x -toluene)_x][B(C₆F₅)₄]₂ (17**) (x = 0, 1)**

The room temperature ¹H NMR spectrum of **17** features one CHMe₂ and one CMe₂ signal (Figures 4.22-4.24). Both of these signals are broad, indicative of a rapid migration of the alkyl group between coordination sites above and below the plane of the ligand backbone. The ScCH₂ ¹H and ¹³C NMR signals were

observed at δ 0.70 and 64.1 ppm, respectively, with a $^1J_{C,H}$ coupling constant of 103 Hz, which is suggestive of an α -agostic interaction.

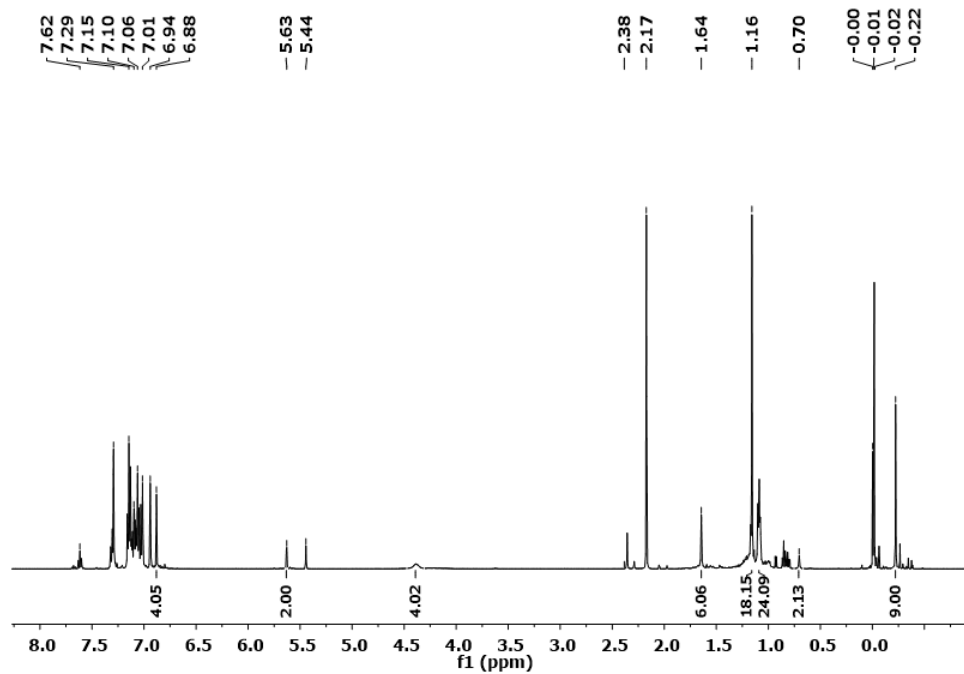


Figure 4.22: ^1H NMR Spectrum of 17 generated in the presence of 5 equivalents of toluene (500 MHz, 298K, $\text{C}_6\text{D}_5\text{Br}$)

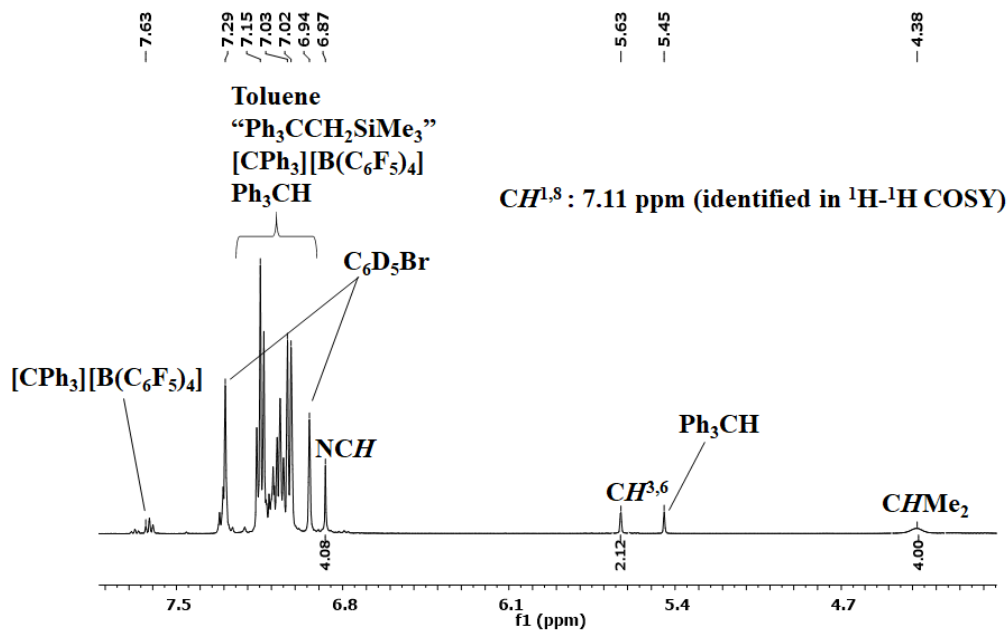


Figure 4.23: Expanded ^1H NMR Spectrum of 17 generated in the presence of 5 equivalents of toluene (161 MHz, 298K, $\text{C}_6\text{D}_5\text{Br}$)

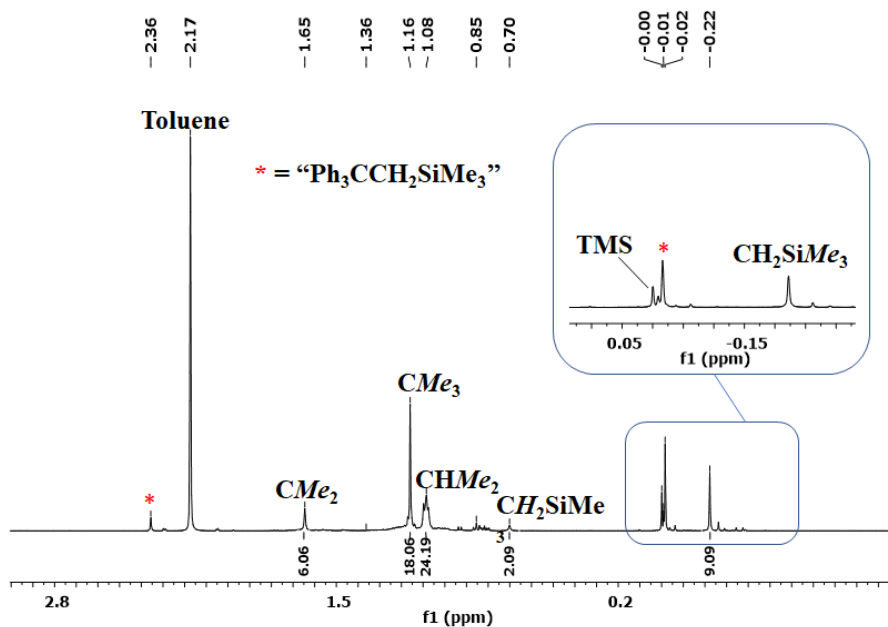


Figure 4.24: Expanded ^1H NMR Spectrum of 17 generated in the presence of 5 equivalents of toluene (161 MHz, 298K, $\text{C}_6\text{D}_5\text{Br}$)

Select examples of C_6F_5 transfer from the $B(C_6F_5)_4$ anion to a cationic rare earth center have been reported in the literature. However, this was not observed for **17**. A single sharp signal was observed at -16.21 ppm in the ^{11}B NMR spectrum (Figure 4.25), and just three signals were observed in the ^{19}F NMR spectrum (Figure 4.26), consistent with intact $B(C_6F_5)_4$ anions.

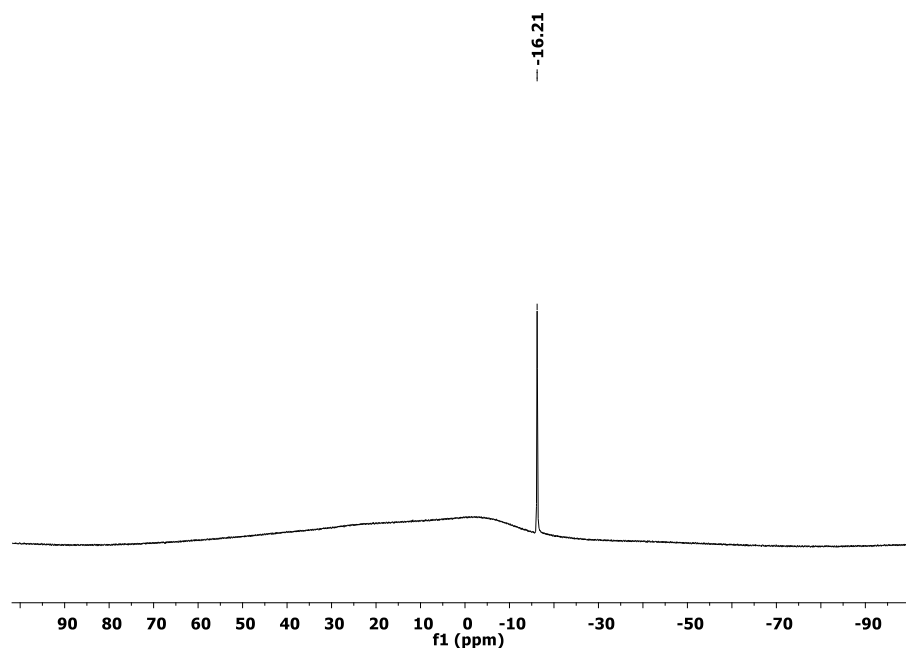


Figure 4.25: ^{11}B NMR Spectrum of **17** generated in the presence of 5 equivalents of toluene (161 MHz, 298K, C_6D_5Br)

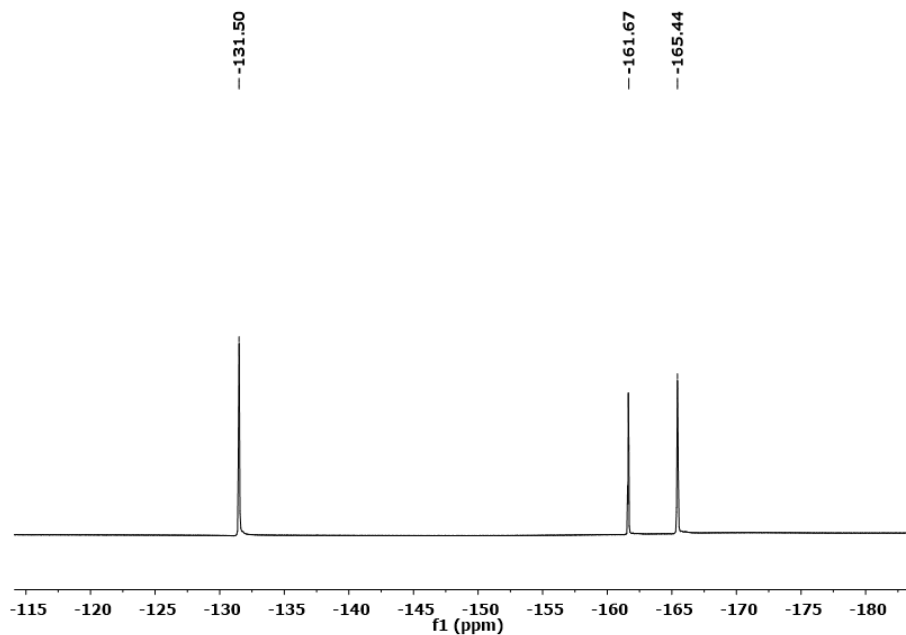


Figure 4.26: ^{19}F NMR Spectrum of **17** generated in the presence of **5** equivalents of toluene (471 MHz, 258K, $\text{C}_6\text{D}_5\text{Br}$)

Complex **17** was generated in the presence of 10 equivalents of toluene in $\text{C}_6\text{D}_5\text{Br}$ and low temperature ^1H NMR spectra (25 °C to -25 °C) were recorded in an effort to observe toluene coordination to afford a C_s symmetric complex (Figure 4.27). However, this proved unsuccessful in the temperature range studied (the freezing point of bromobenzene is -31 °C). Significant broadening of proton signals that lie above/below the xanthene backbone such as the CHMe_2 and CMe_2 signals was observed at lower temperatures as can be seen in Figure 4.26. Significant precipitation of a dark orange oil was also seen at -25 °C. Complex **17**

proved to be unstable in CH_2Cl_2 and is insoluble in toluene, which prevented studies at a temperatures lower than $-25\text{ }^\circ\text{C}$.

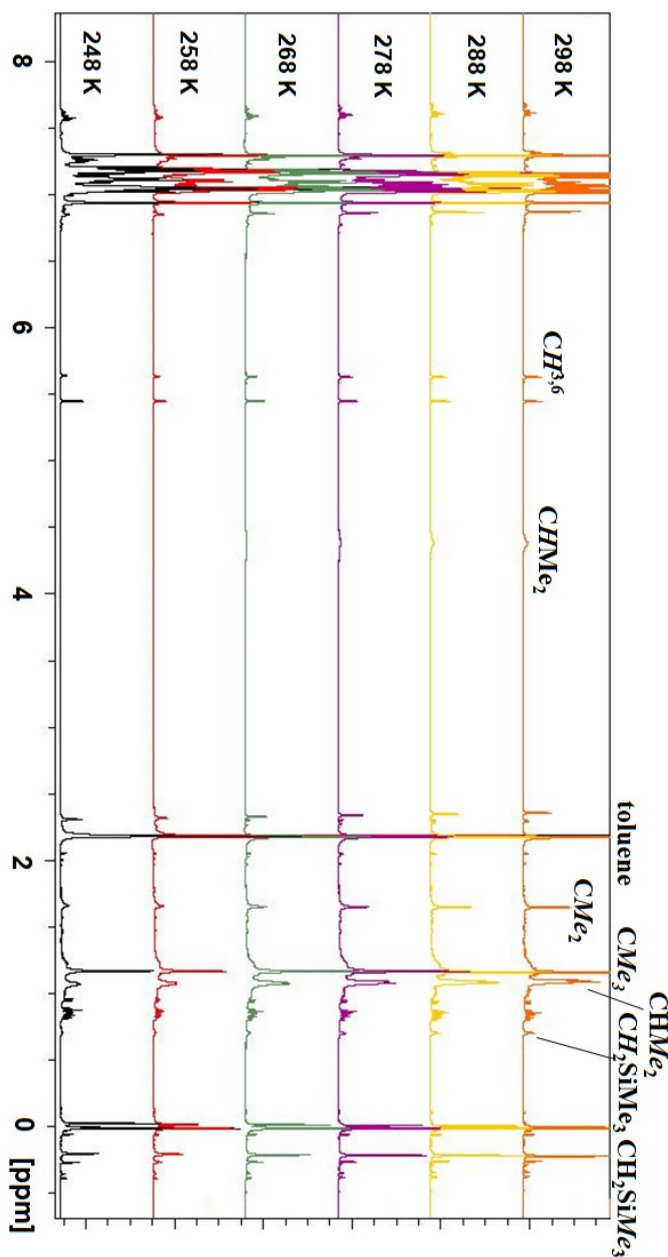
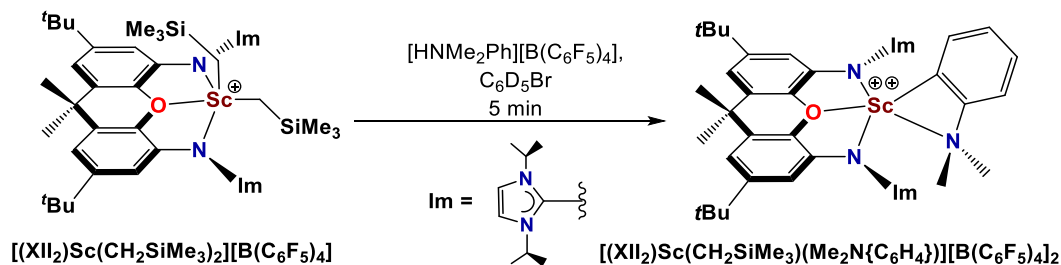


Figure 4.27: Variable Temperature ^1H NMR Spectra of 17 (500 MHz, $\text{C}_6\text{D}_5\text{Br}$)

4.8.3 In-situ generation of the dicationic [(XII₂)Sc(C₆H₄NMe₂)]₂[B(C₆F₅)₄]₂ (**17**) complex

Apart from Lewis acidic B(C₆F₅)₃ and CPh₃⁺, the Brønsted acid co-reactant [HNMe₂Ph][B(C₆F₅)₄] is often utilized to access cationic rare earth complexes. A 1:1 reaction of [HNMe₂Ph][B(C₆F₅)₄] and **15** resulted in the liberation of 2 equivalents of TMS, as opposed to the expected 1 equivalent (Scheme 4.10), yielding [(XII₂)Sc(C₆H₄NMe₂)]₂[B(C₆F₅)₄]₂ (**18**) in-situ.



Scheme 4.10: In-situ generation of [(XII₂)Sc(C₆H₄NMe₂)]₂[B(C₆F₅)₄]₂ (18**)**

Solution NMR spectra indicate the formation of a *C_s* symmetric complex, with a loss of top bottom symmetry, as evidenced by the presence of two distinct *CHMe₂* signals (δ 4.21 and 4.08 ppm) and two *CMe₂* signals (δ 1.56, 1.49 ppm) (Figure 4.28). Both *CHMe₂* signals integrate to 2H, and are septets, which indicate that cyclometallation of the isopropyl groups has not occurred. The N,N-

dimethylaniline byproduct is occasionally found to coordinate to the cationic rare earth centers, either through σ -donation via the nitrogen or η^6 -coordination of the phenyl ring (Section 1.5.3). Piers and coworkers observed that η^6 -coordinated *N,N*-dimethylaniline resulted in a significant low frequency shift for the para and ortho-phenyl resonances (e.g. $[(\text{NacNac}^{\text{Me,Dipp}})\text{Y}(\text{CH}_2\text{Ph})(\eta^6\text{-Ph-NMe}_2)][\text{B}(\text{C}_6\text{F}_5)_4]$ *p*-phenyl = 5.79 ppm, *o*-phenyl = 6.11 ppm in $\text{C}_6\text{D}_5\text{Br}$), which was not observed for **18**.⁴⁸ The presence of a single peak for the NMe_2 group integrating to 6 in addition to 4 distinct C–H phenyl environments observed in the ^{13}C NMR, as well as an additional quaternary aromatic resonance at 174.80 ppm suggests C–H bond activation of the phenyl ring of *N,N*-dimethylaniline. Only one other example of C–H bond activation of *N,N*-dimethylaniline by a monocationic rare earth center has been reported. In the aforementioned literature example by Anwender and coworkers, the ortho-phenyl is C–H activated.¹²⁴ X-ray quality crystals of **18** were not successfully grown, and overlapping C_6H_4 ^1H NMR signals prevented definitive identification of the site of C–H activation. However, it is likely that the *ortho*-phenyl position is C–H bond activated due to initial NMe_2 coordination to scandium (and in order to maintain NMe_2 coordination). ^{19}F and ^{11}B NMR spectra are consistent with the intact $\text{B}(\text{C}_6\text{F}_5)_4$ anions (Figures 4.29-4.30).

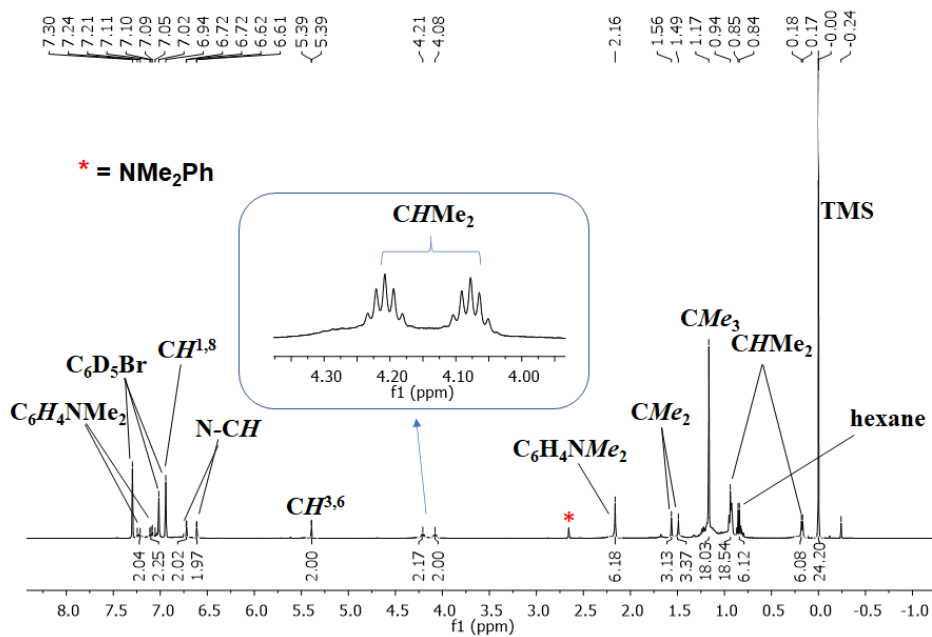


Figure 4.28: ^1H NMR Spectrum of in-situ generated 18 (600 MHz, 298K, $\text{C}_6\text{D}_5\text{Br}$)

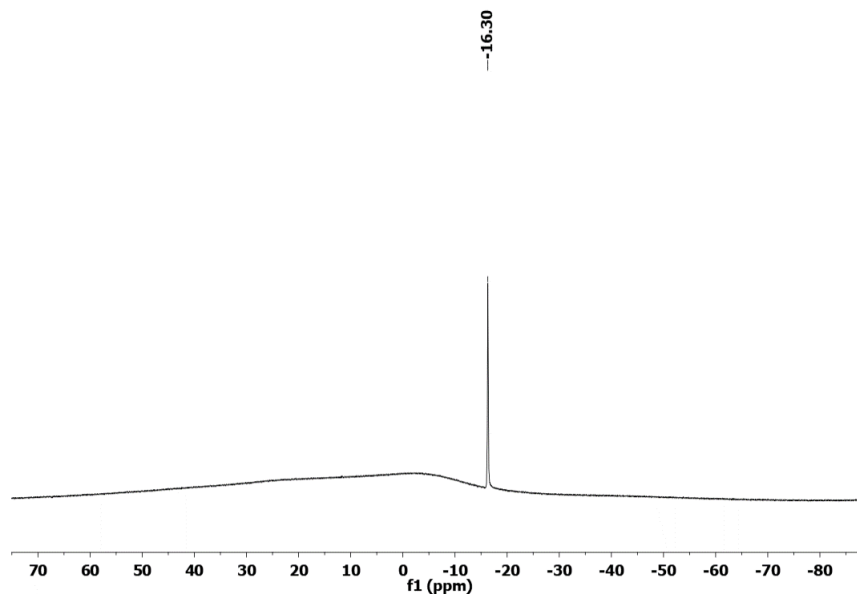


Figure 4.29: ^{11}B NMR Spectrum of in-situ generated 18 (161 MHz, 298K, $\text{C}_6\text{D}_5\text{Br}$)

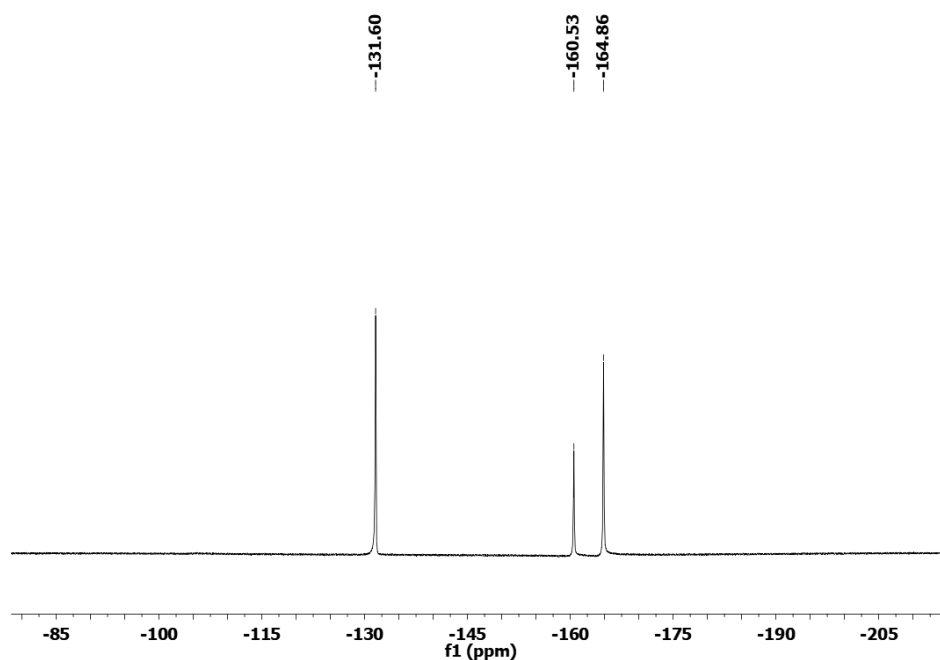


Figure 4.30: ^{19}F NMR Spectrum of in-situ generated **18** (471 MHz, 298K, $\text{C}_6\text{D}_5\text{Br}$)

Complex **18** slowly decomposes to generate a midnight blue complex that is slightly soluble in bromobenzene and is accompanied by the generation of free dimethyl aniline. This complex is yet to be identified and appears to be paramagnetic due to the absence of corresponding signals in the ^1H NMR spectrum.

4.9 Ethylene Polymerization Catalysis Using $[(XII)_2Sc(CH_2SiMe_3)][B(C_6F_5)_4]_2$

Select examples of dicationic rare earth alkyl complexes have proven to be efficient olefin polymerization catalysts as previously outlined in Section 1.5.6. Only two examples of spectroscopically observed unsaturated dicationic rare earth monoalkyl complexes are reported in the literature, which consequently proved to be highly efficient olefin polymerization catalysts.^{42, 60}

The dicationic monoalkyl complex **16** was investigated for its potential as an ethylene polymerization catalyst. However, the compound was inactive towards ethylene polymerization. This may be attributed to the strong contact ion pair formation with the $MeB(C_6F_5)_3$ anion, which prevents the ethylene coordination required for polymerization.

In contrast, complex **17** proved to be a potent ethylene polymerization catalyst when generated in the presence of toluene at 24 °C and placed under 1 atm of ethylene as summarized in Table 4.1. Complex **17** has higher activity when polymerization is terminated after 3 minutes as opposed to 5 minutes. This can be attributed to the catalyst either decomposing partially due to the highly exothermic nature of the polymerization or due to the catalyst becoming ensnared in the precipitated polyethylene. Run times longer than 5 minutes were not attempted due to the significant precipitation of polyethylene which prevented stirring of the solution. The polydispersity is rather narrow for Entry 2 and 3 (1.40, 1.41),

however at a higher run time of 5 minutes (Entry 3) the polydispersity is slightly broader (2.06), which can be similarly be attributed to significant precipitation of polyethylene. The M_w of the resulting polyethylene increases with run time as is to be expected. The moderately narrow polydispersity suggests that the catalyst is active during the entirety of the polymerization run.

Table 4.1: Ethylene polymerization by **17**

Entry	Time (min)	Yield (g)	^a Activity	M_w (g/mol)	M_w/M_n	Solvent
1	2	0.239	741	65 700	1.40	4:1 (toluene: <i>o</i> -C ₆ H ₄ F ₂)
2	3	0.420	868	111 880	1.41	4:1 (toluene: <i>o</i> -C ₆ H ₄ F ₂)
3	5	0.456	565	202 100	2.06	4:1 (toluene: <i>o</i> -C ₆ H ₄ F ₂)
4	3	0.135	168	170 550	1.29	<i>o</i> -C ₆ H ₄ F ₂

^a Activity in kg PE mol⁻¹ h⁻¹ atm⁻¹. Polymerization conditions: 25 °C, 1 atm of ethylene. Entry 1-3: Catalyst (**17**) is generated in solution by reacting 0.01 mmol of **15** and 0.01 mmol of [CPh₃][B(C₆F₅)₄] in 2 mL (1:1 toluene/*o*-C₆H₄F₂) and stirred for 2 hours. The reaction is then diluted with 50 mL of a 4:1 mixture of toluene:*o*-C₆H₄F₂. Entry 4: Catalyst is generated in solution by reacting 0.01 mmol of **15** and 0.01 mmol of [CPh₃][B(C₆F₅)₄] in 2 mL of *o*-C₆H₄F₂ and stirred for 30 minutes. The reaction is then diluted with 50 mL of *o*-C₆H₄F₂.

The activity dramatically decreased when the catalyst was generated, and the polymerization was conducted, in the absence of toluene (Entry 4). This can be attributed to a requirement for stabilization of the dicationic catalyst by toluene coordination. Nevertheless, the polydispersity of the resulting polymer is still rather narrow (1.29), suggesting that one active species is responsible for the catalysis.

Complex **17**'s ethylene polymerization activity compares favorably with other non-cyclopentadienyl scandium catalysts. Okuda and coworkers, in-situ generated a dicationic complex (from the reaction of $[\text{Sc}(\text{CH}_2\text{SiMe}_3)_3(\text{THF})_2]$ and 5 eq. $[\text{HNMe}_2\text{Ph}][\text{B}(\text{C}_6\text{F}_5)_4]$ in toluene), which showed low activity ($1 \text{ kg mol}^{-1} \text{ h}^{-1} \text{ atm}^{-1}$) for ethylene polymerization.⁵⁷ Similarly, monocationic scandium catalysts such as Piers' $[(\text{NacNac}^{\text{iBu,Dipp}})\text{Sc}(\text{CH}_3)][\text{MeB}(\text{C}_6\text{F}_5)_3]$ ($59 \text{ kg mol}^{-1} \text{ h}^{-1} \text{ atm}^{-1}$) and Hessen's $[\text{PhC}(\text{N}\{\text{Diip}\})(\text{N}\{\text{Diip}\})\text{Sc}(\text{CH}_2\text{SiMe}_3)(\text{THF})][\text{B}(\text{C}_6\text{F}_5)_4]$ ($24 \text{ kg mol}^{-1} \text{ h}^{-1} \text{ atm}^{-1}$) both exhibited lower ethylene polymerization activities than **17**.^{39, 54} . Complex **17** is approaching the high activity for ethylene polymerization observed by Trifonov for his monocationic $[(2,6\text{-}^i\text{Pr}_2\text{C}_6\text{H}_3)\text{NC}(\text{Me})\text{CHPPH}_2\text{N}(2,6\text{-Me}_2\text{C}_6\text{H}_3)\text{Sc}(\text{CH}_2\text{SiMe}_3)][\text{B}(\text{C}_6\text{F}_5)_4]$ complex ($2460 \text{ kg P.E mol}^{-1} \text{ h}^{-1} \text{ bar}^{-1}$).¹²⁵

4.10 Summary and Conclusions

Initial attempts to synthesize the XII₂ ligand via the Staudinger reaction instead afforded the triazene intermediate XIA₂. The XIA₂ ligand was utilized in

isolation of a neutral yttrium complex, [(XIA)Y(CH₂SiMe₃)₃] (**10**). However, this complex slowly decomposed at room temperature.

A rare example of a Buchwald-Hartwig ‘imination’ using an imidazol-2-imine was utilized in order to isolate XII₂. Subsequent protonation of XII₂ using [H(Et₂O)₂][B(C₆F₅)₄] and reaction with [M(CH₂SiMe₃)₃(THF)₂] (M= Sc, Y) yielded the dialkyl cations [(XII₂)Y(CH₂SiMe₃)₂][B(C₆F₅)₄](**14**) [(XII₂)Sc(CH₂SiMe₃)₂][B(C₆F₅)₄] (**15**). Complex **15** was utilized to generate rare examples of dicationic rare earth alkyl complexes. The reaction of **15** with the Lewis acid B(C₆F₅)₃ yielded [(XII₂)Sc(CH₂SiMe₂CH₂SiMe₃)][(MeB(C₆F₅)₃)] [B(C₆F₅)₄] **16**, which is the first spectroscopically observed dicationic group 3 contact ion pair. Reaction of **15** with [CPh₃][B(C₆F₅)₄] resulted in a rare example of a spectroscopically observed monoalkyl dication [(XII₂)Sc(CH₂SiMe₃)(η^x-toluene)_x][B(C₆F₅)₄]₂ (**17**). Complex **17** proved to be a highly efficient ethylene polymerization catalyst that rivals the activities of other non-metallocene rare earth alkyl olefin polymerization catalysts.

Chapter 5

Synthesis of an Alkyl Yttrium Cation Utilizing A Monoanionic Rigid Asymmetric NON-Donor Ligand

5.1 Introduction

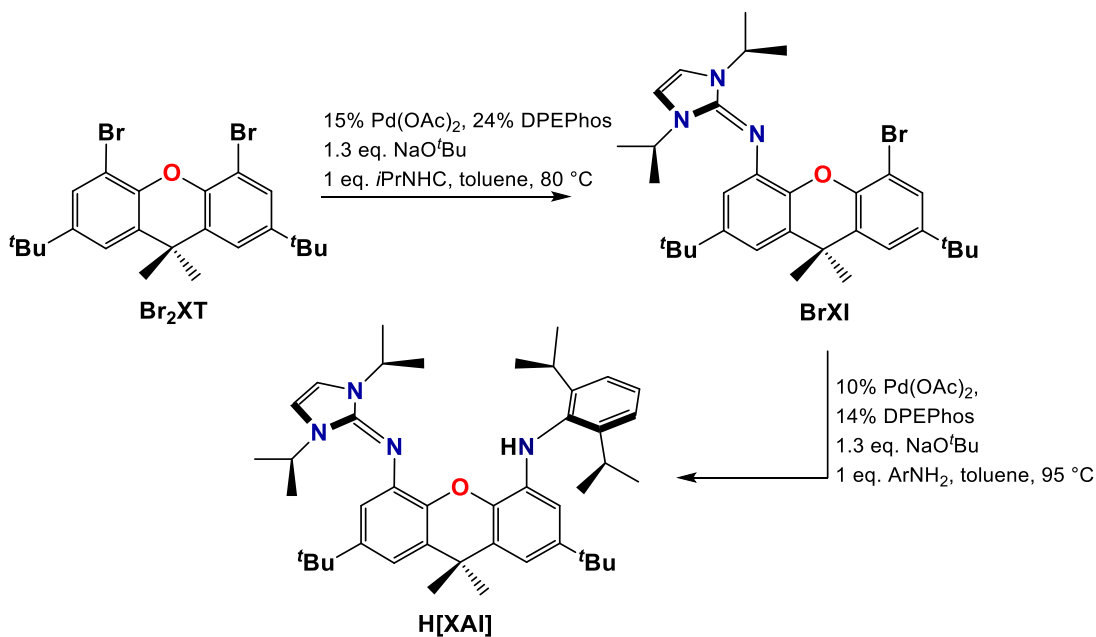
Rare earth alkyl complexes are often thermally unstable due to their propensity to follow decomposition pathways such as cyclometallation.⁴⁰ Furthermore, cationic rare earth alkyl complexes are scarce due to their highly reactive nature. Careful ligand design which incorporates steric protection and high electron donation, in addition to cyclometallation resistance is required to access potential cationic rare earth alkyl complexes.^{40, 61}

Previously, the Emslie group has reported the synthesis of dianionic 4,5-bis(arylamido)xanthene ligands (XA_2 and XN_2 ; Figure 5.1) which have been shown to be highly effective for the isolation of reactive organometallic complexes.^{23, 63-65, 68, 104} Specifically, XA_2 was successfully utilized in the isolation of a cationic thorium alkyl complex and a rare example of a dicationic thorium complex.^{66, 68} XN_2 was successfully utilized in accessing neutral yttrium and lutetium monoalkyl complexes which demonstrated cyclometallation resistance at room temperature.^{23, 97} A limitation of 4,5-bis(amido)xanthene ligands is that their 2- charge does not

allow for the synthesis of cationic alkyl complexes of the rare earth elements. This led to the design of the monoanionic AII₂ ligand (Chapter 3) where a zwitterionic resonance structure can be expected to allow the imidazole rings to lie perpendicular to the plane of the acridanide backbone. This provides a steric profile similar to that of the XA₂ dianion (albeit with isopropyl groups slightly further removed from the metal coordination pocket due to their attachment in the *ortho* positions of a 5-membered rather than a 6-membered ring), and as a consequence, complexes of the AII₂ ligand were expected to demonstrate similar cyclometallation resistance. Although AII₂ was successfully utilized to prepare a cationic yttrium alkyl complex in-situ (Chapter 3), the complex decomposed within 45 minutes at room temperature, and the reduced steric bulk of the AII₂ ligand relative to the XA₂ and XN₂ ligands may be responsible for this low stability.

In order to access a stable monocationic yttrium monoalkyl complex, we became interested in designing a monoanionic ligand with increased steric protection. This led to the design of the XAI ligand which utilizes a neutral xanthene backbone with one flanking neutral imidazol-2-imine donor and one flanking 2,6-diisopropylanilido anionic donor.

position yielding BrXI (Scheme 5.1). Subsequent Buchwald-Hartwig amination with 2,6-diisopropylaniline yielded H[XAI] as seen in Scheme 5.1.



Scheme 5.1: Synthesis of H[XAI]

Solution NMR spectra for H[XAI] are consistent with the expected *C_s*-symmetric structure (Figures 5.2-5.4); a single *CMe*₂ signal was observed by ¹H and ¹³C NMR spectroscopy, while two distinct *CMe*₃ signals were observed by ¹H and ¹³C NMR. The *NH* signal appears as a sharp singlet at δ 5.17 ppm, which is in the region expected for secondary amines.

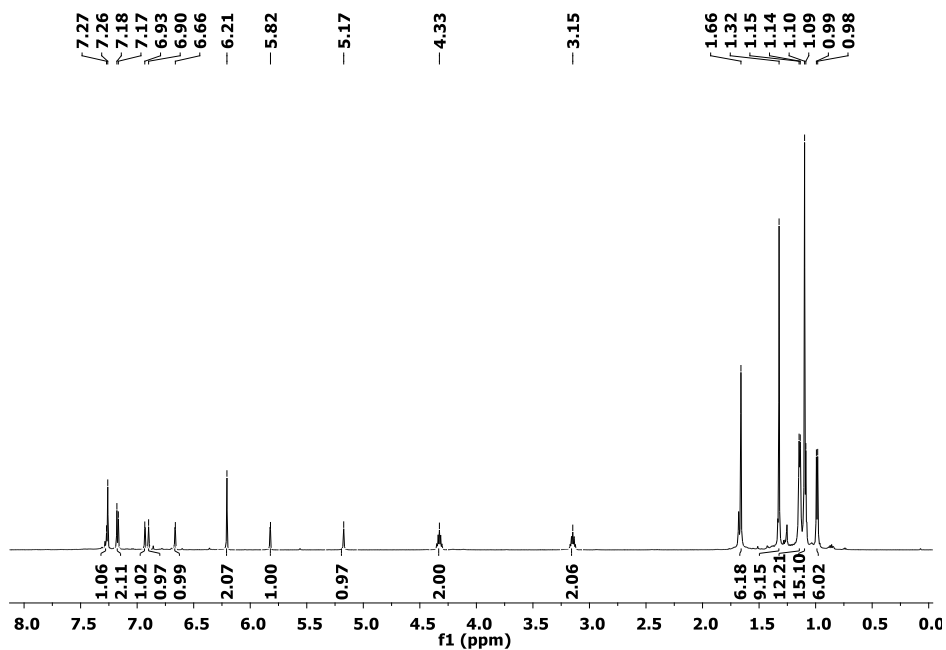


Figure 5.2: ^1H NMR Spectrum of H[XAI] (600 MHz, CDCl_3)

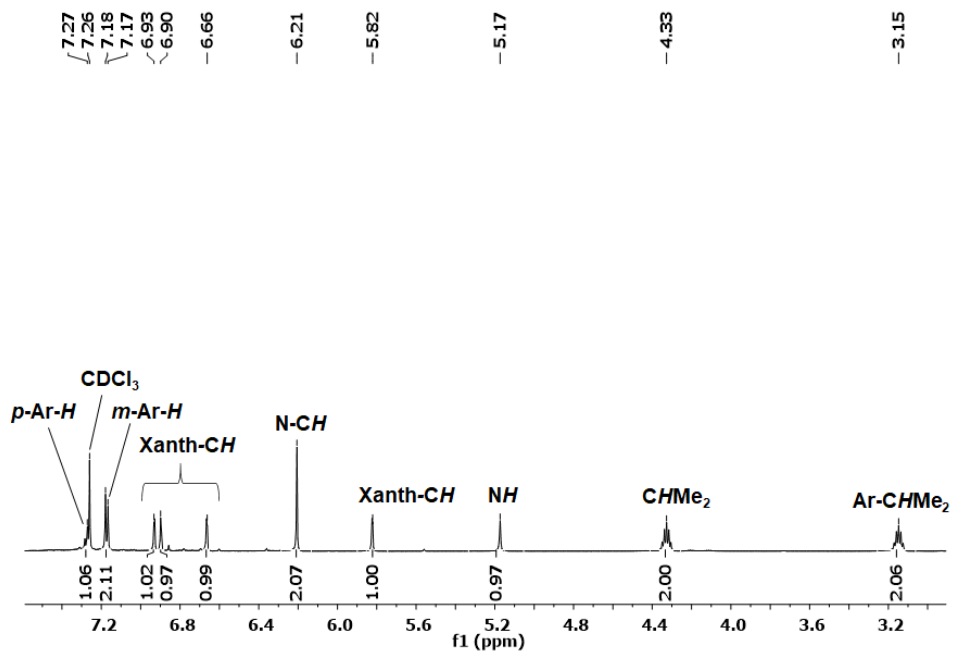


Figure 5.3: Expanded Region - ^1H NMR Spectrum of H[XAI] (600 MHz, CDCl_3)

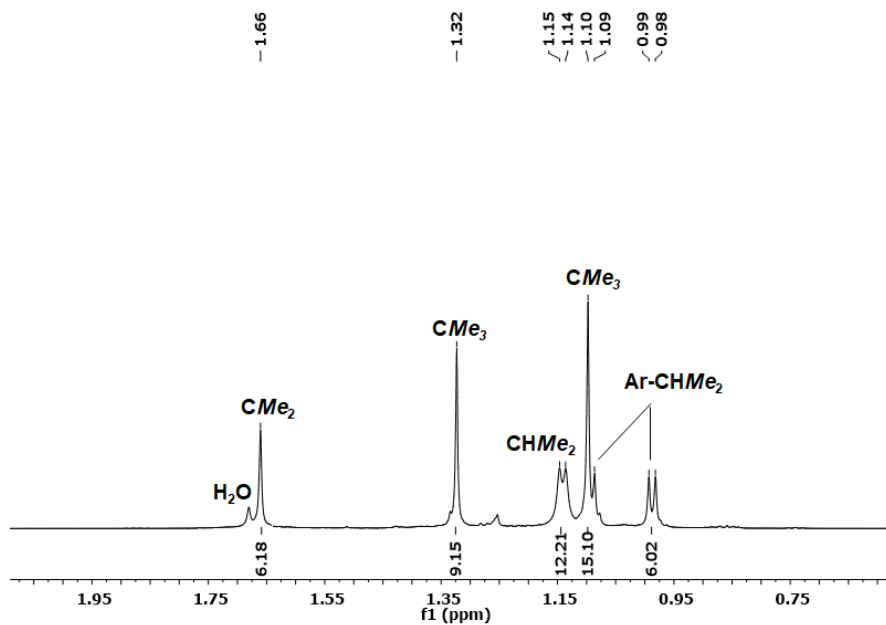
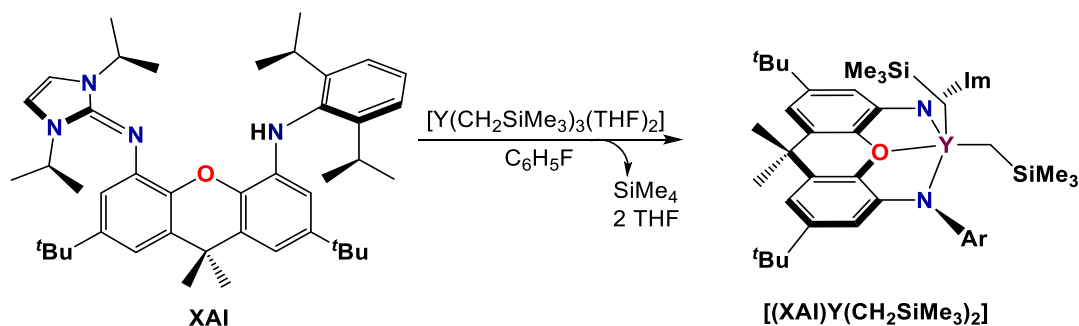


Figure 5.4: Expanded Region - ^1H NMR Spectrum of $\text{H}[\text{XAl}]$ (600 MHz, CDCl_3)

5.3 Synthesis of $[(\text{XAl})\text{Y}(\text{CH}_2\text{SiMe}_3)_2]$

A 1:1 reaction of $\text{H}[\text{XAl}]$ with $[\text{Y}(\text{CH}_2\text{SiMe}_3)_3(\text{THF})_2]$ in $\text{C}_6\text{H}_5\text{F}$ resulted in the elimination of 1 equivalent of tetramethylsilane to afford $[(\text{XAl})\text{Y}(\text{CH}_2\text{SiMe}_3)_2]$ (**20**) as an analytically pure beige powder (Scheme 5.2). $[(\text{XAl})\text{Y}(\text{CH}_2\text{SiMe}_3)_2]$ is stable in solution at room temperature and is stable up to 60 °C in solution for 24 hours. Heating at temperatures above 60 °C resulted in the evolution of tetramethylsilane accompanied by various unknown products.



Scheme 5.2: Synthesis of $[(\text{XAl})\text{Y}(\text{CH}_2\text{SiMe}_3)_2]$

Solution NMR spectra for **19** are consistent with apparent C_s -symmetry (Figures 5.5-5.7). For example, a single CMe_2 signal in both the ^{13}C and ^1H NMR, and two distinct CHMe_2 signals suggest that top-bottom symmetry on the NMR timescale. Rapid ligand cyclometallation has been observed for rare earth alkyl complexes. However, based on the expected integration of the alkyl signals, it is evident that no such cyclometallation occurred in this case. The $\text{Y}-\text{CH}_2$ protons of each alkyl ligand are diastereotopic, resulting in overlapping, ill defined broad signals at -0.67 to -0.64 ppm in the ^1H NMR spectrum, whereas the $\text{Y}-\text{CH}_2$ signal was observed as a doublet at 34.86 ppm in the ^{13}C NMR spectrum, with a $^1J_{\text{C},\text{Y}}$ coupling constant of 36 Hz, which is comparable to literature examples of neutral yttrium alkyl complexes.^{37, 58}

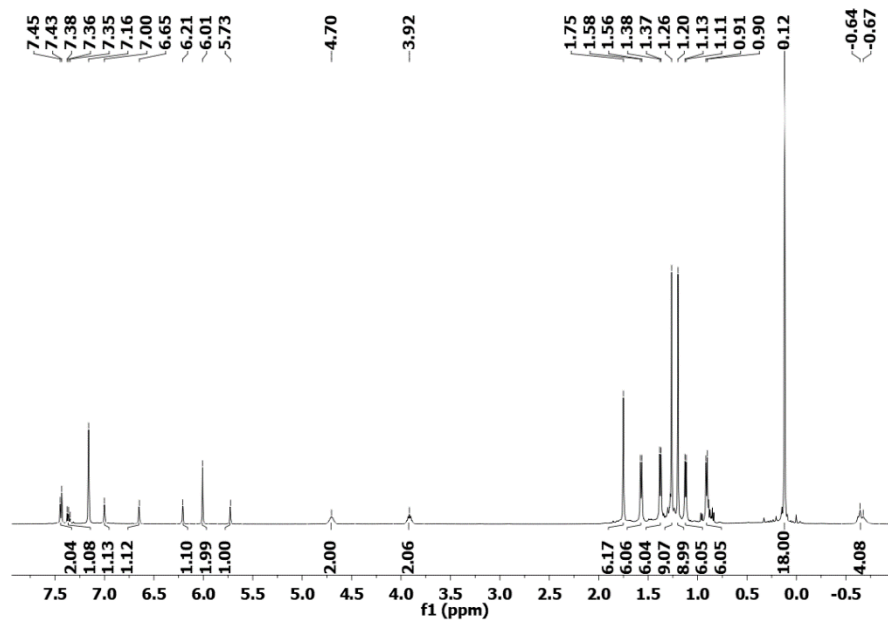


Figure 5.5: ^1H NMR Spectrum of $[(\text{XAl})\text{Y}(\text{CH}_2\text{SiMe}_3)_2]$ (600 MHz, C_6D_6)

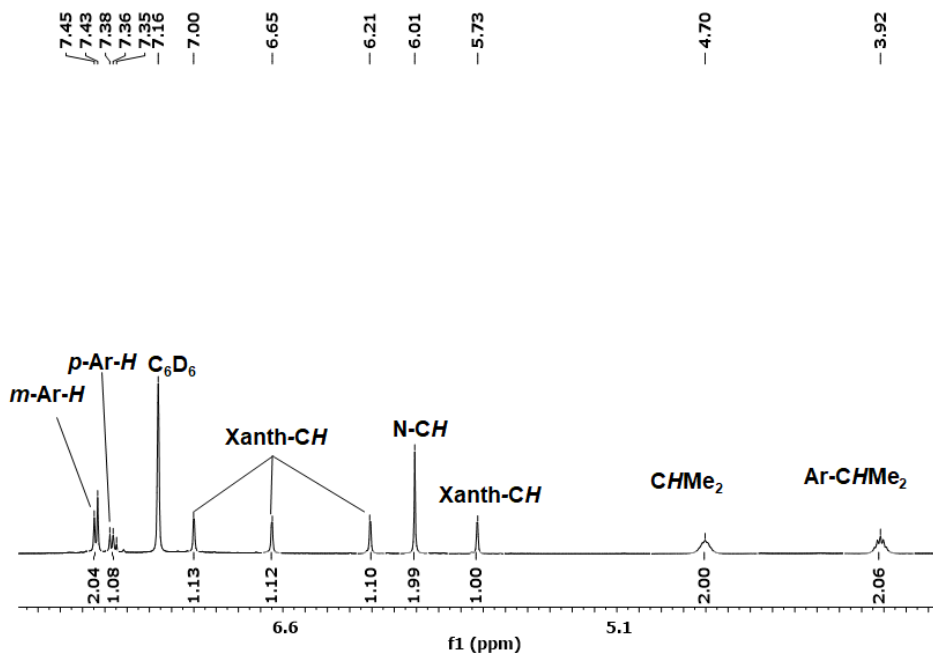


Figure 5.6: Expanded Region - ^1H NMR Spectrum of $[(\text{XAl})\text{Y}(\text{CH}_2\text{SiMe}_3)_2]$ (600 MHz, C_6D_6)

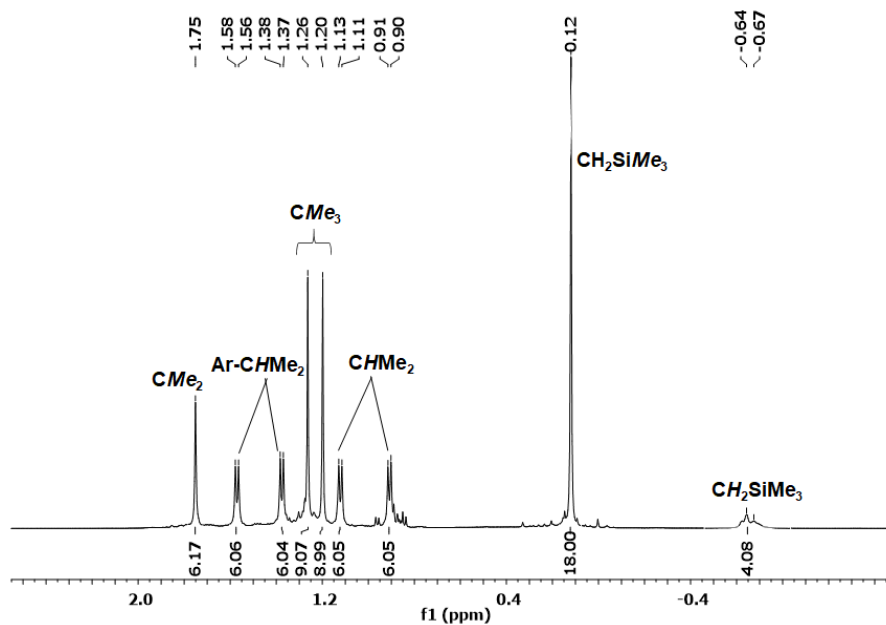


Figure 5.7: Expanded Region - ^1H NMR Spectrum of $[(\text{XAl})\text{Y}(\text{CH}_2\text{SiMe}_3)_2]$ (600 MHz, C_6D_6)

Apparent C_s symmetry is likely the result of rapid migration of alkyl groups between coordination sites above and below the ligand plane. Therefore, low temperature NMR spectra were collected in d^8 -toluene (Figure 5.8). At 198 K, a loss of top-bottom symmetry was observed, as evidenced by four distinct broad CHMe_2 signals. In addition, the diastereotopic Y-CH_2 protons appear as four broad signals at δ 0.28, -0.09 , -0.97 and -1.49 ppm. Similarly, the CH_2SiMe_3 signals are observed as two distinct broad peaks at δ 0.15 and 0.35 ppm.

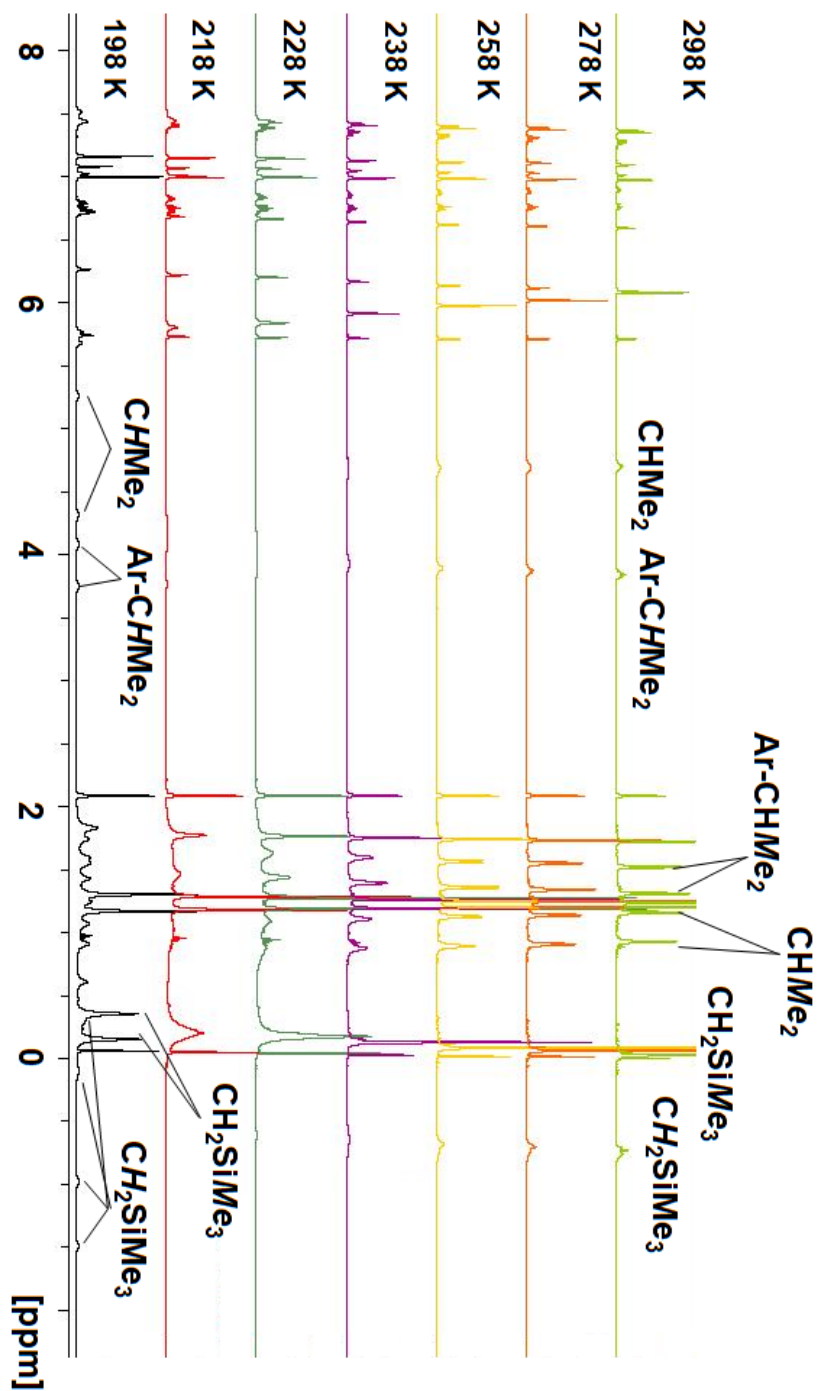
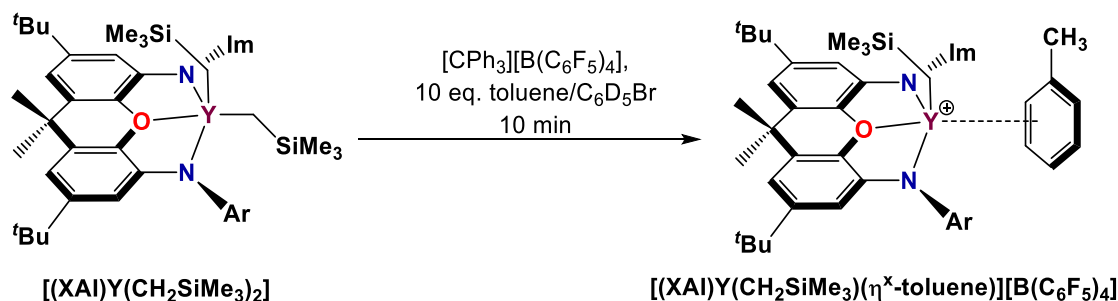


Figure 5.8: Variable Temperature- ^1H NMR of $[(\text{XAD})\text{Y}(\text{CH}_2\text{SiMe}_3)_2]$ (500 MHz, d^8 -toluene)

5.3.1 Synthesis of $[(XAI)Y(CH_2SiMe_3)(\eta^x\text{-toluene})][B(C_6F_5)_4]$

The reaction of **20** with 1 equivalent of $[CPh_3][B(C_6F_5)_4]$ in C_6D_5Br in the presence of 10 equivalents of toluene, afforded a cationic monoalkyl complex $[(XAI)Y(CH_2SiMe_3)(\eta^x\text{-toluene})][B(C_6F_5)_4]$ (**21**; Scheme 5.3), accompanied by the usual byproducts of trimethylsilylmethyl group abstraction by the trityl cation; Ph_3CH , and $SiMe_3$ signals (δ 2.06 ppm, -0.27 ppm) attributed to one isomer of “ $Ph_3CCH_2SiMe_3$ ”.^{66, 123} Complex **21** is fairly stable at room temperature in solution. Significant decomposition of **21** was seen after 2 days at room temperature, or more rapidly at 50 °C producing tetramethylsilane and several unidentified products. In the absence of toluene, the expected monocationic yttrium alkyl complex was not observed and instead several unidentified products were observed, strongly suggesting that toluene coordination stabilizes **21**.



Scheme 5.3: In-situ generation of $[(XAI)Y(CH_2SiMe_3)(\eta^x\text{-toluene})][B(C_6F_5)_4]$ (**21**)

Solution NMR at 298 K was consistent with a C_1 -symmetric structure as evidenced by four distinct broad signals for the $CHMe_2$ environments in the 1H NMR spectrum (Figures 5.9-5.11). However further characterization was not possible at 298 K due to broadening of the signals corresponding to proton environments that lie above and below the plane of the ligand backbone, which is most likely attributed to the rapid migration of the alkyl group between the coordination sites above and below the ligand plane. Therefore, variable temperature NMR spectra (298 K – 248 K) were recorded, and at 248 K significant sharpening of the signals (those which were broad at room temperature) were observed. At this temperature, the diastereotopic $Y-CH_2$ signals were observed as two distinct doublets (-0.84 ppm, -0.93 ppm) with a $^2J_{H,H}$ coupling constant of 11 Hz. Additionally, coordinated toluene was observed, affording five distinct aryl proton environments, the identity of which was further confirmed by 2D COSY NMR spectroscopy (Figure 5.12). The ortho and meta proton signals for coordinated toluene were observed at a significantly lower frequency than the respective signals for free toluene, which was similarly observed for literature examples of toluene-coordinated cationic rare earth complexes.¹²⁶ The para proton signal for the coordinated toluene was obscured in the aromatic region and was identified via 2D COSY NMR spectra (Figure 5.12). The CH_3 signal for coordinated toluene signal is coincidental with the signal for free toluene.

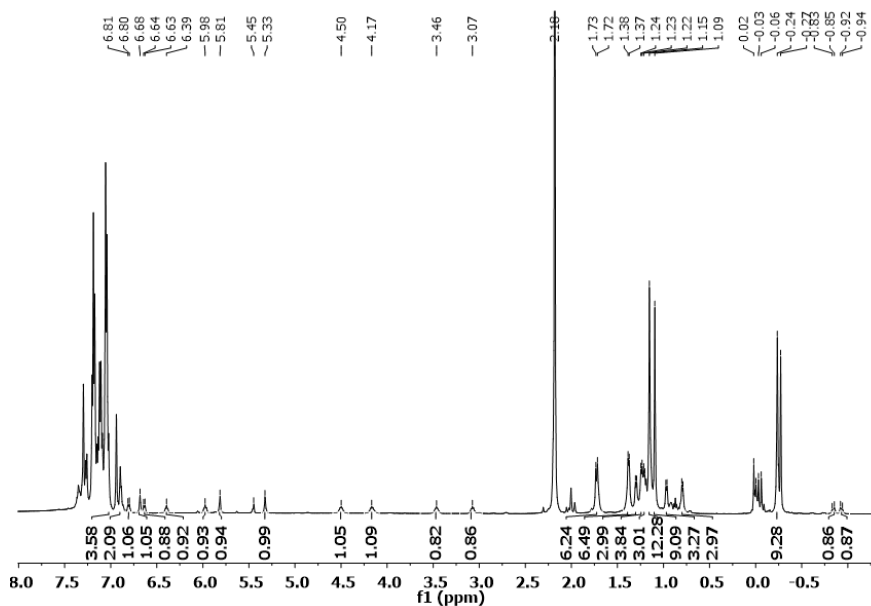


Figure 5.9: ^1H NMR Spectrum of $[(\text{XAI})\text{Y}(\text{CH}_2\text{SiMe}_3)(\eta^x\text{-toluene})][\text{B}(\text{C}_6\text{F}_5)_4]$ (500 MHz, 248 K, $\text{C}_6\text{D}_5\text{Br}$)

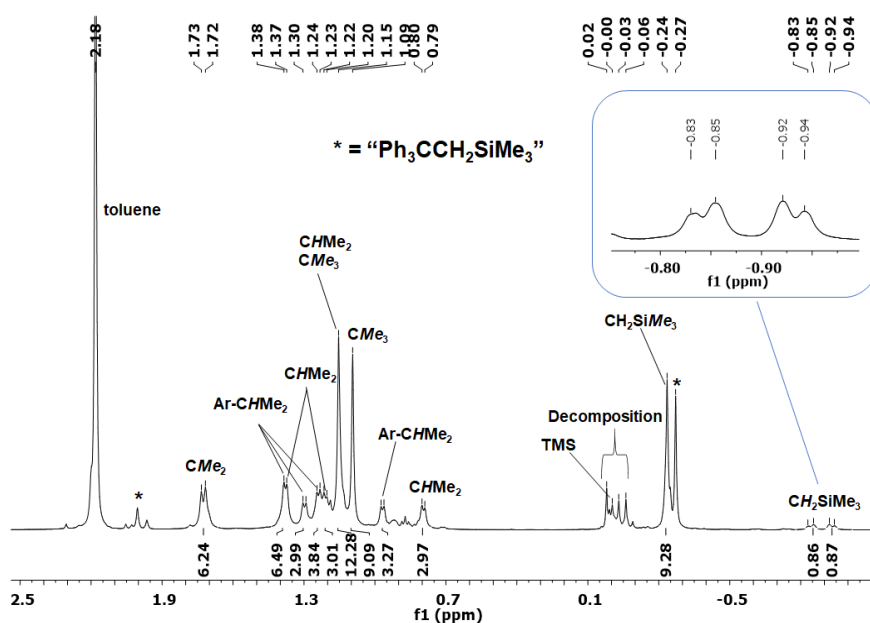


Figure 5.10: Expanded Region of the ^1H NMR Spectrum of $[(\text{XAI})\text{Y}(\text{CH}_2\text{SiMe}_3)(\eta^x\text{-toluene})][\text{B}(\text{C}_6\text{F}_5)_4]$ (500 MHz, 248 K, $\text{C}_6\text{D}_5\text{Br}$)

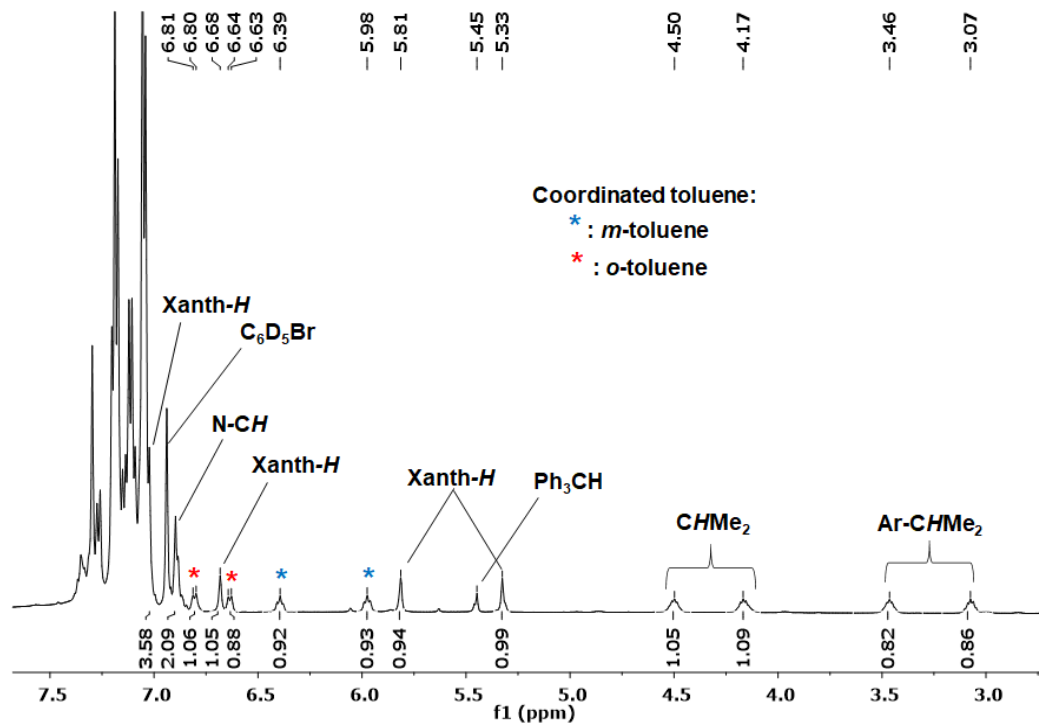


Figure 5.11: Expanded Region of the ¹H NMR Spectrum of [(XAl)Y(CH₂SiMe₃)(η^x-toluene)][B(C₆F₅)₄] (500 MHz, 248 K, C₆D₅Br)

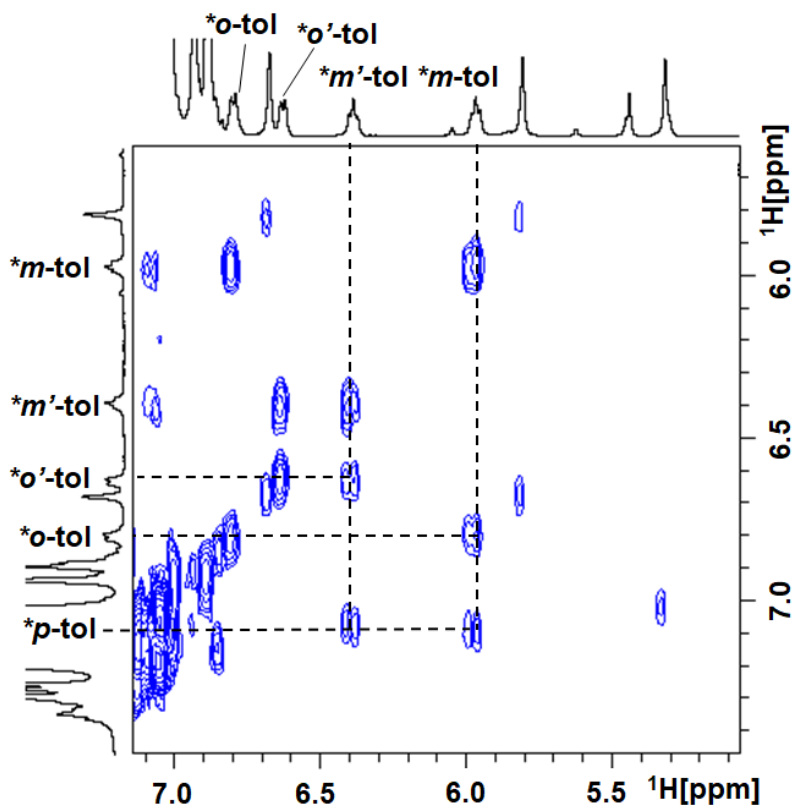


Figure 5.12: ^1H - ^1H COSY NMR Spectrum of $[(\text{XAl})\text{Y}(\text{CH}_2\text{SiMe}_3)(\eta^x\text{-toluene})][\text{B}(\text{C}_6\text{F}_5)_4]$ (500 MHz, 248 K, $\text{C}_6\text{D}_5\text{Br}$)

A ^1H - ^1H EXSY NMR at 248 K revealed the exchange of coordinated toluene and free toluene as evidenced by the clear cross peaks for the coordinated para- and meta-toluene signals and the corresponding free toluene signals (Figure 5.13).

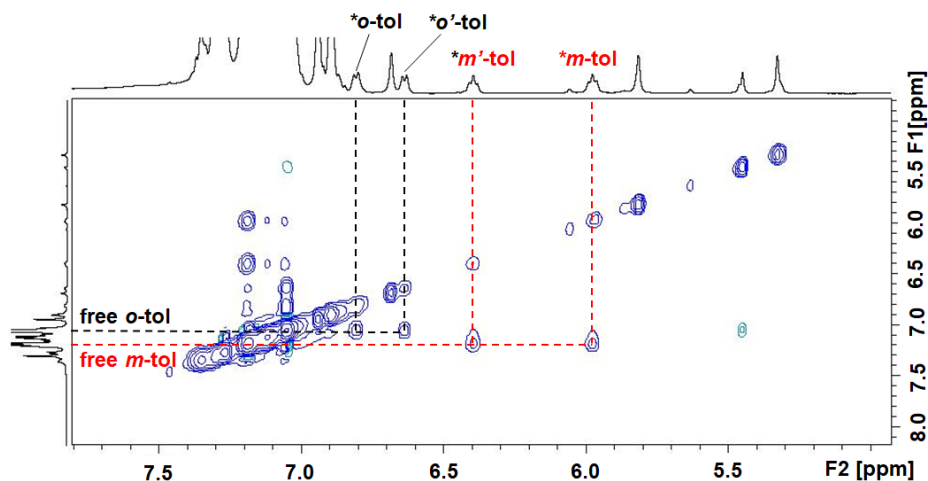


Figure 5.13: ^1H - ^1H EXSY NMR Spectrum of $[(\text{XAl})\text{Y}(\text{CH}_2\text{SiMe}_3)(\eta^x\text{-toluene})][\text{B}(\text{C}_6\text{F}_5)_4]$ (500 MHz, 248 K, $\text{C}_6\text{D}_5\text{Br}$ – D[8] mixing time 0.8 s.

A ^1H - ^1H NOESY NMR spectrum at 248 K revealed a cross peak between the Y-CH_2 and the coordinated Me -toluene signal (Figure 5.14), suggesting that the coordinated toluene is oriented placing the methyl adjacent to the yttrium alkyl group, as depicted in Scheme 5.3.

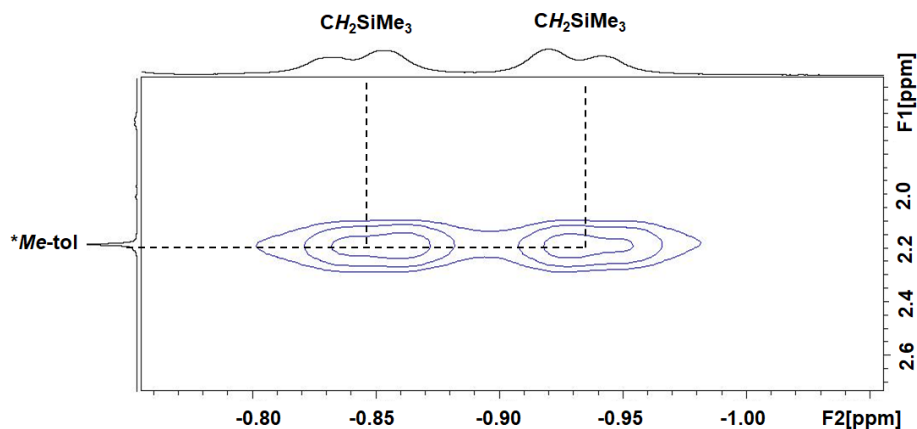


Figure 5.14: ^1H - ^1H NOESY NMR Spectrum of $[(\text{XAl})\text{Y}(\text{CH}_2\text{SiMe}_3)(\eta^x\text{-toluene})][\text{B}(\text{C}_6\text{F}_5)_4]$ (500 MHz, 248 K, $\text{C}_6\text{D}_5\text{Br}$ – D[8] mixing time 0.2 s.

The ^{11}B NMR spectrum is consistent with the expected $\text{B}(\text{C}_6\text{F}_5)_4$ anion as evidenced by a single sharp peak at -16.2 ppm (Figure 5.15).

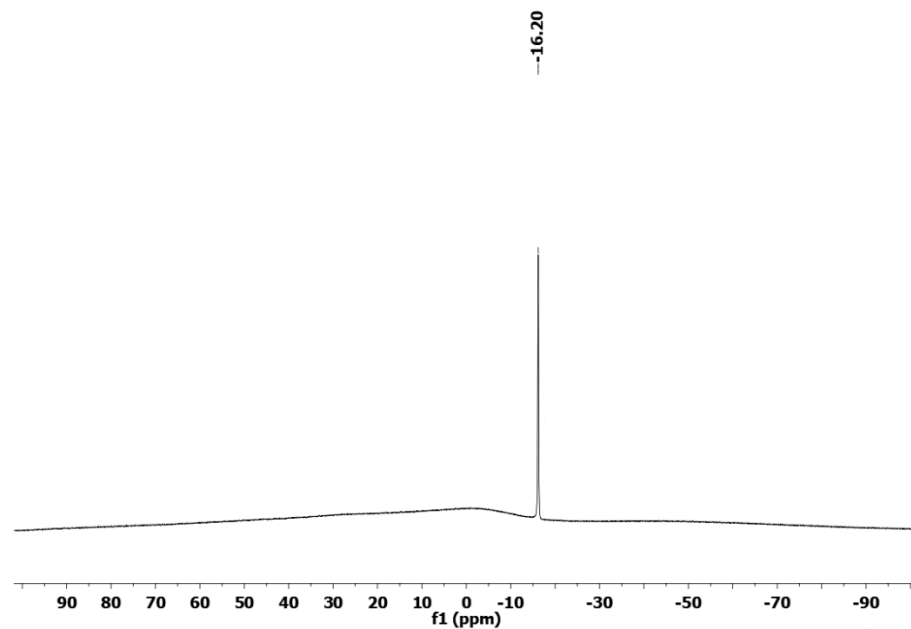


Figure 5.15: ^{11}B NMR Spectrum of $[(\text{XAl})\text{Y}(\text{CH}_2\text{SiMe}_3)(\eta^x\text{-toluene})][\text{B}(\text{C}_6\text{F}_5)_4]$ (161 MHz, $\text{C}_6\text{D}_5\text{Br}$)

Similarly, the ^{19}F NMR spectrum is consistent with the expected intact $\text{B}(\text{C}_6\text{F}_5)_4$ anion as evidenced by three distinct ^{19}F signals (Figure 5.16).

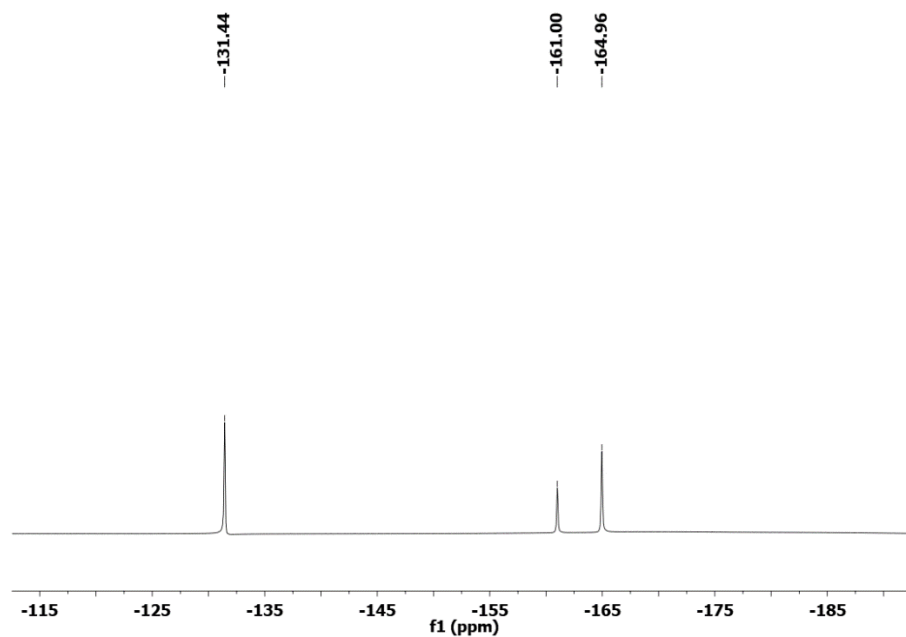


Figure 5.16: ^{19}F NMR Spectrum of $[(\text{XAl})\text{Y}(\text{CH}_2\text{SiMe}_3)(\eta^x\text{-toluene})][\text{B}(\text{C}_6\text{F}_5)_4]$ (471 MHz, $\text{C}_6\text{D}_5\text{Br}$)

Arene coordinated cationic group 4 complexes are well established, and a handful of arene-coordinated rare earth cations have similarly been reported. For example, Piers and coworkers have structurally characterized a series of arene coordinated derivatives of $[(\text{NacNac}^{\text{Me,Dipp}}\text{Sc}(\text{CH}_3)(\eta^6\text{-arene}))]^+$ as highlighted in Section 1.5.4, and were additionally able to observe the coordinated arene spectroscopically.^{53, 126} Piers and coworkers further postulated a dynamic exchange between coordinated and free toluene based on addition of excess d^8 -toluene resulting in the disappearance of the coordinated toluene signals in $[(\text{NacNac}^{\text{Me,Dipp}}\text{Sc}(\text{CH}_3)(\eta^6\text{-toluene}))]^+$.¹²⁶ Similarly, select examples of coordination of PhNMe_2 via the aryl ring have been spectroscopically observed by

Piers et al. (Section 1.5.3), as well as spectroscopically and structurally observed by Hou in the synthesis of $[(C_5Me_4SiMe_3)Sc(\eta^3-C_3H_5)(NMe_2Ph)]^+$.^{48, 51, 127}

Complex **21** is a rare example of an arene coordinated rare earth cationic alkyl complex, and the EXSY spectrum at 248 K highlights the dynamic exchange of coordinated and free toluene.

5.4 Ethylene Polymerization

The cationic monoalkyl complex **21** was investigated for its potential utility for ethylene polymerization. Attempts at ethylene polymerization in *o*-C₆H₅F₂ in the presence of 10 equivalents of toluene resulted in low activity (below 20 kg P.E/ atm/ mol of Y). The toluene coordination described in Section 5.3 suggests that toluene coordination may compete with ethylene for metal coordination, lowering the ethylene polymerization activity.

However, ethylene polymerization in *o*-C₆H₅F₂ in the absence of a competing coordinating arene such as toluene, resulted in inactivity towards ethylene polymerization. This is unsurprising, given that coordinating arene is required for the stabilization of the cationic complex (**21**), as previously described in section 5.3.

5.5 Intramolecular Hydroamination

The high activity of the cationic yttrium monoalkyl complex (**7**) for intramolecular hydroamination led us to investigate whether **21** would demonstrate similar hydroamination activity.

A 2 % loading of **21** was able to cyclize 1-amino-2,2-diphenyl-4-pentene within 8 minutes (Entry 1 in Table 5.1). By contrast, the neutral precursor **20** was much more sluggish, requiring 5.6 hours to cyclize the same substrate.

Complex **21** (2 mol %; Entry 2 in Table 5.1) similarly cyclized 1-amino-2,2-diphenyl-4-methyl-4-pentene (>99% completion) in 50 min, which is significantly more active than complex **8**, which took 1 hour at 5 % catalyst loading.

Additionally, **21** (5 mol%; Entry 3 in Table 5.1) cyclized 1-amino-2,2-diphenyl-5-hexene (>99% completion) in just 15 minutes at room temperature. This substrate is much more challenging than 1-amino-2,2-diphenyl-4-pentene due to the less favourable six- versus five-membered ring formation. Comparatively, complex **7** took 1.1 hours to perform the same cyclization.

Attempts to cyclize 1-amino-5-hexene proved unsuccessful at 24 °C (Entry 4 in Table 5.1), as was similarly observed for complex **8**. This can be attributed to the absence of cyclization promoting phenyl groups (Thorpe-Ingold effect), and strong coordination of the sterically unencumbered substrate to the cationic yttrium centre.

Table 5.1: Intramolecular hydroamination catalyzed by 21

	Substrate	Product	Time (h)	% ^a	$N_t(h^{-1})$
1			≤ 0.13	≥ 99	≥ 385
2			0.83	> 99	60
3			0.25	> 99	80
4 ^b			36	0	0

{2 mol % (Entry 1 and 2) or 5 mol % (Entries 3-4)} generated *in situ* from **20** and $[CPh_3][B(C_6F_5)_4]$ at 25 °C. Reactions were conducted in 0.8 mL C_6D_5Br . Reaction progress was monitored via 1H NMR with a ferrocene internal standard (1:1 with hydroamination substrate)

Complex **21** proved to be a more potent intramolecular hydroamination catalyst than complex **7** as evidenced by the highly efficient cyclization of 1-amino-2,2-diphenyl-4-methyl-4-pentene and 1-amino-2,2-diphenyl-5-hexene. This can potentially be attributed to the greater steric crowding around the metal center afforded by the XAI ligand than the AlI_2 ligand, which in turn may promote cyclization by disfavoring strong association of the substrate to the metal center. The increased room temperature stability of complex **21** in comparison to **7** would

similarly result in increased catalytic efficiency since a fraction of the latter complex will have decomposed before addition of the substrate. By contrast, **21** shows minimal decomposition after 24 hours in solution at room temperature. Room temperature cyclization of 1-amino-2,2-diphenyl-4-methyl-4-pentene and 1-amino-2,2-diphenyl-5-hexene is rare, and the reactivity of complex **21** is on par with the most efficient rare earth intramolecular hydroamination catalysts, such as previously reported $[(\text{XN}_2)\text{Y}(\text{CH}_2\text{SiMe}_3)(\text{THF})]$.²³ This work highlights the utility of cationic rare earth alkyl complexes for intramolecular aminoalkene hydroamination.

5.6 Summary and Conclusions

A new rigid asymmetric monoanionic xanthene-based ligand precursor, $\text{H}[\text{XAI}]$ was synthesized. This new ligand incorporates a formally neutral imidazol-2-imine donor alongside a monoanionic diisopropylanilido donor. $\text{H}[\text{XAI}]$ was utilized to access a neutral yttrium dialkyl complex (**20**). Complex **20** was reacted with $[\text{CPh}_3][\text{B}(\text{C}_6\text{F}_5)_4]$ in the presence of 10 equivalents of toluene to access a rare example of a toluene-coordinated cationic yttrium complex, **21**. Complex **21** is a rare example of a cationic hydroamination catalyst capable of room temperature cyclization of 1-amino-2,2-diphenyl-5-hexene and 1-amino-2,2-diphenyl-5-pentene.

Chapter 6

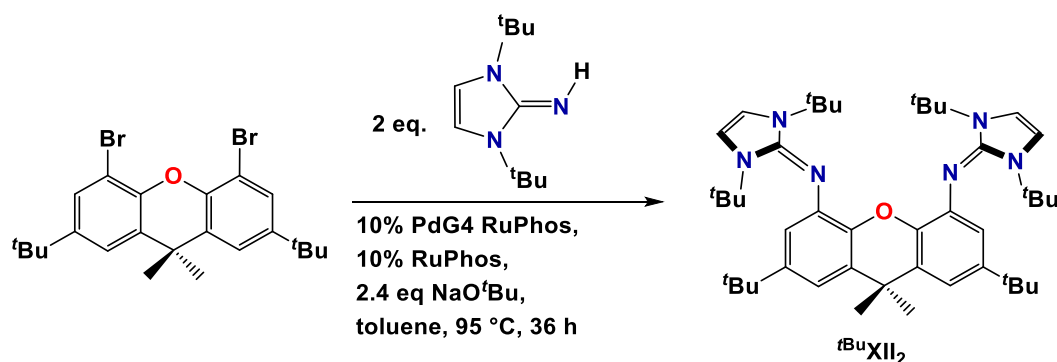
Future Directions and Conclusions

6.1 Future directions of rigid neutral NON donor ligands employing imidazol-2-imine donors

The work in this thesis has demonstrated the potential of imidazol-2-imine donors in stabilizing rare examples of monocationic alkyl complexes of both scandium and yttrium. Additionally, the utilization of imidazol-2-imine donors in the design of the neutral XII₂ ligand allowed access to rare examples of dicationic scandium complexes as highlighted in Chapter 5. [(XII₂)Sc(CH₂SiMe₃)(η^x-toluene)_x][B(C₆F₅)₄]₂ (**17**) was observed to be fairly stable at room temperature in solution and proved to be a potent ethylene polymerization catalyst. However, attempts to access an yttrium analogue proved futile. A dicationic yttrium monoalkyl complex is of interest since its larger ionic radius compared to scandium would potentially result in a more efficient olefin polymerization catalyst. In addition, yttrium is less expensive than scandium, making it more economically viable in industry. Increasing the steric protection afforded by the supporting ligand could allow access to a dicationic yttrium alkyl complex, as well as a more thermally robust/industrially viable analogue of **17**. This section highlights neutral ligand designs that aim to achieve the aforementioned goals.

6.1.1 A Bulky Symmetric NON donor ligand - ^tBuXII₂

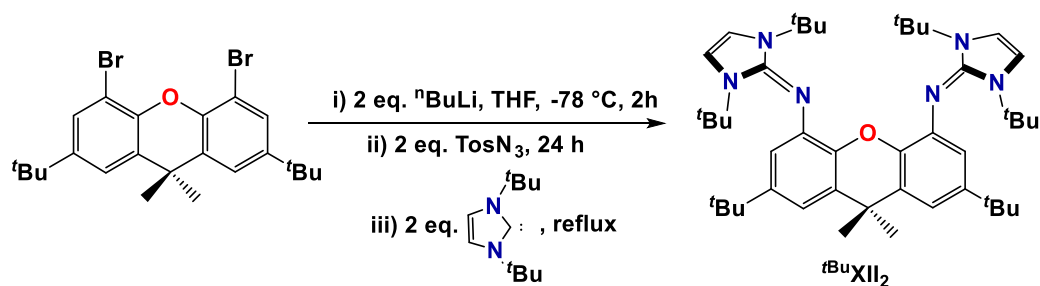
Designing derivatives of XII₂ that employ greater steric bulk could potentially allow access to dicationic yttrium alkyl complexes. A fine balance in steric bulk must be achieved as to impart stability without preventing coordination of the olefin to the metal center. Utilizing 1,3-di-*tert*-butylimidazol-2-imine donors in place of 1,3-diisopropyl-imidazol-2-imine may provide the increased steric protection required to access a dicationic yttrium monoalkyl complex. Buchwald-Hartwig ‘imination’ utilizing the PdG4RuPhos/RuPhos system could allow isolation of the targeted ^tBuXII₂ ligand (Scheme 6.1).



Scheme 6.1: Buchwald-Hartwig Synthetic route for ^tBuXII₂

Initial attempts at accessing XII₂ via the Staudinger reaction did not yield the desired product, and instead led to the isolation of the triazene intermediate XIA₂. The failure of this synthetic route could potentially be attributed to the lack of solubility of the triazene intermediate in toluene. Utilizing THF instead of

toluene (Scheme 6.2) may provide the solubility of the triazene intermediate required for the elimination of N₂, thus providing the target ligand. The Staudinger reaction may therefore provide an alternative route to access the ^tBuXII₂ ligand.

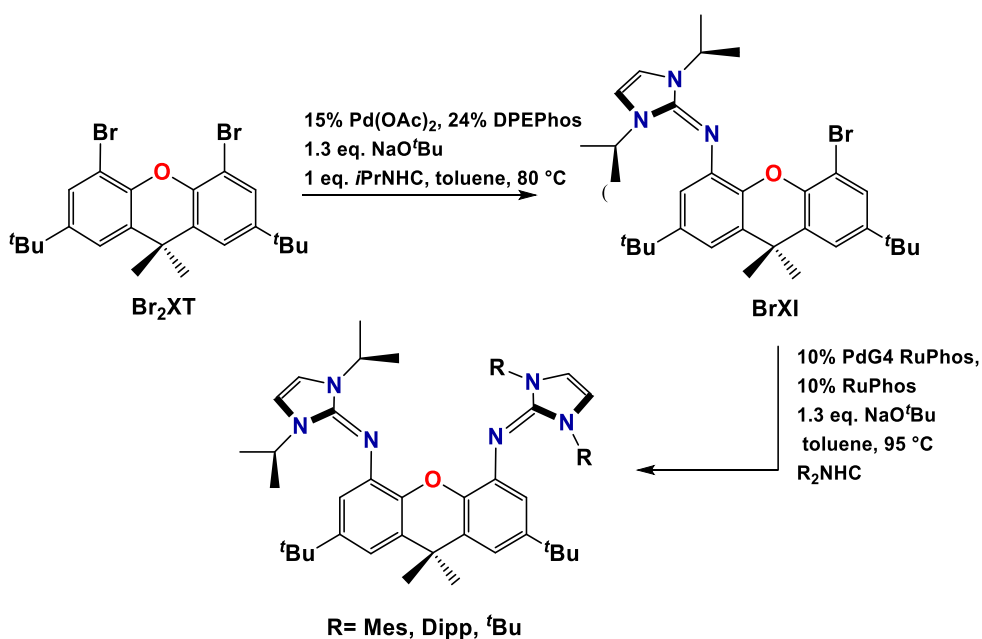


Scheme 6.2: Staudinger reaction synthetic route to ^tBuXII₂

6.1.2 A Bulky Asymmetric NON donor ligand

Symmetric derivatives of XII₂ employing highly bulky imidazol-2-imine donors that replace isopropyl groups with mesityl or 2,6-diisopropylphenyl would potentially either prevent olefin coordination or an inability to incorporate the metal center into the binding pocket of the ligand. Therefore, it may be desirable to replace just one of the imidazol-2-imine groups in XII₂ with a bulkier derivative. In chapter 5, selective cross-coupling of one of the aryl bromide positions of Br₂XT with 1,3-diisopropylimidazol-2-imine was achieved. This allows for the synthesis of asymmetric NON donor ligands, thus allowing for finer control of the steric character of the potential ligands. Replacing just one of the imidazol-2-imine

donors of XII_2 with a bulkier derivative, as outlined in Scheme 6.3, would potentially allow for an increase in steric protection without the aforementioned negative consequences of drastically increasing the steric bulk of the ligand.



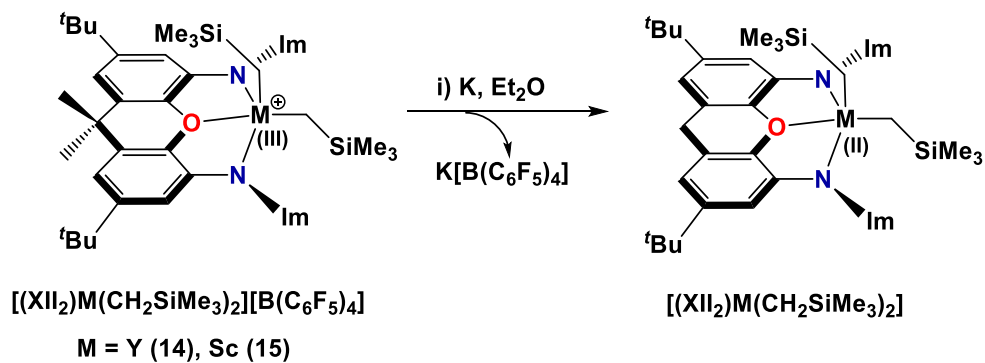
Scheme 6.3: Buchwald-Hartwig synthetic route for an asymmetric NON-donor ligand

6.2 Reductive chemistry of dicationic rare earth complexes

In the past 20 years, significant advances have been made in rare-earth reduction chemistry, demonstrating that all lanthanides (with the exception of radioactive promethium) can form molecular species containing rare earth metals in the +2 oxidation state.^{5, 7, 128, 129, 130} Nevertheless, low valent rare earth chemistry

is still very much in its infancy. The Evans group has reported several Ln(II) complexes with the vast majority employing cyclopentadienyl supporting ligands.^{5, 128} Access to divalent rare earth complexes is achieved by reduction of neutral Ln(III) complexes or by metal vapour synthetic techniques.^{7, 129} Cationic rare earth complexes are potentially ideal candidates for reduction due to their inherent electron-deficient character. Nevertheless, reduction of cationic rare earth complexes has not been reported in the literature to the best of our knowledge.

The monocationic complexes $[(XII)_2Sc(CH_2SiMe_3)_2][B(C_6F_5)_4]$ and $[(XII)_2Y(CH_2SiMe_3)_2][B(C_6F_5)_4]$ can potentially be investigated for reduction as outlined in Scheme 6.4.



Scheme 6.4: Proposed reduction of complexes 14 and 15

The resulting divalent neutral dialkyl complex $[(XII)M(CH_2SiMe_3)_2]$ complex could subsequently be reacted with a Brønsted acid or Lewis acid co-

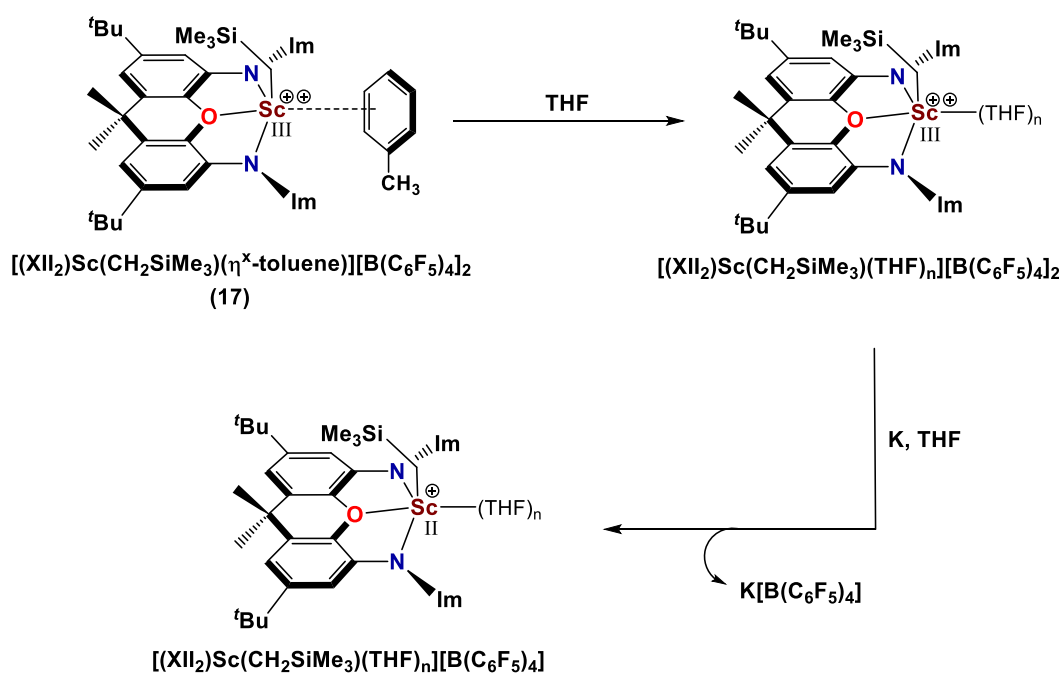
reactant to access a cationic alkyl complex in which the group 3 metal is divalent. Reactivity with small molecules (CO_2 , N_2 , CO) could be explored due to the novelty presented by having a group 3 metal that is cationic in the divalent state (d^1) while possessing a reactive alkyl ligand.

In chapter 4, the dicationic complex $[(\text{XII}_2)\text{Sc}(\text{C}_6\text{H}_4\text{NMe}_2)][\text{B}(\text{C}_6\text{F}_5)_4]_2$ (**18**) was observed to decompose slowly to a dark blue unidentified product and free dimethyl aniline byproduct. The dark blue complex appears to be paramagnetic due to the absence of corresponding signals in the ^1H NMR spectrum. This decomposition product could potentially result from reduction of Sc(III) to afford a low valent Sc species. Although this seems unlikely, a decomposition pathway involving reduction in the absence of a strong reducing agent could potentially be accessed due to the highly electron deficient metal center in dicationic **18**.

Due to the highly electron deficient nature of the metal center in dicationic complexes **16-18**, reduction of these complexes via a strong reducing agent (e.g. K) could additionally be explored. Low valent scandium complexes have been scarcely reported in literature. Recently Evans and coworkers reported the synthesis of the first structurally characterized Sc(II) complex employing bis(trimethylsilyl)amide ligands.¹³¹

Reduction of **17** could potentially yield a monocationic divalent alkyl complex and may potentially be further reduced to a rare example of a monovalent scandium complex. The reductive chemistry of dicationic rare earth metal

complexes could provide ease of access to divalent chemistry and potentially monovalent chemistry. Reduction of these complexes would require a suitable non-halide solvent such as Et₂O or THF, which would result in a solvent coordinated dicationic complex as proposed in Scheme 6.5. Subsequent treatment with K could potentially result in the desired low valent species (Scheme 6.5). Similarly, reduction of complexes **16** and **18** can be investigated.



Scheme 6.5: Reduction of $[(XII_2)Sc(CH_2SiMe_3)(\eta^x\text{-toluene})_x][B(C_6F_5)_4]$ (**17**) ($x = 0, 1$)

6.3 Cationic Aluminum Alkyl Complexes

The utilization of neutral ligands to access dicationic metal chemistry of group 3 metals can potentially be extended to the group 13 trivalent metalloids, specifically Al(III). A plethora of monocationic aluminum complexes have been reported in the literature.¹³² In contrast, only two examples of monometallic dicationic aluminum complexes have been reported in the literature. In 2016, Stephan and coworkers reported a dicationic aluminum hydride complex supported by NHC ancillary ligands (Figure 6.1 a), and Cowley and coworkers reported the coordinatively saturated β -diketiminato complex in (Figure 6.1 b).¹³³ Dicationic aluminum alkyl complexes have not been reported in the literature to the best of our knowledge.

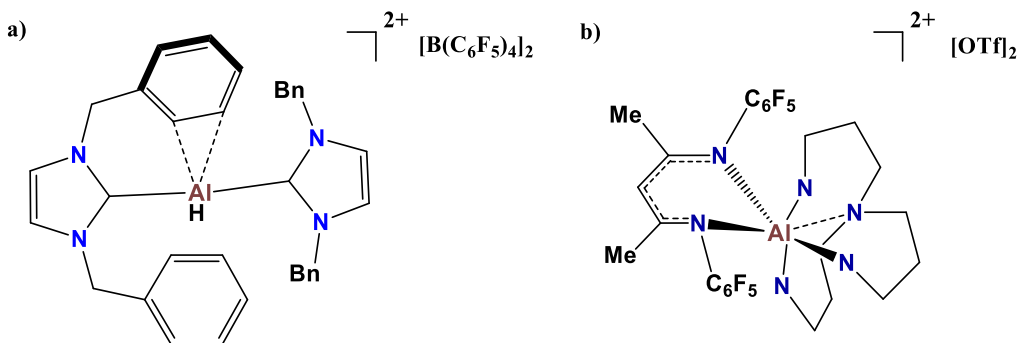
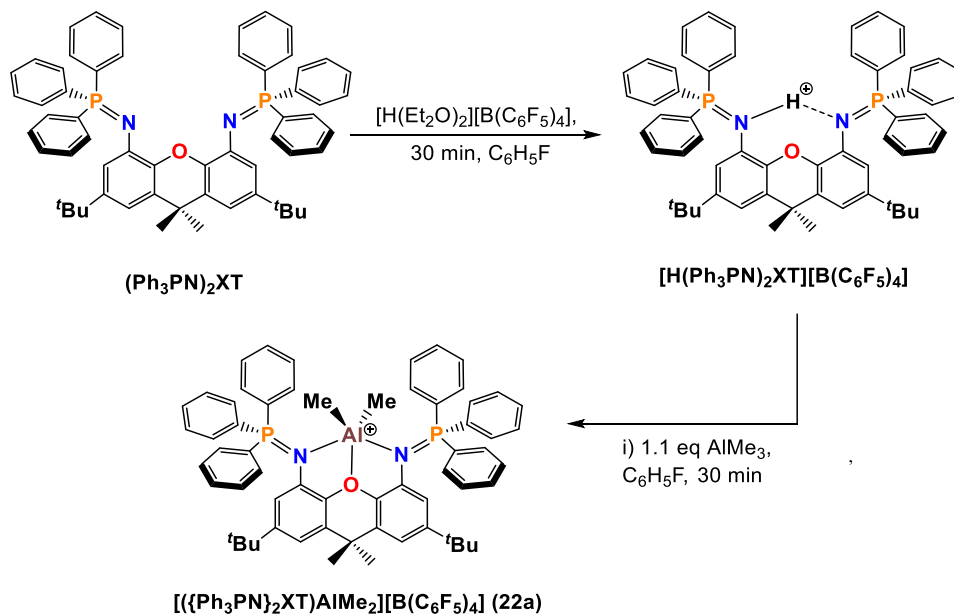


Figure 6.1: Dicationic Aluminum complexes in the literature

Monomeric monocationic aluminum alkyl complexes demonstrate an inability to polymerize olefins due to the rather high energy demand of the olefin insertion step as determined by computational studies conducted by Ariaifard and coworkers.¹³⁴ However, similar studies have not been conducted on dicationic aluminum alkyl complexes and therefore these complexes may potentially be viable olefin polymerization catalysts. The neutral ligands described in this thesis may allow access to dicationic aluminum alkyl complexes. This section describes the preliminary synthesis of select monocationic aluminium dialkyl complexes that can potentially be utilized to access dicationic aluminum alkyl complexes.

6.3.1 Synthesis of $[(\{\text{Ph}_3\text{PN}\}_2\text{XT})\text{AlMe}_2][\text{B}(\text{C}_6\text{F}_5)_4]$

The 1:1 reaction of $(\text{Ph}_3\text{PN})_2\text{XT}$ (**1**) and $[\text{H}(\text{Et}_2\text{O})_2][\text{B}(\text{C}_6\text{F}_5)_4]$ in $\text{C}_6\text{H}_5\text{F}$ yielded the in-situ generation of $[\text{H}(\text{Ph}_3\text{PN})_2\text{XT}][\text{B}(\text{C}_6\text{F}_5)_4]$. Subsequent reaction of in-situ generated $[\text{H}(\text{Ph}_3\text{PN})_2\text{XT}][\text{B}(\text{C}_6\text{F}_5)_4]$ with 1.1 equivalents of AlMe_3 yielded the cationic $[(\{\text{Ph}_3\text{PN}\}_2\text{XT})\text{AlMe}_2][\text{B}(\text{C}_6\text{F}_5)_4]$ (**22a**) complex (Scheme 6.6).



Scheme 6.6: Synthesis of $[(\text{Ph}_3\text{PN})_2\text{XT}]\text{AlMe}_2[\text{B}(\text{C}_6\text{F}_5)_4]$ (22a)

Solution NMR spectra are consistent with a C_{2v} symmetric structure as evidenced by a single CMe_2 and CMe_3 signal observed in the ^1H (Figure 6.2) and ^{13}C NMR spectra. The AlMe_2 signal was observed as a sharp signal at $\delta -0.77$ ppm.

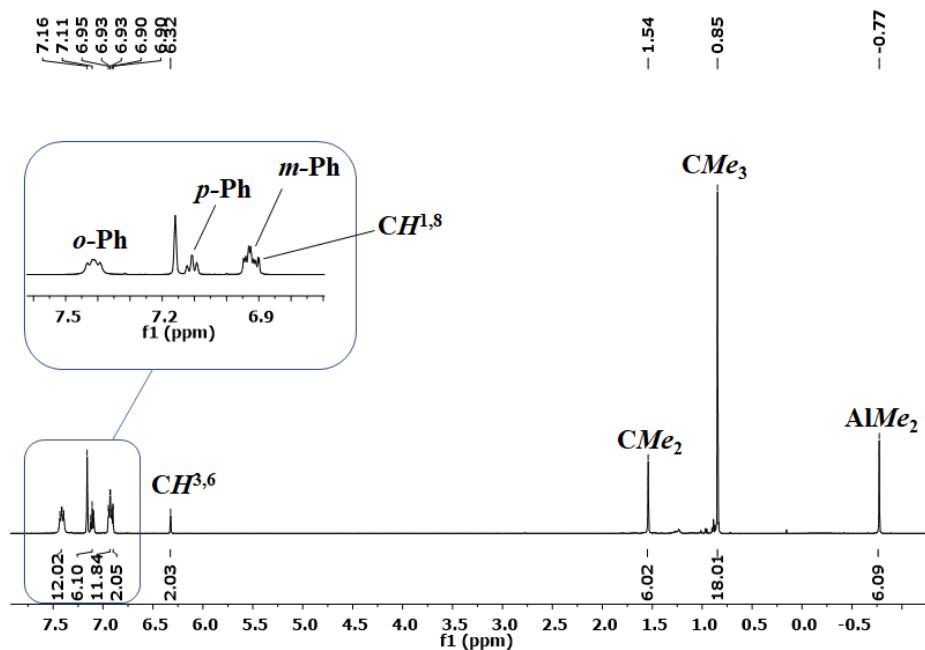


Figure 6.2: ^1H NMR Spectrum of $[(\{\text{Ph}_3\text{PN}\}_2\text{XT})\text{Al}(\text{CH}_3)_2][\text{B}(\text{C}_6\text{F}_5)_4]$ (**22a**) (500 MHz, C_6D_6)

As expected, a single ^{31}P NMR signal at δ 25.46 ppm was observed for complex **22a** as seen in Figure 6.3. A single sharp peak was observed at δ -15.85 ppm in the ^{11}B NMR spectrum, consistent with an intact $\text{B}(\text{C}_6\text{F}_5)_4$ anion (Figure 6.4).

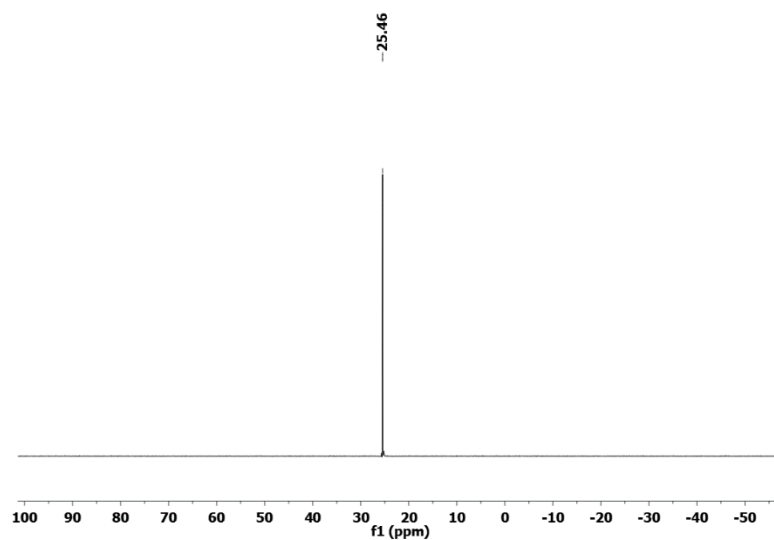


Figure 6.3: ^{31}P NMR Spectrum of $[(\{\text{Ph}_3\text{PN}\}_2\text{XT})\text{Al}(\text{CH}_3)_2][\text{B}(\text{C}_6\text{F}_5)_4]$ (22a) (203 MHz, C_6D_6)

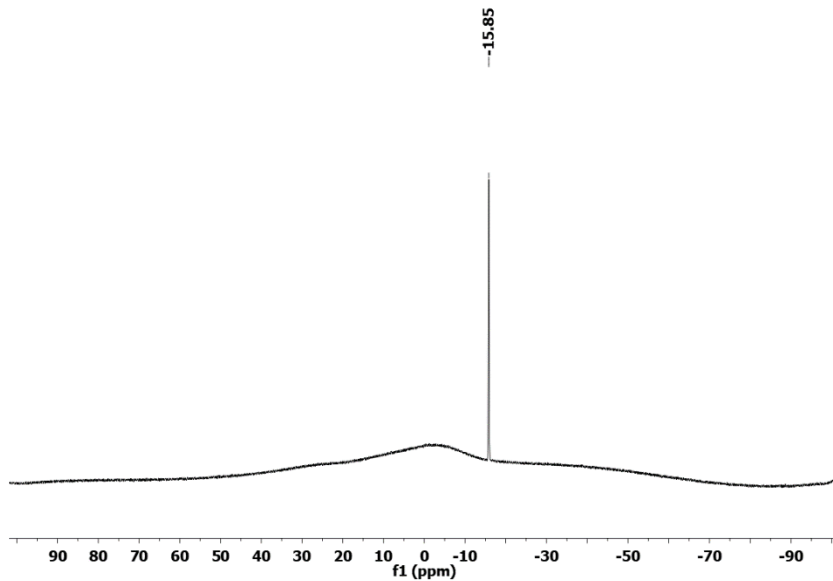


Figure 6.4: ^{11}B NMR Spectrum of $[(\{\text{Ph}_3\text{PN}\}_2\text{XT})\text{Al}(\text{CH}_3)_2][\text{B}(\text{C}_6\text{F}_5)_4]$ (22aa) (161 MHz, C_6D_6)

Repeated attempts at growing X-ray quality crystals of **22a** proved unsuccessful. Therefore, an identical synthesis in which the $B(C_6F_5)_4$ anion was replaced with a $[B(C_6H_3\{CF_3\}_2)_4]$ anion was investigated, yielding $[(\{Ph_3PN\}_2XT)Al(CH_3)_2][B(C_6H_3\{CF_3\}_2)_4]$ (**22b**). X-ray quality crystals of **22b** were grown by layering hexanes onto a solution of **22b** in toluene and cooling to $-28\text{ }^\circ\text{C}$ (Figure 6.5). Complex **22b** is 5 coordinate and adopts a distorted trigonal bipyramidal geometry. The P–N distances are $1.621(2)\text{ \AA}$ and $1.617(2)\text{ \AA}$ respectively, which are slightly elongated in comparison to those in uncomplexed phosphinimine ligands, which typically range from 1.56 to 1.58 \AA .¹⁰⁵ This elongation of the P–N bond suggests some contribution from the zwitterionic resonance structure (with a positive charge on phosphorus and a negative charge on nitrogen).

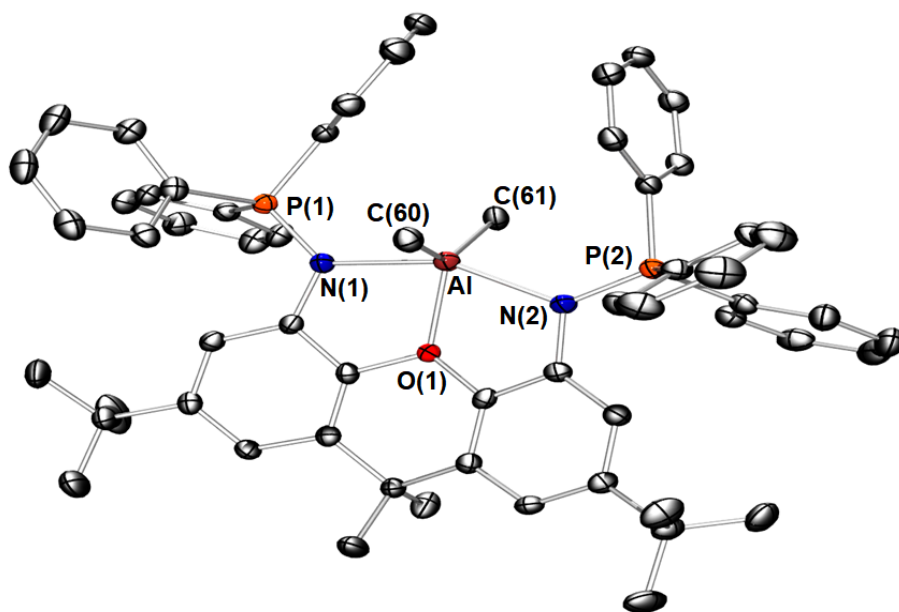
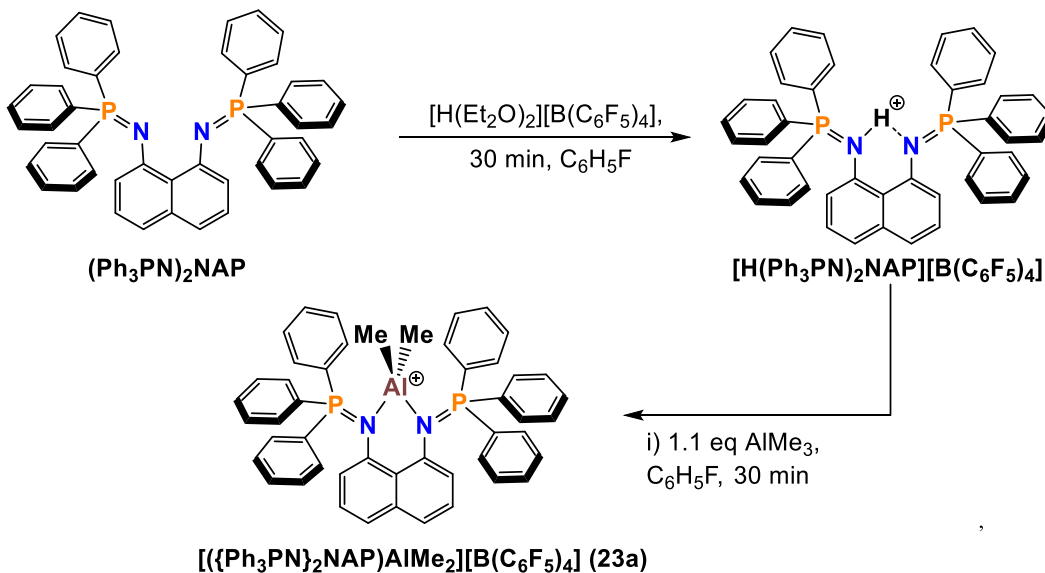


Figure 6.5: X-Ray crystal structure of $[(\{\text{Ph}_3\text{PN}\}_2\text{XT})\text{Al}(\text{CH}_3)_2][\text{B}(\text{C}_6\text{H}_3\{\text{CF}_3\}_2)_4]$ (22b**). Ellipsoids are set to 50 % probability. For clarity, hydrogen atoms, $[\text{B}(\text{C}_6\text{H}_3\{\text{CF}_3\}_2)_4]$ anion and toluene are omitted. Selected bond lengths (Å) and angles (°): Al–C(60) 1.971(3), Al–C(61) 1.977(3), Al–N(1) 2.132(2), Al–N(2) 2.141(2), Al–O(1) 1.990(2), N(1)–P(1) 1.621(2), N(2)–P(2) 1.617(2), C(60)–Al–C(61) 137.9(1), N(1)–Al–N(2) 154.36(9), O(1)–Al–N(1) 77.50(8), O(1)–Al–N2 76.96(8), O(1)–Al–C(60) 110.0 (1), O(1)–Al–C(61) 112.0 (1). R= 6.78 %.**

As previously mentioned, the xanthene backbone has been observed to bend at the central non-aromatic ring, and is most often observed upon coordination to small metal ions.^{23, 102} In the case of **22b**, a 15.68° bend was observed.

6.3.2 Synthesis of $[(\{\text{Ph}_3\text{PN}\}_2\text{NAP})\text{AlMe}_2][\text{B}(\text{C}_6\text{F}_5)_4]$

Several three coordinate monocationic aluminium complexes have been reported in the literature, and the previously described $(\text{Ph}_3\text{PN})_2\text{NAP}$ ligand (chapter 2), can potentially be utilized to synthesize a three coordinate dicationic aluminum alkyl complex. The 1:1 reaction of $(\text{Ph}_3\text{PN})_2\text{NAP}$ and $[\text{H}(\text{Et}_2\text{O})_2][\text{B}(\text{C}_6\text{F}_5)_4]$ in $\text{C}_6\text{H}_5\text{F}$ resulted in the in-situ generation of $[\text{H}(\text{Ph}_3\text{PN})_2\text{NAP}][\text{B}(\text{C}_6\text{F}_5)_4]$. Subsequent reaction of $[\text{H}(\text{Ph}_3\text{PN})_2\text{NAP}][\text{B}(\text{C}_6\text{F}_5)_4]$ with 1.1 equivalents of AlMe_3 yielded the cationic $[(\{\text{Ph}_3\text{PN}\}_2\text{NAP})\text{AlMe}_2][\text{B}(\text{C}_6\text{F}_5)_4]$ (**23a**) complex (Scheme 6.7). A small amount of residual AlMe_3 was observed in the product via ^1H NMR. Heating the solid under vacuum should remove the slight excess in AlMe_3 .



Scheme 6.7: Synthesis of $[(\{\text{Ph}_3\text{PN}\}_2\text{NAP})\text{AlMe}_2][\text{B}(\text{C}_6\text{F}_5)_4]$ (23a**)**

Solution NMR spectra are consistent with a C_{2v} symmetric structure as evidenced by a three distinct Ar-*H* signals for the naphthalene backbone along with three distinct aryl phosphinimine peaks in the ^1H and ^{13}C NMR spectra. The AlMe_2 signal was observed as a sharp signal at $\delta -1.29$ ppm (Figures 6.6-6.7). As expected, a single signal is seen in the ^{31}P NMR (Figure 6.8) for **23a**.

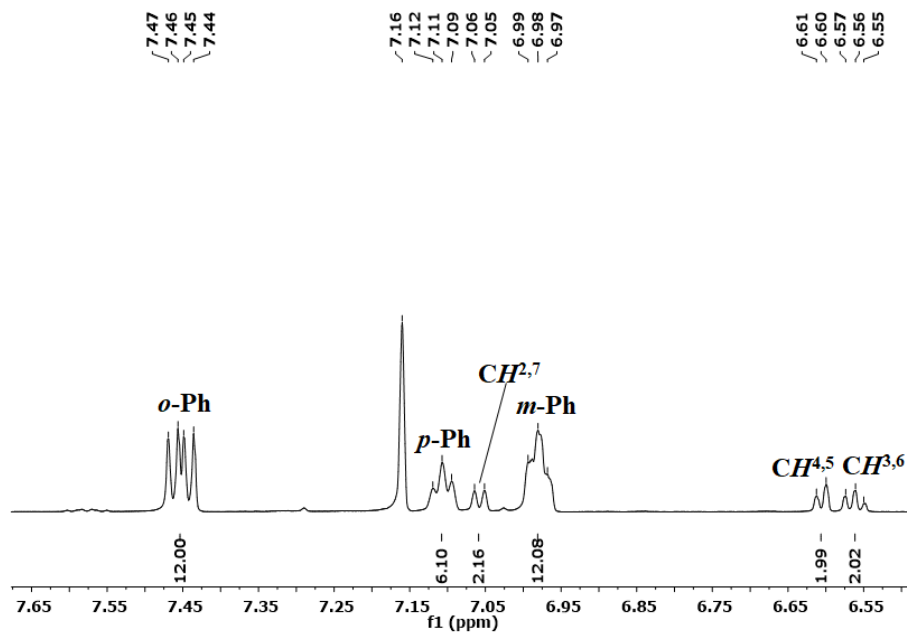


Figure 6.6: Expanded region - ^1H NMR Spectrum of $[(\{\text{Ph}_3\text{PN}\}_2\text{NAP})\text{Al}(\text{CH}_3)_2][\text{B}(\text{C}_6\text{F}_5)_4]$ (23a) (600 MHz, C_6D_6)

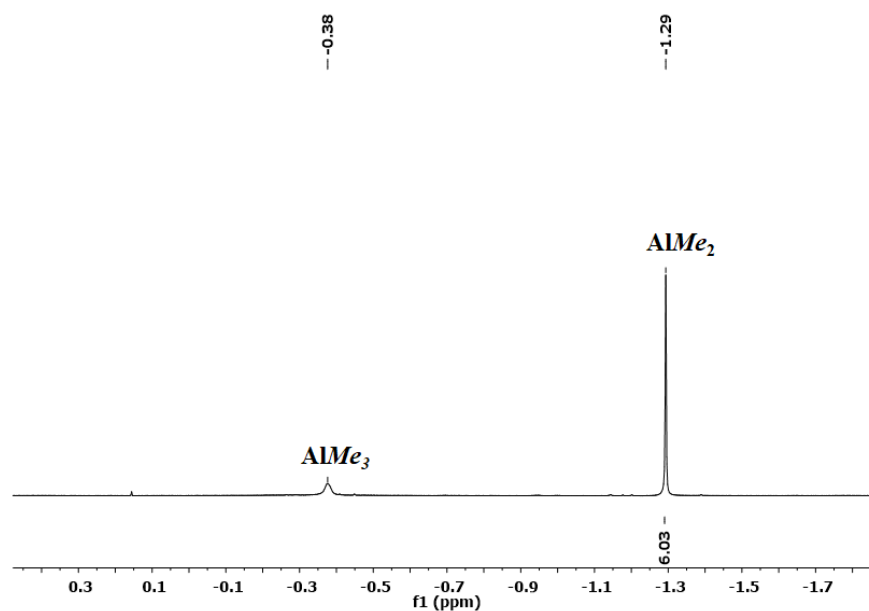


Figure 6.7: Expanded region - ^1H NMR Spectrum of $[(\{\text{Ph}_3\text{PN}\}_2\text{NAP})\text{Al}(\text{CH}_3)_2][\text{B}(\text{C}_6\text{F}_5)_4]$ (23a) (600 MHz, C_6D_6)

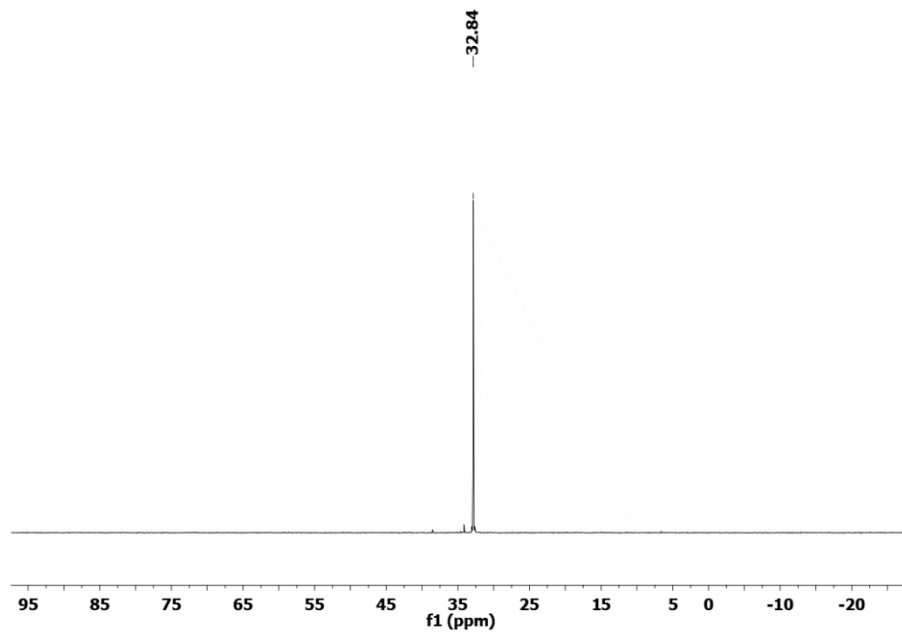


Figure 6.8: ^{31}P NMR Spectrum of $[(\{\text{Ph}_3\text{PN}\}_2\text{NAP})\text{Al}(\text{CH}_3)_2][\text{B}(\text{C}_6\text{F}_5)_4]$ (**23a**) (243 MHz, C_6D_6)

A single sharp peak was observed at $\delta -16.1$ ppm in the ^{11}B NMR spectrum (Figure 6.9), consistent with an intact $\text{B}(\text{C}_6\text{F}_5)_4$ anion.

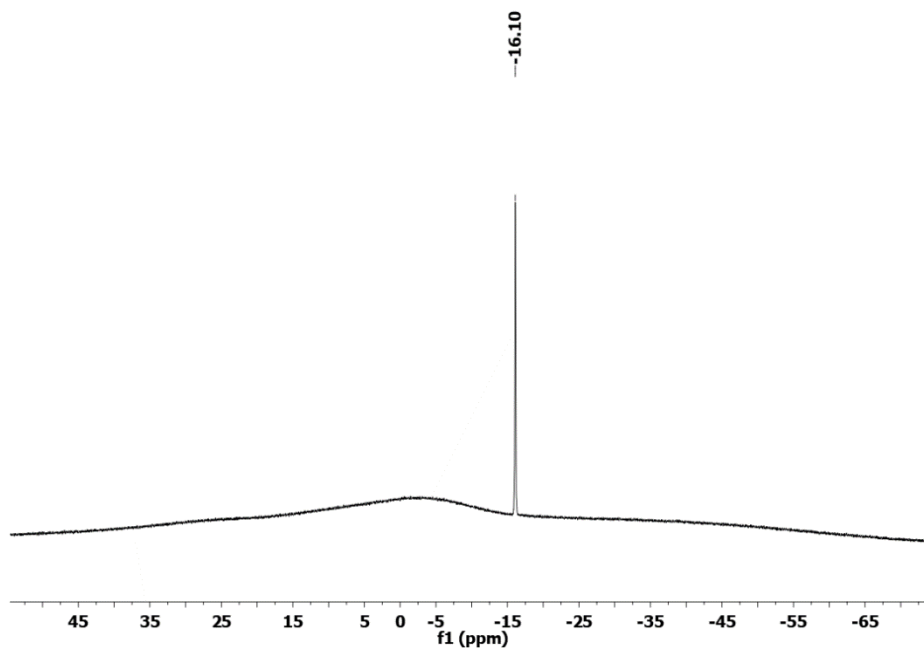


Figure 6.9: ^{11}B NMR Spectrum of $[({\text{Ph}}_3\text{PN})_2\text{NAP})\text{Al}(\text{CH}_3)_2][\text{B}(\text{C}_6\text{F}_5)_4]$ (**23a**) (161 MHz, C_6D_6)

Similar to **22a**, repeated attempts at growing X-ray quality crystals of **23a** proved unsuccessful. Therefore, an identical synthesis in which the $\text{B}(\text{C}_6\text{F}_5)_4$ anion was replaced with $[\text{B}(\text{C}_6\text{H}_3\{\text{CF}_3\}_2)_4]$ was investigated yielding $[({\text{Ph}}_3\text{PN})_2\text{NAP})\text{Al}(\text{CH}_3)_2][\text{B}(\text{C}_6\text{H}_3\{\text{CF}_3\}_2)_4]$ (**23b**) (Figure 6.10). X-ray quality crystals of **23b** were grown by layering hexanes onto a solution of **23b** in toluene followed by cooling to $-28\text{ }^\circ\text{C}$ (Figure 6.10). Complex **23b** is 4-coordinate and adopts a distorted tetrahedral geometry. Similar to **23a**, The P–N distances are $1.639(2)\text{ \AA}$ and $1.618(2)\text{ \AA}$ respectively, which are slightly elongated in comparison

to those in uncomplexed phosphinimine ligands, which typically range from 1.56 to 1.58 Å.¹⁰⁵ Aluminum lies 0.736 Å out of the P(1)—N(1)—C(1) plane as opposed to 0.216 Å out of the P(2)—N(2)—C(8) plane. As a result of the constraints imposed by the ligand framework, the Al-N distances (1.961(2) and 1.916(2) Å) are fairly different from one another due to the non-ideal orientation of the lone pair of N(1) relative to Al.

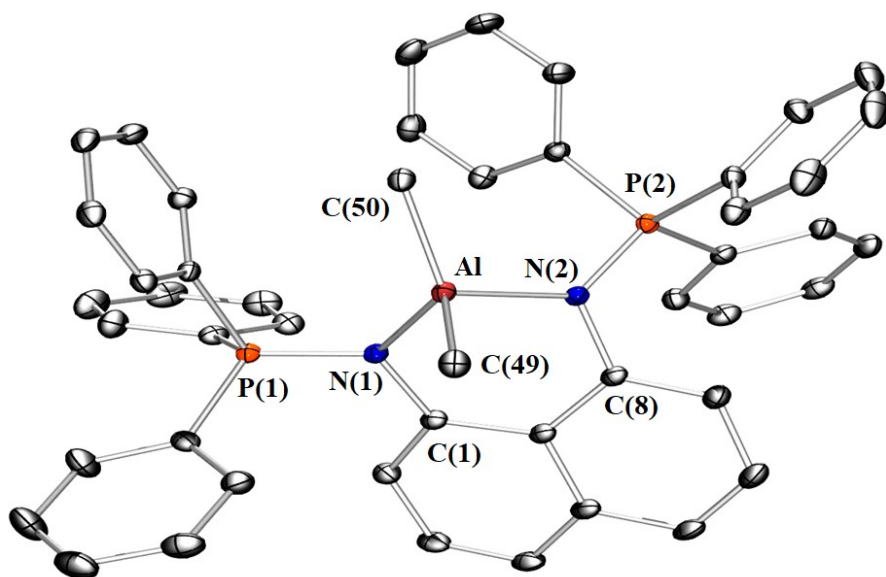


Figure 6.10: X-Ray crystal structure of [(Ph₃PN)₂NAP)Al(CH₃)₂][B(C₆H₃{CF₃})₄] (23b). Ellipsoids are set to 50 % probability. For clarity, hydrogen atoms, [B(C₆H₃{CF₃})₄] anion and toluene are omitted. Selected bond lengths (Å) and angles (°): Al—C(49) 1.962(3), Al—C(50) 1.969(2), Al—N(1) 1.961(2), Al—N(2) 1.916(2), N(1)—P(1) 1.639(2), N(2)—P(2) 1.618(2), C(60)—Al—C(61) 112.5(1), N(1)—Al—N(2) 91.15(7), N(1)—Al—C(49) 107.74(8), N(2)—Al—C(50) 111.58(8). R = 4.83 %.

Through the successful isolation of complexes 22 and 23, forthcoming research can focus on accessing dicationic aluminum alkyl complexes using Lewis acid and Brønsted acid co-reactants. Further research could also focus on the ethylene polymerization capability of the potential dicationic aluminum alkyl complexes. Due to the success in accessing dicationic scandium alkyl complexes employing the XII₂ supporting ligand, analogous aluminium chemistry using XII₂ could similarly prove viable.

6.4 Summary and Conclusions

In conclusion, this thesis describes the synthesis of a variety of rigid neutral and monoanionic ligands. In addition, this thesis describes the utility of imidazol-2-imine donors in stabilizing rare earth alkyl complexes, specifically highly electron-deficient cations and rare examples of dicationic rare earth complexes. The monocationic rare earth alkyl complexes (**7**, **21**) described in this thesis were found to be highly potent intramolecular hydroamination catalysts, but were inefficient ethylene polymerization catalysts. In an effort to synthesize a more electrophilic complex, a series of dicationic scandium complexes were generated in-situ. Of these complexes, [(XII₂)Sc(CH₂SiMe₃)(η^x-toluene)_x][B(C₆F₅)₄]₂ (**17**) (x = 0, 1), proved to be a highly efficient ethylene polymerization catalyst. Future work in this area would focus on designing derivatives of the XII₂ ligand to access more thermally robust/industrially viable dicationic rare earth complexes. Furthermore,

the highly electron deficient dicationic complexes may present a feasible avenue to access low valent chemistry of the rare-earth metals. In addition, the neutral supporting ligands developed in this thesis could be applied to the synthesis of dicationic aluminum alkyl complexes.

Chapter 7

Experimental Methods

7.1 General Details

7.1.1 Laboratory Equipment and Apparatus

An argon-filled M-Braun UNIlab glovebox equipped with a $-28\text{ }^{\circ}\text{C}$ freezer was employed for the manipulation and storage of all air sensitive compounds, and reactions were performed on a double manifold high vacuum line (with all glass-glass connections, rather than connections via hose tubing) using standard techniques. A Fisher Scientific Ultrasonic FS-30 bath was used to sonicate reaction mixtures where indicated. Yttrium and scandium compounds reported in this thesis are very air and moisture sensitive, and the vacuum line operated at $<5\text{ mTorr}$. The argon stream was further purified using an Oxisorb-W scrubber from Matheson Gas Products. A VWR Clinical 200 Large Capacity Centrifuge (with 28° fixed-angle rotors that hold 12 x 15 mL Kimble Chase glass centrifuge tubes) located within a glovebox was utilized when required. Commonly utilized specialty glassware includes a J-Young NMR tubes, thick walled flasks equipped with Teflon stopcocks and a swivel frit assembly.

7.1.2 Solvents

Pentane, Hexanes, toluene, benzene, tetrahydrofuran (THF), and diethyl ether (Et₂O) were initially dried and distilled at atmospheric pressure from Na/Ph₂CO. Unless otherwise stated all protio solvents were stored over an appropriate drying agent (Hexanes, pentane = Na/Ph₂CO/tetraglyme; benzene, toluene, Et₂O, THF = Na/Ph₂CO). Solvents C₆H₅F, *o*-C₆H₄F₂, C₆D₅Br, CH₃OH, 1,4-dioxane and CH₂Cl₂ were dried over 4Å molecular sieves for 4 days, prior to vacuum distillation to a storage flask. Deuterated solvents (C₆D₆, d₈-toluene) were purchased from Cambridge Isotope Laboratories and dried over Na/Ph₂CO unless otherwise stated.

7.1.3 Starting Materials

1,3-diisopropylimidazol-2-imine,⁹¹ 1,3-diisopropylimidazol-2-ylidene,¹³⁵
 4,5-dibromo-2,7,9,9-tetramethylacridan,¹¹⁷ 4,5-dibromo-2,7-di-*tert*-butyl-9,9-
 dimethylxanthene,⁹⁸ tosyl azide,¹³⁶ [H(Et₂O)₂][B(C₆F₅)₄],¹³⁷
 [H(Et₂O)₂][B(C₆H₃{CF₃}₂)₄],¹³⁸ [Y(CH₂SiMe₃)₃(THF)₂]¹³⁹ and
 [Sc(CH₂SiMe₃)₃(THF)₂]¹³⁹ were prepared according to literature procedures. 1-
 Amino-5-hexene was purchased from GFS Chemicals, dried over CaH₂ and
 distilled prior to use. LiCH₂SiMe₃ (1.0M in pentane), 1,3-diisopropylimidazolium
 chloride, *n*BuLi (1.6M in hexanes) anhydrous YCl₃, anhydrous ScCl₃, PPh₃,

NaO^tBu, RuPhos (PCy₂{*o*-C₆H₄(C₆H₃{OⁱPr}_{2-2,6})}), "RuPhos Pd G4" ((RuPhos)Pd(C₆H₄{*o*-C₆H₄(*o*-NHMe)})(OMs)]; OMs = OSO₂Me), Pd(OAc)₂ and DPEPhos were purchased from Sigma Aldrich. Solid LiCH₂SiMe₃ were obtained by removal of solvent *in vacuo*. YCl₃(THF)_{3.5} and ScCl₃(THF)₃ were obtained by refluxing anhydrous MCl₃ (M = Y, Sc) in dry THF for 24 hours, followed by removal of solvent under vacuum. [CPh₃][B(C₆F₅)₄] was purchased from Alfa Aesar. [HNMe₂Ph][B(C₆F₅)₄] was purchased from Strem Chemicals. C₆F₅Br (utilized in the synthesis of B(C₆F₅)₃) was purchased from Oakwood Chemicals and distilled from molecular sieves prior to use. B(C₆F₅)₃ was prepared from C₆F₅MgBr and BF₃·Et₂O according to literature procedure.¹⁴⁰

7.1.4 Instrumentation and Analysis

Combustion elemental analyses were performed by Midwest Microlab, LLC, Indianapolis, IN, USA. NMR Spectroscopy (¹H, ¹³C{H}, ³¹P{H}, ¹¹B, ¹⁹F, DEPT-Q, COSY, ¹H-¹³C HSQC, ¹H-¹³C HMBC) was performed on Bruker AV-200, AV-500 and AV-600 spectrometers. ¹H-²⁹Si HMBC, EXSY, NOESY and Variable Temperature NMR spectroscopy was conducted exclusively on a Bruker AV-500 Spectrometer. All ¹H NMR and ¹³C NMR spectra were referenced relative to SiMe₄ using the resonance of the deuterated solvent (¹³C NMR) or the protio impurity in the deuterated solvent; (¹H NMR) - C₆D₆ (7.16 ppm), C₆D₅Br (7.30, 7.02–6.94 ppm), d₈-toluene (7.09, 7.01, 6.97, 2.08 ppm) CD₂Cl₂ (5.32 ppm), CDCl₃ (7.26 ppm); (¹³C NMR) - C₆D₆ (128.06 ppm), C₆D₅Br (130.90, 129.41, 126.24,

122.17 ppm), d^8 -toluene (137.48, 128.87, 127.96, 125.13, 20.43 ppm), $CDCl_3$ (77.16 ppm), CD_2Cl_2 (53.84 ppm). $^{31}P\{^1H\}$ NMR spectra were referenced using an external standard of 85% H_3PO_4 in D_2O (0.0 ppm). ^{19}F NMR were referenced using an external standard of CFC_3 (0.0 ppm). ^{11}B NMR were referenced using an external standard of $BF_3 \cdot Et_2O$ (0.0 ppm). To reference ^{31}P , ^{11}B and ^{19}F NMR spectra, the spectrum for the test compound was acquired first, after which the reference standard was run unlocked at the same field.

X-ray crystallographic analyses were performed on suitable crystals coated in Paratone oil and mounted on a SMART APEX II diffractometer with a 3 kW Sealed tube Mo generator in the McMaster Analytical X-ray (MAX) Diffraction Facility. In all cases, non-hydrogen atoms were refined anisotropically and H atoms were generated in ideal positions and updated with each cycle of refinement.

7.2 Synthetic Procedures and Characterization Pertaining to the Work of Chapter 2

Synthesis of (Ph₃PN)₂XT (1)

A 1.6M solution of *n*BuLi in hexanes (1.02 mL, 1.66 mmol) was added under a stream of argon to a solution of 4,5-dibromo-2,7-di-*tert*-butyl-9,9-dimethylxanthene (400 mg, 0.83 mmol) in 50 mL of THF at $-78\text{ }^{\circ}\text{C}$, and the reaction was stirred for 2 h. A solution of tosyl azide (328 mg, 1.66 mmol) in approximately 2 mL of THF was added dropwise to the reaction at $-78\text{ }^{\circ}\text{C}$, which was then allowed to warm to room temperature, and stirred for 24h. A solution of PPh₃ (437 mg, 1.66 mmol) in approximately 5 mL of THF was added to the reaction at room temperature and the reaction was stirred for a further 24 h. Solvent was then evaporated in vacuo to afford a brown-yellow residue, which was purified in air; $\sim 20\text{ mL}$ of Et₂O was added, followed by sonication, filtration, and washing of the solid with water ($2\times\sim 20\text{ mL}$), Et₂O ($3\times\sim 10\text{ mL}$), and hexanes ($2\times\sim 20\text{ mL}$). The solid was dried under vacuum at $45\text{ }^{\circ}\text{C}$ for 16 h, yielding (Ph₃PN)₂XT as a bright yellow powder (523 mg, 72 %). This ligand is moisture sensitive in solution, but air- and water-stable as a solid. **¹H NMR (C₆D₆, 600 MHz, 298K):** δ 8.02-7.99 (m, 12H, *o*-phenyl), 7.08 (dd, 2H, $^4J_{\text{H,H}} 2\text{ Hz}$, $J_{\text{P,H}} 1\text{ Hz}$, $\text{CH}^{1,8}$), 6.98-6.96 (m, 6H, *p*-phenyl), 6.88-6.85 (m, 12H, *m*-phenyl), 6.56 (appt. t, 2H, $^4J_{\text{H,H}} 2\text{ Hz}$, $^4J_{\text{P,H}} 2\text{ Hz}$, $\text{CH}^{3,6}$), 1.87 (s, 6H, CMe_2), 1.22 (s, 18H, CMe_3) ppm. **¹³C{¹H} NMR (C₆D₆, 151**

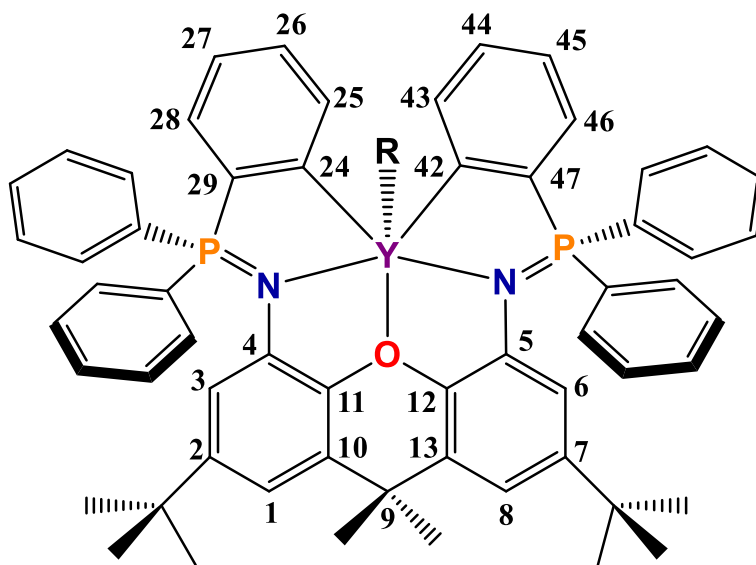
MHz, 298K): δ 144.74 (d, $^2J_{P,C}$ 18 Hz, $C^{4,5}$), 143.16 (s, $C^{2,7}$), 139.37 (s, $C^{11,12}$), 133.59 (d, $^2J_{P,C}$ 9 Hz, *o*-Ph), 132.87 (s, *ipso*-Ph), 131.00 (s, *p*-Ph), 129.99 (s, $C^{10,13}$), 128.39 (d, $^3J_{P,C}$ 12 Hz, *m*-Ph), 118.80 (d, $^3J_{P,C}$ 9 Hz, $CH^{3,6}$), 111.93 (s, $CH^{1,8}$), 35.66 (s, CMe_2), 34.32 (s, CMe_3), 33.54 (s, CMe_2), 31.91 (s, CMe_3) ppm. $^{31}P\{^1H\}$ NMR (C_6D_6 , 243 MHz, 298K): δ -1.95 (s) ppm. $C_{59}H_{58}O_1N_2P_2$ (873.05 g mol $^{-1}$): calcd. C 81.17, H 6.70, 3.21 %; found C 80.95, H 6.82, N 3.05 %.

NOTE: Organic azides can potentially be explosive and have to be handled with caution. The reaction was conducted with a blast shield in place.

Synthesis of [({Ph₂(C₆H₄)PN}₂XT)Y(CH₂SiMe₃)] (2)

A solution of (Ph₃PN)₂XT (1) (160 mg, 0.18 mmol) in toluene (15 mL) was added dropwise to a solution of [Y(CH₂SiMe₃)₃(THF)₂] (100 mg, 0.20 mmol) in toluene (10 mL) at room temperature. The reaction was stirred for 1 hour and then the solvent was removed in vacuo to afford an off white solid. This solid was redissolved in 25 mL of toluene and the solvent was again removed in vacuo, in order to remove residual THF. This solid was washed with hexanes (3 × ~2 mL) and then dried under vacuum for 4 hours, yielding 2 as a highly air-sensitive off-white solid (128 mg, 68%). 1H NMR (C_6D_6 , 600 MHz, 298K): δ 8.30 (d, 2H, $^3J_{H,H}$ 7 Hz, $CH^{25,43}$), 8.08-8.04 (m, 4H, *o*-Ph), 7.74-7.70 (m, 4H, *o*-Ph), 7.21-7.18 (m, 2H, $CH^{26,44}$), 7.17-7.15 (m, 2H, $CH^{28,46}$), 7.12-7.08 (m, 4H, *m*-Ph), 7.07-7.03 (m, 2H, *p*-Ph), 6.99-6.96 (m, 2H, $CH^{27,45}$), 6.93 (d, 2H, $^4J_{H,H}$ 2 Hz, $CH^{1,8}$), 6.92-6.90

(m, 2H, *p*-Ph), 6.86-6.83 (m, 4H, *m*-Ph), 6.83 (d, 2H, $^4J_{\text{H,H}}$ 2 Hz, $\text{CH}^{3,6}$) 1.71, 1.69 (s, 2 x 3H, CMe_2), 1.04 (s, 18H, CMe_3), 0.20 (s, 9H, CH_2SiMe_3), 0.19 (d, 2H, $^2J_{\text{H,Y}}$ 3 Hz, CH_2SiMe_3) ppm. $^{13}\text{C}\{^1\text{H}\}$ NMR (C_6D_6 , 151 MHz, 298K): δ 199.63 (dd, $^1J_{\text{Y,C}}$, $^2J_{\text{P,C}}$ 44 Hz, 38 Hz, $\text{C}^{24,42}$), 146.14 (s, $\text{C}^{2,7}$), 143.82 (d, $^2J_{\text{Y,C}}$ 18 Hz, $\text{C}^{11,12}$), 142.34 (d, $^2J_{\text{Y,C}}$ 26 Hz, $\text{CH}^{25,43}$), 140.21 (s, *ipso*-Ph), 139.31 (s, $\text{C}^{29,47}$), 138.93 (s, *ipso*-Ph), 133.51 (d, $^2J_{\text{P,C}}$ 10 Hz, *o*-Ph), 133.31 (d, $^2J_{\text{P,C}}$ 10 Hz, *o*-Ph), 132.05 (s, *p*-Ph), 131.75 (s, *p*-Ph), 130.84 (s, $\text{C}^{10,13}$), 130.28 (dd, $^2J_{\text{Y,C}}$, $^2J_{\text{P,C}}$, 25 Hz, 80 Hz, $\text{C}^{4,5}$), 129.04 (s, $\text{CH}^{26,44}$), 128.96 (s, *m*-Ph), 128.86 (s, $\text{CH}^{28,46}$), 128.79 (s, *m*-Ph), 124.87 (d, $^3J_{\text{P,C}}$ 16 Hz, $\text{CH}^{27,45}$), 117.78 (d, $^3J_{\text{P,C}}$ 11 Hz, $\text{CH}^{3,6}$), 111.86 (s, $\text{CH}^{1,8}$), 35.37 (s, CMe_2), 35.31, 28.13 (2 x s, CMe_2), 34.63 (s, CMe_3), 34.68 (d, $^1J_{\text{Y,C}}$ 37 Hz, CH_2SiMe_3), 31.47 (s, CMe_3), 4.75 (s, CH_2SiMe_3) ppm. $^{31}\text{P}\{^1\text{H}\}$ NMR (C_6D_6 , 243 MHz, 298K): δ 28.85 (d, $^2J_{\text{Y,P}}$ 11.4 Hz). $\text{C}_{63}\text{H}_{67}\text{O}_1\text{N}_2\text{P}_2\text{SiY}$ (1047.16 g mol $^{-1}$): calcd. C 72.26, H 6.45, 2.68; found C 71.79, H 6.80, N 2.61. X-ray quality crystals of $[(\{\text{Ph}_2(\text{C}_6\text{H}_4)\text{PN}\}_2\text{XT})\text{Y}(\text{CH}_2\text{SiMe}_3)(\text{THF})]\cdot 2\text{THF}$ (**2-THF** $\cdot 2\text{THF}$) were grown by layering hexanes onto a saturated solution of **2** in THF, and cooling to -28 °C.



Synthesis of $(\text{Ph}_3\text{PN})_2\text{NAP}$ (3)

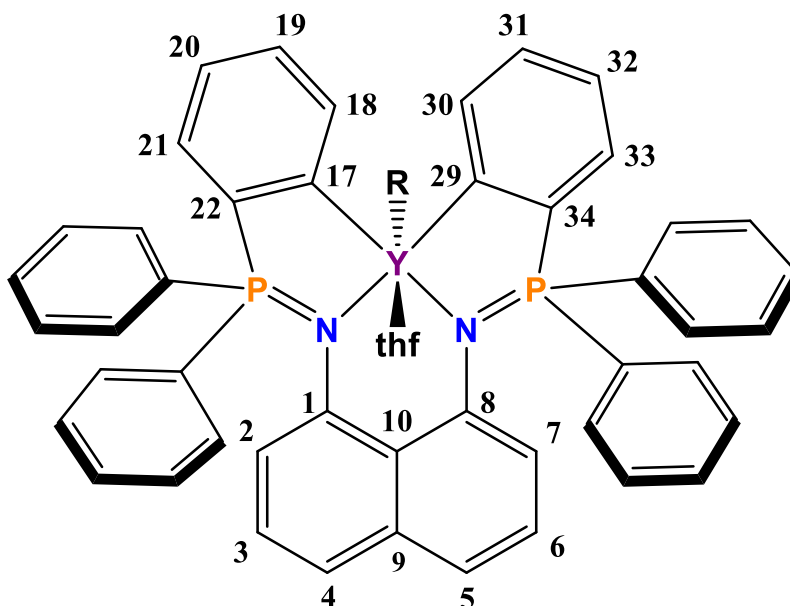
A 100 mL round bottom flask was loaded with 1,8-diaminonaphthalene (100 mg, 0.63 mmol) and Ph_3PBr (533 mg, 1.26 mmol), and ~50 mL of CH_2Cl_2 was condensed into the flask at $-78\text{ }^\circ\text{C}$. Excess Et_3N (1 mL, 7.16 mmol) was added to the reaction at $-78\text{ }^\circ\text{C}$, and the reaction mixture was allowed to warm up to room temperature. After stirring for 1 h, solvent was removed in vacuo, and ~50 mL of THF was condensed into the flask, followed by sonication to suspend all the solid. The reaction was cooled to $-45\text{ }^\circ\text{C}$, and a solution of $\text{KN}(\text{SiMe}_3)_2$ (502 mg, 2.52 mmol) in 10 mL of THF was added slowly. The reaction was then brought to room temperature, and stirred for 1h prior to removal of solvent in vacuo to afford a bright yellow solid. This solid was purified in air; ~20 mL of Et_2O was added to the flask,

followed by sonication to suspend the yellow solid, filtration, and washing of the solid with water (~20 mL), Et₂O (2 × ~20 mL), and then hexanes (2 × ~20 mL). Bright yellow (Ph₃PN)₂NAP was then dried at 45°C in vacuo for 16 h (351 mg, 82 %). **¹H NMR (CD₂Cl₂, 600 MHz, 298K):** δ 7.95-7.92 (m, 12 H, *o*-Ph), 7.41-7.39 (m, 6H, *p*-Ph), 7.23-7.20 (m, 12H, *m*-Ph), 6.85 (d, 2H, ³J_{H,H} 8 Hz, CH^{4,5}), 6.73 (appt. t, 2H, ³J_{H,H} 8 Hz, CH^{3,6}), 6.25 (d, ³J_{H,H} 8 Hz, CH^{2,7}) ppm. **¹³C{¹H} NMR (CD₂Cl₂, 151 MHz, 298K):** δ 150.52 (s, C^{1,8}), 138.91 (s, C⁹), 133.52 (d, ²J_{P,C} 10 Hz, *o*-Ph). 132.64 (s, *ipso*-Ph), 131.99 (s, C¹⁰), 131.51 (s, *p*-Ph), 128.54(d, ³J_{P,C} 12 Hz, *m*-Ph), 125.24 (s, CH^{3,6}), 116.95 (s, CH^{4,5}), 116.17 (d, ³J_{P,C} 14 Hz, C^{2,7}). **³¹P{¹H} NMR (CD₂Cl₂, 243 MHz, 298K):** δ -3.39 ppm. **C₄₆H₃₆N₂P₂ (678.74 g mol⁻¹):** calcd. C 81.40, H 5.35, N 4.13 %; found. C 81.18, H 5.61, N 4.06 %.

Synthesis of [(Ph₂(C₆H₄)PN)₂NAP]Y(CH₂SiMe₃)(THF) (4)

A solution of (Ph₃PN)₂NAP (**3**) (124 mg, 0.18 mmol) in toluene (15 mL) was added dropwise to a solution of [Y(CH₂SiMe₃)₃(THF)₂] (100 mg, 0.20 mmol) in toluene (10 mL) at room temperature. The reaction was stirred for 1 hour and then the solvent was removed in vacuo to afford an off white solid. This solid was then washed with hexanes (3 × ~2 mL), and then dried under vacuum for 4 hours, yielding **4-THF** as an off white solid (121 mg, 72.6%). **¹H NMR (C₆D₆, 600 MHz, 298K):** δ 8.52 (d, 2H, ³J_{H,H} 7 Hz, CH^{18,30}), 7.74-7.71 (m, 4H, *o*-Ph), 7.48-7.45 (m, 4H, *o*-Ph), 7.30-7.28 (m, 2H, CH^{19,31}), 7.14 (d, 2H, ³J_{H,H} 8 Hz, CH^{4,5}), 7.07-7.03

(m, 2H, $CH^{21,33}$), 6.99-6.96 (broad m, 2H, *p*-Ph), 6.99-6.96 (br m, 4H, *m*-Ph), 6.96-6.93 (m, 2H, $CH^{2,7}$), 6.96-6.93 (m, 2H, $CH^{20,32}$), 6.92-6.88 (m, 2H, *p*-Ph), 6.83 (app. t, 2H, $^3J_{H,H}$ 8 Hz, $^3J_{H,H}$ 8 Hz, $CH^{3,6}$), 6.72-6.69 (m, 4H, *m*-Ph), 3.67 (m, 4H, THF), 1.22 (m, 4H, THF), 0.41 (s, 9H, CH_2SiMe_3), -0.15 (d, 2H, $^2J_{Y,H}$ 2 Hz, CH_2SiMe_3) ppm. $^{13}C\{^1H\}$ NMR (C_6D_6 , 151 MHz, 298K): δ 197.52 (app. t, J 42 Hz, $C^{17,29}$), 145.26 (d, $^2J_{P,C}$ 6 Hz, $C^{1,8}$), 139.48 (d, $^2J_{Y,C}$ 26 Hz, $CH^{18,30}$), 138.50 (app. t, J 70 Hz, $C^{22,34}$), 133.61 (d, $^2J_{P,C}$ 9 Hz, *o*-Ph), 133.49 (d, $^2J_{P,C}$ 9 Hz, *o*-Ph), 133.23 (s, *ipso*-Ph), 132.71 (s, *ipso*-Ph), 131.54 (s, *p*-Ph), 131.23 (s, *p*-Ph), 130.30, 129.76 (2 \times s, C^9 and C^{10}), 129.34 (s, $CH^{19,31}$), 129.13 (d, $^2J_{P,C}$ 4 Hz, $CH^{21,33}$), 128.78 (d, $^3J_{P,C}$ 11 Hz, *m*-Ph), 128.43 (d, $^3J_{P,C}$ 11 Hz, *m*-Ph), 125.35 (d, $^3J_{P,C}$ 16 Hz, $CH^{20,32}$), 125.04 (s, $CH^{3,6}$), 122.29 (s, $CH^{4,5}$), 121.38 (d, $^3J_{P,C}$ 13 Hz, $CH^{2,7}$), 69.05 (s, THF), 25.33 (s, THF), 30.82 (d, $^1J_{Y,C}$ 34 Hz, CH_2SiMe_3), 5.02 (s, CH_2SiMe_3) ppm. $^{31}P\{^1H\}$ NMR (C_6D_6 , 243 MHz, 298K): δ 28.49 (d, $^2J_{Y,P}$ 12 Hz) ppm. $C_{54}H_{53}ON_2P_2SiY$ (924.95 g mol $^{-1}$): calcd. C 70.12, H 5.78, N 3.03 %; found C 69.31, H 5.79, N 2.58 % (some thermal decomposition likely occurred during transport to Indianapolis for elemental analysis). X-ray quality crystals of [$\{Ph_2(C_6H_4)PN\}_2NAP\}Y(CH_2SiMe_3)(DME)\cdot hexane$] (**4-DME**·hexane) were grown by layering a saturated solution of **4** in DME with hexanes, followed by cooling to -28 °C.



7.3 Synthetic Procedures and Characterization Pertaining to the Work of Chapter 3

Synthesis of H[AlI₂] (5)

Under argon, a mixture of [(RuPhos)Pd(C₆H₄{*o*-C₆H₄(*o*-NHMe)})(OMs)] ("RuPhos Pd G4"; 214 mg, 0.252 mmol), RuPhos (117.9 mg, 0.252) and sodium *tert*-butoxide (0.584 g, 6.07 mmol) was dissolved in approximately 10 mL of 1,4-dioxane and stirred for 5 minutes in a 100 mL sealed flask. This was followed by the addition of 1,3-diisopropylimidazol-2-imine (0.888 g, 5.31 mmol) and 4,5-dibromo-2,7,9,9-tetramethylacridan (1.00 g, 2.53 mmol) in approximately 30 mL of 1,4-dioxane. The sealed reaction flask was heated at 100 °C in an oil bath

for 36 h yielding a dark brown solution. Under air, the reaction solution was passed through a pad of Celite and volatiles were removed under reduced pressure to afford a dark brown oil. The product was extracted using approximately 30 mL of CH_2Cl_2 and was washed with 60 mL of water. The resulting aqueous layer was additionally extracted with 30 mL of CH_2Cl_2 and the organic layers were combined. The organic layer was dried over MgSO_4 and gravity filtered. Volatiles were removed from the filtrate under reduced pressure to afford a sticky dark brown solid. This solid was dissolved in approximately 60 mL of hot hexanes and was passed through a pad of Celite, yielding a dark orange filtrate. The filtrate was concentrated to 20 mL and was allowed to re-crystallize at $-10\text{ }^\circ\text{C}$ overnight. The resulting brown-orange powder was dried for 12 h at $80\text{ }^\circ\text{C}$ under reduced pressure to yield 846 mg of $\text{H}[\text{AlI}_2]$ (**5**) (59 % yield). $^1\text{H NMR}$ (C_6D_6 , 600 MHz, 298K): δ 8.39 (s, 1H, NH), 6.98 (s, 2H, $\text{CH}^{1,8}$), 6.72 (s, 2H, $\text{CH}^{3,6}$), 5.90 (s, 4H, N-CH), 4.49 (sept, $^3J_{\text{H,H}}$ 6.0 Hz, 4H, CHMe_2), 2.39 (s, 6H, Ar-Me), 1.82 (s, 6H, CMe_2), 0.92 (d, $^3J_{\text{H,H}}$ 6.0 Hz, 24H, CHMe_2) ppm. $^{13}\text{C}\{^1\text{H}\}$ NMR (C_6D_6 , 600 MHz, 298K): δ 146.45 (s, NCN), 137.27 (s, $\text{C}^{4,5}$), 131.64 (s, $\text{C}^{11,12}$), 128.94 (s, $\text{C}^{10,13}$), 127.28 (s, $\text{C}^{2,7}$), 116.83 (s, $\text{CH}^{3,6}$), 116.24 (s, $\text{CH}^{1,8}$), 108.61 (s, N-CH), 45.69 (s, CHMe_2), 37.33 (s, C^9), 29.96 (s, CMe_2), 21.83 (s, Ar-Me), 21.42 (s, CHMe_2) ppm. $\text{C}_{35}\text{H}_{49}\text{N}_7$ (567.83 g mol $^{-1}$): calcd. C 74.03, H 8.70, N 17.27 %; found. C 73.75, H 8.85, N 17.05 %.

Synthesis of [(AlI₂)Y(CH₂SiMe₃)₂] (**6**)

A solution of H[AlI₂] (**5**) (484 mg, 0.852 mmol) in 20 mL of toluene was added dropwise to a solution of [Y(CH₂SiMe₃)₃(THF)₂] (422 mg, 0.852 mmol) in toluene (15 mL) at room temperature. The reaction was stirred for 1 hour and then the solvent was removed in vacuo to afford a dark brown oil. 30 mL of hexanes was added to the oil and the mixture was sonicated to obtain a brown solid. Solvent was removed in vacuo and the solid was washed with hexanes (3 x ~ 5 mL). The solid was dried under vacuum for 4 hours, yielding **6** as a highly air-sensitive brown solid (658 mg, 93 % yield). X-ray quality crystals of **6** were grown by cooling a concentrated toluene solution to -29 °C. ¹H NMR (C₆D₆, 600 MHz, 298K): δ 6.92 (s, 2H, CH^{1,8}), 6.06 (s, 4H, N-CH), 5.56 (s, 2H, CH^{3,6}), 4.88 (sept, ³J_{H,H} 7 Hz, 4H, CHMe₂), 2.27 (s, 6H, Ar-Me), 1.96 (s, 6H, CMe₂), 1.19 (d, ³J_{H,H} 7 Hz, 12H, CHMe₂), 0.99 (d, ³J_{H,H} 7 Hz, 12H, CHMe₂), 0.19 (s, 18H, CH₂SiMe₃), -0.81 (d, ²J_{H,Y} 2 Hz, 4H, CH₂SiMe₃) ppm. ¹³C{¹H} NMR (C₆D₆, 600 MHz, 298K): δ 152.21 (s, NCN), 144.31 (s, C^{4,5}), 139.33 (s, C^{2,7}), 127.77 (s, C^{11,12}), 123.48 (s, C^{10,13}), 118.04 (s, CH^{1,8}), 112.45 (s, N-CH), 111.71 (s, CH^{3,6}), 47.62 (s, CHMe₂), 37.11 (s, C⁹), 34.46 (s, CMe₂), 28.32 (d, ¹J_{C,Y} 36 Hz, CH₂SiMe₃), 23.06 (s, CHMe₂), 22.29 (s, CHMe₂), 21.94 (s, Ar-Me), 4.62 (s, CH₂SiMe₃) ppm. C₄₃H₇₀N₇Si₂Y (830.16 g mol⁻¹): calcd. C 62.21, H 8.50, N 11.81 %; found. C 61.68, H 8.44, N 11.25 %.

Synthesis of $[(AlI_2)Y(CH_2SiMe_3)][B(C_6F_5)_4]$ (7**)**

- 1) 15 mg (0.018 mmol) of $[(AlI_2)Y(CH_2SiMe_3)]$ (**6**) was dissolved in approximately 0.4 mL of C_6D_5Br to afford a light brown solution. To this solution was added $[CPh_3][B(C_6F_5)_4]$ (16.6 mg, 0.018 mmol) in approximately 0.4 mL of C_6D_5Br , resulting in a deep purple solution, which was allowed to react for 10 minutes. At room temperature, solutions of cation **7** were completely decomposed after 45 minutes. Therefore, some product decomposition accompanies this room temperature synthesis.
- 2) 15 mg (0.018 mmol) of $[(AlI_2)Y(CH_2SiMe_3)]$ (**6**) was dissolved in approximately 0.4 mL of C_6D_5Br to afford a light brown solution and cooled to $-28\text{ }^\circ\text{C}$. To this solution was added a cooled solution ($-28\text{ }^\circ\text{C}$) of 16.6 mg (0.018 mmol) $[CPh_3][B(C_6F_5)_4]$ in approximately 0.4 mL C_6D_5Br , resulting in a deep purple solution. The reaction was maintained at $-28\text{ }^\circ\text{C}$ for 45 minutes for complete conversion. This procedure was followed to minimize the decomposition of $[(AlI_2)Y(CH_2SiMe_3)]$.

Several ^{13}C NMR signals are not visible in the $^{13}\text{C}\{^1\text{H}\}$ NMR (16 000 scans) at 258 K due to significant precipitation of **7**. These peaks are reported as identified from ^1H - ^{13}C HSQC at 258 K. ^1H NMR (C_6D_5Br , 500 MHz, 298K): δ 6.72 (s, 2H, $CH^{1,8}$), 6.65 (s, 2H, N-CH), 6.63 (s, 2H, N-CH), 5.53 (s, 2H, $CH^{3,6}$), 5.01 (sept, $^3J_{H,H}$ 7 Hz, 2H, $CHMe_2$), 4.17 (sept, $^3J_{H,H}$ 7 Hz, 2H, $CHMe_2$), 2.07 (s, 6H, Ar-Me), 1.82 (s, 3H, CMe_2), 1.52 (s, 3H, CMe_2), 1.42 (d, $^3J_{H,H}$ 7 Hz, 6H, $CHMe_2$), 1.22 (appt t, $^3J_{H,H}$

7 Hz, 12H, CHMe_2), 1.10 (d, $^3J_{\text{H,H}}$ 7 Hz, 6H, CHMe_2), -0.44 (s, 9H, CH_2SiMe_3), -0.88 (appt s, 2H, CH_2SiMe_3) ppm. $^{13}\text{C}\{^1\text{H}\}$ NMR (C_6D_6 , 500 MHz, 258K) 149.36 ($\text{B}(\text{C}_6\text{F}_5)_4$), 147.47 ($\text{B}(\text{C}_6\text{F}_5)_4$), 137.39 ($\text{B}(\text{C}_6\text{F}_5)_4$), 135.50 ($\text{B}(\text{C}_6\text{F}_5)_4$), 118.65 ($\text{CH}^{1,8}$), 113.79 (N-CH), 113.81 ($\text{CH}^{3,6}$), 47.98 (s, CHMe_2), 47.86 (s, CHMe_2), 36.44 (CMe_2), 33.92 (CH_2SiMe_3), 30.99 (CMe_2) 24.36 (s, CHMe_2), 22.80 (s, CHMe_2), 21.84 (s, Ar-Me), 21.26 (s, CHMe_2), 20.77 (s, CHMe_2), 3.59 (s, CH_2SiMe_3) ppm. $^{11}\text{B}\{^1\text{H}\}$ NMR ($\text{C}_6\text{D}_5\text{Br}$, 161 MHz, 258K): -16.17 (s, $\text{B}(\text{C}_6\text{F}_5)_4$) ppm. ^{19}F NMR ($\text{C}_6\text{D}_5\text{Br}$, 161 MHz, 258K): -131.29 (appt s, *o*-F $\text{B}(\text{C}_6\text{F}_5)_4$) ppm.

Synthesis of $[(\text{AlI}_2)\text{Sc}(\text{CH}_2\text{SiMe}_3)_2]$ (**8**)

A solution of $\text{H}[\text{AlI}_2]$ (**5**) (100 mg, 0.176 mmol) in 10 mL of toluene was added dropwise to a solution of $[\text{Sc}(\text{CH}_2\text{SiMe}_3)_3(\text{THF})_2]$ (87.3 mg, 0.193 mmol) in toluene (10 mL) at room temperature. The reaction was stirred for 1 hour and then the solvent was removed in vacuo to afford a dark brown oil. Approximately 20 mL of hexanes was added to the oil and the mixture was sonicated to obtain a brown solid. Solvent was removed in vacuo and the solid was washed with hexanes (3 x ~ 2 mL). The solid was dried under vacuum for 4 hours yielding **8** as a highly air-sensitive brown solid (135 mg, 98 % yield). X-ray quality crystals of **8** were grown by cooling a concentrated toluene solution to -28 °C. ^1H NMR (C_6D_6 , 600 MHz, 298K): δ 6.88 (s, 2H, $\text{CH}^{1,8}$), 6.11 (s, 4H, N-CH), 5.47 (s, 2H, $\text{CH}^{3,6}$), 4.98 (sept, $^3J_{\text{H,H}}$ 7 Hz, 4H, CHMe_2), 2.28 (s, 6H, Ar-Me), 1.97 (s, 6H, CMe_2), 1.22 (d, $^3J_{\text{H,H}}$ 7

Hz, 12H, CHMe_2), 1.02 (d, $^3J_{\text{H,H}}$ 7 Hz, 12H, CHMe_2), 0.13 (s, 18H, CH_2SiMe_3), – 0.50 (s, 4H, CH_2SiMe_3) ppm. $^{13}\text{C}\{^1\text{H}\}$ NMR (C_6D_6 , 600 MHz, 298K): δ 153.03 (s, NCN), 145.26 (s, $\text{C}^{4,5}$), 138.23 (s, $\text{C}^{2,7}$), 126.67 (s, $\text{C}^{11,12}$), 123.81 (s, $\text{C}^{10,13}$), 117.18 (s, $\text{CH}^{1,8}$), 112.68 (s, N-CH), 110.22 (s, $\text{CH}^{3,6}$), 47.56 (s, CHMe_2), 36.98 (s, C^9), 34.35 (s, CMe_2), 30.97 (s, CH_2SiMe_3), 23.55 (s, CHMe_2), 22.13 (s, CHMe_2), 22.13 (s, Ar-Me), 4.31 (s, CH_2SiMe_3) ppm. $\text{C}_{43}\text{H}_{70}\text{N}_7\text{Si}_2\text{Sc}$ (786.19 g mol⁻¹): calcd. C 65.69, H 8.97, N 12.47 %; found. C 65.42, H 8.78, N 11.91 %.

General Procedure for in-situ Hydroamination using $[(\text{AlI}_2)\text{Y}(\text{CH}_2\text{SiMe}_3)_2]$ (6)

In the glovebox, $[(\text{AlI}_2)\text{Y}(\text{CH}_2\text{SiMe}_3)_2]$ (6) (5 mg, 0.006 mmol) was dissolved in 0.8 mL of C_6D_6 and added to the hydroamination substrate 1-amino-2,2-diphenyl-4-pentene (0.12 mmol) and the internal standard (0.12 mmol ferrocene) measured in a separate vial. The solution was then immediately placed in a PTFE valved NMR tube, and the reaction was monitored at 24 °C by ^1H NMR spectroscopy.

Kinetic study of the hydroamination of 1-amino-2,2-diphenyl-pent-5-ene by $[(\text{AlI}_2)\text{Y}(\text{CH}_2\text{SiMe}_3)_2]$ (6)

The experiment was carried out as described in the general procedure for *in-situ* hydroamination using $[(\text{AlI}_2)\text{Y}(\text{CH}_2\text{SiMe}_3)_2]$.

**General procedure for in-situ Hydroamination using
[(AlI₂)Y(CH₂SiMe₃)] [B(C₆F₅)₄] (7)**

Entry 1 - In the glovebox, [(AlI₂)Y(CH₂SiMe₃)₂] (**6**) (10 mg, 0.012 mmol) was dissolved in 0.5 mL of C₆D₅Br. Similarly, [CPh₃][B(C₆F₅)₄] (11.1 mg, 0.012 mmol) was dissolved in 0.5 mL and added to the solution of (**6**) resulting in a deep purple solution. After 10 minutes, 0.2 mL of the catalyst solution (**7**) was measured and added to 1-amino-2,2-diphenyl-pent-4-ene (0.12 mmol) and ferrocene (0.12 mmol) in 0.6 mL of C₆D₅Br. The solution was then immediately placed in a PTFE-valved NMR tube, and the reaction was monitored at 24 °C by ¹H NMR spectroscopy.

Entries (2-4) - In the glovebox, [(AlI₂)Y(CH₂SiMe₃)₂] (5 mg, 0.006 mmol) was dissolved in 0.4 mL of C₆D₅Br. Similarly, [CPh₃][B(C₆F₅)₄] (5.6 mg, 0.006 mmol) was dissolved in 0.4 mL and added to the solution of **6** resulting a deep purple solution. After 10 minutes, this catalyst solution was added to the hydroamination substrate (0.12 mmol) and the internal standard (0.12 mmol ferrocene) measured in a separate vial. The solution was then immediately placed in a PTFE valved NMR tube, and the reaction was monitored at 24 °C by ¹H NMR spectroscopy.

Kinetic study of the hydroamination of 1-amino-2,2-diphenyl-4-methylpent-4-ene by [(AlI₂)Y(CH₂SiMe₃)] [B(C₆F₅)₄] (7)

(10 mg, 0.012 mmol) of **6** was dissolved in 0.5 mL of C₆D₅Br. Similarly, [CPh₃][B(C₆F₅)₄] (11.1 mg, 0.012 mmol) was dissolved in 0.5 mL of C₆D₅Br and

added to the solution of **6** resulting a deep purple solution. After 10 minutes, the appropriate volume of catalyst solution was measured using a glass microsyringe (0.26 mL, 2% catalyst loading) and added to 1-amino-2,2-diphenyl-4-methylpent-4-ene (0.16 mmol) and the internal standard (0.16 mmol ferrocene) measured in a separate vial and dissolved in 0.6 mL of C₆D₅Br. The solution was then immediately placed in a PTFE valved NMR tube, and the reaction was monitored at 24 °C by ¹H NMR spectroscopy.

Kinetic study of the hydroamination of 1-amino-2,2-diphenyl-hex-5-ene by [(AlI₂)Y(CH₂SiMe₃)] [B(C₆F₅)₄] (7**)**

(5.31 mg, 0.0064 mmol) of **6** was dissolved in 0.4 mL of C₆D₅Br. Similarly, [CPh₃][B(C₆F₅)₄] (5.9 mg, 0.0064 mmol) was dissolved in 0.4 mL of C₆D₅Br and added to the solution of **6** resulting in a deep purple solution. After 10 minutes, the catalyst solution was subsequently added to 1-amino-2,2-diphenyl-hex-5-ene (0.16 mmol) and the internal standard (0.16 mmol ferrocene) measured in a separate vial. The solution was then immediately placed in a PTFE valved NMR tube, and the reaction was monitored at 24 °C by ¹H NMR spectroscopy.

7.4 Synthetic Procedures and Characterization Pertaining to the Work of Chapter 4

Synthesis of XIA₂ (9)

250 mg (0.52 mmol) of Br₂XT was placed in a 100 mL round bottom flask in the glove box and equipped with a reflux condenser. Approximately 50 mL of THF was vacuum transferred to the reaction flask resulting in a clear solution. 0.64 mL (1.04 mmol) of 1.63 M *n*BuLi was added to the reaction flask at -78°C under a heavy flow of argon and was allowed to stir for 2 hours. 205 mg (1.04 mmol) of TosN₃ was dissolved in approximately 5 mL of THF in the dry box and was then added dropwise to the reaction flask under a heavy flow of argon at -78°C . The resulting bright yellow solution was stirred for 16 h and was allowed to come to room temperature. The solvent was removed in vacuo resulting in a yellow solid. Approximately 50 mL of toluene was vacuum transferred to the reaction flask. 158 mg (1.04 mmol) of 1,4-diisopropyl-imidazolin-2-ylidene was dissolved in approximately 5 mL of toluene in a drybox and was added to the reaction flask under a heavy flow of argon at room temperature. The resulting orange solution was heated to reflux for 3 days. The solvent was removed in vacuo and the resulting yellow solid was dissolved in approximately 30 mL of CH₂Cl₂. This solution was gravity filtered and the filtrate was subsequently washed 3 times with 20 mL of water. CH₂Cl₂ was then removed in vacuo and the resulting solid was washed with approximately 30 mL of diethyl ether, resulting in 207 mg of bright yellow solid

(0.32 mmol, 61%). ^1H NMR (CD_2Cl_2 , 600 MHz, 298K): δ 7.33 (d, $^3J_{\text{H,H}}$ 6.0 Hz, 2H, $\text{CH}^{3,6}$), 7.27 (d, $^3J_{\text{H,H}}$ 6.0 Hz, 2H, $\text{CH}^{1,8}$), 6.72 (s, 4H, N-CH), 5.27 (sept, $^3J_{\text{H,H}}$ 6.0 Hz, 4H, CHMe_2), 1.69 (s, 6H, CMe_2), 1.43 (d, $^3J_{\text{H,H}}$ 6.0 Hz, 24H, CHMe_2), 1.35 (s, 18H, CMe_3) ppm. $^{13}\text{C}\{^1\text{H}\}$ NMR (CD_2Cl_2 , 600 MHz, 298K): δ 150.62 (s, NCN), 144.81 (s, $\text{C}^{2,7}$), 142.99 (s, $\text{C}^{11,12}$), 140.28 (s, $\text{C}^{4,5}$), 130.32 (s, $\text{C}^{10,13}$), 119.82 (s, $\text{C}^{3,6}$), 112.86 (s, $\text{C}^{1,8}$), 111.64 (s, N-CH), 48.42 (s, CHMe_2), 34.94 (s, CMe_3), 34.87 (s, C^9), 33.12 (s, CMe_2), 31.73 (s, CHMe_2), 22.74 (s, CMe_3) ppm. $\text{C}_{41}\text{H}_{60}\text{N}_{10}\text{O}_1$ (786.19 g mol $^{-1}$).

NOTE: Organic azides can potentially be explosive and have to be handled with caution. The reaction was conducted with a blast shield in place.

Synthesis of $[(\text{XIA}_2)\text{Y}(\text{CH}_2\text{SiMe}_3)_3]$ (10)

200 mg (0.25 mmol) of XIA_2 was placed in a 50 mL round bottom flask and dissolved in approximately 20 mL of toluene in a dry box. To this was added a solution consisting of 125.9 mg (0.25 mmol) of $[\text{Y}(\text{CH}_2\text{SiMe}_3)_3(\text{THF})_2]$ in 10 mL of toluene resulting in a merlot colored solution. The solvent was then removed in vacuo resulting in 260 mg (0.065 mmol, 85%) of merlot colored solid. ^1H NMR (C_6D_6 , 600 MHz, 298K): δ 7.89 (d, $^3J_{\text{H,H}}$ 6.0 Hz, 2H, $\text{CH}^{3,6}$), 7.43 (d, $^3J_{\text{H,H}}$ 6.0 Hz, 2H, $\text{CH}^{1,8}$), 6.04 (s, 4H, N-CH), 5.31 (sept, $^3J_{\text{H,H}}$ 6.0 Hz, 4H, CHMe_2), 1.79 (s, 6H, CMe_2), 1.35 (s, 18H, CMe_3), 1.24 (d, $^3J_{\text{H,H}}$ 6.0 Hz, 24H, CHMe_2), 0.10 (br s, 27H, CH_2SiMe_3), -0.55 (br s, 2H, CH_2SiMe_3), -0.67 (br s, 4H, CH_2SiMe_3) ppm. ^{13}C

NMR: (C₆D₆, 600 MHz, 298K): δ 151.06 (s, NCN), 145.64 (s, C^{2,7}), 142.18 (s, C^{4,5}), 130.37 (s, C^{10,13}), 128.08 (s, C^{11,12}), 120.28 (s, C^{1,8}), 113.09 (s, N-CH), 111.06 (s, C^{3,6}), 49.09 (s, CHMe₂), 34.95 (s, CMe₃) 32.99 (s, CMe₂), 31.78 (s, CMe₃), 23.09 (s, CHMe₂), 22.01 (d, ²J_{C,Y} 24 Hz, CH₂SiMe₃), 21.43 (s, C⁹), 5.01 (s, CH₂SiMe₃), 4.73 (s, CH₂SiMe₃) ppm. **C₅₃H₉₃N₁₀O₁Si₃Y (1059.53 g mol⁻¹).**

Synthesis of XII₂ (11)

The catalyst mixture of Pd(OAc)₂ (46.7 mg, 0.208 mmol), DPEPhos (156 mg, 0.29 mmol), sodium *tert*-butoxide (479 mg, 2.49 mmol) were dissolved in approximately 20 mL of toluene and stirred at room temperature for 10 minutes in the glovebox. 1,3-diisopropylimidazol-2-imine (720 mg, 4.3 mmol) and 4,5-dibromo-2,7-di-*tert*-butyl-9,9-dimethylxanthene (1 g; 2.08 mmol) were dissolved in approximately 30 mL of toluene in the glovebox and added to the reaction mixture. The reaction mixture was placed in a sealed 100 mL flask and heated to 95°C in an oil bath outside the glovebox for 48 h. Under air, the reaction solution was passed through a pad of Celite and volatiles were removed under reduced pressure to afford a dark brown oil. The product was extracted using approximately 60 mL of CH₂Cl₂ and was washed with 60 mL of water. The resulting aqueous layer was additionally extracted with 30 mL of CH₂Cl₂ and the organic layers were combined. The organic layer was dried over MgSO₄ and gravity filtered. Volatiles were removed from the filtrate under reduced pressure to afford a sticky dark brown solid. This solid was

dissolved in approximately 50 mL of hexanes and was passed through a pad of Celite, yielding a dark orange filtrate. The filtrate was concentrated to approximately 10 mL and was allowed to re-crystallize at $-10\text{ }^{\circ}\text{C}$ overnight. The resulting beige powder was dried for 12 h at $80\text{ }^{\circ}\text{C}$ under reduced pressure to yield 609 mg of XII₂ (45 % yield). **¹H NMR (C₆D₆, 600 MHz, 298K):** δ 7.13 (s, 2H, CH^{1,8}), 7.13 (s, 2H, CH^{3,6}), 5.92 (s, 4H, N-CH), 4.45 (sept, 4H, ³J_{H,H} 7 Hz, CHMe₂), 1.82 (s, 6H, CMe₂), 1.38 (s, 18H, CMe₃) 1.00 (d, ³J_{H,H} 7 Hz, 24H) ppm. **¹³C{¹H} NMR (C₆D₆, 151 MHz, 298K):** δ 144.64 (s, NCN), 144.48 (s, C^{2,7}), 142.77 (s, C^{4,5}), 140.10 (s, C^{11,12}) 130.46 (s, C^{10,13}), 118.00 (s, CH^{1,8}), 112.03 (CH^{3,6}), 107.74 (s, N-CH), 45.26 (s, CHMe₂), 35.57 (s, C⁹). 34.58 (s, CMe₃), 32.03 (s, CMe₂), 32.03 (s, CMe₃), 21.78 (s, CHMe₂) ppm. **C₄₁H₆₀N₆O₁ (652.95 g mol⁻¹):** calcd. C 75.42, H 9.26, N 12.87 %; found. C 75.63, H 9.47, N 12.51 %.

NOTE: The reaction had to be heated slowly from room temperature to $95\text{ }^{\circ}\text{C}$. Several unidentified products were seen when the reaction was placed directly in a $95\text{ }^{\circ}\text{C}$ oil bath.

Synthesis of [(XII₂)YCl₃] (12)

A solution of XII₂ (11) (100 mg, 0.153 mmol) in 5 mL of THF was added dropwise to a solution of [YCl₃(THF)_{3.5}] (69 mg, 0.153 mmol) in THF (5 mL) at room temperature and the reaction was stirred for 1 hour. Approximately 40 mL of hexanes was added to the reaction resulting in the precipitation of white solid. The

solution was decanted, and the white solid was further dried under vacuum for 1 hour. The solid was further washed with hexanes (3 x ~ 5 mL) and further dried under vacuum for 2 hours, yielding **12** as an air-sensitive white solid (106 mg, 82 % yield). **¹H NMR (CD₂Cl₂, 600 MHz, 298K):** δ 7.07 (s, 4H, N-CH), 6.81 (s, 2H, CH^{1,8}), 5.66 (s, 2H, CH^{3,6}), 5.08 (sept, ³J_{H,H} 7 Hz, 4H, CHMe₂), 1.73 (s, 6H, CMe₂), 1.54 (d, ³J_{H,H} 7 Hz, 12H, CHMe₂), 1.29 (d, ³J_{H,H} 7 Hz, 12H, CHMe₂), 1.21 (s, 18H, CMe₃) ppm. **¹³C{¹H} NMR (CD₂Cl₂, 151 MHz, 298K):** δ 148.39 (s, NCN), 147.12 (s, C^{2,7}), 141.66 (s, C^{4,5}), 137.89 (C^{11,12}), 129.23 (s, C^{10,13}), 114.79 (s, N-CH), 112.94 (s, CH^{1,8}), 109.72 (s, CH^{3,6}), 48.81 (s, CHMe₂), 34.76 (s, CMe₃), 34.38 (s, C⁹), 34.04 (s, CMe₂), 31.50 (s, CMe₃), 23.63 (s, CHMe₂), 23.33 (s, CHMe₂) ppm. **C₄₁H₆₀N₆O₁Cl₃Y (848.22 g mol⁻¹):** calcd. C 58.06, H 7.13, N 9.91 %; found. C 58.33, H 7.16, N 9.43 %.

Synthesis of [H(XII₂)] [B(C₆F₅)₄] · 0.5 hexane (**13**)

A solution of [H(Et₂O)₂][B(C₆F₅)₄] (127 mg, 0.153 mmol) in approximately 10 mL of C₆H₅F was added dropwise to a solution of XII₂ (**11**) (100 mg, 0.153 mmol) in C₆H₅F (5 mL) at room temperature. The reaction was stirred for 1 hour and 40 mL of hexanes was added, which resulted in precipitation of white solid. The solution was decanted, and the solid was dried under vacuum. The solid was further washed with hexanes (3 x ~ 5 mL) and further dried under vacuum for 4 hours, yielding **13** as a white solid (182 mg, 86 % yield). **¹H NMR (CD₂Cl₂, 600 MHz, 298K):** δ 7.03

(s, 2H, *xanth-H*), 6.83 (br s, 4H, N-*CH*), 6.40 (br s, 2H, *xanth-H*), 5.85 (br s, 1H, *NH*), 4.38 (sept, $^3J_{\text{H,H}}$ 7 Hz, 4H, *CHMe*₂), 1.67 (s, 6H, *CMe*₂), 1.29 (d, $^3J_{\text{H,H}}$ 7 Hz, 24H), 1.26 (s, 18H, *CMe*₃) ppm. $^{13}\text{C}\{^1\text{H}\}$ NMR (CD_2Cl_2 , 151 MHz, 298K): δ 146.61 (s, *C*^{2,7}), 139.38 (s, *C*^{4,5}), 138.67 (s, *C*^{10,11,12,13}), 137.86 (s, N-*CN*), 130.55 (s, *C*^{10,11,12,13}), 115.42 (s, *xanth-H*), 113.22 (s, *xanth-H*), 113.22 (s, N-*CH*), 35.36 (s, *C*⁹), 34.86 (s, *CMe*₃), 32.45 (s, *CMe*₂), 31.57 (s, *CMe*₃), 22.24 (s, *CHMe*₂) ppm. **C₆₈H₆₈N₆O₁F₂₀B₁ (1376.08 g mol⁻¹):** calcd. C 59.35, H 4.98, N 6.11 %; found. C 59.75, H 5.48, N 5.55 %.

Synthesis of [(XII₂)Y(CH₂SiMe₃)₂][B(C₆F₅)₄] (**14**)

A solution of [H(XII₂)] [B(C₆F₅)₄] · 0.5 hexane (**13**) (300 mg, 0.218 mmol) in 10 mL of C₆H₅F was added dropwise to a solution of [Y(CH₂SiMe₃)₃(THF)₂] (108 mg, 0.218 mmol) in C₆H₅F (5 mL) at room temperature and the reaction was stirred for 1 hour. Approximately 40 mL of hexanes was added to the reaction resulting in the precipitation of white solid. The solution was decanted, and the white solid was dried under vacuum for 1 hour. The solid was further washed with hexanes (3 x ~ 5 mL) and dried under vacuum for 2 hours, yielding **14** as a highly air-sensitive white solid (323 mg, 93 % yield). X-ray quality crystals of **14** were grown by layering hexanes on top of a solution of **14** in C₆H₅F and cooling to -29 °C. ^1H NMR ($\text{C}_6\text{D}_5\text{Br}$, 600 MHz, 298K): δ 6.96 (s, 2H, *CH*^{1,8}), 6.73 (s, 4H, N-*CH*), 5.65 (s, 2H, *CH*^{3,6}), 4.63 (sept, $^3J_{\text{H,H}}$ 7 Hz, 4H, *CHMe*₂), 1.68 (s, 6H, *CMe*₂), 1.32 (d,

$^3J_{\text{H,H}}$ 7 Hz, 12H, CHMe_2), 1.16 (s, 18H, CMe_3), 1.10 (d, $^3J_{\text{H,H}}$ 7 Hz, 12H, CHMe_2), -0.19 (s, 18H, CH_2SiMe_3), -0.77 (appt s, 2H, CH_2SiMe_3) ppm. $^{13}\text{C}\{^1\text{H}\}$ NMR ($\text{C}_6\text{D}_5\text{Br}$, 151 MHz, 298K): δ 148.37 (s, $\text{C}^{2,7}$), 147.34 (s, NCN), 140.37 (s, $\text{C}^{4,5}$), 137.89 ($\text{C}^{11,12}$), 130.11 (s, $\text{C}^{10,13}$), 114.56 (s, N-CH), 112.78 (s, $\text{CH}^{1,8}$), 109.16 (s, $\text{CH}^{3,6}$), 48.37 (s, CHMe_2), 37.51 (d, $^3J_{\text{H,H}}$ 42 Hz, CH_2SiMe_3), 34.45 (s, CMe_3), 34.37 (s, C^9), 32.02 (s, CMe_2), 31.07 (s, CMe_3), 22.94 (s, CHMe_2), 21.80 (s, CHMe_2), 3.34 (s, CH_2SiMe_3) ppm. C 59.75, H 5.48, N 5.55 %; found. C 59.35, H 4.98, N 6.11 %. $\text{C}_{73}\text{H}_{82}\text{N}_6\text{O}_1\text{Si}_2\text{YF}_{20}\text{B}_1$ (1595.32 g mol $^{-1}$): calcd. C 54.96, H 5.18, N 5.27 %; found. C 54.63, H 5.23, N 4.91 %.

Synthesis of $[(\text{XII}_2)\text{Sc}(\text{CH}_2\text{SiMe}_3)_2][\text{B}(\text{C}_6\text{F}_5)_4]$ (**15**)

A solution of $[\text{H}(\text{XII}_2)][\text{B}(\text{C}_6\text{F}_5)_4] \cdot \text{hexane}$ (**13**) (300 mg, 0.218 mmol) in 10 mL of $\text{C}_6\text{H}_5\text{F}$ was added dropwise to a solution of $[\text{Sc}(\text{CH}_2\text{SiMe}_3)_3(\text{THF})_2]$ (98 mg, 0.218 mmol) in $\text{C}_6\text{H}_5\text{F}$ (5 mL) at room temperature and the reaction was stirred for 1 hour. Approximately 40 mL of hexanes was added to the reaction resulting in the precipitation of white solid. The solution was decanted, and the white solid was dried under vacuum for 1 hour. The solid was further washed with hexanes (3 x ~ 5 mL) and dried under vacuum for 2 hours, yielding **15** as a highly air-sensitive white solid (308 mg, 91 % yield). X-ray quality crystals of **15** grown by layering hexanes on top of a solution of **15** in $\text{C}_6\text{H}_5\text{F}$ and cooling to -29 °C. ^1H NMR ($\text{C}_6\text{D}_5\text{Br}$, 600 MHz, 298K): 6.94 (s, 2H, $\text{CH}^{1,8}$), 6.76 (s, 4H, N-CH), 5.62 (s, 2H,

$CH^{3,6}$), 4.69 (br s, 4H, $CHMe_2$), 1.66 (s, 6H, CMe_2), 1.32 (d, $^3J_{H,H}$ 6 Hz, 12H, $CHMe_2$), 1.16 (s, 18H, CMe_3), 1.10 (d, $^3J_{H,H}$ 6 Hz, 12H, $CHMe_2$), -0.25 (s, 18H, CH_2SiMe_3), -0.35 (br s, 4H, CH_2SiMe_3) ppm. $^{13}C\{^1H\}$ NMR (C_6D_5Br , 151 MHz, 298K): 148.44 (s, NCN), 147.90 (s, $C^{2,7}$), 140.74 (s, $C^{4,5}$), 137.73 ($C^{11,12}$), 129.69 (s, $C^{10,13}$), 114.66 (s, N-CH), 112.14 (s, $CH^{1,8}$), 108.32 (s, $CH^{3,6}$), 48.34 (s, $CHMe_2$), 34.57 (s, C^9), 34.46 (s, CMe_3), 31.10 (s, CMe_2), 31.10 (s, CMe_3), 23.21 (s, $CHMe_2$), 21.54 (s, $CHMe_2$), 2.87 (s, CH_2SiMe_3) ppm. $C_{73}H_{82}N_6O_1F_{20}B_1Si_2Sc$ (1551.37 g mol⁻¹): calcd. C 56.52, H 5.33, N 5.42 %; found. C 56.21, H 5.46, N 5.08 %.

NOTE: The ^{13}C NMR signal for CH_2SiMe_3 was not located in either the 1H - ^{13}C HSQC or the ^{13}C NMR spectrum due to broadening at 298 K and at 318 K.

In-situ synthesis of $[(XII)_2Sc(CH_2SiMe_2CH_2SiMe_3)][MeB(C_6F_5)_3][B(C_6F_5)_4]$ (16)

A solution of $B(C_6F_5)_3$ (9 mg, 0.0176 mmol) in 0.4 mL of C_6D_5Br was added dropwise to a solution of $[(XII)_2Sc(CH_2SiMe_3)_2][B(C_6F_5)_4]$ (15) (25 mg, 0.0161 mmol) in C_6D_5Br (0.4 mL) at room temperature and the reaction was stirred for 2 hours. 1H NMR (C_6D_5Br , 500 MHz, 258K): δ 7.09 (s, 2H, $C^{1,8}$), 6.79 (d, $^3J_{H,H}$ 2 Hz, 2H, N-CH), 6.77 (d, $^3J_{H,H}$ 2 Hz, 2H, N-CH), 5.46 (s, 2H, $C^{3,6}$), 4.90 (sept, $^3J_{H,H}$ 7 Hz, 2H, $CHMe_2$), 4.26 (sept, $^3J_{H,H}$ 7 Hz, 2H, $CHMe_2$), 1.71 (s, 6H, CMe_2), 1.50 (br s, 3H, $MeB(C_6F_5)_3$), 1.26 (d, $^3J_{H,H}$ 7 Hz, 6H, $CHMe_2$), 1.17 (d, $^3J_{H,H}$ 7 Hz, 6H, $CHMe_2$), 1.15 (s, 18H, CMe_3), 0.99 (d, $^3J_{H,H}$ 7 Hz, 6H, $CHMe_2$), 0.85 (s, 2H,

CH_2SiMe_2), 0.82 (d, $^3J_{\text{H,H}}$ 7 Hz, 6H, CHMe_2), -0.13 (s, 9H, CH_2SiMe_3), -0.31 (s, 6H, CH_2SiMe_2), -0.66 (s, 2H, CH_2SiMe_3) ppm. $^{13}\text{C}\{^1\text{H}\}$ NMR ($\text{C}_6\text{D}_5\text{Br}$, 126 MHz, 258K): δ 149.89 (s, $\text{C}^{2,7}$), 144.72 (s, NCN), 139.43 (s, $\text{C}^{4,5}$), 136.61 (s, $\text{C}^{11,12}$), 122.29 (s, $\text{C}^{10,13}$), 115.98 (s, N-CH), 115.38 (s, N-CH), 114.87 (s, $\text{C}^{1,8}$), 109.04 (s, $\text{C}^{3,6}$), 65.64 (s, CH_2SiMe_2), 49.31 (s, CHMe_2), 48.46 (s, CHMe_2), 34.59 (s, CMe_3), 34.56 (s, CMe_2), 34.30 (s, C^9), 30.85 (s, CMe_3), 30.02 (s, CMe_2), 23.32 (s, CHMe_2), 22.61 (s, CHMe_2), 21.59 (s, CHMe_2), 21.11 (s, CHMe_2), 6.59 (s, CH_2SiMe_3), 2.45 (s, CH_2SiMe_2), 1.22 (s, CH_2SiMe_3) ppm. ^{11}B NMR ($\text{C}_6\text{D}_5\text{Br}$, 161 MHz, 258K): -15.02 (s, $\text{MeB}(\text{C}_6\text{F}_5)_3$), -16.20 (s, $\text{B}(\text{C}_6\text{F}_5)_4$) ppm. ^{19}F NMR ($\text{C}_6\text{D}_5\text{Br}$, 471 MHz, 258 K): -131.76 (br s, $o\text{-B}(\text{C}_6\text{F}_5)_4$), -133.27 (d, $^3J_{\text{F,F}}$ 22 Hz, $o\text{-MeB}(\text{C}_6\text{F}_5)_3$), -157.57 (t, $^3J_{\text{F,F}}$ 20 Hz, $p\text{-MeB}(\text{C}_6\text{F}_5)_3$), -161.76 (d, $^3J_{\text{F,F}}$ 20 Hz, $m\text{-MeB}(\text{C}_6\text{F}_5)_3$), -162.09 (d, $^3J_{\text{F,F}}$ 20 Hz, $p\text{-B}(\text{C}_6\text{F}_5)_4$), -165.58 (br s, $m\text{-B}(\text{C}_6\text{F}_5)_4$) ppm.

NOTE: The ^{13}C NMR signal for $\text{Sc-CH}_2\text{SiMe}_2$ (δ 65.64 ppm) was located via $^1\text{H-}^{13}\text{C}$ HSQC NMR spectroscopy.

In-situ synthesis of $[(\text{XII})_2\text{Sc}(\text{CH}_2\text{SiMe}_3)\{\eta^x\text{-toluene}\}_x][\text{B}(\text{C}_6\text{F}_5)_4]_2$ (**17**) ($x = 0, 1$)

A solution of $[\text{CPh}_3][\text{B}(\text{C}_6\text{F}_5)_4]$ (15.5 mg, 0.0168 mmol) in 0.4 mL of $\text{C}_6\text{D}_5\text{Br}$ was added dropwise to a solution of $[(\text{XII})_2\text{Sc}(\text{CH}_2\text{SiMe}_3)_2][\text{B}(\text{C}_6\text{F}_5)_4]$ (**15**) (20 mg, 0.0129 mmol) and 10 equivalents of toluene (11.9 mg) in $\text{C}_6\text{D}_5\text{Br}$ (0.4 mL) at room temperature. The reaction was stirred vigorously for 2 hours. ^1H NMR ($\text{C}_6\text{D}_5\text{Br}$,

600 MHz, 298K): δ 7.11 (s, 2H, $CH^{1,8}$), 6.87 (s, 4H, N-CH), 5.63 (s, 2H, $CH^{3,6}$), 4.38 (br s, 4H, $CHMe_2$), 1.65 (s, 6H, CMe_2), 1.16 (s, 18H, CMe_3), 1.08 (appt t, $^3J_{H,H}$ 6 Hz, 24 H, $CHMe_2$), 0.70 (s, 2H, CH_2SiMe_3), -0.22 (s, 9H, CH_2SiMe_3) ppm. **$^{13}C\{^1H\}$ NMR (C_6D_5Br , 151 MHz, 298K** δ 151.14 (s, $C^{2,7}$), 144.06 (s, NCN), 138.01 (s, $C^{11,12}$), 142.07 (s, $C^{4,5}$), 131.02 (s, $C^{10,13}$), 116.19 (s, N-CH), 115.24 (s, $CH^{1,8}$), 109.06 (s, $CH^{3,6}$), 63.88 (s, CH_2SiMe_3), 49.39 (s, $CHMe_2$), 35.16 (s, C^9), 34.86 (s, CMe_3), 30.98 (s, CMe_3), 30.62 (s, CMe_2), 22.84 (s, $CHMe_2$), 21.51 (s, $CHMe_2$), 1.81 (s, CH_2SiMe_3) ppm. **^{11}B NMR (C_6D_5Br , 161 MHz, 298K):** δ -16.21 (s, $B(C_6F_5)_4$) ppm. **^{19}F NMR (C_6D_5Br , 471 MHz, 298 K):** δ -131.50 (br s, *o*- $B(C_6F_5)_4$), -161.67 (d, $^3J_{F,F}$ 20 Hz, *p*- $B(C_6F_5)_4$), -165.44 (br s, *m*- $B(C_6F_5)_4$) ppm.

Note: The CMe_2 and CH_2SiMe_3 signals were identified via 1H - ^{13}C HSQC NMR spectroscopy.

In-situ synthesis of $[(XII)_2Sc(C_6H_4NMe_2)][B(C_6F_5)_4]_2$ (**18**)

A solution of $[HNMe_2Ph][B(C_6F_5)_4]$ (10.3 mg, 0.013 mmol) in 0.4 mL of C_6D_5Br was added to a solution of $[(XII)_2Sc(CH_2SiMe_3)_2][B(C_6F_5)_4]$ (**15**) (20 mg, 0.013 mmol) in C_6D_5Br (0.4 mL) at room temperature and subsequently transferred to a J-Young tube. **1H NMR (C_6D_5Br , 600 MHz, 298K):** δ 7.23 (m, 2H, $C_6H_4NMe_2$), 7.09 (m, 2H, $C_6H_4NMe_2$), 7.01 (d, $^4J_{H,H}$ 2 Hz, 2H, $CH^{1,8}$), 6.72 (d, $^3J_{H,H}$ 2 Hz, 2H, N-CH), 6.61 (d, $^3J_{H,H}$ 2 Hz, 2H, N-CH), 5.39 (d, $^4J_{H,H}$ 2 Hz, 2H, $CH^{3,6}$), 4.21 (sept, $^3J_{H,H}$ 7 Hz, 2H, $CHMe_2$), 4.08 (sept, $^3J_{H,H}$ 7 Hz, 2H, $CHMe_2$), 2.16 (s, 6H,

$C_6H_4NMe_2$), 1.56 (s, 3H, CMe_2), 1.49 (s, 3H, CMe_2), 1.17 (s, 6H, CMe_3), 0.94 (m, 18H, $CHMe_2$), 0.18 (d, $^3J_{H,H}$ 7 Hz, 6H, $CHMe_2$) ppm. $^{13}C\{^1H\}$ NMR (C_6D_5Br , 151 MHz, 298K): δ 175.60 (s, $q-NMe_2Ph$), δ 153.31 (s, $q-NMe_2Ph$), 149.49 (s, $C^{2,7}$), 145.33 (s, NCN), 138.96 (s, $C^{4,5}$), 136.20 (s, $C^{11,12}$), 133.0 (s, NMe_2Ph), 131.2 (s, NMe_2Ph), 130.50 (s, $C^{10,13}$), 128.27 (s, NMe_2Ph), 117.88 (s, NMe_2Ph), 115.54 (s, N-CH), 115.51 (s, N-CH), 115.38 (s, $CH^{1,8}$), 109.01 (s, $CH^{3,6}$), 49.66 (s, $CHMe_2$), 48.82 (s, $CHMe_2$), 46.87 (s, NMe_2Ph), 34.61 (s, CMe_3), 34.04 (s, CMe_2), 33.88 (s, C^9), 30.84 (s, CMe_3), 30.80 (s, CMe_2), 23.45 (s, $CHMe_2$), 22.39 (s, $CHMe_2$), 21.23 (s, $CHMe_2$), 20.14 (s, $CHMe_2$) ppm.

Ethylene Polymerization with $[(XII)_2Sc(CH_2SiMe_3)_2][B(C_6F_5)_4]$ (**15**) activated using $[CPh_3][B(C_6F_5)_4]$

(Entries 1-3 in Table 4.1) In the glovebox 15 mg of $[(XII)_2Sc(CH_2SiMe_3)_2][B(C_6F_5)_4]$ (**15**) was dissolved in approximately 1 mL of *o*- $C_6H_5F_2$. To this was added a solution of 9 mg of $[CPh_3][B(C_6F_5)_4]$ in 1 mL of toluene, and was allowed to react for 2 hours at 24 °C. The solution was diluted with an additional 40 mL of toluene and an additional 10 mL of *o*- $C_6H_4F_2$ and was briefly evacuated before placing the flask under dynamic ethylene (1 atm). After the appropriate amount of time the solution was opened to air and approximately 5 mL of acidified methanol (10 % HCl) was added. The solid was filtered and washed with methanol and acetone, followed by drying at 50 °C under high vacuum.

(Entry 4 in Table 4.1) In the glovebox 15 mg of $[(\text{XII})_2\text{Sc}(\text{CH}_2\text{SiMe}_3)_2][\text{B}(\text{C}_6\text{F}_5)_4]$ (**15**) was dissolved in approximately 1 mL of *o*-C₆H₅F₂. To this was added a solution of 9 mg of $[\text{CPh}_3][\text{B}(\text{C}_6\text{F}_5)_4]$ in 1 mL of *o*-C₆H₅F₂, and was allowed to react for 30 minutes at 24 °C. The solution was diluted with an additional 50 mL of *o*-C₆H₄F₂ and was briefly evacuated before placing the flask under dynamic ethylene (1 atm). After the appropriate amount of time the solution was opened to air and approximately 5 mL of acidified methanol (10 % HCl) was added. The solid was filtered and washed with methanol and acetone, followed by drying at 50 °C under high vacuum.

7.5 Synthetic Procedures and Characterization Pertaining to the Work of Chapter 5

Synthesis of H[XAI] (**19**)

The catalyst mixture of Pd(OAc)₂ (70 mg, 0.312 mmol), DPEPhos (269.2 mg, 0.499 mmol), sodium *tert*-butoxide (260 mg, 2.7 mmol) were dissolved in approximately 20 mL of toluene and stirred at room temperature for 10 minutes in the glovebox. 1,3-diisopropylimidazol-2-imine (383 mg, 2.29 mmol) and 4,5-dibromo-2,7-di-*tert*-butyl-9,9-dimethylxanthene (1 g; 2.08 mmol) were dissolved in approximately 40 mL of toluene in the glovebox and added to the reaction mixture. The reaction mixture was placed in a sealed 100 mL flask and heated to

80°C in an oil bath outside the glovebox for 18 h. The reaction was cooled to room temperature and a solution of 2,6-diisopropylaniline (406 mg, 2.29 mmol), Pd(OAc)₂ (46.7 mg, 0.21 mmol), DPEPhos (157 mg, 0.29 mmol) and sodium *tert*-butoxide (280 mg, 2.91 mmol) dissolved in 15 mL of toluene was syringed into the reaction under a flow of argon, and was subsequently heated at 95 °C for 24 hours. Under air, the reaction solution was passed through a pad of Celite and volatiles were removed under reduced pressure to afford a dark brown oil. The product was extracted using approximately 60 mL of CH₂Cl₂ and was washed with 60 mL of water. The resulting aqueous layer was additionally extracted with 30 mL of CH₂Cl₂ and the organic layers were combined. The organic layer was dried over MgSO₄ and gravity filtered. Volatiles were removed from the filtrate under reduced pressure to afford a dark brown oil. The crude product was purified by basic alumina gel column chromatography (30 % ethyl acetate/hexanes solution) to obtain H[XAI] (**19**) as a beige solid (318 mg, 28 % yield) **¹H NMR (CDCl₃, 600 MHz, 298K):** δ 7.27 (t, 1H, ³J_{H,H} 8 Hz, *p*-Ar-*H*), 7.18 (d, 2H, ³J_{H,H} 8 Hz, *m*-Ar-*H*), 6.93 (d, 1H, ⁴J_{H,H} 2 Hz, xanth-*H*), 6.90 (d, 1H, ⁴J_{H,H} 2 Hz, xanth-*H*), 6.66 (d, 1H, ⁴J_{H,H} 2 Hz, xanth-*H*), 6.21 (s, 2H, N-*CH*), 5.82 (d, 1H, ⁴J_{H,H} 2 Hz, xanth-*H*), 5.17 (s, 1H, *NH*), 4.33 (sept, 2H, ³J_{H,H} 7 Hz, *CHMe*₂), 3.15 (sept, 2H, ³J_{H,H} 7 Hz, Ar-*CHMe*₂), 1.66 (s, 6H, *CMe*₂), 1.32 (s, 9H, *CMe*₃), 1.15 (d, 12H, ³J_{H,H} 7 Hz, *CHMe*₂), 1.10 (s, 9H, *CMe*₃), 1.09 (d, 6H, ³J_{H,H} 7 Hz, Ar-*CHMe*₂), 0.99 (d, 6H, ³J_{H,H} 7 Hz, Ar-*CHMe*₂) ppm. **¹³C{¹H} NMR (CDCl₃, 151 MHz, 298K):** δ 148.21 (s, Ar-*C*_{ipso}), 145.23 (s, *NCN*), 145.23 (s, *C*^{2,7}), 144.28 (s, *C*^{2,7}), 139.95 (*C*^{4,5}), 137.84 (s, *C*^{4,5}),

135.88 (s, $C^{11,12}$), 135.48 (s, Ar- C_{ortho}), 135.17 (s, $C^{11,12}$), 128.46 (s, $C^{10,13}$), 128.00 (s, $C^{10,13}$), 127.14 (s, Ar- CH_{para}), 123.69 (s, Ar- CH_{meta}), 118.77 (s, *xanth*-H), 113.70 (s, *xanth*-H), 110.52 (s, *xanth*-H), 108.09 (s, N-CH), 106.99 (s, *xanth*-H), 45.27 (s, $CHMe_2$), 34.66 (s, C^9), 34.55 (s, CMe_3), 34.51 (s, CMe_3), 33.41 (s, CMe_2), 31.77 (s, CMe_3), 31.54 (s, CMe_3), 27.91 (s, Ar- $CHMe_2$), 24.52 (s, Ar- $CHMe_2$), 24.09 (s, Ar- $CHMe_2$), 21.95 (s, $CHMe_2$) ppm. $C_{44}H_{62}N_4O_1$ (662.99 g mol⁻¹): calcd. C 79.71, H 9.43, N 8.45 %; found. C 80.00, H 9.35, N 8.12 %.

Synthesis of [(XAl)Y(CH₂SiMe₃)₂] (20)

A solution of H[XAl₂] (19) (156 mg, 0.235 mmol) in 20 mL of C₆H₅F was added dropwise to a solution of [Y(CH₂SiMe₃)₃(THF)₂] (128 mg, 0.258 mmol) in C₆H₅F (15 mL) at room temperature. The reaction was stirred for 1 hour and then the solvent was removed in vacuo to afford a brown oil. 30 mL of hexanes was added to the oil and the mixture was sonicated to obtain a brown solid. Solvent was removed in vacuo and the solid was washed with hexanes (3 x ~ 5 mL). The solid was dried under vacuum for 4 hours, yielding 20 as a highly air-sensitive brown solid (178 mg, 82 % yield). ¹H NMR (C₆D₆, 600 MHz, 298K): δ 7.44 (s, 2H, ³J_{H,H} 8 Hz, Ar- CH_{meta}), 7.36 (s, 1H, ³J_{H,H} 8 Hz, Ar- CH_{para}), 7.00 (d, ⁴J_{H,H} 2 Hz, *xanth*-H), 6.65 (d, 1H, ⁴J_{H,H} 2 Hz, *xanth*-H), 6.21 (d, 1H, ⁴J_{H,H} 2 Hz, *xanth*-H), 6.01 (s, 2H, N-CH), 5.73 (d, 1H, ⁴J_{H,H} 2 Hz, *xanth*-H), 4.70 (sept, 2H, ³J_{H,H} 7 Hz, $CHMe_2$),

3.92 (sept, 2H, $^3J_{\text{H,H}}$ 7 Hz, Ar-CHMe₂), 1.75 (s, 6H, CMe₂), 1.57 (d, 6H, $^3J_{\text{H,H}}$ 7 Hz, Ar-CHMe₂), 1.38 (d, 6H, $^3J_{\text{H,H}}$ 7 Hz, Ar-CHMe₂), 1.26 (s, 9H, CMe₃), 1.20 (s, 9H, CMe₃), 1.12 (sept, 6H, $^3J_{\text{H,H}}$ 7 Hz, CHMe₂), 0.91 (sept, 6H, $^3J_{\text{H,H}}$ 7 Hz, CHMe₂), 0.12 (s, 18H, CH₂SiMe₃), -0.64 (br m, 4H, CH₂SiMe₃) ppm. **¹³C{¹H} NMR (C₆D₆, 151 MHz, 298K):** δ 150.11 (s, NCN), 147.85 (s, C^{2,7}), 147.57 (s, C^{4,5}), 146.96 (s, C^{2,7}), 146.42 (s, Ar-C_{ortho}), 143.51 (s, Ar-C_{ipso}), 142.41 (s, C^{4,5}), 140.81 (s, C^{11,12}), 139.89 (s, C^{11,12}), 132.62 (s, C^{10,13}), 128.06 (s, C^{10,13}), 125.50 (s, Ar-CH_{para}), 124.49 (s, Ar-CH_{meta}), 113.49 (s, N-CH), 111.68 (s, *xanth*-H), 109.73 (s, *xanth*-H), 108.38 (s, *xanth*-H), 105.00 (s, *xanth*-H), 48.15 (s, CHMe₂), 35.34 (s, C⁹), 34.99 (s, CMe₃), 34.71 (s, CMe₃), 33.85 (d, $^1J_{\text{C,Y}}$ 41 Hz, CH₂SiMe₃), 31.85 (s, CMe₃), 31.66 (s, CMe₃), 31.00 (s, CMe₂), 28.45 (s, Ar-CHMe₂), 26.50 (s, Ar-CHMe₂), 24.99 (s, Ar-CHMe₂), 23.20 (s, CHMe₂), 21.97 (s, CHMe₂), 4.13 (s, CH₂SiMe₃) ppm.

Synthesis of [(XAl)Y(CH₂SiMe₃)(η^x -toluene)][B(C₆F₅)₄] (21)

A solution of [CPh₃][B(C₆F₅)₄] (20 mg, 0.0216 mmol) in 0.4 mL of C₆D₅Br was added dropwise to a solution of **20** (20 mg, 0.0216 mmol) and 10 equivalents of toluene (11.9 mg) in C₆D₅Br (0.4 mL) at room temperature yielding a bright orange solution. The solution was transferred to a J-Young tube and allowed to react for 10 minutes. **¹H NMR (C₆D₅Br, 500 MHz, 248K):** δ 7.32 (2H, Ar-CH_{meta}), 7.07 (1H, *p*-tol), 7.02 (s, 1H, *xanth*-H), 6.93 (1H, Ar-CH_{para}) 6.89 (s, 2H, N-CH), 6.81

(d, 1H, $^3J_{\text{H,H}}$ 8 Hz, *o*-tol), 6.68 (s, 1H, xanth-*H*), 6.64 (d, 1H, $^3J_{\text{H,H}}$ 8 Hz, *o*-tol), 6.39 (t, 1H, $^3J_{\text{H,H}}$ 8 Hz, *m*-tol), 5.98 (t, 1H, $^3J_{\text{H,H}}$ 8 Hz, *m*-tol), 5.81 (s, 1H, xanth-*H*), 5.33 (s, 1H, xanth-*H*), 4.50 (sept, 1H, $^3J_{\text{H,H}}$ 7 Hz, CHMe₂), 4.17 (sept, 1H, $^3J_{\text{H,H}}$ 7 Hz, CHMe₂), 3.46 (sept, 1H, $^3J_{\text{H,H}}$ 7 Hz, Ar-CHMe₂), 3.07 (sept, 1H, $^3J_{\text{H,H}}$ 7 Hz, Ar-CHMe₂), 2.18 (s, 3H, *Me*-tol), 1.73 (s, 3H, CMe₂), 1.72 (s, 3H, CMe₂), 1.38 (d, 3H, $^3J_{\text{H,H}}$ 7 Hz, Ar-CHMe₂), 1.38 (d, 3H, $^3J_{\text{H,H}}$ 7 Hz, Ar-CHMe₂), 1.30 (d, 3H, $^3J_{\text{H,H}}$ 7 Hz, Ar-CHMe₂), 1.24 (d, 3H, $^3J_{\text{H,H}}$ 7 Hz, Ar-CHMe₂), 1.21 (d, 3H, $^3J_{\text{H,H}}$ 7 Hz, CHMe₂), 1.15 (d, 3H, $^3J_{\text{H,H}}$ 7 Hz, CHMe₂), 1.15 (s, 9H, CMe₃), 1.09 (s, 9H, CMe₃), 0.97 (d, 3H, $^3J_{\text{H,H}}$ 7 Hz, CHMe₂), 0.80 (d, 3H, $^3J_{\text{H,H}}$ 7 Hz, CHMe₂), -0.24 (s, 9H, CH₂SiMe₃), -0.84 (d, 1H, $^2J_{\text{H,H}}$ 11 Hz, CH₂SiMe₃), -0.93 (d, 1H, $^2J_{\text{H,H}}$ 11 Hz, CH₂SiMe₃) ppm. **¹³C{¹H} NMR (C₆D₅Br, 126 MHz, 248K):** δ 149.21 (s, NCN), 147.42 (s, C^{2,7}), 147.38 (s, C^{2,7}), 145.68 (s, Ar-C_{ipso}), 145.05 (s, Ar-C_{ortho}), 139.17 (s, q-C), 138.45 (s, q-C), 138.11 (s, q-C), 134.41 (s, *m*-tol), 133.57 (*o*-tol), 131.55 (s, *o*-tol), 128.30 (s, *m*-tol), 124.58 (s, Ar-CH_{meta}), 124.37 (s, Ar-CH_{meta}), 115.22 (s, N-CH), 115.06 (s, N-CH), 113.59 (s, *Ar*-H), 110.24 (s, *Ar*-H), 108.99 (s, *Ar*-H), 107.97 (s, *Ar*-H), 48.54 (s, CHMe₂), 48.36 (s, CHMe₂), 39.14 (s, CH₂SiMe₃), 35.07 (s, CMe₂), 34.45 (s, CMe₃), 34.33 (s, CMe₃), 34.11 (s, C⁹), 31.21 (s, CMe₃), 31.02 (s, CMe₃), 29.34 (s, CMe₂), 27.79 (s, Ar-CHMe₂), 27.30 (s, Ar-CHMe₂), 27.26 (s, CHMe₂), 25.85 (s, CHMe₂), 24.41 (s, CHMe₂), 23.81 (s, Ar-CHMe₂), 23.57 (s, Ar-CHMe₂), 22.68 (s, CHMe₂), 21.29 (Ar-CHMe₂), 20.88 (Ar-CHMe₂), 3.00 (CH₂SiMe₃) ppm. **¹¹B NMR (C₆D₅Br, 161 MHz, 248K):** δ -16.20 (s, B(C₆F₅)₄)

ppm. ^{19}F NMR ($\text{C}_6\text{D}_5\text{Br}$, 471 MHz, 248 K): δ -131.44 (s, *o*-B(C_6F_5)₄), -161.00 (s, *p*-B(C_6F_5)₄), -164.96 (s, *m*-B(C_6F_5)₄) ppm.

NOTE: The ^1H NMR signals at 7.07 (1H, *p*-tol) and 2.18 (s, 3H, *Me*-tol) were identified via ^1H - ^1H COSY and ^1H - ^{13}C HMBC. Similarly, the Ar- CH_{meta} signal was assigned on the basis of ^1H - ^{13}C HMBC and ^1H - ^{13}C HSQC. The Ar- CH_{para} signal could not be located in the ^{13}C NMR spectrum, presumably because it is obscured by signals due to “ $\text{Ph}_3\text{CCH}_2\text{SiMe}_3$ ” and “ Ph_3CH ” byproducts. The CH_2SiMe_3 ^{13}C signal (39.14 ppm) was identified in the ^1H - ^{13}C HSQC.

General Procedure for in-situ Hydroamination using [(XAl)Y(CH₂SiMe₃)₂] (20)

In the glovebox, [(XAl)Y(CH₂SiMe₃)₂] (**20**) (5.6 mg, 0.006 mmol) was dissolved in 0.8 mL of C_6D_6 and added to the hydroamination substrate 1-amino-2,2-diphenyl-5-pentene (0.12 mmol) and the internal standard (0.12 mmol ferrocene) measured in a separate vial. The solution was then immediately placed in a PTFE valved NMR tube, and the reaction was monitored at 24 °C by ^1H NMR spectroscopy.

General procedure for in-situ Hydroamination using [(XAI)Y(CH₂SiMe₃)(η^x -toluene)][B(C₆F₅)₄] (21**)**

Entries 1 and 2 in Table 5.1- In the glovebox, [(XAI)Y(CH₂SiMe₃)₂] (**20**) (11.1 mg, 0.012 mmol) was dissolved in 0.5 mL of C₆D₅Br along with toluene (11.05 mg, 0.12 mmol). Similarly, [CPh₃][B(C₆F₅)₄] (11.2 mg, 0.012 mmol) was dissolved in 0.5 mL of C₆D₅Br, and added to the solution of **20**, resulting in a deep orange solution. After 10 minutes, 0.2 mL of the catalyst solution **21** was added to the hydroamination substrate (0.12 mmol) and ferrocene (0.12 mmol) in 0.6 mL of C₆D₅Br. The solution was then immediately placed in a PTFE-valved NMR tube, and the reaction was monitored at 24 °C by ¹H NMR spectroscopy.

Entries 3 and 4 in Table 5.1- In the glovebox, [(XAI)Y(CH₂SiMe₃)₂] (**20**) (5.5 mg, 0.006 mmol) was dissolved in 0.4 mL of C₆D₅Br along with toluene (5.6 mg, 0.06 mmol). Similarly, [CPh₃][B(C₆F₅)₄] (5.6 mg, 0.006 mmol) was dissolved in 0.4 mL of C₆D₅Br and added to the solution of **20**, resulting a deep orange solution. After 10 minutes, this catalyst solution was added to the hydroamination substrate (0.12 mmol) and the internal standard (0.12 mmol ferrocene) measured in a separate vial. The solution was then immediately placed in a PTFE valved NMR tube, and the reaction was monitored at 24 °C by ¹H NMR spectroscopy.

7.6 Synthetic Procedures and Characterization Pertaining to Future Work - Chapter 6

Synthesis of $[(\{\text{Ph}_3\text{PN}\}_2\text{XT})\text{Al}(\text{CH}_3)_2][\text{B}(\text{C}_6\text{F}_5)_4]$ (**22a**)

A solution of $[\text{H}(\text{Et}_2\text{O})_2][\text{B}(\text{C}_6\text{F}_5)_4]$ (142 mg, 0.172 mmol) in approximately 10 mL of $\text{C}_6\text{H}_5\text{F}$ was added dropwise to a solution of $(\text{Ph}_3\text{PN})_2\text{XT}$ (**1**) (150 mg, 0.172 mmol) in $\text{C}_6\text{H}_5\text{F}$ (5 mL) at room temperature. The reaction was stirred for 30 min and then the solvent was removed under vacuo yielding a yellow oil. The yellow oil was dissolved in 5 mL of $\text{C}_6\text{H}_5\text{F}$ and added dropwise to a solution of 13.6 mg (0.189 mmol) of AlMe_3 in 5 mL of $\text{C}_6\text{H}_5\text{F}$. Approximately 40 mL of hexanes was added to the reaction resulting in the precipitation of white solid. The solution was decanted, and the white solid was further dried under vacuum for 1 hour. The solid was washed with hexanes (3 x ~ 5 mL) and further dried under vacuum for 2 hours, yielding **22a** as a highly air-sensitive white solid (214 mg, 77 % yield).

^1H NMR (C_6D_6 , 500 MHz, 298K): δ 7.43-7.39 (m, 12H, *o*-Ph), 7.12-7.09 (m, 6H, *p*-Ph), 6.95-6.92 (m, 12H, *m*-Ph), 6.90 (d, $^4J_{\text{H,H}}$ 2 Hz, 2H, $\text{CH}^{1,8}$), 6.32 (d, $^4J_{\text{H,H}}$ 2 Hz, 2H, $\text{CH}^{3,6}$), 1.54 (s, 6H, CMe_2), 0.85 (s, 18H, CMe_3), -0.77 (s, 6H, AlMe_2) ppm. **^{13}C NMR (C_6D_6 , 126 MHz, 298K):** δ 147.99 (s, $\text{C}^{2,7}$), 137.51 (d, $^3J_{\text{P,C}}$ 18 Hz, $\text{C}^{11,12}$), 135.59 (d, $^2J_{\text{P,C}}$ 2 Hz, $\text{C}^{4,5}$), 134.25 (d, $^2J_{\text{P,C}}$ 8 Hz, *o*-Ph), 133.67 (d, $^4J_{\text{P,C}}$ 2 Hz, *p*-Ph), 129.35 (d, $^3J_{\text{P,C}}$ 13 Hz, *m*-Ph), 128.82 (s, $\text{C}^{10,13}$), 124.18 (d, $^1J_{\text{P,C}}$ 99 Hz, *ipso*-Ph), 118.1 (d, $^3J_{\text{P,C}}$ 12 Hz, $\text{CH}^{3,6}$), 113.69 (s, $\text{CH}^{1,8}$), 34.55 (s,

CMe_3), 34.47 (s, C^9), 33.44 (s, CMe_2), 30.85 (s, CMe_3), 3.54 (s, AlMe_2) ppm. ^{31}P NMR: (C_6D_6 , 243 MHz, 298K): δ 25.47 (s, NPh_3) ppm. ^{11}B NMR (C_6D_6 , 126 MHz, 298K): -15.84 (s, $\text{B}(\text{C}_6\text{F}_5)_4$) ppm. ^{19}F NMR ($\text{C}_6\text{D}_5\text{Br}$, 471 MHz, 298 K): -131.69 (br s, $o\text{-B}(\text{C}_6\text{F}_5)_4$), -162.85 (t, $^3J_{\text{F,F}}$ 20 Hz, $p\text{-B}(\text{C}_6\text{F}_5)_4$), -166.52 (t, $^3J_{\text{F,F}}$ 20 Hz, $m\text{-B}(\text{C}_6\text{F}_5)_4$) ppm.

Synthesis of $[(\{\text{Ph}_3\text{PN}\}_2\text{XT})\text{Al}(\text{CH}_3)_2][\text{B}(\text{C}_6\text{H}_3\{\text{CF}_3\}_2)_4]$ (**22b**)

A solution of $[\text{H}(\text{Et}_2\text{O})_2][\text{B}(\text{C}_6\text{H}_3\{\text{CF}_3\}_2)_4]$ (116 mg, 0.115 mmol) in approximately 10 mL of $\text{C}_6\text{H}_5\text{F}$ was added dropwise to a solution of $(\text{Ph}_3\text{PN})_2\text{XT}$ (**1**) (100 mg, 0.115 mmol) in $\text{C}_6\text{H}_5\text{F}$ (5 mL) at room temperature. The reaction was stirred for 30 min and then the solvent was removed under vacuo yielding a yellow oil. The yellow oil was dissolved in 5 mL of $\text{C}_6\text{H}_5\text{F}$ and added dropwise to a solution of 9 mg (0.127 mmol) of AlMe_3 in 5 mL of $\text{C}_6\text{H}_5\text{F}$. Approximately 40 mL of hexanes was added to the reaction resulting in the precipitation of a white solid. The solution was decanted, and the white solid was dried under vacuum for 1 hour. The solid was further washed with hexanes (3 x ~ 5 mL) and dried under vacuum for 2 hours, yielding **22b** as a highly air-sensitive white solid (168 mg, 82 % yield). X-ray quality crystals of **22b** were grown by layering hexanes onto a solution of **22b** in toluene, followed by cooling to $-29\text{ }^\circ\text{C}$

^1H NMR (C_6D_6 , 500 MHz, 298K): δ 7.43-7.39 (m, 12H, *o*-Ph), 7.12-7.09 (m, 6H, *p*-Ph), 6.95-6.92 (m, 12H, *m*-Ph), 6.90 (d, $^4J_{\text{H,H}}$ 2 Hz, 2H, $\text{CH}^{1,8}$), 6.32 (d, $^4J_{\text{H,H}}$ 2 Hz, 2H, $\text{CH}^{3,6}$), 1.54 (s, 6H, CMe_2), 0.85 (s, 18H, CMe_3), -0.77 (s, 6H, AlMe_2) ppm.

^{13}C NMR (C_6D_6 , 126 MHz, 298K): Identical to 22a

Synthesis of $[(\{\text{Ph}_3\text{PN}\}_2\text{NAP})\text{Al}(\text{CH}_3)_2][\text{B}(\text{C}_6\text{F}_5)_4]$ (**23a**)

A solution of $[\text{H}(\text{Et}_2\text{O})_2][\text{B}(\text{C}_6\text{F}_5)_4]$ (244 mg, 0.295 mmol) in approximately 10 mL of $\text{C}_6\text{H}_5\text{F}$ was added dropwise to a solution of $(\text{Ph}_3\text{PN})_2\text{NAP}$ (**3**) (200 mg, 0.295 mmol) in $\text{C}_6\text{H}_5\text{F}$ (5 mL) at room temperature. The reaction was stirred for 30 min and then the solvent was removed under vacuo yielding a yellow oil. The yellow oil was dissolved in 5 mL of $\text{C}_6\text{H}_5\text{F}$ and added dropwise to a solution of 23.4 mg (0.325 mmol) of AlMe_3 in 5 mL of $\text{C}_6\text{H}_5\text{F}$ and stirred for 30 minutes. The solution was removed under vacuo yielding **23a** as a highly air-sensitive white solid (356 mg, 85 % yield).

^1H NMR (C_6D_6 , 600 MHz, 298K): δ 7.45 (m, 12H, *o*-Ph), 7.11 (m, 6H, *p*-Ph), 7.07 (d, $^3J_{\text{H,H}}$ 6 Hz, 2H, $\text{C}^{2,7}$), 7.00-6.97 (m, 12H, *m*-Ph), 6.62-6.59 (m, 2H, $\text{C}^{4,5}$), 6.58-6.55 (m, 2H, $\text{C}^{3,6}$), -1.29 (s, 6H, AlMe_2) ppm. **^{13}C NMR (C_6D_6 , 151 MHz, 298K):** δ 148.6 (s, C^{10}), 141.4 (s, C^9), 136.8 (s, $\text{C}^{4,5}$), 134.5 (s, *p*-Ph), 134.4 (d, $^2J_{\text{C,P}}$ 60 Hz, *o*-Ph), 129.9 (d, $^2J_{\text{C,P}}$ 60 Hz, *m*-Ph), 125.4 (s, $\text{C}^{3,6}$), 124.7 (d, $\text{C}^{2,7}$), 124.1 (s, $\text{C}^{4,5}$), 123.3 (d, $^2J_{\text{C,P}}$ 60 Hz, *ipso*-Ph) 1.63 ppm (s, 6H, AlMe_2) ppm. **^{31}P**

NMR: (C₆D₆, 243 MHz, 298K): δ 32.84 (s, NPh₃) ppm. **¹¹B NMR (C₆D₆, 126 MHz, 298K):** -16.10 (s, B(C₆F₅)₄) ppm.

Synthesis of [(Ph₃PN)₂NAP]Al(CH₃)₂[B(C₆H₃{CF₃)₂]₄] (**23b**)

A solution of [H(Et₂O)]₂[B(C₆H₃{CF₃)₂]₄] (149 mg, 0.147 mmol) in approximately 5 mL of C₆H₅F was added dropwise to a solution of (Ph₃PN)₂NAP (**3**) (100 mg, 0.147 mmol) in C₆H₅F (5 mL) at room temperature. The reaction was stirred for 30 min and then the solvent was removed under vacuo yielding a yellow oil. The yellow oil was dissolved in 5 mL of C₆H₅F and added dropwise to a solution of 11.7 mg (0.162 mmol) of AlMe₃ in 5 mL of C₆H₅F. The solution was removed under vacuo yielding **23b** as a highly air-sensitive white solid (356 mg, 85 % yield). (178 mg, 76 % yield). X-ray quality crystals of **23b** were grown by layering hexanes onto a solution of **23b** in toluene and cooling to -29 °C

¹H NMR (C₆D₆, 600 MHz, 298K): δ 7.45 (m, 12H, *o*-Ph), 7.11 (m, 6H, *p*-Ph), 7.07 (d, ³J_{H,H} 6 Hz, 2H, C^{2,7}), 7.00-6.97 (m, 12H, *m*-Ph), 6.62-6.59 (m, 2H, C^{4,5}), 6.58-6.55 (m, 2H, C^{3,6}), -1.29 (s, 6H, AlMe₂) ppm. **¹³C NMR (C₆D₆, 151 MHz, 298K):** δ 148.6 (s, C¹⁰), 141.4 (s, C⁹), 136.8 (s, C^{4,5}), 134.5 (s, *p*-Ph), 134.4 (d, ²J_{C,P} 60 Hz, *o*-Ph), 129.9 (d, ²J_{C,P} 60 Hz, *m*-Ph), 125.4 (s, C^{3,6}), 124.7 (d, C^{2,7}), 124.1 (s, C^{4,5}), 123.3 (d, ²J_{C,P} 60 Hz, *ipso*-Ph) 1.63 ppm (s, 6H, AlMe₂) ppm. **³¹P NMR:** (C₆D₆, 243 MHz, 298K): δ 32.87 (s, NPh₃) ppm.

Bibliography

1. J. Voncken, *The Rare Earth Elements*, Springer International Publishing Switzerland, 2016.
2. C. E. S. Housecroft, A.G., *Inorganic Chemistry*, Pearson Education Limited, Essex, England, 2nd edn., 2005.
3. A. J. J. Ryan, J. W. Ziller and W. J. Evans, *Chem. Sci.*, 2020, **11**, 2006-2014.
4. D. A. Atwood, *The Rare Earth Elements: Fundamentals and Applications*, Wiley, Lexington, Kentucky, 2012; W. J. Evans, *Coord. Chem. Rev.*, 2000, **206**, 263-283.
5. M. R. MacDonald, J. E. Bates, J. W. Ziller, F. Furche and W. J. Evans, *J. Am. Chem. Soc.*, 2013, **135**, 9857-9868.
6. a) M. C. Cassani, D. J. Duncalf and M. F. Lappert, *J. Am. Chem. Soc.*, 1998, **120**, 12958-12959; b) Y. K. Gun'ko, P. B. Hitchcock and M. F. Lappert, *Organometallics*, 2000, **19**, 2832-2834.
7. M. N. Bochkarev, *Coord. Chem. Rev.*, 2004, **248**, 835-851.
8. R. D. Shannon, *Acta Crystallographica Section A*, 1976, **32**, 751-767.
9. C. Elschenbroich, *Organometallics*, Wiley-VCH, Weinheim, Germany, 2006, third completely revised and extended ed.
10. M. E. Thompson, S. M. Baxter, A. R. Bulls, B. J. Burger, M. C. Nolan, B. D. Santarsiero, W. P. Schaefer and J. E. Bercaw, *J. Am. Chem. Soc.*, 1987, **109**, 203-219.

11. D. W. Sauter, M. Taoufik and C. Boisson, *Polymers*, 2017, **9**, 1-13.
12. G. J. Natta, *J. Am. Chem. Soc.*, 1955, **77**, 1708-1710; K. Ziegler, E. Holzkamp, H. Breil, H. Martin, *Angew. Chem.* 1955, **67**, 426.
13. A. Keyes, H. E. B. Alhan, E. Ordonez, U. Ha, D. B. Beezer, H. Dau, Y. S. Liu, E. Tsogtgerel, G. R. Jones and E. Harth, *Angew. Chem. Int., Ed.*, 2019, **58**, 12370-12391.
14. G. W. Coates, *Chem. Rev.*, 2000, **100**, 1223-1252.
15. Z. Tadmor, C. G. Gogos, *Principles of Polymer Processing*, Wiley, United States of America, 1979.
16. E. J. Arlman, P. Cossee, *J. Catal.*, 1964, **3**, 99-104.
17. M. Brookhart and M. L. H. Green, *J. Organomet. Chem.*, 1983, **250**, 395-408.
18. P. Margl, L. Q. Deng and T. Ziegler, *J. Am. Chem. Soc.*, 1999, **121**, 154-162.
19. A. S. Hoffman, B. A. Fries, P. C. Condit, *J Polym Sci Pol Sym.*, 1963, **4**, 109.
20. E. Quintanilla, F. di Lena and P. Chen, *Chem. Commun.*, 2006, **41**, 4309-4311.
21. T. E. Muller, K. C. Hultsch, M. Yus, F. Foubelo and M. Tada, *Chem. Rev.*, 2008, **108**, 3795-3892.
22. a) D. V. Gribkov, K. C. Hultsch and F. Hampel, *J. Am. Chem. Soc.*, 2006, **128**, 3748-3759; b) S. W. Hong, S. Tian, M. V. Metz and T. J. Marks, *J.*

- Am. Chem. Soc.*, 2003, **125**, 14768-14783; c) A. L. Reznichenko and K. C. Hultzs, *Organometallics*, 2013, **32**, 1394-1408.
23. K. S. A. Motolko, D. J. H. Emslie and H. A. Jenkins, *Organometallics*, 2017, **36**, 1601-1608.
24. S. Bambirra, H. Tsurugi, D. van Leusen and B. Hessen, *Dalton Trans.*, 2006, **9**, 1157-1161.
25. S. Z. Ge, A. Meetsma and B. Hessen, *Organometallics*, 2008, **27**, 5339-5346.
26. F. Lauterwasser, P. G. Hayes, S. Brase, W. E. Piers and L. L. Schafer, *Organometallics*, 2004, **23**, 2234-2237.
27. A. A. Trifonov, *Coord. Chem. Rev.*, 2010, **254**, 1327-1347.
28. a) M. E. Jung and G. Piizzi, *Chem. Rev.*, 2005, **105**, 1735-1766; b) Beesley, R. M.; Ingold, C. K.; Thorpe, J. F. *J. Chem. Soc.*, **1915**. 107, 1080.
29. M. R. Crimmin, M. Arrowsmith, A. G. M. Barrett, I. J. Casely, M. S. Hill and P. A. Procopiou, *J. Am. Chem. Soc.*, 2009, **131**, 9670-9685.
30. a) A. A. Trifonov, I. V. Basalov and A. A. Kissel, *Dalton Trans.*, 2016, **45**, 19172-19193; b) S. Hong and T. J. Marks, *Accounts Chem. Res.*, 2004, **37**, 673-686; c) A. L. Reznichenko, A. J. Nawara-Hultzs, K. C. Hultzs, *Top. Curr. Chem.*, 2014. **343**, 191-260; d) A. L. Reznichenko, K. C. Hultzs, *Top. Organomet. Chem.*, 2011. **43**, 51-114.
31. J. E. Baldwin, *Chem. Commun.*, 1976, **18**, 734-736..
32. M. Zimmermann and R. Anwander, *Chem. Rev.*, 2010, **110**, 6194-6259.

33. H. M. Dietrich, G. Raudaschl-Sieber and R. Anwander, *Angew. Chem. Int., Ed.*, 2005, **44**, 5303-5306.
34. M. Zimmermann, F. Estler, E. Herdtweck, K. W. Toernroos and R. Anwander, *Organometallics*, 2007, **26**, 6029-6041.
35. a) G. Li, C. Zuccaccia, C. Tedesco, I. D'Auria, A. Macchioni and C. Pellecchia, *Chem. Eur. J.*, 2014, **20**, 232-244; b) L. Luconi, J. Klosin, A. J. Smith, S. Germain, E. Schulz, J. Hannedouche and G. Giambastiani, *Dalton Trans.*, 2013, **42**, 16056-16065.
36. a) D. D. Graf, R. R. Schrock, W. M. Davis and R. Stumpf, *Organometallics*, 1999, **18**, 843-852; b) R. R. Schrock, F. Schattenmann, M. Aizenberg and W. M. Davis, *Chem. Commun.*, 1998, **2**, 199-200.
37. A. A. Trifonov and D. M. Lyubov, *Coord. Chem. Rev.*, 2017, **340**, 10-61.
38. P. M. Zeimentz, S. Arndt, B. R. Elvidge and J. Okuda, *Chem. Rev.*, 2006, **106**, 2404-2433.
39. P. G. Hayes, W. E. Piers and R. McDonald, *J. Am. Chem. Soc.*, 2002, **124**, 2132-2133.
40. K. R. D. Johnson and P. G. Hayes, *Chem. Soc. Rev.*, 2013, **42**, 1947-1960.
41. H. Vanderheijden, C. J. Schaverien and A. G. Orpen, *Organometallics*, 1989, **8**, 255-258.
42. B. D. Ward, L. Lukesova, H. Wadepohl, S. Bellemin-Laponnaz and L. H. Gade, *Eur. J. Inorg. Chem.*, 2009, **7**, 866-871.
43. S. Arndt, T. P. Spaniol and J. Okuda, *Chem. Commun.*, 2002, **42**, 896-897.

44. E. Y. X. Chen and T. J. Marks, *Chem. Rev.*, 2000, **100**, 1391-1434.
45. J. N. Pedeutour, K. Radhakrishnan, H. Cramail and A. Deffieux, *Macromol. Rapid Commun.*, 2001, **22**, 1095-1123.
46. T. M. Cameron, J. C. Gordon, R. Michalczyk and B. L. Scott, *Chem. Commun.*, 2003, **18**, 2282-2283.
47. P. G. Hayes, W. E. Piers and M. Parvez, *Organometallics*, 2005, **24**, 1173-1183.
48. A. L. Kenward, W. E. Piers and M. Parvez, *Organometallics*, 2009, **28**, 3012-3020.
49. a) M. W. Bouwkamp, P. H. M. Budzelaar, J. Gercama, I. D. Morales, J. de Wolf, A. Meetsma, S. I. Troyanov, J. H. Teuben and B. Hessen, *J. Am. Chem. Soc.*, 2005, **127**, 14310-14319; b) X. F. Li, M. Nishiura, K. Mori, T. Mashiko and Z. M. Hou, *Chem. Commun.*, 2007, **40**, 4137-4139; c) J. J. Liu, D. Reta, J. A. Cleghorn, Y. X. Yeoh, F. Ortu, C. A. P. Goodwin, N. F. Chilton and D. P. Mills, *Chem. Eur. J.*, 2019, **25**, 7749-7758.
50. A. F. R. Kilpatrick, J. C. Buffet, P. Norby, N. H. Rees, N. P. Funnell, S. Sripothongnak and D. O'Hare, *Chem. Mat.*, 2016, **28**, 7444-7450.
51. A. L. Kenward, J. A. Ross, W. E. Piers and M. Parvez, *Organometallics*, 2009, **28**, 3625-3628.
52. C. J. Schaverien, *Organometallics*, 1992, **11**, 3476-3478.
53. P. G. Hayes, W. E. Piers and M. Parvez, *J. Am. Chem. Soc.*, 2003, **125**, 5622-5623.

54. S. Bambirra, M. W. Bouwkamp, A. Meetsma and B. Hessen, *J. Am. Chem. Soc.*, 2004, **126**, 9182-9183.
55. S. Bambirra, D. van Leusen, A. Meetsma, B. Hessen and J. H. Teuben, *Chem. Commun.*, 2003, **4**, 522-523.
56. D. M. Lyubov, L. Luconi, A. Rossin, G. Tuci, A. V. Cherkasov, G. K. Fukin, G. Giambastiani and A. A. Trifonov, *Chem. Eur. J.*, 2014, **20**, 3487-3499.
57. S. Arndt, T. P. Spaniol and J. Okuda, *Angew. Chem. Int., Ed.*, 2003, **42**, 5075-5079.
58. S. Arndt and J. Okuda, *Adv. Synth. Catal.*, 2005, **347**, 339-354.
59. S. Arndt, B. R. Elvidge, P. M. Zeimentz, T. P. Spaniol and J. Okuda, *Organometallics*, 2006, **25**, 793-795.
60. Y. Pan, T. Q. Xu, Y. S. Ge and X. B. Lu, *Organometallics*, 2011, **30**, 5687-5694.
61. W. E. Piers and D. J. H. Emslie, *Coord. Chem. Rev.*, 2002, **233**, 131-155.
62. E. Peris and R. H. Crabtree, *Chem. Soc. Rev.*, 2018, **47**, 1959-1968.
63. C. A. Cruz, D. J. H. Emslie, L. E. Harrington, J. F. Britten and C. M. Robertson, *Organometallics*, 2007, **26**, 692-701.
64. K. S. A. Motolko, J. S. Price, D. J. H. Emslie, H. A. Jenkins and J. F. Britten, *Organometallics*, 2017, **36**, 3084-3093.
65. N. R. Andreychuk, S. Ilango, B. Vidjayacoumar, D. J. H. Emslie and H. A. Jenkins, *Organometallics*, 2013, **32**, 1466-1474.

66. C. A. Cruz, D. J. H. Emslie, L. E. Harrington and J. F. Britten, *Organometallics*, 2008, **27**, 15-17.
67. Andreychuk, N. *Rigid NON-Donor Pincer Ligands in Organoactinide Chemistry*. Chemistry, Ph.D. Thesis, McMaster University: Hamilton, ON, 2018
68. C. A. Cruz, D. J. H. Emslie, C. M. Robertson, L. E. Harrington, H. A. Jenkins and J. F. Britten, *Organometallics*, 2009, **28**, 1891-1899.
69. X. J. Xing, S. G. Zhang, L. M. Thierer, M. R. Gau, P. J. Carroll and N. C. Tomson, *Dalton Trans.*, 2020, **49**, 7796-7806.
70. H. Staudinger, J. Meyer, *Chim. Acta.*, 1919, **2**, 635-646.
71. R. Keat, M. C. Miller, R. A Shaw, *J. Chem. Soc.*, 1967, 1404-1408.
72. a) K. A. Rufanov, A. R. Petrov, V. V. Kotov, F. Laquai and J. Sundermeyer, *Eur. J. Inorg. Chem.*, 2005, **19**, 3805-3807; b) N. K. Hangaly, A. R. Petrov, M. Elfferding, K. Harms and J. Sundermeyer, *Dalton Trans.*, 2014, **43**, 7109-7120; c) Z. Jian, N. K. Hangaly, W. Rong, Z. Mou, D. Liu, S. Li, A. A. Trifonov, J. Sundermeyer and D. Cui, *Organometallics*, 2012, **31**, 4579-4587.
73. a) N. K. Hangaly, A. R. Petrov, K. A. Rufanov, K. Harms, M. Elfferding and J. r. Sundermeyer, *Organometallics*, 2011, **30**, 4544-4554; b) Z. Jian, A. R. Petrov, N. K. Hangaly, S. Li, W. Rong, Z. Mou, K. A. Rufanov, K. Harms, J. Sundermeyer and D. Cui, *Organometallics*, 2012, **31**, 4267-4282.

74. N. S. Hillesheim, M. Elfferding, T. Linder and J. Sundermeyer, *Z. Anorg. Allg. Chem.*, 2010, **636**, 1776-1782.
75. W. F. Rong, D. T. Liu, H. P. Zuo, Y. P. Pan, Z. B. Jian, S. H. Li and D. M. Cui, *Organometallics*, 2013, **32**, 1166-1175.
76. K. D. Conroy, W. E. Piers and M. Parvez, *J. Organomet. Chem.*, 2008, **693**, 834-846.
77. D. Wang, S. H. Li, X. L. Liu, W. Gao and D. M. Cui, *Organometallics*, 2008, **27**, 6531-6538.
78. N. Y. Rad'kova, A. O. Tolpygin, V. Y. Rad'kov, N. M. Khamaletdinova, A. V. Cherkasov, G. K. Fukin and A. A. Trifonov, *Dalton Trans.*, 2016, **45**, 18572-18584.
79. J. L. Brosmer and P. L. Diaconescu, *Organometallics*, 2015, **34**, 2567-2572.
80. Z. C. Zhang and D. M. Cui, *Chem. Eur. J.*, 2011, **17**, 11520-11526.
81. a) K. R. Johnson and P. G. Hayes, *Dalton Trans.*, 2014, **43**, 2448-2457; b) K. R. D. Johnson and P. G. Hayes, *Organometallics*, 2011, **30**, 58-67.
82. K. R. D. Johnson, B. L. Kamenz and P. G. Hayes, *Can. J. Chem.*, 2016, **94**, 330-341.
83. K. R. D. Johnson and P. G. Hayes, *Organometallics*, 2009, **28**, 6352-6361.
84. K. R. D. Johnson and P. G. Hayes, *Organometallics*, 2013, **32**, 4046-4049.
85. K. R. D. Johnson and P. G. Hayes, *Inorg. Chim. Acta*, 2014, **422**, 209-217.
86. K. R. Johnson, M. A. Hannon, J. S. Ritch and P. G. Hayes, *Dalton Trans.*, 2012, **41**, 7873-7875.

87. M. T. Zamora, K. R. Johnson, M. M. Hanninen and P. G. Hayes, *Dalton Trans.*, 2014, **43**, 10739-10750.
88. N. Kuhn, R. Fawzi, M. Steimann, J. Wiethoff, D. Blaser and R. Boese, *Z.Naturforsch.(B)*, 1995, **50**, 1779-1784.
89. X. Wu and M. Tamm, *Coord. Chem. Rev.*, 2014, **260**, 116-138.
90. T. K. Panda, D. Petrovic, T. Bannenberg, C. G. Hrib, P. G. Jones and M. Tamm, *Inorg. Chim. Acta*, 2008, **361**, 2236-2242.
91. M. Tamm, D. Petrovic, S. Randoll, S. Beer, T. Bannenberg, P. G. Jones and O. Grunenberg, *Org. Biomol. Chem.*, 2007, **5**, 523-530.
92. D. Petrovic, T. Bannenberg, S. Randoll, P. G. Jones and M. Tamm, *Dalton Trans.*, 2007, **26**, 2812-2822.
93. K. Jess, V. Derdau, R. Weck, J. Atzrodt, M. Freytag, P. G. Jones and M. Tamm, *Adv. Synth. Catal.*, 2017, **359**, 629-638.
94. T. K. Panda, C. G. Hrib, P. G. Jones, J. Jenter, P. W. Roesky and M. Tamm, *Eur. J. Inorg. Chem*, 2008, **27**, 4270-4279.
95. a) F. T. Edelmann, D. M. M. Freckmann and H. Schumann, *Chem. Rev.*, 2002, **102**, 1851-1896; b) F. T. Edelmann, *Chem. Soc. Rev.*, 2012, **41**, 7657-7672; c) T. S. Li, S. Kaercher and P. W. Roesky, *Chem. Soc. Rev.*, 2014, **43**, 42-57; d) M. Nishiura and Z. M. Hou, *Nat. Chem.*, 2010, **2**, 257-268.
96. a) C. A. Cruz, D. J. H. Emslie, H. A. Jenkins and J. F. Britten, *Dalton Trans.*, 2010, **39**, 6626-6628; b) N. R. Andreychuk, D. J. H. Emslie, H. A. Jenkins and J. F. Britten, *J. Organomet. Chem.*, 2018, **857**, 16-24.

97. K. S. A. Motolko, D. J. H. Emslie and J. F. Britten, *RSC Adv.*, 2017, **7**, 27938-27945.
98. J. S. Nowick, P. Ballester, F. Ebmeyer and J. Rebek, *J. Am. Chem. Soc.*, 1990, **112**, 8902-8906.
99. a) E. L. Lu, W. Gan and Y. F. Chen, *Dalton Trans.*, 2011, **40**, 2366-2374; P. L. Watson, *Chem. Commun.*, 1983, **6**, 276-277; b) A. L. Wayda, J. L. Atwood and W. E. Hunter, *Organometallics*, 1984, **3**, 939-941.
100. P. M. Zeimentz and J. Okuda, *Organometallics*, 2007, **26**, 6388-6396.
101. a) K. H. Denhaan, J. L. Deboer, J. H. Teuben, A. L. Spek, B. Kojicprodic, G. R. Hays and R. Huis, *Organometallics*, 1986, **5**, 1726-1733; b) D. A. Pantazis, J. E. McGrady, M. Besora, F. Maseras and M. Etienne, *Organometallics*, 2008, **27**, 1128-1134; c) A. F. Dunlop-Briere, P. H. M. Budzelaar and M. C. Baird, *Organometallics*, 2012, **31**, 1591-1594.
102. C. A. Cruz, T. Chu, D. J. H. Emslie, H. A. Jenkins, L. E. Harrington and J. F. Britten, *J. Organomet. Chem.*, 2010, **695**, 2798-2803.
103. a) N. R. Andreychuk, T. Dickie, D. J. H. Emslie and H. A. Jenkins, *Dalton Trans.*, 2018, **47**, 4866-4876; b) K. S. A. Motolko, D. J. H. Emslie, H. A. Jenkins and J. F. Britten, *Eur. J. Inorg. Chem.*, 2017, **22**, 2920-2927.
104. B. Vidjayacoumar, S. Ilango, M. J. Ray, T. Chu, K. B. Kolpin, N. R. Andreychuk, C. A. Cruz, D. J. H. Emslie, H. A. Jenkins and J. F. Britten, *Dalton Trans.*, 2012, **41**, 8175-8189.

105. Based on a search of the Cambridge Structural Database conducted on September 2019. C. R. Groom, I. J. Bruno, M. P. Lightfoot and S. C. Ward, *Acta Cryst.* (2016). B72, 171-179
106. S. Bambirra, S. J. Boot, D. van Leusen, A. Meetsma and B. Hessen, *Organometallics*, 2004, **23**, 1891-1898.
107. S. Bambirra, A. Meetsma, B. Hessen and A. P. Bruins, *Organometallics*, 2006, **25**, 3486-3495.
108. D. M. Lyubov, A. V. Cherkasov, G. K. Fukin and A. A. Trifonov, *Organometallics*, 2016, **35**, 126-137.
109. S. Bradbury, C. W. Rees, R. C. Storr, *J. Chem. Soc. Perkin Trans. I*, 1972, **1**, 68-71.
110. a) L. Anthore-Dalion, A. D. Benischke, B. Wei, G. Berionni and P. Knochel, *Angew. Chem. Int., Ed*, 2019, **58**, 4046-4050; b) A. D. Benischke, L. Anthore-Dalion, G. Berionni and P. Knochel, *Angew. Chem. Int., Ed*, 2017, **56**, 16390-16394; c) A. D. Benischke, L. Anthore-Dalion, F. Kohl and P. Knochel, *Chem. Eur. J.*, 2018, **24**, 11103-11109.
111. a) C. E. Hayes and D. B. Leznoff, *Dalton Trans.*, 2012, **41**, 5743-5753; b) M. E. O'Reilly and A. S. Veige, *Chem. Soc. Rev.*, 2014, **43**, 6325-6369.
112. J. Hicks, P. Vasko, J. M. Goicoechea and S. Aldridge, *Nature*, 2018, **557**, 92-95.
113. A. Heilmann, J. Hicks, P. Vasko, J. M. Goicoechea and S. Aldridge, *Angew. Chem. Int., Ed.*, 2020, **59**, 4897-4901.

114. J. Hicks, A. Heilmann, P. Vasko, J. M. Goicoechea and S. Aldridge, *Angew. Chem. Int., Ed.*, 2019, **58**, 17265-17268.
115. J. Hicks, A. Mansikkamaki, P. Vasko, J. M. Goicoechea and S. Aldridge, *Nat. Chem.*, 2019, **11**, 237-241.
116. A. Nicolay, M. S. Ziegler, L. Rochlitz and T. D. Tilley, *Polyhedron*, 2020, **180**, 9.
117. E. W. Y. Wong and D. J. H. Emslie, *Dalton Trans.*, 2015, **44**, 11601-11612.
118. D. Maiti, B. P. Fors, J. L. Henderson, Y. Nakamura and S. L. Buchwald, *Chem. Sci.*, 2011, **2**, 57-68.
119. R. A. Kunetskiy, S. M. Polyakova, J. Vavrik, I. Cisarova, J. Saame, E. R. Nerut, I. Koppel, I. A. Koppel, A. Kutt, I. Leito and I. M. Lyapkalo, *Chem. Eur. J.*, 2012, **18**, 3621-3630.
120. S. A. Filimon, D. Petrovic, J. Volbeda, T. Bannenberg, P. G. Jones, C. G. F. von Richthofen, T. Glaser and M. Tamm, *Eur. J. Inorg. Chem.*, 2014, **35**, 5997-6012.
121. P. D. Bolton, N. Adams, E. Clot, A. R. Cowley, P. J. Wilson, M. Schroeder and P. Mountford, *Organometallics*, 2006, **25**, 5549-5565.
122. A. D. Horton, *Organometallics*, 1996, **15**, 2675-2677.
123. P. D. Bolton, E. Clot, N. Adams, S. R. Dubberley, A. R. Cowley and P. Mountford, *Organometallics*, 2006, **25**, 2806-2825.
124. C. O. Hollfelder, L. N. Jende, H. M. Dietrich, K. Eichele, C. Maichle-Mossmer and R. Anwander, *Chem. Eur. J.*, 2019, **25**, 7298-7302.

125. D. F. Li, S. H. Li, D. M. Cui, X. Q. Zhang and A. A. Trifonov, *Dalton Trans.*, 2011, **40**, 2151-2153.
126. P. G. Hayes, W. E. Piers and M. Parvez, *Chem. Eur. J.*, 2007, **13**, 2632-2640.
127. N. Yu, M. Nishiura, X. F. Li, Z. F. Xi and Z. M. Hou, *Chem.-Asian J.*, 2008, **3**, 1406-1414.
128. a) M. A. Angadol, D. H. Woen, C. J. Windorff, J. W. Ziller and W. J. Evans, *Organometallics*, 2019, **38**, 1151-1158; b) T. F. Jenkins, D. H. Woen, L. N. Mohanam, J. W. Ziller, F. Furche and W. J. Evans, *Organometallics*, 2018, **37**, 3863-3873; c) S. A. Moehring, M. Miehllich, C. J. Hoerger, K. Meyer, J. W. Ziller and W. J. Evans, *Inorg. Chem.*, 2020, **59**, 3207-3214; d) C. T. Palumbo, L. E. Darago, C. J. Windorff, J. W. Ziller and W. J. Evans, *Organometallics*, 2018, **37**, 900-905.
129. M. C. Cassani, Y. K. Gun'ko, P. B. Hitchcock, A. G. Hulkes, A. V. Khvostov, M. F. Lappert and A. V. Protchenko, *J. Organomet. Chem.*, 2002, **647**, 71-83.
130. a) F. G. N. Cloke, *Chem. Soc. Rev.*, 1993, **22**, 17-24; M. E. Fieser, M. R. MacDonald, B. T. Krull, J. E. Bates, J. W. Ziller, F. Furche and W. J. Evans, *J. Am. Chem. Soc.*, 2015, **137**, 369-382; b) D. N. Huh, S. R. Ciccone, S. Bekoe, S. Roy, J. W. Ziller, F. Furche and W. J. Evans, *Angew. Chem. Int., Ed.*, DOI: 10.1002/anie.202006393; c) D. N. Huh, J. W. Ziller and W. J. Evans, *Inorg. Chem.*, 2019, **58**, 9613-9617; d) M. R. MacDonald, J. E.

- Bates, M. E. Fieser, J. W. Ziller, F. Furche and W. J. Evans, *J. Am. Chem. Soc.*, 2012, **134**, 8420-8423; e) M. R. MacDonald, J. W. Ziller and W. J. Evans, *J. Am. Chem. Soc.*, 2011, **133**, 15914-15917.
131. D. H. Woen, G. P. Chen, J. W. Ziller, T. J. Boyle, F. Furche and W. J. Evans, *Angew. Chem. Int., Ed.*, 2017, **56**, 2050-2053.
132. D. Franz and S. Inoue, *Chem. Eur. J.*, 2019, **25**, 2898-2926.
133. a) L. L. Cao, E. Daley, T. C. Johnstone and D. W. Stephan, *Chem. Commun.*, 2016, **52**, 5305-5307; b) D. Vidovic, M. Findlater, G. Reeske and A. H. Cowley, *J. Organomet. Chem.*, 2007, **692**, 5683-5686.
134. E. S. Tabatabaie, S. Dehghanpour, E. Mosaddegh, R. Babaahmadi, A. Chipman, B. F. Yates and A. Ariafard, *Dalton Trans.*, 2019, **48**, 6997-7005.
135. T. Schaub, U. Radius, A. Brucks, M. P. Choules, M. T. Olsen and T. B. Rauchfuss, in *Inorganic Syntheses*, ed. 2010, vol. 35, pp. 78-83.
136. H. Xiong, Y. Gu, S. N. Zhang, F. P. Lu, Q. Ji, L. L. Liu, P. X. Ma, G. Yang, W. Hou and H. T. Xu, *Chem. Commun.*, 2020, **56**, 4692-4695.
137. P. Jutzi, C. Muller, A. Stammler and H. G. Stammler, *Organometallics*, 2000, **19**, 1442-1444.
138. M. Brookhart, B. Grant and A. F. Volpe, *Organometallics*, 1992, **11**, 3920-3922.
139. F. Estler, G. Eickerling, E. Herdtweck and R. Anwander, *Organometallics*, 2003, **22**, 1212-1222.
140. J. Pohlmann, F. Brickmann, *Z. Naturforsch* 1965, **B20**, 5.